

Utilising a High Pressure, Cross Flow, Stainless Steel Fintube Heat Exchanger for Direct Steam Generation from Recovered Waste Heat

Karl Paul Martin Wipplinger

**Thesis presented for the degree of MScEng
in Mechanical Engineering at the
University of Stellenbosch**



Thesis supervisors:

Dr T.M. Harms
esl (energy systems laboratories)

Dr A.B. Taylor
CAE (Centre for Automotive Engineering)

April 2004

DECLARATION

I, Karl Paul Martin Wipplinger, submit this thesis in partial fulfilment of the requirements of the degree MScEng at the University of Stellenbosch and hereby declare that the work contained in this thesis is my own original work and that I have not previously, in its entirety or in part, submitted it at any university for a degree.

Signed:

Date:

ABSTRACT

Around the world the implementation of heat recovery systems is playing an increasingly important role in the engineering industry. The recovered energy is utilised in the plants and saves companies millions in expenses per year. Not only is this seen on the grand scale of industry, but also in everyday life, where for instance turbochargers are used to boost the performance of automobiles by utilising the wasted energy expelled along with exhaust gasses.

The aim of this project is to investigate a small scale waste heat recovery system, and to determine the optimum method by which to convert the recovered energy into electrical energy, which can be used as a secondary energy source.

The research contained in this thesis, centres on the main components and theory needed for the construction of a small scale waste heat recovery system. Also included, is a theoretical analysis concerning the design and construction of the system, utilising researched theory and a simulation program of the recovery system. The simulation is control volume-based and generates property data on the fluid and exhaust gas throughout the heat exchanger.

The final design included a finite element stress analysis of certain parts of the system to ensure safe testing at high pressures and temperatures.

The final design resulted in a high pressure, cross flow, stainless steel fin tube heat exchanger that, by using a continuous combustion unit as energy source and water as the working fluid, reached efficiencies of up to 74% in direct steam generation testing. The tube-side of the heat exchanger was designed to withstand pressures of up to 2MPa (20bar), which is imperative for the implementation of the next phase, where a turbocharger will be connected to the heat exchanger.

The completion of this part of the project has paved the way for further development and implementation of the heat recovery system.

OPSOMMING

Die herwinning van energie begin 'n toenemend belangrike rol in die ingenieurs industrie speel. Die herwonne energie word in fabriek benut en spaar maatskappye miljoene aan uitgawes per jaar. Hierdie beginsel word nie net in die grootskaalse nywerhede toegepas nie, maar ook in die alledaagse lewe, soos byvoorbeeld in voertuie waar turbo-aanjaers gebruik word om die energie-uitset van enjins te verhoog deur bloot gebruik te maak van die verlore energie wat saam met die uitlaatgasse in die atmosfeer gepomp word.

Die doel van hierdie projek is om 'n kleinskaalse energieherwinningstelsel te ondersoek en die mees effektiewe metode te vind om die herwinde energie na elektriese energie om te skakel wat as 'n sekondêre energiebron gebruik kan word.

Die navorsing bevat in die tesis, kyk na al die hoofkomponente en teoretiese kennis wat nodig is vir die konstruksie van 'n kleinskaalse hitteherwinningstelsel. Ook ingesluit is 'n teoretiese analise ten opsigte van die ontwerp en konstruksie van die sisteem. Dit behels die gebruik van nagevorsde teorie saam met 'n simulatie program van die herwinnings stelsel. Die simulatie program is op kontrole volumes gebaseer en genereer uitlaatgas- en water eienskappe soos dit deur die hitteruiler vloei.

Die finale ontwerp bevat 'n eindige element spannings analise van sekere kritiese komponente in die stelsel om die veilige gebruik van die sisteem by hoë drukke en temperature te verseker.

Die finale ontwerp was 'n hoëdruk, kruisvloei, vlekvrystaal finbuis hitteruiler. Deur 'n konstante verbrandingseenheid as energiebron te gebruik saam met water as werksvloei, het die hitteruiler effektiwiteit van tot 74% in direkte stoomgenerasie-toetse bereik. Die hitteruiler is ontwerp om hoë drukke van tot 2MPa (20bar) te hanteer wat baie belangrik is vir die implementasie van die volgende fase van die projek waar 'n turbo-aanjaer aan die stelsel gekoppel sal.

Die suksesvolle voltooiing van hierdie fase van die projek het die weg gebaan vir die verdere ontwikkeling en implimentasie van die energieherwinningsstelsel.

DEDICATION

To my loving family. You have always believed in me and supported me in everything I have done. A special thanks to Marga for all her time and effort.

Above all I want to praise God for being true, for giving me all the opportunities I have and always helping me fulfil my dreams.

ACKNOWLEDGEMENTS

I would like to sincerely thank the following persons for their assistance and contributions during the course of this study:

Firstly Dr T M Harms, for believing in me, always making time for me (even if it was only for a quick chat) and for his continuous support during this project.

Dr A B Taylor for his help, guidance and continuous support.

Mr C F Zietsman and Moses, who put up with all my demands and helped me acquire all the correct hardware for this project.

The guys from SMD, especially Graham, Riaan and Menno. This project would never have been a success without your technical expertise.

The Centre for Automotive Engineering, for letting me use part of their facilities while testing the heat exchanger.

TABLE OF CONTENTS

	Page
DECLARATION	ii
ABSTRACT	iii
OPSOMMING	iv
DEDICATION	v
ACKNOWLEDGEMENTS	vi
TABLE OF CONTENTS	vii
LIST OF FIGURES	x
LIST OF TABLES	xiv
LIST OF SYMBOLS	xvi
1. INTRODUCTION	1
2. PROJECT OUTLINE	3
3. THE WASTE HEAT RECOVERY SYSTEM	5
4. LITERATURE REVIEW	8
4.1 INTERNET SEARCHES	8
4.1.1 Turbine introduction as from Micro Hydropower Basics (2000)	8
4.1.2 Impulse Turbines	9
4.1.3 Reaction Turbines	11
4.1.4 TurbochargersNZ (2001)	12
4.1.5 TurboGenset (2003)	14
4.1.6 Bowman Power (2002)	15
4.2 PUBLISHED PAPERS AND TEXTBOOKS	16
4.2.1 Energy Recovery Cycles	16
4.2.2 Two-phase Flow inside Tubes	17
4.2.3 Boiling Heat Transfer Coefficient	20
4.2.4 U-tubes	21
4.2.5 Stainless Steel Corrosion	23
4.2.6 Turbocharger Design	24
4.2.7 Power Generation utilising High Speed Generators	27
4.2.8 Material Research	29
4.3 RESEARCH DONE AT THE UNIVERSITY OF STELLENBOSCH	32
4.3.1 Joubert (1996)	32
4.3.2 Koorts (1998)	33
4.3.3 Lotun (1999 & 2001)	33

Table of Contents (<i>continued</i>)	Page
4.3.4 Wipplinger (2001)	34
4.3.5 Conclusion	35
5. THEORETICAL ANALYSIS	36
5.1 THE CONTINUOUS COMBUSTION UNIT AND ENERGY AVAILABILITY	36
5.1.1 Combustion Analysis	36
5.2 FINTUBE AND U-BEND DESIGN CONSIDERATIONS	37
5.3 EQUATIONS AND THEORIES	38
5.3.1 Implicit Geometries	38
5.3.2 Preheating Theory	40
5.3.3 Single-phase Liquid Pressure Drop across a Tube	41
5.3.4 Single-phase Liquid Pressure Drop across a U-bend	42
5.3.5 Boiler Theory	43
5.3.6 Two-phase Pressure Drop in a Tube	44
5.3.7 Two-phase Pressure Drop across a U-bend	45
5.3.8 Superheated Theory	45
5.3.9 Single-phase Vapour Pressure Drop across a Tube	46
5.3.10 Single-phase Vapour Pressure Drop across a U-bend	47
5.3.11 Gas side Pressure Drop Theory	48
5.3.12 Fin Efficiency	49
5.3.13 Overall Heat Transfer Coefficient for a Control Volume	49
5.3.14 Heat Exchanger Effectiveness	49
5.3.15 Gas Heat Transfer Coefficient	50
5.3.16 Water Liquid Heat Transfer Coefficient	52
5.3.17 Water Vapour Heat Transfer Coefficient	52
5.3.18 Final Energy Balance Calculations	53
5.3.19 Conclusion	54
5.4 MICROSOFT® EXCEL 2002 SPREADSHEET	55
5.4.1 Introduction	55
5.4.2 Main Sheet	55
5.4.3 Energy Balance	55
5.4.4 Different Phase Stages	56
5.4.5 Rankine Cycle	57
5.4.6 Exhaust and Water Pressure Drop	57
5.4.7 Conclusion	57
5.5 MICROSOFT® VISUAL BASIC 6.0 SIMULATION PROGRAM (HESP)	58
5.5.1 Introduction	58
5.5.2 Simulation	60
5.5.3 Conclusion	67
6. STRESS ANALYSIS	68
6.1 INTRODUCTION	68
6.2 FINITE ELEMENT ANALYSIS	68
6.2.1 U-bend	70
6.2.2 Fintube	71

	Page
Table of Contents (<i>continued</i>)	
6.3 CONCLUSION	71
7. PRACTICAL TESTING OF THE HEAT EXCHANGER	72
7.1 SYSTEM DESIGN	72
7.2 CONSTRUCTION AND TROUBLESHOOTING	73
7.3 FINAL SYSTEM CONFIGURATION AND TESTING	77
7.4 EXPERIMENTAL VS. SIMULATED RESULTS	80
7.4.1 Testing Strategy	80
7.4.2 Testing Procedure	81
7.4.3 Result Discussion	82
7.4.4 Further Simulated Testing	90
7.4.5 Conclusion	93
8. PROJECT CONCLUSION	95
9. RECOMMENDATIONS	96
REFERENCES	97
APPENDIX A - Manufacturer's Turbocharger Design Drawing (<i>AlliedSignal, 2002</i>)	A1
APPENDIX B - Manufacturer's Turbocharger Maps (<i>AlliedSignal, 2002</i>)	B1
APPENDIX C - Air Based Feasibility & Chocking Calculations	C1
APPENDIX D - Water Based Feasibility Calculations	D1
APPENDIX E - Continuous Combustion Unit	E1
APPENDIX F - Correlations	F1
APPENDIX G - Microsoft® Excel 2002 Spreadsheet	G1
APPENDIX H - Microsoft® Visual Basic 6.0 Simulation Program	H1
APPENDIX I - Microsoft® Visual Basic 6.0 Program Flow Chart	I1
APPENDIX J - Energy Availability	J1
APPENDIX K - Heat Exchanger Design Drawings	K1
APPENDIX L - Heat Exchanger Test Results	L1
APPENDIX M - Stress Analysis	M1

LIST OF FIGURES

	Page
<i>Figure 1.1: Energy distribution of a typical turbocharged diesel engine (Wipplinger, 2000)</i>	2
<i>Figure 3.1: Air-based lab configuration for waste heat recovery system</i>	5
<i>Figure 3.2: Water-based lab configuration for open loop recovery system</i>	7
<i>Figure 4.1: The runner of a Pelton wheel (Micro Hydropower Basics, 2000)</i>	9
<i>Figure 4.2: The Pelton working configuration</i>	10
<i>Figure 4.3: The runner of a Turgo turbine</i>	11
<i>Figure 4.4: The Turgo working configuration</i>	11
<i>Figure 4.5: The Francis turbine and guide vanes</i>	12
<i>Figure 4.6: Turbocharger layout (Volkswagen, 2003)</i>	13
<i>Figure 4.7: Inside schematic of the TurboGenset motor/generator</i>	14
<i>Figure 4.8: Photograph showing the power output cables</i>	15
<i>Figure 4.9: The Bowman Power motor/generator design</i>	16
<i>Figure 4.10: Flow patterns for horizontal flow of a liquid and gas or vapour (Mills, 1995)</i>	18
<i>Figure 4.11: Variation of heat transfer coefficient and flow regime with change in quality</i>	19
<i>Figure 4.12: The flow regime with the influence of the return bend</i>	22
<i>Figure 4.13: Flow pattern where $G=50\text{kg/m}^2\text{s}$ for $2R/D=3$ and $2R/D=7.1$ and $D=6.9\text{mm}$: (a) $x=0.0005$, $2R/D=3$, top view; (b) downstream $x=0.1$, $2R/D=3$, side view; (c) bend $x=0.1$, $2R/D=3$, top view; (d) bend $x=0.3$, $2R/D=3$, top view; (e) bend $x=0.4$, $2R/D=3$, top view; (f) bend $x=0.4$, $2R/D=7.1$, top view. (Wang et al., 2003)</i>	23
<i>Figure 4.14: Surge line illustration</i>	26
<i>Figure 4.15: Electrical Turbocompound (ETC) system schematic</i>	28
<i>Figure 4.16: Turbocompound (TC) limitations</i>	29
<i>Figure 4.17: Maximum allowable stress in brass with rising temperature</i>	31
<i>Figure 4.18: Fin configurations</i>	32
<i>Figure 5.1: Fintube and U-bend spacing geometries</i>	38
<i>Figure 5.2: Heat exchanger geometries</i>	39
<i>Figure 5.3: Implicit heat exchanger geometries</i>	39
<i>Figure 5.4: Control volume used in theoretical analysis</i>	39
<i>Figure 5.5: Flow directions inside the heat exchanger</i>	58

List of Figures (<i>continued</i>)	Page
<i>Figure 5.6: Davis-Swann method (Papalambros and Wilde, 2000)</i>	59
<i>Figure 5.7: Temperature and error convergence</i>	60
<i>Figure 5.8: Exhaust and water temperature distribution across the heat exchanger</i>	62
<i>Figure 5.9: Water heat transfer coefficient and quality using equation 5.5.2</i>	63
<i>Figure 5.10: Water heat transfer coefficient and quality using equation 5.5.3</i>	64
<i>Figure 5.11: Exhaust and water velocities across the heat exchanger</i>	65
<i>Figure 5.12: Pressure drop across the heat exchanger</i>	65
<i>Figure 5.13: Exhaust and water specific heat across the heat exchanger</i>	66
<i>Figure 5.14: Water heat transfer coefficient versus temperature</i>	67
<i>Figure 6.1: U-bend NASTRAN analysis: Bottom Von Mises stress [MPa]</i>	70
<i>Figure 6.2: U-bend NASTRAN analysis: Top Von Mises stress [MPa]</i>	70
<i>Figure 6.3: Fintube NASTRAN analysis: Von Mises stress [MPa]</i>	71
<i>Figure 7.1: Deformation and shearing of the fintube</i>	73
<i>Figure 7.2: Completed fintube</i>	74
<i>Figure 7.3: Preparation for the assembly process</i>	74
<i>Figure 7.4: Final product of the sub assembly</i>	75
<i>Figure 7.5: Heat exchanger cover (left), end caps covering the U-bends (right)</i>	75
<i>Figure 7.6: Diffuser/nozzle ducting (left), connecting pipe (right)</i>	76
<i>Figure 7.7: Service hatch on the diffuser ducting</i>	76
<i>Figure 7.8: Final system configuration</i>	78
<i>Figure 7.9: Measurements taken on the heat exchanger</i>	79
<i>Figure 7.10: Measurements taken on the inlet manifold</i>	79
<i>Figure 7.11: The error between the simulated and measured exhaust and water temperatures</i>	85
<i>Figure 7.12: Experimental and simulated exhaust and water temperatures</i>	85
<i>Figure 7.13: Heat exchanger experimental and simulated energy balance</i>	86
<i>Figure 7.14: Test point 9: Actual versus simulated temperatures inside the heat exchanger</i>	87
<i>Figure 7.15: Exhaust gas distribution inside the ducting</i>	87
<i>Figure 7.16: Test point comparisons</i>	89
<i>Figure 7.17: Water temperature distribution</i>	91

List of Figures (<i>continued</i>)	Page
<i>Figure 7.18</i> : Water outlet pressures	91
<i>Figure 7.19</i> : Water thermal heat transfer coefficient	91
<i>Figure 7.20</i> : Water quality	92
<i>Figure 7.21</i> : Water enthalpy	92
<i>Figure A1</i> : Turbocharger design drawing	A2
<i>Figure C1</i> : Recovery system diagram	C2
<i>Figure E1</i> : Continuous combustion unit	E6
<i>Figure G1</i> : Main excel sheet	G2
<i>Figure G2</i> : Energy balance excel sheet	G3
<i>Figure G3</i> : Preheating excel sheet	G3
<i>Figure G4</i> : Boiler (water only) excel sheet	G4
<i>Figure G5</i> : Boiler (steam only) excel sheet	G4
<i>Figure G6</i> : Superheating excel sheet	G5
<i>Figure G7</i> : Rankine cycle excel sheet	G5
<i>Figure G8</i> : Pressure drop excel sheet	G6
<i>Figure H1</i> : Main interface	H3
<i>Figure H2</i> : Running conditions	H3
<i>Figure H3</i> : Heat exchanger geometries	H4
<i>Figure H4</i> : Implicit geometries	H4
<i>Figure H5</i> : Simulation results	H5
<i>Figure H6</i> : Save file textbox	H5
<i>Figure H7</i> : Writing data to text file	H6
<i>Figure H8</i> : Finished simulated run	H6
<i>Figure H9</i> : Plot interface	H7
<i>Figure H10</i> : Choosing the axis	H7
<i>Figure H11</i> : Water plot	H8
<i>Figure H12</i> : Gas plot	H9
<i>Figure I1</i> : Execute program	18
<i>Figure I2</i> : Subfunction 1	19

List of Figures (<i>continued</i>)	Page
<i>Figure I3</i> : Subfunction 2	I10
<i>Figure I4</i> : Preheater	I11
<i>Figure I5</i> : Boiler	I12
<i>Figure I6</i> : Superheater	I13
<i>Figure I7</i> : Result plot	I14
<i>Figure M1</i> : U-bend NASTRAN analysis: Bottom major principal stress [MPa]	M2
<i>Figure M2</i> : U-bend NASTRAN analysis: Bottom minor principal stress [MPa]	M2
<i>Figure M3</i> : U-bend NASTRAN analysis: Bottom Von Mises [MPa]	M3
<i>Figure M4</i> : U-bend NASTRAN analysis: Top major principal stress [MPa]	M3
<i>Figure M5</i> : U-bend NASTRAN analysis: Top minor principal stress [MPa]	M4
<i>Figure M6</i> : U-bend NASTRAN analysis: Top Von Mises [MPa]	M4
<i>Figure M7</i> : Fintube NASTRAN analysis: Azimuth stress [MPa]	M5
<i>Figure M8</i> : Fintube NASTRAN analysis: Radial stress [MPa]	M5
<i>Figure M9</i> : Fintube NASTRAN analysis: Axial stress [MPa]	M6
<i>Figure M10</i> : Fintube NASTRAN analysis: Von Mises stress [MPa]	M6

LIST OF TABLES

	Page
<i>Table 4.1:</i> Turbine classifications (Micro Hydropower Basics, 2000)	8
<i>Table 4.2:</i> Technical characteristics of the HSG10- and HSG50 high speed generators	15
<i>Table 4.3:</i> Material properties	30
<i>Table 4.4:</i> Experimental results obtained by Lotun (2001)	33
<i>Table 4.5:</i> Finned heat exchanger specifications	34
<i>Table 4.6:</i> Experimental results obtained by Wipplinger (2001)	35
<i>Table 5.1:</i> Gas/fluid input values	60
<i>Table 5.2:</i> Simulation program input and output summary	61
<i>Table 6.1:</i> Stainless steel data from ASME (2001)	68
<i>Table 7.1:</i> Heat exchanger experimental testing and simulation results	83
<i>Table 7.2:</i> Heat exchanger experimental and simulated energy balance	84
<i>Table 7.3:</i> Flow conditions inside the ducting	88
<i>Table 7.4:</i> Input values to the simulation program	90
<i>Table B1:</i> Turbocharger map: 1/10 open	B2
<i>Table B2:</i> Turbocharger map: 1/5 open	B3
<i>Table B3:</i> Turbocharger map: 2/5 open	B4
<i>Table B4:</i> Turbocharger map: 3/5 open	B5
<i>Table B5:</i> Turbocharger map: 4/5 open	B6
<i>Table B6:</i> Turbocharger map: fully open	B7
<i>Table C1:</i> Ideal Brayton cycle	C2
<i>Table C2:</i> Case study 1	C3
<i>Table C3:</i> Case study 2	C3
<i>Table C4:</i> Case study 3	C4
<i>Table C5:</i> Case study 4	C4
<i>Table C6:</i> Case study 5	C5
<i>Table C7:</i> Case study 6	C5
<i>Table D1:</i> Water based feasibility results	D2
<i>Table J1:</i> Combustion enthalpy values	J2

List of Tables (<i>continued</i>)	Page
<i>Table L1</i> : Test data on 27-10-2003	L2
<i>Table L2</i> : Test data on 30-10-2003	L3
<i>Table L3</i> : Test data on 30-10-2003 (<i>continued</i>)	L4
<i>Table L4</i> : Test data on 5-10-2003	L5

LIST OF SYMBOLS

Nomenclature

A	Area, [m ²]
BH	Boilerheating
b	Fin efficiency constant
CV	Control volume
C	Capacity ratio
C _f	Skin friction coefficient
C _{ffo}	Skin friction coefficient for fluid only
C _{max}	Maximum capacity
C _{min}	Minimum capacity
C _p	Specific heat at constant pressure, [J/kg.K]
c	Mach number
D	Diameter, [m]
dt	Time derivative
eff	Efficiency, [%]
F	Enhancement factor; Fin efficiency [%]
f	Friction factor
G	Mass flux, [kg/m ² .s]
Gr	Grashof number
G _{ai}	Mass velocity through minimum free flow area of the core, [kg/m ² .s]
g	Gravitational constant, [m/s ²]
H	Height, [m]
h	Heat transfer coefficient, [W/m ² .K]; Enthalpy [J/kg]
h ₂₉₈ ^o	Reference enthalpy at 298K, [J/kg]
h _f ^o	Enthalpy of formation, [J/kg]
h _{fg}	Enthalpy of vaporization, [J/kg]
h _{is}	Instantaneous isentropic enthalpy, [J/kg]
h _{mac}	Macroscopic heat transfer coefficient (bulk convective, Chen's correlation), [W/m ² .K]
h _{mic}	Microscopic heat transfer coefficient (nucleate boiling, Chen's correlation), [W/m ² .K]
Id	Inner diameter, [m]
k	Thermal conductivity, [W/m.K]; Gas constant
L	Length, [m]
<i>m</i>	Mass flow rate, [kg/s]
Nu	Nusselt number

N_r	Number of tube rows
N_t	Number of tubes
n	Number of transfer units
Od	Outer diameter, [m]
P	Pressure, [Pa]
PH	Preheating
Pr	Prandtl number
P_L	Dimensionless longitudinal pitch
P_T	Dimensionless transverse pitch
p	Pitch, [m]
Q	Power, [W]
R	Gas constant, [J/kg.K]; Radius [m]
Ra	Rayleigh number
Re	Reynolds number
S	Suppression factor
SH	Superheating
$Stan$	Stanton number
S_L	Longitudinal tube pitch, [m]
S_T	Transverse tube pitch, [m]
T	Temperature, [K or °C]
t	Thickness, [m]
U	Overall heat transfer coefficient, [W/m ² .K]
Vel	Velocity, [m/s]
V_0	Empty duct velocity, [m/s]
V_{max}	Maximum velocity, [m/s]
X_{tt}	Turbulent-turbulent Lockhart-Martinelli parameter
x	Quality

Greek symbols

α	Void fraction
Δ	Difference, finite increment
η_T	Turbine efficiency, [%]
η_{TS}	Turbine total-to-static efficiency, [%]
μ	Dynamic viscosity, [m.s/kg]
ν	Kinematic viscosity, [kg/m.s]
ρ	Density, [kg/m ³]
σ	Surface tension, [N/m]; Area ratio, eq's 5.3.103 and 5.3.105; Stress, eq 6.2.1, [MPa]

τ	Wall shear stress, [N/m ²]
ϕ	Diameter, [m]; Fin efficiency constant (p. 49)
ϕ_{10}^2	Two-phase multiplier (Friedel's correlation)
χ	Tube bank pressure drop correction factor
ω	Rotational speed, [rpm]

Subscripts

1	Inlet
2	Outlet
accel	Acceleration
av	Average
crit	Critical
cv	Control volume
e	Equivalent
eff	Efficiency
enth	Enthalpy
f	Fin
fo	Fluid only
fr	Frontal
fric	Friction
g	Gas
grav	Gravity
H.E.	Heat exchanger
homo	Homogeneous
hyd	Hydraulic
l	Liquid
lo	Liquid only
max	Maximum
min	Minimum
o	Reference value
p	Products
r	Reactants
s	Surface
sat	Saturated
sep	Separated
T	Temperature
t	Tube

tot Total
transf Transfer
w Water

Abbreviations

DBPT Density by using Pressure and Temperature
DLBT Density of Liquid by using Temperature
DVBT Density of Vapour by using Temperature
CPBPT Specific Heat at Constant Pressure by using Pressure and Temperature
CPLBT Specific Heat at Constant Pressure of Liquid by using Temperature
CPVBT Specific Heat at Constant Pressure of Vapour by using Temperature
HBPT Enthalpy by using Pressure and Temperature
HLBT Enthalpy of Liquid by using Temperature
HVBT Enthalpy of Vapour by using Temperature
PBT Pressure by using Temperature
TBP Temperature by using Pressure
TBPH Temperature by using Pressure and Enthalpy

Superscripts

* Critical

Overscore

. Per time unit

1. INTRODUCTION

The mid 20th century has proven to be a time during which the world has had a rude awakening from its relaxed attitude towards the usage of our depleting natural resources. Proof of this is the waste heat recovery systems that have been in use in industries all over the world for the last 50 years.

An example of this is the integration of various factory sections where the waste heat from one section is used in another section. This is common practise in the food industry and not only saves money, but streamlines the whole system and makes it more efficient.

None the less, a large amount of energy is still being lost in the form of heat generated by everyday industrial- and domestic equipment. Waste heat can be identified in the form of unburned but combustible fuel, sensible heat discharge in drain water and sensible and latent heat discharge from exhaust gasses, according to Al Rabghi et al. (1993).

The motivation behind the whole energy recovery process is not just the slow depletion of natural resources like fossil fuels and the rising cost of obtaining these resources, but also the degradation of the environment.

Twenty five percent of the energy consumption in the western world is centred in the transportation sector. Automobiles and trucks account for approximately 80% of all transportation energy expenditures. Koehler et al. (1997) states that these thermal engines operate with a thermal efficiency between 30 and 40%.

According to Corrado (1985), of the 80% of transportation vehicles, a large amount uses diesel engines. Figure 1.1 indicates the energy balance for a typical turbocharged diesel engine which was done at the Centre for Automotive Engineering (CAE) in Stellenbosch.

Figure 1.1 clearly indicates that approximately one third of the total energy released by the combustion process is lost along with the exhaust gas, while one third is transferred to the cooling fluids and the rest is converted to actual mechanical power.

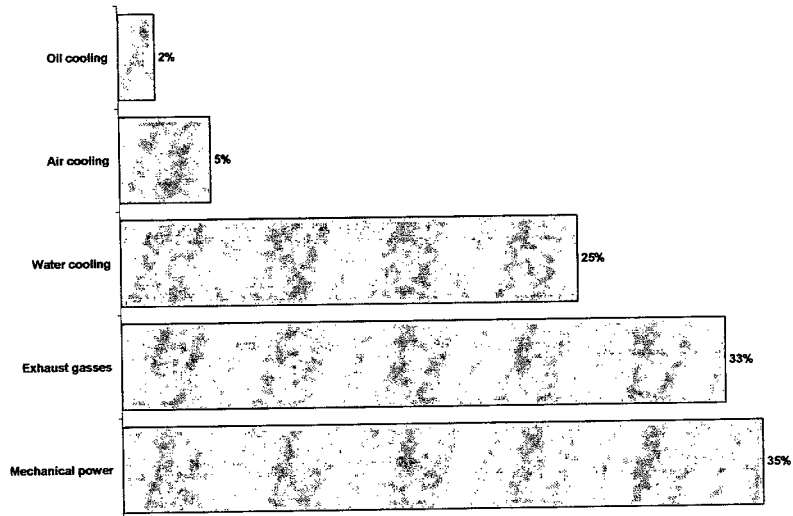


Figure 1.1: Energy distribution of a typical turbocharged diesel engine (Wipplinger, 2000)

The cooling fluids are a necessary loss which prevents the catastrophic failure due to overheating. These losses will inevitably become smaller as our knowledge of composite materials increase.

But the energy lost along with the exhaust gas, can be ascribed to the inefficient utilisation of the available energy, which makes research into the recovery of the wasted energy and subsequent efficiency and fuel utilization improvement, a viable option.

2. PROJECT OUTLINE

This project focuses on thermal waste heat recovery and the conversion of the recovered energy into a useful form, for example electrical energy. Undergraduate studies by Koorts (1998) and Wipplinger (2001) as well as post-graduate research by Lotun (2001) have been done on the same subject matter.

The initial aim of this project was to build forth on previous research done at the University of Stellenbosch and to construct a working heat recovery system which would convert recovered thermal energy into electrical energy by means of a heat exchanger, a turbine and an electrical generator. The key factor being that the system would have to work at high temperatures and pressures to enable the maximum energy recovery as determined by Wipplinger (2001).

The turbine assembly available for the project was a turbocharger from a Golf TDi 1900 donated by the Centre for Automotive Engineering (CAE). The high speed electrical generator had to be acquired. Two sources were found in the United Kingdom, however, both the generators proved to be unobtainable due to the high costs involved.

The heat exchanger that was to be used in the project was proposed by Lotun (2001). However, in the feasibility study, it was determined that the heat exchanger designed and tested by Lotun (2001), was inadequate for the proposed project. The problem being that it was unable to withstand a combination of high pressures and temperatures. This led to the decision that the heat exchanger would have to be redesigned.

The result was that the project's focus shifted from the construction of the recovery system as a whole, to the designing and testing of a suitable heat exchanger, which could be used in further studies on the same subject matter.

As the turbocharger was already available for the project, research was done on the implementation and design theory of turbochargers in order to enable its smooth integration into the system.

The project followed a logical layout and began with the research needed for the design process. Alternative recovery cycles were investigated, for example the utilisation of air as the recovery medium instead of a water-based system (as proposed by Bolland et al. (1995) in their investigation of the Air Bottoming Cycle) as well as the various parts needed to construct a fully integrated recovery system. The internet, published papers and research done at the University of Stellenbosch was consulted in order to acquire the necessary knowledge on turbines, generators, two-phase flow, corrosive resistant materials (due to the corrosive nature of exhaust gasses) and various other applicable theories.

After the necessary research was finished, the knowledge acquired was implemented in the design process which consisted of two phases: firstly a spreadsheet was written in order to serve as a theory familiarisation tool, after which a control volume based simulation program of a cross flow, fin tube heat exchanger was written. The results of the simulation program were used in the final design of the heat exchanger.

Stress analyses were done using a finite element analysis package to ensure that the heat exchanger would withstand the high temperature- and pressure induced stresses.

Finally the heat exchanger was constructed and tested. The practical test results were compared to that of the simulation program which proved to be a good estimate and confirmed that the simulation program would accurately predict the heat exchanger behaviour under specified inlet conditions.

This document discusses the motivation, research, design and practical implementation and testing of the proposed system and forms part of the proposal for an MScEng degree done by Mr K.P.M. Wipplinger. The project is being supervised by Dr T.M. Harms as well as Dr A.B. Taylor and builds forth on the projects done by Koorts (1998), Lotun (2001) and Wipplinger (2001).

3. THE WASTE HEAT RECOVERY SYSTEM

Different waste heat recovery methods have been investigated in this project. In the following, the implication of utilising air or water as working fluids is briefly discussed.

The greatest advantage of utilising air as the main recovery medium is the simplicity of the system. Because of the abundance of air, a closed loop system would be deemed unnecessary. This would result in a less costly open loop system which is easier to construct and maintain.

A possible system configuration, if air were to be used as working fluid, is illustrated in figure 3.1. The flow path of the exhaust air, working air, cooling oil and generated electrical power is shown. As seen below, a turbine and motor/generator is included in the system in order to convert the recovered energy into electrical energy. Other means of utilising the recovery energy could however be accomplished by using a piston engine or Stirling engine.

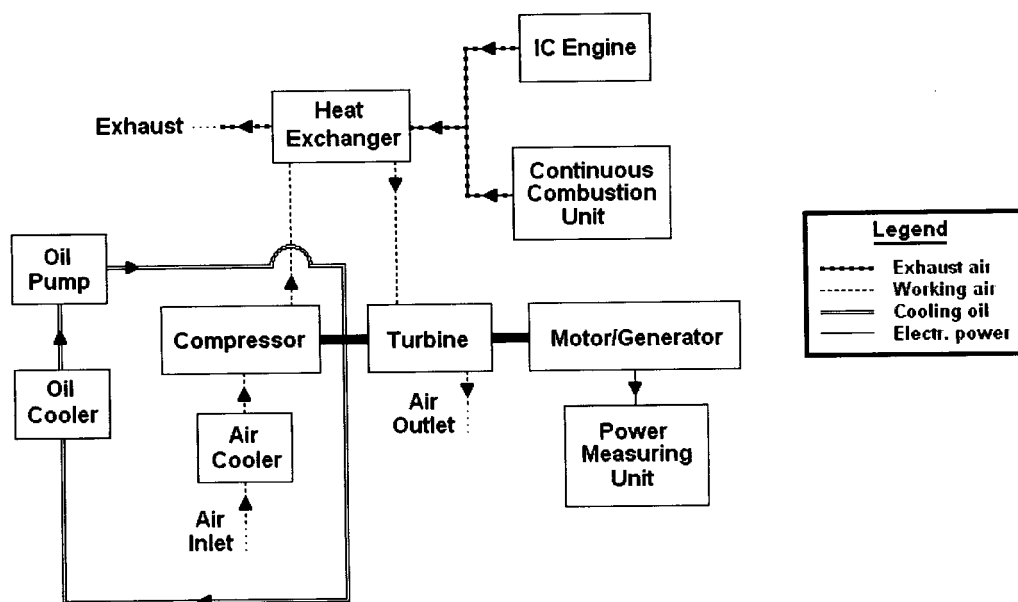


Figure 3.1: Air-based laboratory configuration for waste heat recovery system

Air, however, was found to be unsuitable for the intended application because of very low efficiencies and the size of the heat exchanger required (*for a more detailed analysis, see appendix C and section 4.3.5*).

Also investigated, was the possibility of using water as an energy transfer medium in a Rankine steam turbine cycle. From preliminary calculations it is clear that when water is used as the recovery medium, the system can yield a much higher efficiency, but the design of the system becomes more cumbersome, if one is working with a preheated section, two-phase section, and superheated section in a direct steam generation system. There are also additional costs involved when looking at a closed loop system, because of the necessity of a condenser. The open loop system, which excludes the condenser, was chosen for this project because of time and funding limitations.

The main hardware components required for the project were identified as follows:

- Heat exchanger for heat recovery
- Turbocharger for energy conversion
- Generator for electrical generation

Of the three main components, only two could be acquired: the heat exchanger (initially proposed by Lotun (2001) but later redesigned) and the turbocharger (which was used in the final year project described in Wipplinger (2001) for the degree of BEng at the University of Stellenbosch). The generator could not be obtained due to the costs involved. However, the turbocharger could be used as a viable substitute, as it consists of a turbine and compressor unit on one shaft and, by measuring the compressor output, one could have an approximation of the energy recovered by the turbine section.

The components already installed in the laboratory, were:

- A pipe-ducting system connected with the exhaust of an IC engine at the CAE's testing laboratories
- A heat exchanger used in the thesis of D. Lotun (1999), which was found to be inadequate for this project and which had to be redesigned (*see chapters 5 to 7*)
- A continuous combustion unit, utilising either propane-gas or diesel as fuel

The system configuration, if water was to be used as the working fluid, can be seen in figure 3.2 and illustrates the flow path of the exhaust air, working fluid, cooling oil and generated electrical power.

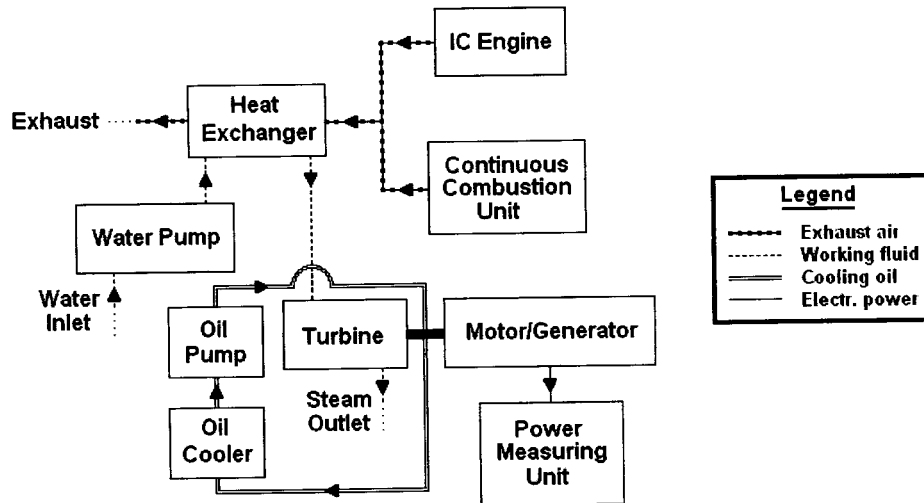


Figure 3.2: Water-based laboratory configuration for open loop recovery system

The design would have to take into account the framework needed to support the whole system as well as all the data-measuring equipment. It was decided that the continuous combustion unit be used as a source of “waste” heat energy and not the IC-engine exhaust gasses from CAE, because of increased losses that would occur along the ducting connecting the test cells of CAE to the laboratory and because of its nearby convenience and availability.

The following information was identified as data that needed to be recorded:

Pressures at the...

- outlet of the continuous combustion unit
- inlet and outlet of the heat exchanger
- inlet and outlet of the exhaust manifold
- ambient conditions

Temperatures at the...

- outlet of the continuous combustion unit
- inlet, middle and outlet of every row in the heat exchanger
- inlet and outlet of the exhaust manifold
- ambient conditions

Other information needed...

- exhaust gas flow rate exiting the continuous combustion unit
- water mass flow rate entering the heat exchanger

4. LITERATURE REVIEW

This chapter consists of subject matter critical to the proposed project, and has been researched using the following media:

- Internet searches
- Published papers and textbooks
- Research done at the University of Stellenbosch

4.1 INTERNET SEARCHES

The following section shows information that has been reviewed relating to the hardware needed for this project. The source data was found on websites as noted in the references.

4.1.1 Turbine introduction as from *Micro Hydropower Basics* (2000)

A turbine converts energy, in the form of fluid- or gas-flow, into rotating shaft power. The selection of the appropriate turbine depends on the desired running speed of the generator, or other devices loading the turbine. Other considerations, such as whether the turbine is expected to produce power under part-flow conditions, also play an important role in the selection. All turbines have a power-speed characteristic. They will tend to run most efficiently at a particular speed, head and flow combination.

A turbine design speed is largely determined by the head under which it operates. Turbines can be classified as high, medium or low head machines. They are also divided by their principle way of operating and can be either impulse or reaction turbines.

Impulse and Reaction Turbines			
	High Head	Medium Head	Low Head
Impulse	Pelton Turgo	Cross-flow Multi-jet Pelton Turgo	Cross-flow
Reaction		Francis	Propeller Kaplan

Table 4.1: Turbine classifications (Micro Hydropower Basics, 2000)

The rotating blades, or “runner”, of a reaction turbine is fully immersed in the fluid and is enclosed in a pressure casing. The blades are profiled so that pressure differences across them impose lift forces, like those on aircraft wings, which cause the runner to rotate.

In contrast, an impulse turbine runner operates in air, driven by a jet (or jets) of fluid. Here the fluid remains at atmospheric pressure before and after making contact with the runner blades. In this case a nozzle converts the pressurised low velocity fluid into a high speed jet. The runner blades deflect the jet so as to maximise the change of momentum of the fluid thus maximising the force on the blades.

Impulse turbines are usually cheaper than reaction turbines because there is no need for a specialist pressure casing or for carefully engineered clearances, but they are also only suitable for relatively high heads.

4.1.2 Impulse Turbines

Pelton wheel

A Pelton wheel (*see figure 4.1*) is an impulse turbine and consists of a set of specially shaped buckets mounted on a periphery of a circular disc. It is turned by jets of water which are discharged from one or more nozzles and strike the buckets. The buckets are split into two halves so that the central area does not act as a dead spot incapable of deflecting water away from the oncoming jet. The cutaway on the lower lip allows the next bucket to move further before cutting off the jet propelling the bucket ahead of it. It also permits a smoother entrance of the bucket into the jet. The Pelton bucket is designed to deflect the jet through 165° , which is the maximum angle possible without the return jet interfering with the next bucket.

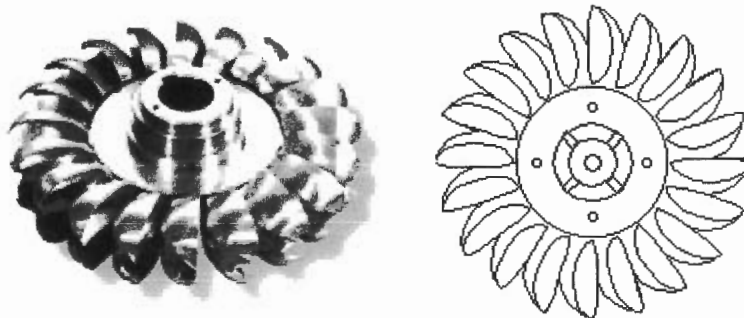


Figure 4.1: The runner of a Pelton wheel (Micro Hydropower Basics, 2000)

For large scale plants Pelton wheels are normally only considered for heads above 150m (14.7bar), but heads as low as 20m (1.9bar) can be applied to micro Pelton turbine applications. If the runner size and low speed do not pose a problem for a particular installation, a Pelton turbine can be used efficiently with fairly low heads.

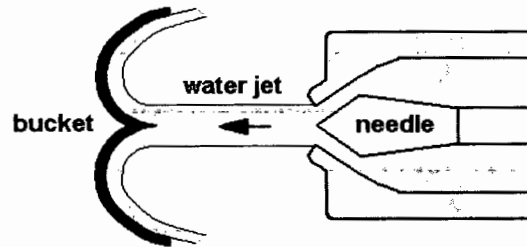


Figure 4.2: The Pelton working configuration

There are two options if a higher running speed and smaller runner are required:

- Increasing the number of jets

Two or more jets enable a smaller runner to be used for a given flow and increase the rotational speed. The required power can still be attained and the part-flow efficiency is especially good because the wheel can be run on a reduced number of jets, with each jet in use still receiving the optimum flow.

- Twin runners

Two runners can be placed on the same shaft - either side by side or on opposite sides of the generator. This configuration is unusual and would only be used if the number of jets per runner had already been maximised. However, it allows the use of smaller diameter and hence faster rotating runners.

Turgo turbine

The Turgo turbine is similar to a Pelton turbine but was designed to have a higher specific speed. In this case the jets strike the plane of the runner on one side and exits on the other side. Therefore the flow rate is not limited by the discharged fluid interfering with the incoming jet and as a consequence, a Turgo turbine can have a smaller diameter runner than a Pelton for the equivalent power. With smaller faster spinning runners, it is more likely to be able to connect Turgo turbines directly to the generator rather than having to go via a costly speed-increasing transmission.

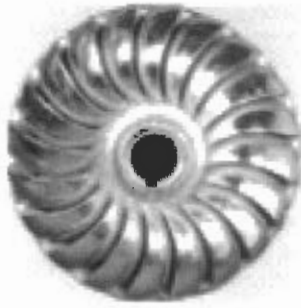


Figure 4.3: The runner of a Turgo turbine

Like the Pelton, the Turgo is efficient over a wide range of speeds and shares the general characteristics of impulse turbines listed for the Pelton, including the fact that it can be mounted either horizontally or vertically. According to *Micro Hydropower Basics* (2000), a Turgo runner is more difficult to manufacture than a Pelton wheel and the vanes of the runner are more fragile than Pelton buckets.

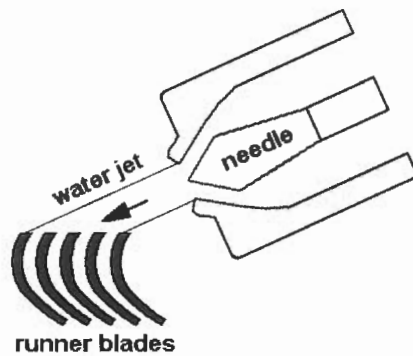


Figure 4.4: The Turgo working configuration

4.1.3 Reaction Turbines

Francis turbine

Francis turbines can either be volute-cased or open-flume machines. The spiral casing is tapered to distribute water uniformly around the entire perimeter of the runner and the guide vanes feed the water into the runner at the correct angle. The runner blades are profiled in a complex manner and direct the water so that it exits axially from the centre of the runner. In doing so, the water imparts most of its pressure energy to the runner before leaving the turbine via a draft tube.

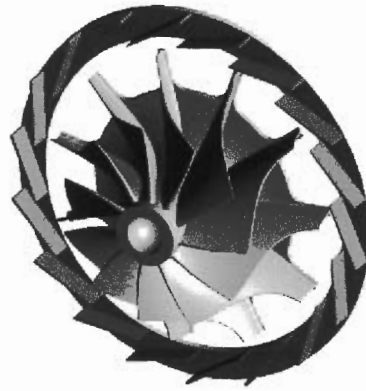


Figure 4.5: The Francis turbine and guide vanes

The Francis turbine is generally fitted with adjustable guide vanes. These guide vanes regulate the water flow as it enters the runner and are usually linked to a governing system which matches flow to turbine loading in the same way as a spear valve or deflector plate in a Pelton turbine. When the flow is reduced, the efficiency of the turbine falls away. The information source for this section was *Micro Hydropower Basics* (2000).

4.1.4 TurbochargersNZ (2001)

This site was used as a source of information on the workings of a Francis turbine-based turbocharger. Summarised below is the useful data acquired from the site.

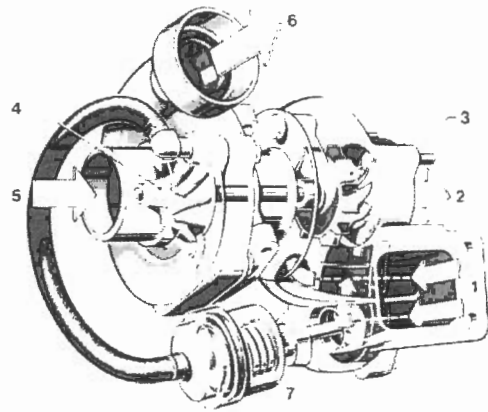
The turbine stage of a turbocharger comprises two components: the turbine wheel and the collector (or housing, as it is commonly referred to). High-speed engines generally use turbochargers with radial turbines. On larger engines such as ship propulsion, axial turbines are used.

The exhaust gas is guided into the turbine wheel by the housing. The energy in the exhaust gas turns the turbine. Significant amounts of power can be generated in the region of 50kW on a typical 12 litre diesel engine.

Once the gas has passed through the blades of the wheel, it leaves the turbine housing via the exhaust outlet. The speed of the engine determines how fast the turbine wheel spins. If the engine is in idle mode, the wheel will be spinning, but at a minimal speed. As one put one's foot on the accelerator, the exhaust gasses increase and the turbine wheel starts to spin faster, thus driving the compressor.

Small turbochargers can spin at up to 140000rpm (or 2333rps). The more gas that passes through the turbine housing, the faster the turbine wheel will rotate.

The compressor stage comprises two sections, the impeller or wheel and the housing. The compressor wheel is connected to the turbine by a forged steel shaft. As the compressor wheel spins, air enters through an area known as the inducer and is compressed through the blades, leaving the exducer at a high velocity.



1. Exhaust gases to turbine
2. Exhaust gas outlet
3. Turbine wheel
4. Compressor wheel
5. Intake air to compressor
6. Compressed air to engine
7. Wastegate controle

**Figure 4.6: Turbocharger layout
(Volkswagen, 2003)**

The housing is designed to convert the high-velocity, low-pressure air stream into a high-pressure, low-velocity air stream through diffusion. Air enters the compressor at a temperature equivalent to that of the atmosphere. However, it leaves the compressor cover at a temperature of up to 200°C.

Because the density of the air increases as it is cooled down, even more air can be forced into the engine if the air is cooled after the compressor. This is called intercooling or aftercooling and is achieved by cooling the charge air with either water or air.

The turbocharger bearing system is lubricated by oil from the engine. The oil is fed under pressure into the bearing housing, through to the journal bearings and thrust system. The oil also acts as a coolant, taking away heat generated by the turbine.

The journal bearings are a free-floating rotational type. To perform correctly, the journal bearings should float between a film of oil (i.e. between bearing and shaft, and bearing and bearing housing.) The bearing clearances are very small - less than the width of a human hair. Dirty oil, or blockages in the oil supply holes, can cause serious damage to the turbocharger. Piston ring seals can be found at both ends of the turbocharger. They are designed to keep the exhaust and air pressure out of the bearing housing.

4.1.5 TurboGenset (2003)

The TurboGenset Company was established in 1993 to develop the technology related to small-scale electricity generation. Its particular expertise lies in the development of high-speed motors/generators in combination with turbomachinery. They have developed a high-speed motor/generator applicable for portable and stand-by power generation, using gas and/or steam turbines, co-generation using gas turbines, gas expanders and hybrid electric vehicles. They currently have two high-speed motor/generator models available: the HSG10 and HSG50 (including the option of customisation).



Figure 4.7: Inside schematic of the TurboGenset motor/generator

The motor/generator uses disc technology instead of the traditional drum design. This means that the magnetic field is axial and not radial. Therefore the strengthening of the rotor does not interfere with the magnetic field. As the magnets have poor tensile strength, they must be supported under the extreme centrifugal loads, making this one of the key aspects of the motor/generator design. Because the motor/generator can run at very high speeds, the use of a reduction gearbox linking the turbine and generator is eliminated, which subsequently reduces system losses.

Specifications for both models can be seen in table 4.2.

Technical Characteristics		
	HSG10	HSG50
Electrical output	10kVA, 4kHz, 3-phase AC	50kVA, 4kHz, 3-phase AC
Rectified output	140V DC	720V DC
Operating speed	60,000 rpm	60,000 rpm
Electrical efficiency	95%	95%
Overall efficiency including integral cooling fan	90%	90%
Regulation	6%	6%
Weight	4kg	9kg
Size	170mm diam x 129mm long	170mm diam x 220mm long

Table 4.2: Technical characteristics of the HSG10- and HSG50 high speed generators

The 50kW alternator was designed to operate at 60000rpm, compatible with the relevant commercial turbo machinery. Although the 50kW alternator is roughly the same size as a car alternator, it produces over 50 times the electrical power.



Figure 4.8: Photograph showing the power output cables

In addition to the current 50kW unit, the Company is finalizing the development of the 100kW unit with the 250kW unit currently under development. Using the disc technology design, around 2MW of electrical power is considered to be achievable.

4.1.6 Bowman Power (2002)

Bowman Power has been doing the research and development of their product line on much the same subject matter as TurboGenset. They have also designed a motor/generator that can run at high rotational speeds, thus allowing the elimination of a reduction gearbox in the turbine-generator configuration. The Bowman Power generator can generate between 20kW and 1.5MW. It is also much more compact than the product TurboGenset

can provide. The weight of the generator is unknown, but it makes use of the same disc technology that is incorporated into the HSG10 and HSG50 models available from TurboGenset.

Their design consists of a rare earth, brushless, permanent magnet rotor designed to integrate directly onto the turbo machinery shaft in micro turbine generators. The high speed alternator acts as the starter and electrical generator, and eliminates the need for a starter motor and for a large, heavy, expensive speed reduction gearbox. High overall efficiencies in excess of 98% are achievable through carefully controlled ohmic, core, fluid dynamic and stray eddy current losses. The stator output voltages can also be tailored to satisfy a wide range of applications. The cooling options range between oil, water and air. The operating temperature is between -10°C and $+45^{\circ}\text{C}$ and the power ranges vary from 20kW to 1.5MW.

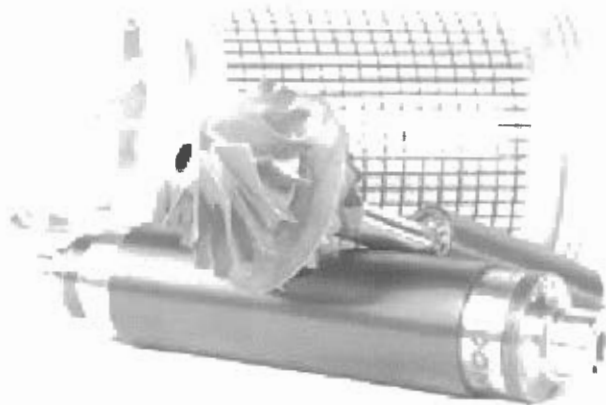


Figure 4.9: The Bowman Power motor/generator design

4.2 PUBLISHED PAPERS AND TEXTBOOKS

The following section contains information gathered from papers and textbooks concerning subject matters applicable to this project.

4.2.1 Energy recovery cycles

Bolland et al. (1995)

This paper presents a thermodynamic analysis of the Air Bottoming Cycle (ABC) as well as the results of a feasibility study on using the ABC for gas turbine waste heat recovery/power generation on oil/gas platforms in the North Sea. The basis of the feasibility study was to utilize the exhaust gas heat from an LM2500PE gas turbine. The

combined gas turbine and ABC shaft efficiency was calculated as 46.6%. The LM2500PE gas turbine contributes 36.1%, while the ABC adds 10.5% to the gas turbine efficiency. These results show that the ABC is an economical option for power generation.

Najjar (2000)

In this article, 12 research investigations carried out by the author and associates during the last 10 years are briefly reviewed. These investigations cover 12 gas turbine systems which would contribute towards the efficient use of energy. They entail fundamental studies in addition to applications of combined systems in the industry including: the closed gas turbine cycle; the organic Rankine cycle; re-powering; integrated power and refrigeration; cryogenic power; liquefied natural gas (LNG) gasification; and inlet air cooling.

Oomori et al. (1993)

The Rankine bottoming cycle, which operates on the waste heat of engine cooling, has been developed to improve the fuel economy of a passenger car. The evaporative engine cooling system is utilized to obtain high thermal efficiencies and to simplify the Rankine bottoming system. The bottoming system uses HCFC123 as working fluid and a scroll expander as a power conversion unit. The results indicate that energy recovery, which depends on the ambient temperature, is almost 3% of the engine output power at an ambient temperature of 25°C.

4.2.2 Two-phase Flow inside Tubes

Figure 4.10 shows the flow patterns of horizontal flows. The influence of gravity perpendicular to the flow causes the gas or vapour bubbles to rise to the top half of the tube. In bubbly and plug flows, the bubbles tend to flow in the upper half of the pipe. At low liquid and gas flow rates, there is a possibility of stratified flow, where the liquid flows at the bottom of the tube with a relatively smooth surface. As the vapour velocity increases, waves form on the liquid surface. The wave amplitude increases as the vapour velocity increases and can even become large enough to form liquid slugs which wet the upper periphery of the tube wall. A still higher vapour percentage will result in annular flow inside the tube. Eventually the liquid will be dispersed into droplets entrained in the vapour flow.

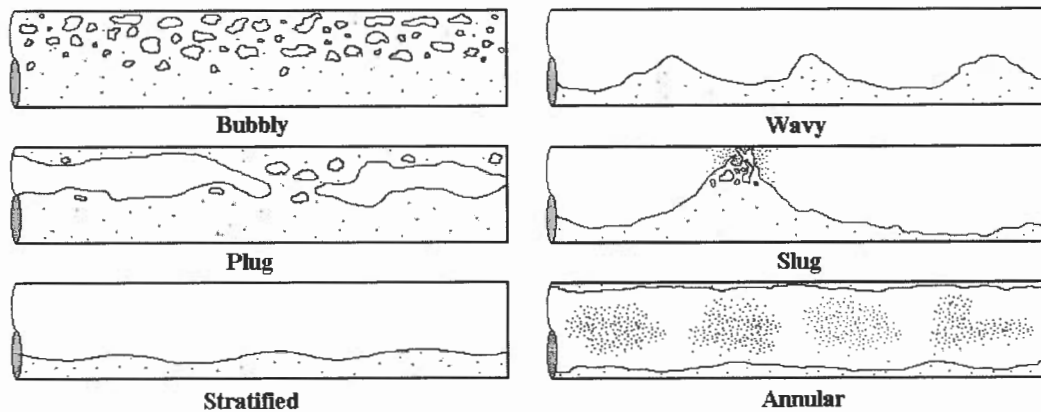


Figure 4.10: Flow patterns for horizontal flow of a liquid and gas or vapour (Mills, 1995)

Carey (1991)

As described above, the two-phase flow inside the tube can be divided into different flow regimes. During bubbly flow and plug flow, nucleate boiling is the dominant result of heat addition. However, when annular flow occurs and the water starts to evaporate from the wetted tube perimeter, nucleate boiling is more and more suppressed.

The portion of the tube wall covered by the liquid film generally decreases with downstream distance until the wall is completely dry around the entire perimeter of the tube. Liquid may, however, still be present in the flow as entrained droplets. Transport of heat from the tube wall to the droplets is necessary if the vaporization process is to continue.

In general, the continued vaporization of the droplets may be accomplished by a combination of mechanisms, including convection through the gas, radiation, and collisions or near collisions of droplets with the wall. These mechanisms are not very effective, and the associated heat transfer coefficient is usually significantly lower than the values associated with nucleate boiling and/or liquid film evaporation. In the mist evaporation process, the heat transfer coefficient usually continues to decrease as the quality increases, until the single-phase vapour value is ultimately attained.

As seen in figure 4.11, the heat transfer coefficient increases as the tube distance increases, especially when annular flow occurs and the water film thickness decreases. The heat transfer coefficient will only start to decrease when the film becomes so thin that

small dry patches of tube wall are exposed. In horizontal flow, the exposure usually starts at the top of the tube due to gravitational forces that drags most of the fluid to the bottom of the tube. This is called “partial dryout”. When the wall is partially dry, heat transfer from the dry portions of the wall surface is negligible compared to that at locations wetted by liquid where film evaporation is occurring. This causes the heat transfer coefficient to drop as the dry area increases.

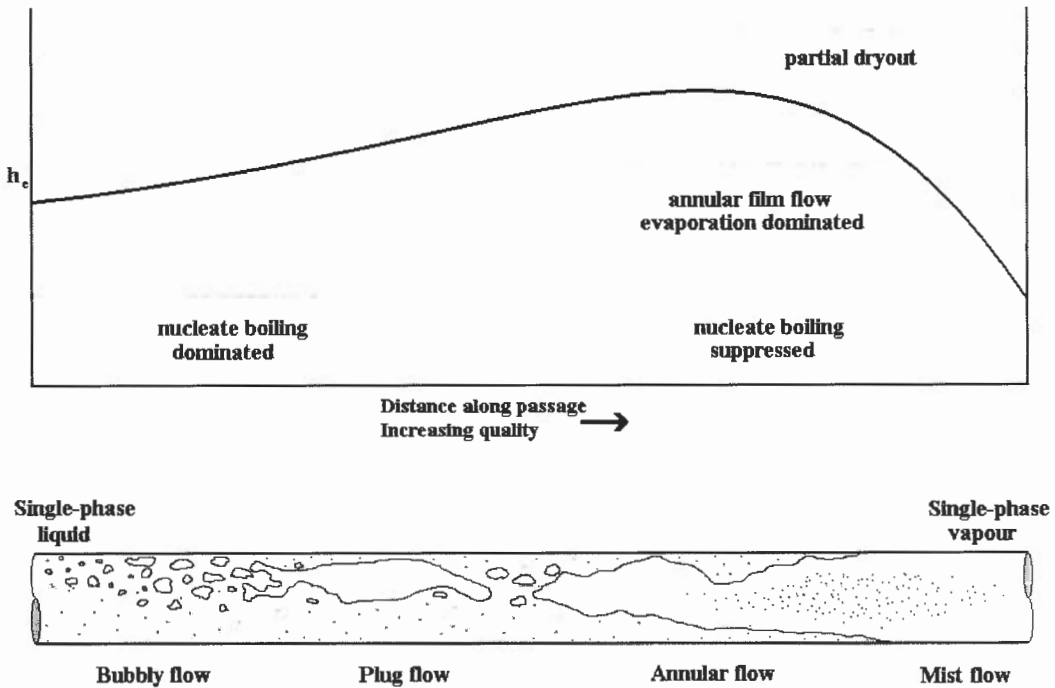


Figure 4.11: Variation of heat transfer coefficient and flow regime with change in quality

Critical heat flux condition (CHF) and boiling burnout are both terms that are used to describe the conditions where the wall temperature rises and/or the heat transfer decreases sharply due to a change in the heat transfer mechanism. In these conditions it is critical that the tube material is able to withstand the increase in temperature and does not start to melt. The term “burnout” is used even when failure of the passage wall does not occur due to overheating and melting, although it does have its origins from conditions where failure has occurred.

4.2.3 Boiling heat transfer coefficient

Yu (2002) and Passos (2000)

The Chen correlation for the boiling heat transfer coefficient has been used for many years for water flowing in tubes. Chen (1963) was the first to introduce the superposition approach of nucleation and forced convection mechanisms. The convective transfer is expressed as a function of the two-phase Reynolds number after Lockhart-Martinelli, and the nucleation transfer is obtained from the nucleate boiling correlation of Forster and Zuber (1955). The Chen (1963) correlation can be expressed as:

$$h = h_{mic} + h_{mac} \quad \dots(4.2.1)$$

The total heat transfer coefficient is equal to the sum of a microscopic (nucleate boiling) contribution, h_{mic} , and a macroscopic (bulk convective) contribution, h_{mac} , where...

$$h_{mic} = 0.00122 \frac{k_l^{0.79} C_{pl}^{0.45} \rho_l^{0.49}}{\sigma^{0.5} \mu_l^{0.29} h_{fg}^{0.24} \rho_g^{0.24}} \Delta T_{sat}^{0.24} \Delta P_{sat}^{0.75} S \quad \dots(4.2.2)$$

$$h_{mac} = 0.023 \left[\frac{G(1-x_z)D}{\mu_l} \right]^{0.8} \left[\frac{\mu C_p}{k} \right]^{0.4} \frac{k_l}{D} F \quad \dots(4.2.3)$$

ΔT_{sat} is the wall superheat in Kelvin and ΔP_{sat} is the difference between the saturation pressures calculated from the wall temperature and the fluid temperature in Pascal.

Parameter S (suppression factor) is calculated as...

$$S = \frac{1}{1 + 2.53 \times 10^{-6} F^{1.25} \frac{G(1-x)D}{\mu_l}} \quad \dots(4.2.4)$$

Parameter S corrects the fully developed nucleate boiling prediction of h_{mic} to account for the fact that, as the macroscopic convective effect increases in strength, nucleation is more strongly suppressed.

Parameter F (enhancement factor) is calculated as...

$$F = \begin{cases} 1.0 & \dots \frac{1}{X_u} \leq 0.1 \\ 2.35 \left(\frac{1}{X_u} + 0.213 \right)^{0.736} & \dots \frac{1}{X_u} > 0.1 \end{cases} \quad \dots(4.2.5)$$

where X_{tt} is the turbulent-turbulent Lockhart-Martinelli parameter...

$$X_{tt} = \left(\frac{1-x}{x} \right)^{0.9} \left(\frac{\rho_g}{\rho_l} \right)^{0.5} \left(\frac{\mu_l}{\mu_g} \right)^{0.1} \quad \dots(4.2.6)$$

4.2.4 U-tubes

Wang et al. (2002) and (2003)

The compact air-cooled coils for evaporators and condensers normally contain many 180° return bends (or hairpins), which are directly linked to straight tubes to compact the heat exchanger size. The presence of a return bend will enhance the heat transfer and frictional pressure drop in the bend and its downstream straight tube due to the presence of the disturbance caused by secondary flow in the U-bend, and carried into the downstream straight section after the U-bend. In a curved tubing, the centrifugal force drives the more rapid flowing fluid in the concave part of the curve channel, while the fluid in the convex part is slowing down, resulting in vortices of the secondary flow. The magnitude of such secondary flow reduces with an increase of the bend radius and a decrease of fluid velocity.

In the two-phase flow application, the flow pattern in the return bend is dramatically affected by the vortices of the secondary flow. Flow patterns are intimately interrelated to both the two-phase heat transfer and pressure drop. As a consequence, the knowledge of the two-phase flow regime in a return bend is very important for an accurate estimation of the performance of an air-cooled heat exchanger.

Two-phase flow in a U-bend can be roughly classified into five regions: (I) upstream region, (II) de-acceleration region, (III) return bend, (IV) recovery region and (V) downstream region. According to tests done by Wang et al. (2002), the length of region (II) will be around 80-120D for $2R/D=3$. The lengths of regions (II) and (IV) varies with flow patterns.

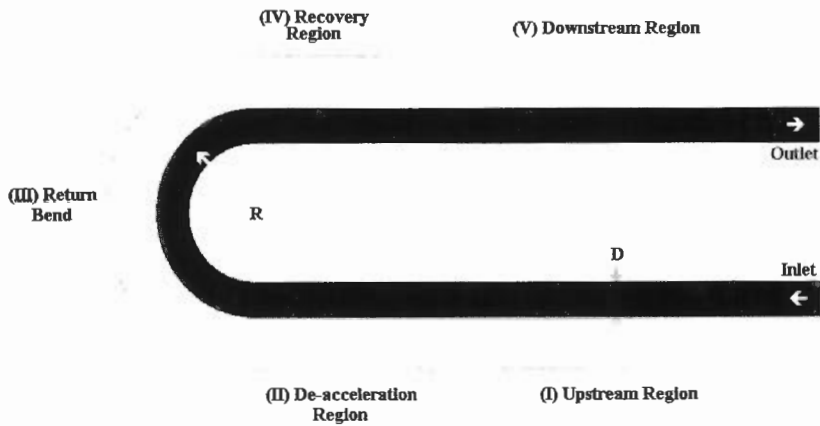


Figure 4.12: The flow regime with the influence of the return bend

Figure 4.13 (a) is an example of plug flow where the quality is equal to 0.0005. The plug is big enough to occupy the whole cross-section of pipe and moves along with the flow without disturbing the flow pattern.

Figure 4.13 (b) shows stratified flow in a pipe for $x=0.1$ and a mass flux of $G=50\text{kg/m}^2\cdot\text{s}$. If, however, a return bend is inserted into the pipe as in figure 4.13 (c), the liquid in the bottom will swirl around the concave part of the bend while the vapour is forced along the convex part. This motion will continue into the recovery region (IV) of the bend due to its inertia and result in the temporary change of the flow pattern into annular flow. Due to the low vapour quantity, the flow will, however, return to stratified flow. If the curvature ratio of the bend were to be increased to $2R/D=7$ or higher, the temporary annular flow would not be observed for the same quality.

If, as in figure 4.13 (d), the quality is increased to 0.3 for a curvature ratio of $2R/D=3$, the flow does not change to annular in region (IV), but stays stratified.

In figure 4.13 (e) the quality is increased to 0.4 and results in a constant annular flow throughout the tube for both $2R/D=3$ and $2R/D=7$. For a higher mass flux of $G=400\text{kg/m}^2\cdot\text{s}$ and $x > 0.02$, the flow pattern is also annular throughout the tube for both $2R/D=3$ and $2R/D=7$ as in figure 4.13 (d).

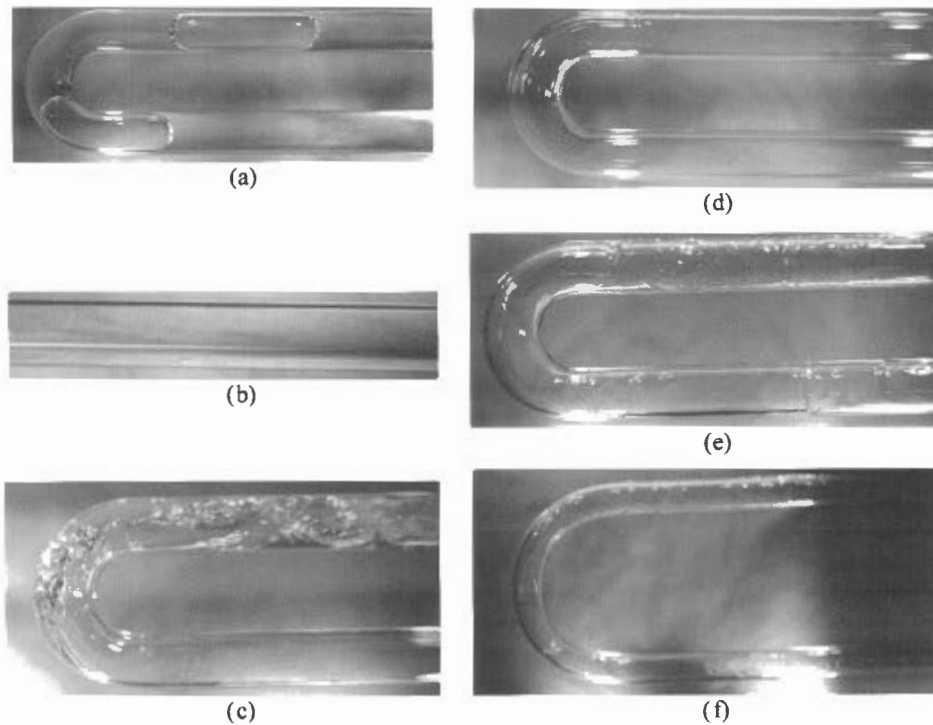


Figure 4.13: Flow pattern where $G=50\text{kg/m}^2\text{s}$ for $2R/D=3$ and $2R/D=7.1$ and $D=6.9\text{mm}$:
 (a) $x=0.0005$, $2R/D=3$, top view; (b) downstream $x=0.1$, $2R/D=3$, side view; (c) bend $x=0.1$, $2R/D=3$, top view; (d) bend $x=0.3$, $2R/D=3$, top view; (e) bend $x=0.4$, $2R/D=3$, top view; (f) bend $x=0.4$, $2R/D=7.1$, top view. (Wang et al., 2002)

In summary:

- 1) When the tube diameter and curvature ratio is reduced, there is a less pronounced change in the flow pattern due to an increase in surface tension and the lack of developing length of swirl flow to overturn the liquid and form annular flow.
- 2) If the quality increases, the change in flow pattern is also less visible due to a lack of the liquid portion of the flow. When the quality goes above 0.4, the flow pattern is annular inside the whole tube for mass flux values between 50 and $700\text{kg/m}^2\text{s}$.
- 3) For curvature ratios bigger than 7.1 and qualities smaller than 0.1 at a mass flux of $50\text{kg/m}^2\text{s}$, the flow is stratified throughout the tube.

4.2.5 Stainless Steel Corrosion

Crawford et al. (1997)

Stainless steels exhibit passivity over a wide range of environments due to the formation of a Cr_2O_3 layer. The stability of this passive oxide film is destroyed by the presence of halogen ions, particularly chloride ions.

Austenitic stainless steels also contain a high proportion of nickel to stabilise the austenite at room temperature and improve corrosion resistance. A certain amount of molybdenum will enhance these stainless steels' ability to resist pitting corrosion. Austenitic stainless steels are subject to pitting and intergranular corrosion.

The most common type of corrosion in austenitic stainless steels is intergranular corrosion. This type of corrosion is a direct result of sensitisation, which is the phenomenon of chromium carbide precipitation at the grain boundaries in the temperature range of 425-815°C. The matrix alloy near the grain boundaries is depleted of chromium while the chromium carbide precipitates are very high in chromium. The chromium depleted zone is less corrosion resistant than the chromium carbide precipitates.

Pitting corrosion results from the failure of the passive oxide film. The attack on the metal is localised and takes place over small areas. Pitting most often occurs in the presence of chloride ions and can occur in various modes: shallow pits, deep pits or wide and shallow pits. Surfaces affected by pitting are often covered by corrosion products. As a result, the pits can only be seen clearly once the surface has been cleaned of the corrosion products.

4.2.6 Turbocharger Design

Included in appendix A is the detailed design drawing of the turbocharger originally considered for this project. The drawing was provided by AlliedSignal, England (AlliedSignal Ltd., 2002). In order to use the turbocharger to generate power from recovered energy, it is imperative to know and understand its working mechanisms and the theory behind the design. Section 4.1.4 has already provided a brief introduction to the working mechanisms. The following paragraphs take a more in-depth look into the theory of turbocharger design. The turbines in small turbochargers are normally radial turbines, whilst in a large turbocharger they are always single-stage axial turbines. The basic difference between the two types of turbines are their speed dependent flow characteristics. The turbine total-to-static efficiency (η_{TS}) will vary with blade speed ratio, turbine rotor speed and admission width.

In the exhaust system of a turbocharged engine, the turbine is presented with pulses of fluctuating pressure and temperature and this produces variations of blade speed ratio and

total-to-static efficiency with time. The average turbine efficiency (η_T), as set out in equation 4.2.7, allows for these fluctuations.

$$\eta_T = \frac{\int \eta_{TS} \dot{m} \Delta h_{is} dt}{\int \dot{m} \Delta h_{is} dt} \quad \dots (4.2.7)$$

\dot{m} is the instantaneous mass flow rate and Δh_{is} is the instantaneous isentropic enthalpy drop (Benson et al., 1979).

The compressor unit of a turbocharger is normally used as a source of additional compressed air in an IC-engine, as previously stated. In the absence of an electrical generator it can also be used to measure the amount of energy recovered by the turbine unit (taking losses into account). The adiabatic efficiencies for compressors are primarily dependent upon three dimensionless variables:

Pressure ratio (outlet over inlet)...

$$\frac{P_2}{P_1} \quad \dots (4.2.8)$$

Mach number based on the wheel tip speed...

$$\frac{1}{2} \omega \frac{D}{c} \quad \dots (4.2.9)$$

Mass flow rate over the critical mass flow rate...

$$\frac{\dot{m}}{\dot{m}^*} \quad \dots (4.2.10)$$

where...

$$\dot{m}^* = 0.578 \left(\frac{\pi D^2}{4} \right) \rho_o c_o \quad \dots (4.2.11)$$

$$\text{with } \begin{aligned} c_o &= \sqrt{kRT} \\ k &= 1.4 \end{aligned} \quad \dots (4.2.12)$$

Choking occurs when somewhere within the compressor the flow reaches the speed of sound. It occurs at values where the ratio of mass flow rate over the critical mass flow rate are less than 1, because the critical mass flow rate is based on the compressor wheel

diameter rather than on the cross section where choking occurs. The value of the ratio varies with tip speed, because the location within the compressor at which choking occurs, depends on the structure of the internal boundary layers (Ferguson, 1986 and White, 1999).

Also of great importance is the surge line shown on the compressor characteristic curve in appendix B. Suppose a compressor is operating at point 3 on the negative slope of the curve in figure 4.14. A reduction in mass flow due to a momentary blockage will cause an increase in the outlet pressure, which will tend to return the mass flow to point 3. Thus, this negative slope represents a region of stable operation. It is self-correcting.

If the flow rate drops to a point corresponding to 2 on the positive slope of the characteristic, the outlet pressure will continue to decrease, causing a further drop in mass flow and a further drop in the outlet pressure, and so on until point 1 is reached, where the mass flow is zero. The mass flow may even become negative through the compressor. When the outlet pressure (back-pressure) has reduced itself sufficiently due to the reduced flow rate, the positive flow becomes established once again and the compressor picks up until the restricted mass flow is again reached, when pressure reduction once again takes place. The pressure therefore surges back and forth in an unstable fashion, which, if severe enough, could lead to failure of parts of the compressor. The research sources were Ferguson (1986) and Sayers (1990).

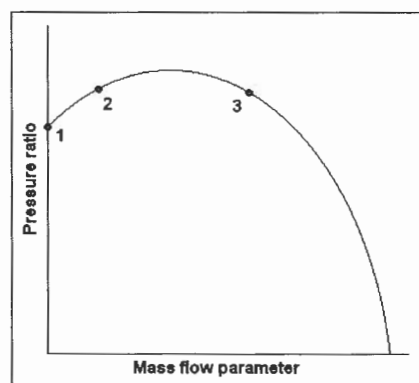


Figure 4.14: Surge line illustration

Although the turbocharger was not implemented in this project due to a change in project scope (*discussed in chapter 2 and appendix C*), all relevant data concerning the turbocharger are documented in this thesis for future reference (*see appendix A and B*).

4.2.7 Power Generation utilising High Speed Generators

According to Hopmann (2002), the DOE Office of Heavy Vehicle Technology and Caterpillar Inc. are currently collaborating in a combined program aimed at demonstrating electric turbocompound technology on a Class 8 truck engine. This is a laboratory demonstration program, with no provision for on-truck testing. The goal is to demonstrate the level of fuel efficiency improvement attainable with an electric turbocompound system. Although the program is somewhat different from the one proposed in this thesis, it still has significant bearing on the subject matter due to the fact that an integrated turbocharger-motor/generator system is used.

Existing turbocompound technology consists of a conventional mechanical turbocompound system. The system includes a conventional turbocharger which recovers exhaust energy in a turbine to boost the air coming into the engine in a conventional fashion. Downstream of the turbocharger turbine, the exhaust gas goes through a second turbine. The energy recovered here is added to the engine torque through a system of shafts, gears and a fluid coupling. The objective of the DOE program is to demonstrate the electrical recovery of exhaust energy by using high speed generator technology. Electric turbocompounding eliminates the mechanical coupling to the engine crank shaft necessary in mechanical turbocompounding. This provides more flexibility in packaging. The electric turbocompound system also provides more control flexibility in that the amount of power extracted can be varied which allows the control of engine boost. Also, the generator can be operated as a motor to spin up the turbo more quickly to improve turbo response. The electric turbocompound is a natural fit in a vehicle equipped with More Electric technology.

More Electric Initiative (MEI) technology can be applied to an on-highway truck. Accessories that are normally driven by a belt or chain off of the engine are electrically driven. Accessories can be installed where packaging and servicing are optimized. Also, accessories can be run only when needed at the required power level. A key component of the MEI truck is the crank starter/generator. This device replaces both the generator and the starter on a conventional truck engine. The crank shaft starter/generator can also be used as a motor to convert electric power to driveline torque power. Electric turbocompounding is a complementary technology to MEI in that the electric power

generated by the electric turbocompound can be used to power the MEI accessories. The electric power can also be added to the power train through the crank shaft starter/motor/generator. Likewise, the flow of power can be reversed to power up the turbocharger if needed.

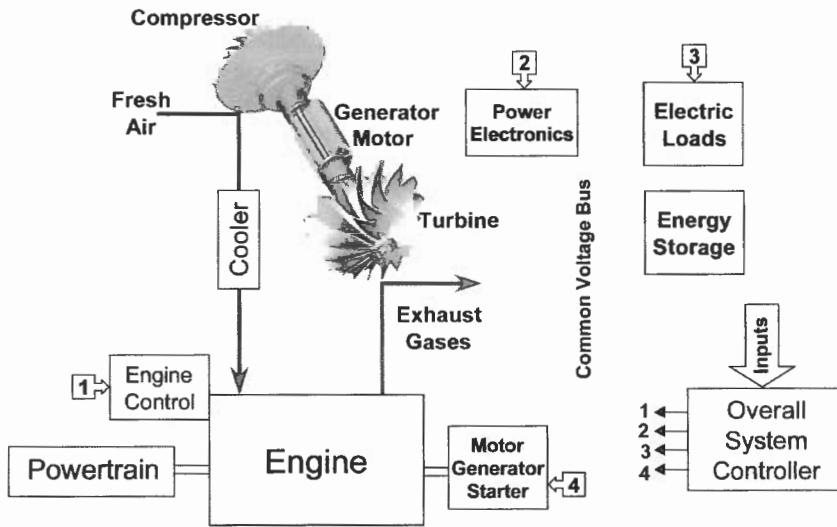


Figure 4.15: Electrical Turbocompound (ETC) system schematic

The graph in figure 4.16 illustrates the operating limits of turbocompounding. The figure applies to a single engine speed. The horizontal axis is the ratio of actual airflow to airflow at the rated condition. The vertical axis is the ratio of exhaust power available for turbocompounding to total exhaust power. The turbocompound is limited in operation on the left by the line that represents maximum turbine inlet temperature, and on the right by the line that represents maximum turbo speed. The various fuelling ratio curves represent different engine power levels. A mechanical system with fixed geometry is limited to a single operating line. The addition of variable geometry to the turbocharger will increase the flexibility of the mechanical system.

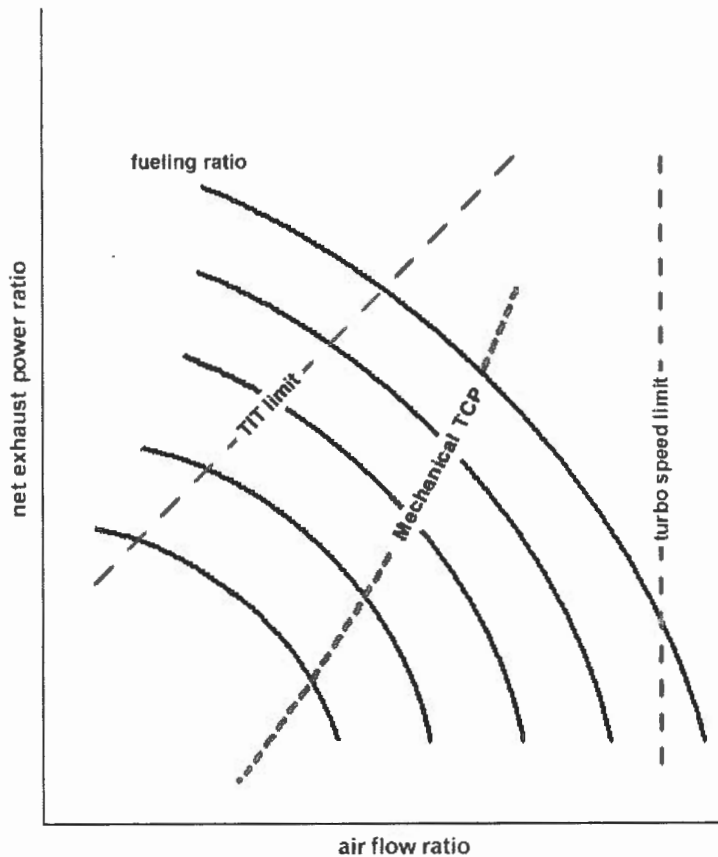


Figure 4.16: Turbocompound (TC) limitations

The electric turbocompound system can operate anywhere along a power curve between the two limits. Operating near the turbine inlet temperature limit maximizes the engine fuel efficiency. In some circumstances, particularly at lower power levels, it may be desirable to operate nearer the turbo speed limit. This would supply excess air to the engine and improve engine response when power demand is increased. This strategy could also improve transient emissions.

The project run by the DOE has the same concerns as the project discussed in this report. The biggest concern is the additional cost and size of applying high speed generator technology to the environment. Another concern is the high frequency of the generator output which complicates the generator design.

4.2.8 Material Research

Due to the combination of high pressures and temperatures present inside the heat exchanger tubes, a tube-material had to be chosen that would withstand the extreme conditions without failing. Another critical part in the design was the fin-material. The

fins are not exposed to very high pressures, but the combination of the high gas temperatures and velocities inside the heat exchanger shell proved to be problematic. Materials like aluminium have a very good conductivity, but they tend to soften at high temperatures. If gas were to be blown across the fins at high velocities, the fins would collapse or deform, decreasing the heat exchanger effectiveness. Copper has a very high melting point, but starts to flake and disintegrate long before it reaches its melting point temperature. The copper would also start “ballooning”, especially at the U-bends, because of the high pressures present inside the heat exchanger.

Another factor which would have to be taken into account is the materials’ resistance to corrosion. Because of the corrosive nature of exhaust gasses, very few materials are able to withstand the extreme conditions. Lastly, there had to be looked at the interface between the tube and fins with regard to expansion at high temperatures and the method of integrating the fins with the tube to form a solid fintube. Another critical design element would be the resistance to heat transfer at the interface. The materials which were considered are set out in the table 4.3.

	Aluminium	Brass	Carbon Steel	Copper	Mild Steel	Stainless Steel 316	3CR12
Density [kg/m ³]	2700	8500	7800	8933	7870	8000	7700
Thermal Conductivity, 0°-600°C [W/m°C]	231	146	49	401	70	17	24
Mean Coefficient of Thermal Expansion, 0°-500°C [m/m°C x 1E-6]	23.9	18.7	10.8	17	13.8	18.25	12.5
Recommended Maximum Service Temperature [°C]	Continuous	--	--	--	500	925	600
	Intermittent	--	--	--	600	870	700

Table 4.3: Material properties

From this table it is clear that aluminium and copper would have been found inappropriate as previously stated. That leaves brass, carbon steel, mild steel, stainless steel and 3CR12.

Brass would be the obvious choice because of its high thermal conductivity, but data received from Maksal Tubes Pty., a South African manufacturer of brass and copper tubing, shows the maximum allowable stress for brass at 200°C is already as low as

20MPa (shown in figure 4.17). Stress calculations in chapter 6 will show that for a tube with an outer diameter of 17.15mm, a wall thickness of 1.65mm and centre-to-centre distance of 42.88mm, the Von Mises stresses will be 12.78MPa. Due to the sharp decline in the allowable maximum stress with an increase in temperature, brass was found to be inadequate.

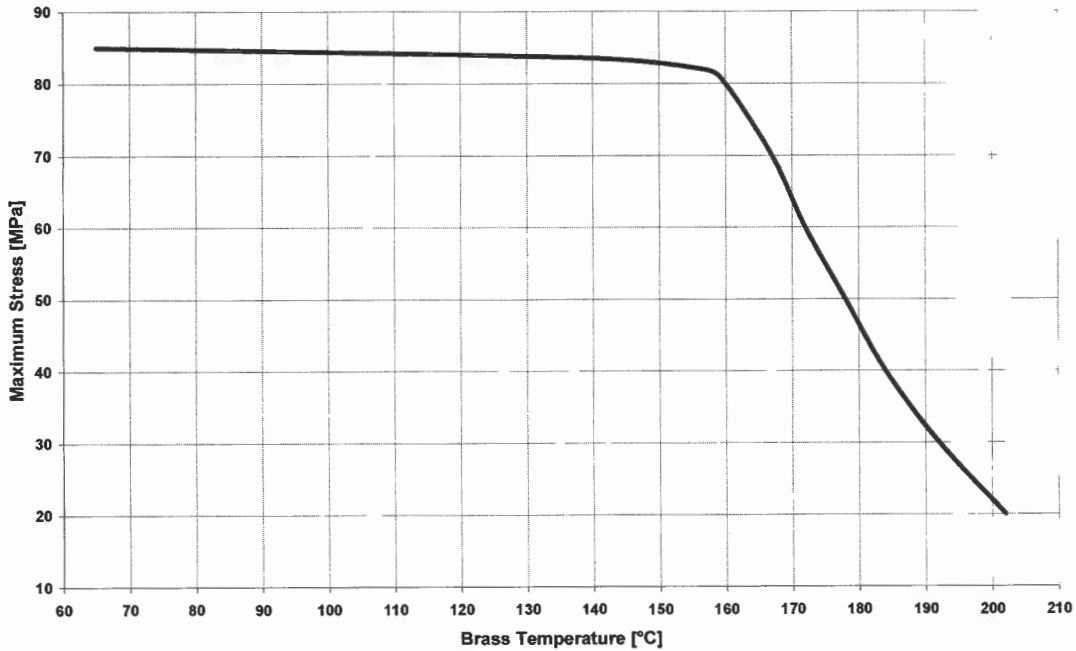


Figure 4.17: Maximum allowable stress in brass with rising temperature

Mild steel could also be eliminated due to its low recommended service temperatures, as seen in table 4.3, as well as carbon steel, which, despite its relatively high thermal conductivity, would corrode and rust in the water/steam environment. This would result in the steady decrease of the heat exchanger effectiveness.

That left stainless steel and 3CR12. It was considered to use stainless steel tubing with 3CR12 fins due to the corrosion problem with 3CR12 and water. However, due to the difference in thermal expansion values, which would result in the buckling of the fins, and ultimate increase in heat transfer resistance between the fins and tubes, 3CR12 was also eliminated.

Stainless steel was left for both the tubing and fins. Despite stainless steel's low thermal conductivity, it has a very good resistance to corrosion and can be used at high temperatures. The most difficult aspect of using this material would be to manufacture the

fin-tube. Stainless steel tends to work harden, so to extrude the fins would be nearly impossible. In the end it was decided to use stainless steel hollow bar and machine cut the fins out with the help of a NC-machine (Numerical Controlled machine). For more details, see section 7.2. An added bonus would be that the resistance to heat transfer between the fins and the tubing would be eliminated (which is not the case in the alternative fin configurations shown below).

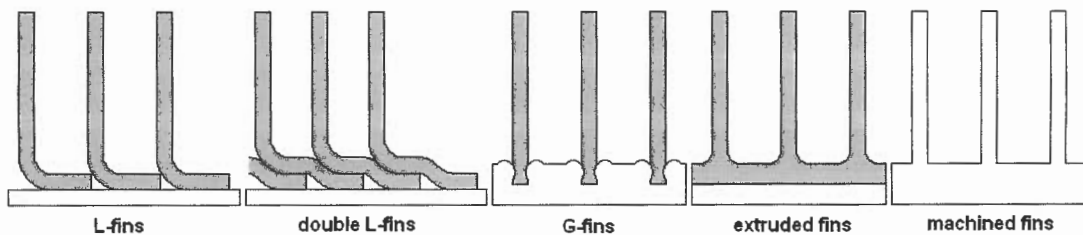


Figure 4.18: Fin configurations

Material properties in this section were obtained from the following sources: Benham et al. (1997), Malan and Paterson (1993), Sassda (2003), Serway (1996) and Shigley and Mischke (1989).

4.3 RESEARCH DONE AT THE UNIVERSITY OF STELLENBOSCH

4.3.1 Joubert (1996)

This project was a technical study of a single pressure waste heat recovery system in a slow speed diesel engine powered ship. The emphasis was on the thermodynamic optimisation of the system in order to obtain the maximum efficiency possible, where after the sizing and layout of the heat exchangers were calculated.

The system made use of the simple Rankine steam cycle and was based on a large diesel engine with known exhaust gas properties. The system was optimised with the aid of a computer. After the system had been optimized, a three stage heat exchanger was designed.

Both the thermodynamic and the heat transfer part of the project were based on theory alone, and no experiments were carried out to confirm the correctness of the results obtained from theory.

The case study showed that a large marine engine producing 9270kW of power had enough heat in its exhaust gas to produce 850kW of electricity. This amounted to a fuel saving of 1620kl of fuel per year.

4.3.2 Koorts (1998)

The project was a technical study and design of a waste heat recovery system under laboratory conditions, utilizing the energy available in exhaust gases. It built forth on the final year project done by Joubert (1996).

The main difference between the two is that this project attempted to develop a smaller scale application, where Joubert (1996) used a marine diesel engine for his study. The emphasis was on the thermodynamic optimisation of the system in order to obtain the maximum efficiency possible, using the design to achieve this.

The case study found that from a 6l capacity engine, 81.02kW of energy was rejected through emissions, and at the optimal design pressure of 600kPa the overall energy recovery was 21.08%.

4.3.3 Lotun (1999 & 2001)

The project investigated the implementation of a small-scale waste heat recovery unit. It included the generation of superheated steam used to operate a Rankine cycle, resulting in the generation of electrical power from the exhaust gasses of a diesel truck engine. Although the project did not reach the electrical generation stage, the following results were obtained from in-depth testing on the exhaust gasses from a continuous combustion unit and from a diesel truck engine. In both cases superheated steam was generated at atmospheric pressure.

	Continuous Combustion Unit	Internal Combustion Engine
Exhaust gas temperature	360°C	212°C
Air enthalpy	642.09 kJ/kg	487.85 kJ/kg
Total energy content	35.31 kW	26.83 kW
Superheated steam	160°C	157°C
Heat transfer efficiency	98.93%	88.97%
Energy recovered	34.93 kW	23.87 kW

Table 4.4: Experimental results obtained by Lotun (2001)

The heat exchanger, a cross-flow copper fintube heat exchanger, was specified by Lotun (2001). The specifications are shown in table 4.5.

Finned Heat Exchanger	
Manufacturing company	YUCON COIL
Company model number	3SC-254/254/10FS/10R Cu/Cu/SS
Pipe material	Copper
Fins material	Copper
Housing	Stainless steel
Width	254 mm
Height	254 mm
Length	254 mm
Number of rows	10
Number of pipes per row	10
Exhaust air finned side	
Fin pitch	3.175 mm
Fin thickness	0.14 mm
Transversal tube pitch	19.05 mm
Longitudinal tube pitch	33.0 mm
Inner tube side	
Pipe outer diameter	9.53 mm
Wall thickness	0.41 mm

Table 4.5: Finned heat exchanger specifications

4.3.4 Wiplinger (2001)

The aims of the project were to do a theoretical analysis to determine the amount of power available for the generation of electrical power and the experimental generation of power using superheated steam and compressed air in conjunction with a turbocharger. Furthermore, the interface design and construction between existing hardware and the turbocharger had to be done.

Lotun (2001) had previously completed the construction and testing of the system responsible for steam generation as well as all the calculations concerning the steam properties.

The power was created by passing the superheated steam and compressed air (in separate experiments) through the turbine and letting the turbine drive the compressor. The turbocharger used, was that of a Golf TDi 1900.

The results of the experimental testing are tabulated in table 4.6.

	Superheated Steam (0.0071 l/s)	Compressed Air (57.84 l/s)
Turbine rotational speed	11396 rpm	42000 rpm
Compressor inlet pressure	100.476 kPa	99.60 kPa
Compressor volume flowrate	0.0089 m ³ /s	0.0289 m ³ /s
Compressor air massflow rate	0.011 kg/s	0.035 kg/s
Compressor power output	0.214 W	7 W

Table 4.6: Experimental results obtained by Wipplinger (2001)

The results showed that the steam cycle was inefficient due to a very low pressure-drop over the turbine, which resulted in a very low volume flow rate and rotational speed of the turbine.

4.3.5 Conclusion

The current project starts with a feasibility study. The aim being to determine whether the heat exchanger proposed by Lotun (2001), could be utilised in an air based recovery system (*see appendix C*). The results showed that the tube diameter in the heat exchanger was too small for the air flow rate required and that choking would occur. As previously stated, it was also determined by Wipplinger (2001) that a system utilising this particular heat exchanger along with water as the working fluid, would be inefficient due to the low maximum pressures obtainable inside the heat exchanger. The limiting factor being that the heat exchanger was primarily made of copper which could not withstand the combination of high temperatures and pressures.

A water-based Rankine cycle recovery system would be much more efficient with the appropriate heat exchanger. The calculations (*see appendix D*) show that a system efficiency of 18% can be achieved if the pump and turbine efficiencies are 80% respectively.

Thus, there was decided to redesign the heat exchanger in order to obtain a higher pressure drop across the turbine and maximize the recovery energy yield.

5. THEORETICAL ANALYSIS

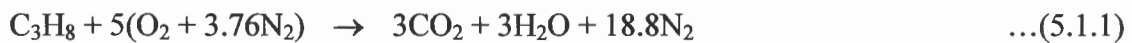
5.1 THE CONTINUOUS COMBUSTION UNIT AND ENERGY AVAILABILITY

For experimental testing purposes, the continuous combustion unit was used as the source of “waste” heat energy (*see appendix E*). By running the unit at various air/propane ratios, it was found that complete combustion (stoichiometric combustion) occurs at a ratio of approximately 16:1, where the air inlet temperature, water inlet temperature and water mass flow rate was held constant during the test procedure.

The following analysis was done on the results obtained, using 16:1 as the stoichiometric air/fuel ratio. All theory concerning the combustion process was provided by Schwack and Harms (2000).

5.1.1 Combustion Analysis

The complete combustion equation is shown in equation 5.1.1.



According to the energy balance of $\text{energy}_{\text{in}} = \text{energy}_{\text{out}}$, the energy distribution can be described as ...

$$Q_{\text{reactants}} = Q_{\text{products}} + Q_{\text{out}} \quad \dots(5.1.2)$$

$$\text{where } Q_{\text{reactants}} = \sum N_r (h_f^\circ + h - h_{298}^\circ) \quad \dots(5.1.3)$$

$$Q_{\text{products}} = \sum N_p (h_f^\circ + h - h_{298}^\circ) \quad \dots(5.1.4)$$

$$Q_{\text{out}} = Q_{\text{water jacket}} + Q_{\text{end plate}} + Q_{\text{exhaust}} \quad \dots(5.1.5)$$

Equation 5.1.5 is a good approximation of the various components of Q_{out} as the other components were deemed negligibly small.

For a ratio of 16:1, equations 5.1.3–5 gave the following results (*see appendix J*)...

$$Q_{\text{reactants}} = -2.6 \text{ kW}$$

$$Q_{\text{products}} = -42.7 \text{ kW}$$

$$Q_{\text{out}} = 40.1 \text{ kW}$$

where Q_{out} consists of ...

$$Q_{\text{water jacket}} = \underline{33.9 \text{ kW}}$$

$$Q_{\text{end plate}} = \underline{0.957 \text{ kW}}$$

$$Q_{\text{exhaust}} = \underline{5.2 \text{ kW}}$$

This means that the recoverable energy available to the heat exchanger will be 5.2kW minus the losses along the piping. The losses can be measured by determining the temperature difference between the continuous combustion unit outlet and the ducting inlet.

As can be seen in appendix L, the losses that have been measured in practical testing are in the range of 0.634kW (depending on the gas mass flow rate and temperature). That means that an energy loss of over 12% occurs in the ducting system. Attempts were made to minimize these losses by using low cost insulation, but failed due to the inability of the insulation to withstand the high temperatures of the ducting. However, as the losses are quite significant, it is recommended that the system is insulated with the correct materials in order to improve future test results.

5.2 FINTUBE AND U-BEND DESIGN CONSIDERATIONS

During the sourcing of the materials of the heat exchanger, it was found that the smallest tube size readily available for the construction of the U-bends, were stainless steel tubes with a 17.15mm OD x 13.84mm ID. This limited the distance of the U-bend from centre-to-centre to 42.88mm (2.5 times the OD).

In addition, the smallest available hollow bar used in the construction of the fin-tubes, was hollow bar with a 32mm OD x 16mm ID. This meant that there would be a shoulder

of 1.16mm where the U-bend and fin-tube would be welded together. To avoid this, a smaller hollow bar, which was not available, would have to be used. Alternatively, the next tube size for the U-bend construction would have had to be used, but a 21.34mm OD x 18.03mm ID would result in a U-bend centre-to-centre distance of 53.35mm, which would produce an inefficient heat exchanger.

Thus, the decision was made to keep the 17.15mm OD x 13.84mm ID U-bends as well as the 32mm OD x 16mm ID hollow bar. The final fintube spacing is illustrated in the figure below.

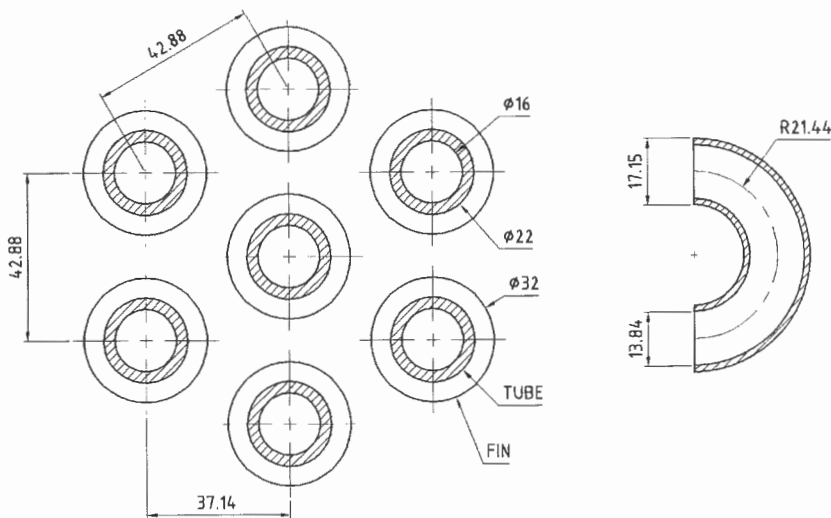


Figure 5.1: Fintube and U-bend spacing geometries

5.3 EQUATIONS AND THEORIES

Various sources were consulted for the equations and theories used in this thesis. What this section will attempt to convey, is a summary of all relevant theory used in the design of the heat exchanger, i.e. theory used in the Excel sheet (which served as a familiarisation tool with the relevant theory) and the Visual Basic simulation program (which was ultimately used to design the heat exchanger). Appendix I (*see pp. 19 – 115*) contains the flow chart of the simulation program. The layout of the theory explanation will approximately follow this flow chart.

5.3.1 Implicit Geometries

Implicit geometries refer to heat exchanger geometries resulting from the specifications supplied by the program user. These specifications include the following:

Heat Exchanger Geometry

Tube Conductivity	18 [W/m.K]	Fin Conductivity	18 [W/m.K]
Tube Length	0.3 [m]	Fin Thickness	0.0005 [m]
Outer Tube Diameter	0.022 [m]	Fin Pitch	0.0025 [m]
Inner Tube Diameter	0.016 [m]	Fin Height	0.005 [m]
Longitudinal Tube Pitch	0.0371 [m]	Nr of Tubes/Row	8 [#]
Transverse Tube Pitch	0.04288 [m]	Nr of Rows	5 [#]

Figure 5.2: Heat exchanger geometries

The data showed above, are the default design values applicable to this project. The geometry values shown in figure 5.2 imply certain standard geometries for the heat exchanger design as seen in figure 5.3. Note that the boundaries of one control volume lies between two fins:

Implicit Geometries

Tube Thickness	0.003 [m]
H.E. Height	0.35874 [m]
Frontal Area	0.107622 [m ²]
Area Exp to Gas	0.0009864 [m ²]
Area Exp to Water	0.0001256 [m ²]

Simulation Results

Nr of Control Volumes/Tube	120 [#]
Total nr of Control Volumes	4800 [#]

Figure 5.3: Implicit heat exchanger geometries

The front and side view of the control volume that has been chosen for the analysis is shown in figure 5.4.

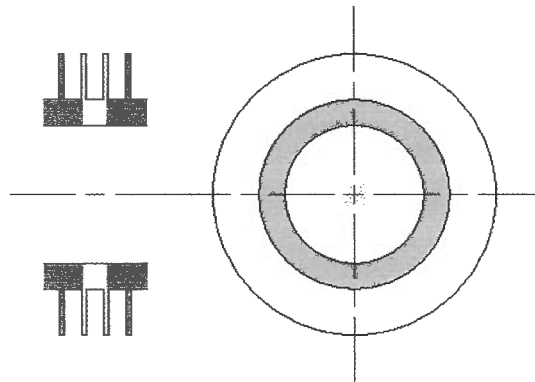


Figure 5.4: Control volume used in theoretical analysis

Tube thickness...

$$t_t = (O_d_t - I_d_t)/2 \quad \dots(5.3.1)$$

Heat exchanger height...

$$H = S_T \cdot N_t + 0.0157 \quad \dots(5.3.2)$$

Heat exchanger frontal area...

$$A_{fr} = H.L_t \quad \dots(5.3.3)$$

Area exposed to gas...

$$A_{gas} = \pi/2((O_d_t + 2H_f)^2 - O_d_t^2) + \pi O_d_t(p_f - t_f) \quad \dots(5.3.4)$$

Area exposed to water...

$$A_w = \pi I_d_t p_f \quad \dots(5.3.5)$$

Control volumes per tube...

$$CV_{tube} = L_t/p_f \quad \dots(5.3.6)$$

The number of control volumes in the heat exchanger...

$$CV_{tot} = L_t.N_t.N_r/p_f \quad \dots(5.3.7)$$

All of the above equations were extensively used in the simulation program.

5.3.2 Preheating Theory

Preheating theory focuses on the heating of a single-phase fluid. In the design, water was used as the working fluid. The “International Association for the Properties of Water and Steam (IAPWS) Industrial Formulation 1997 for the Thermodynamic Properties of Water and Steam” was used to calculate the water (*see Wagner et al. (1997)*).

Some of the equations that follow are preceded by the abbreviation “*IAPWS-IF97*”, which means that a standard function from the IAPWS dll-file has been used to determine the property. For the first control volume of the simulation the temperature, pressure and mass flow rate values of the water and gas inlets are known ($T_w, P_w, \dot{m}_w, T_{gas,in}, P_{gas}, \dot{m}_{gas}$). The values at the outlet of each control volume are calculated in each iteration. The quality (x) and void fraction (α) for single-phase liquid = 0.

Saturated water temperature (*IAPWS-IF97*)...

$$T_{sat} = TBP(P_w/100) \quad \dots(5.3.8)$$

Water liquid enthalpy (*IAPWS-IF97*)...

$$h_{enth} = HBPT(P_w/100, T_w) \quad \dots(5.3.9)$$

Water liquid density (*IAPWS-IF97*)...

$$\rho_w = \text{DBPT}(P_w/100, T_w) \quad \dots(5.3.10)$$

Water liquid velocity...

$$\text{Vel}_w = (4 \dot{m}_w / (\pi I d_t^2)) / \rho_w \quad \dots(5.3.11)$$

Gas heat transfer coefficient (*see section 5.3.15*)

Water liquid heat transfer coefficient (*see section 5.3.16*)

Fin efficiency (*see section 5.3.12*)

Overall heat transfer coefficient (*see section 5.3.13*)

The amount of energy transferred to a specific control volume is...

$$Q_{\text{transf}} = UA_{\text{cv}}(T_{\text{gas,in}} - T_w) \quad \dots(5.3.12)$$

where A_{cv} is the control volume area of the fintube exposed to the gas.

The gas outlet temperature is...

$$T_{\text{gas,out}} = T_{\text{gas,in}} + Q_{\text{gas,tot}} / (\dot{m}_{\text{gas}} \cdot C_{p\text{gas}}) \quad \dots(5.3.13)$$

At this stage it is necessary to clarify the working of the gas temperature in the simulation program. Firstly all the $T_{\text{gas,out}}$'s for a single tube row are determined using the same $T_{\text{gas,in}}$ (equation 5.3.13). The total energy transferred is calculated using equation 5.3.12. From which a new average $T_{\text{gas,in}}$ is determined for the next row. The water outlet temperature is...

$$T_w = T_w + Q_{\text{transf}} / (\dot{m}_w \cdot C_{p_w}) \quad \dots(5.3.14)$$

and the water outlet enthalpy is...

$$h_{\text{enth,out}} = h_{\text{enth,in}} + Q_{\text{transf}} / \dot{m}_w \quad \dots(5.3.15)$$

5.3.3 Single-phase liquid pressure drop across a tube

After the energy balance has been done for one control volume, the pressure drop over the control volume is determined using the Friedel correlation as quoted in Whalley (1987).

Previous average water temperature...

$$t_0 = (T_w^{[-1]} + T_w) / 2 \quad \dots(5.3.16)$$

Current average water temperature...

$$t_1 = (T_w + T_w^{[+1]}) / 2 \quad \dots(5.3.17)$$

Inlet water liquid density (*IAPWS-IF97*)...

$$\rho_0 = 1/\text{DBPT}(P_w/100, t_0) \quad \dots(5.3.18)$$

Outlet water liquid density (*IAPWS-IF97*)...

$$\rho_1 = 1/\text{DBPT}(P_w/100, t_1) \quad \dots(5.3.19)$$

Friction pressure gradient (*IAPWS-IF97*)...

$$U = \dot{m}_w / (\text{DBPT}(P_w/100, t_1) (\pi Id_t^2) / 4) \quad \dots(5.3.20)$$

$$\text{Re} = \text{DBPT}(P_w/100, t_1) \cdot U \cdot Id_t / \mu_w \quad \dots(5.3.21)$$

$$C_f = \begin{cases} 16/\text{Re} & \dots \text{Re} \leq 2000 \\ 0.079 \text{Re}^{-0.25} & \dots \text{Re} > 2000 \end{cases} \quad \dots(5.3.22)$$

$$\tau = 0.5 C_f \cdot \text{DBPT}(P_w/100, t_1) U^2 \quad \dots(5.3.23)$$

which gives...

$$\Delta P_{\text{fric}} = 4\tau \cdot p / Id_t \quad \dots(5.3.24)$$

Gravitational pressure gradient...

$$\Delta P_{\text{grav}} = 0 \quad (\text{for horizontal tubes}) \quad \dots(5.3.25)$$

Accelerational pressure gradient...

$$G = 4 \dot{m}_w / (\pi Id_t^2) \quad \dots(5.3.26)$$

which gives...

$$\Delta P_{\text{accel}} = G^2 (\rho_1 - \rho_0) \quad \dots(5.3.27)$$

The total pressure drop across the tube is...

$$\Delta P = \Delta P_{\text{fric}} + \Delta P_{\text{grav}} + \Delta P_{\text{accel}} \quad \dots(5.3.28)$$

and the new control volume inlet pressure...

$$P_w^{[+1]} = P_w^{[-1]} - \Delta P \quad \dots(5.3.29)$$

5.3.4 Single-phase liquid pressure drop across a U-bend

In the case where the flow has reached the end of the tube and has to pass through the U-bend, it is assumed that the U-bend is well insulated, but that gravitational, accelerational

and frictional pressure loss, play a significant roll. From the terms used in the section 5.3.3, only the gravitational term differs and in the frictional pressure drop, an equivalent length of 0.7m has been used as prescribed by ASHRAE (1985).

$$\Delta P_{\text{grav}} = \text{DBPT}(P_w/100, T_w)g.S_T \quad \dots(5.3.30)$$

The rest of the terms remain the same.

5.3.5 Boiler Theory

The boiler theory also uses Whalley (1987) as well as certain well known correlations such as the Friedel (1979) correlation for two-phase pressure gradients, the CISE correlation for void fraction and the Chen (1963) correlation for boiling heat transfer coefficients in two-phase flow (*see appendix F*).

The two-phase multiplier is determined using the Friedel correlation...

$$\phi_{lo}^2 = \frac{\left(-\frac{dp}{dz}\right)_F}{\left(-\frac{dp}{dz}\right)_{lo}} \quad \dots(F1)$$

The void fraction is determined using the CISE correlation...

$$\alpha = \frac{1}{1 + \left(S \frac{1-x}{x} \frac{\rho_g}{\rho_l}\right)} \quad \dots(F9)$$

The two-phase heat transfer coefficient is determined using Chen's correlation...

$$h_w = h_{\text{mic}} + h_{\text{mac}} \quad \dots(F17)$$

The quality of the two-phase flow (*IAPWS-IF97*) is...

$$x = (h_{\text{enth}} - \text{HLBT}(T_{\text{sat}}))/(\text{HVB}(T_{\text{sat}}) - \text{HLBT}(T_{\text{sat}})) \quad \dots(5.3.31)$$

The homogeneous density of the two-phase mixture (*IAPWS-IF97*) is...

$$\rho_w = (x/\text{DVBT}(T_w) + (1-x)/\text{DLBT}(T_w))^{-1} \quad \dots(5.3.32)$$

The velocity of the two-phase mixture is...

$$\text{Vel}_w = 4 \dot{m}_w / (\pi D_t^2) / \rho_w \quad \dots(5.3.33)$$

Gas heat transfer coefficient (*see section 5.3.15*)

Fin efficiency (*see section 5.3.12*)

Overall heat transfer coefficient (*see section 5.3.13*)

T_{gas} and Q_{transf} are determined in exactly the same manner as in single-phase theory.

The specific heat of the liquid vapour mixture is calculated as (*IAPWS-IF97*)...

$$C_{p_w} = (x \cdot C_{p_{\text{VBT}}}(T_w) + (1 - x) \cdot C_{p_{\text{LBT}}}(T_w)) \quad \dots(5.3.34)$$

The mixtures enthalpy is determined as...

$$h_{\text{enth,out}} = h_{\text{enth,in}} + Q_{\text{transf}} / \dot{m}_w \quad \dots(5.3.35)$$

and the average mixture temperature (*IAPWS-IF97*) is...

$$T_w = \text{TBP}(P_w/100) \quad \dots(5.3.36)$$

5.3.6 Two-phase pressure drop in a tube

When a two-phase liquid flows through a tube, the calculation of the resulting pressure drop must take into account that liquid and vapour exists within the tube.

The homogeneous density (*IAPWS-IF97*) is...

$$\rho_{\text{homo}} = (x/DVBT(T_w) + (1 - x)/DLBT(T_w))^{-1} \quad \dots(5.3.37)$$

the separated density (*IAPWS-IF97*) is...

$$\rho_{\text{sep}} = DVBT(T_w) \cdot \alpha + DLBT(T_w) \cdot (1 - \alpha) \quad \dots(5.3.38)$$

and the friction pressure gradient (*IAPWS-IF97*) with T_w in Kelvin...

$$\mu_l = (6.8523 \times 10^{-13} T_w^6 - 1.8482 \times 10^{-9} T_w^5 + 2.0620 \times 10^{-6} T_w^4 - 1.2185 \times 10^{-3} T_w^3 + 0.4025 T_w^2 - 70.563 T_w + 5138.3) 10^{-4} \quad \dots(5.3.39)$$

$$\text{Re}_{f_0} = G \cdot \text{Id}_t / \mu_l \quad \dots(5.3.40)$$

$$C_{f_0} = \begin{cases} 16/\text{Re}_{f_0} & \dots \text{Re}_{f_0} \leq 2000 \\ 0.079 \text{Re}_{f_0}^{-0.25} & \dots \text{Re}_{f_0} > 2000 \end{cases} \quad \dots(5.3.41)$$

$$\Delta P_{l_0} = 2 C_{f_0} \cdot G^2 / (\text{Id}_t \cdot \text{DLBT}(T_w)) \quad \dots(5.3.42)$$

which gives...

$$\Delta P_{\text{fric}} = p_f \cdot \Delta P_{l_0} \cdot \phi_{l_0}^2 \quad \dots(5.3.43)$$

The gravitational pressure gradient is...

$$\Delta P_{\text{grav}} = 0 \quad (\text{for horizontal tubes}) \quad \dots(5.3.44)$$

Inlet water density (using the previous control volume properties) (*IAPWS-IF97*)...

$$\rho_0 = (x^2/(\alpha.DLBT(T_w)) + (1 - x)^2/((1 - \alpha).DLBT(T_w))) \quad \dots(5.3.45)$$

Outlet water density (using the current control volume properties) (*IAPWS-IF97*)...

$$\rho_1 = (x^2/(\alpha.DVBT(T_w)) + (1 - x)^2/((1 - \alpha).DLBT(T_w))) \quad \dots(5.3.46)$$

Accelerational pressure gradient...

$$\Delta P_{\text{accel}} = G^2(\rho_1 - \rho_0) \quad \dots(5.3.47)$$

The total pressure drop across the tube is then given by...

$$\Delta P = \Delta P_{\text{fric}} + \Delta P_{\text{grav}} + \Delta P_{\text{accel}} \quad \dots(5.3.48)$$

and the new control volume inlet pressure is...

$$P_w^{[+1]} = P_w^{[-1]} - \Delta P \quad \dots(5.3.49)$$

5.3.7 Two-phase pressure drop across a U-bend

Here again, the same equations are used as in the two-phase tube pressure drop calculations in section 5.3.6, with the exception of the gravitational term, and the frictional pressure drop where an equivalent length of 0.7m is again used as prescribed by ASHRAE (1985).

$$\Delta P_{\text{grav}} = DBPT(P_w/100, T_w)g.S_T \quad \dots(5.3.50)$$

The rest of the terms remain the same.

5.3.8 Superheated Theory

The superheated theory is much the same as the preheated theory in the sense that both work with a single-phase fluid or vapour. This makes the calculations for the superheated stage much easier as the properties of the fluid only has to be changed into that of a vapour. (Note that the subscripts referring to the water properties are still with a “w” and not with an “s” or “v”. This was done in order to simplify the simulation programming. The *IAPWS-IF97* automatically compensates for superheated steam.)

The quality (x) and void fraction (α) for single-phase vapour = 1.

The vapour density (*IAPWS-IF97*) is...

$$\rho_w = DBPT(P_w/100, T_w) \quad \dots(5.3.51)$$

and the vapour velocity is...

$$Vel_w = (4 \dot{m}_w / (\pi Id_t^2)) / \rho_w \quad \dots(5.3.52)$$

Gas heat transfer coefficient (*see section 5.3.15*)

Water vapour heat transfer coefficient (*see section 5.3.17*)

Fin efficiency (*see section 5.3.12*)

Overall heat transfer coefficient (*see section 5.3.13*)

The amount of energy transferred to a specific control volume is...

$$Q_{transf} = UA_{cv}(T_{gas,in} - T_w) \quad \dots(5.3.53)$$

and the gas outlet temperature is...

$$T_{gas,out} = T_{gas,in} + Q_{gas,tot} / (\dot{m}_{gas} \cdot Cp_{gas}) \quad \dots(5.3.54)$$

The gas temperature is calculated exactly as in the case of the single-phase liquid.

The vapour outlet temperature is...

$$T_w = T_w + Q_{transf} / (\dot{m}_w \cdot Cp_w) \quad \dots(5.3.55)$$

and the vapour outlet enthalpy is...

$$h_{enth,out} = h_{enth,in} + Q_{transf} / \dot{m}_w \quad \dots(5.3.56)$$

5.3.9 Single-phase vapour pressure drop across a tube

As before, theory from Whalley (1987) is used to calculate the pressure drop over the control volume.

Previous average vapour temp...

$$t_0 = (T_w^{[-1]} + T_w) / 2 \quad \dots(5.3.57)$$

Current average vapour temp...

$$t_1 = (T_w + T_w^{[+1]}) / 2 \quad \dots(5.3.58)$$

Inlet vapour density (*IAPWS-IF97*)...

$$\rho_0 = 1/DBPT(P_w/100, t_0) \quad \dots(5.3.59)$$

Outlet vapour density (*IAPWS-IF97*)...

$$\rho_1 = 1/DBPT(P_w/100, t_1) \quad \dots(5.3.60)$$

Friction pressure gradient (*IAPWS-IF97*)...

$$U = \dot{m}_w / (\text{DBPT}(P_w/100, t_1)(\pi Id_t^2)/4) \quad \dots(5.3.61)$$

$$\text{Re} = \text{DBPT}(P_w/100, t_1).U.Id_t/\mu_w \quad \dots(5.3.62)$$

$$C_f = \begin{cases} 16/\text{Re} & \dots \text{Re} \leq 2000 \\ 0.079 \text{Re}^{-0.25} & \dots \text{Re} > 2000 \end{cases} \quad \dots(5.3.63)$$

$$\tau = 0.5C_f.\text{DBPT}(P_w/100, t_1)U^2 \quad \dots(5.3.64)$$

which gives...

$$\Delta P_{\text{fric}} = 4\tau.P_f/Id_t \quad \dots(5.3.65)$$

Gravitational pressure gradient...

$$\Delta P_{\text{grav}} = 0 \quad (\text{for horizontal tubes}) \quad \dots(5.3.66)$$

Accelerational pressure gradient...

$$G = 4 \dot{m}_w / (\pi Id_t^2) \quad \dots(5.3.67)$$

which gives...

$$\Delta P_{\text{accel}} = G^2(\rho_1 - \rho_0) \quad \dots(5.3.68)$$

The total pressure drop across the tube is then given by...

$$\Delta P = \Delta P_{\text{fric}} + \Delta P_{\text{grav}} + \Delta P_{\text{accel}} \quad \dots(5.3.69)$$

and the new control volume inlet pressure is...

$$P_w^{[+1]} = P_w^{[-1]} - \Delta P \quad \dots(5.3.70)$$

5.3.10 Single-phase vapour pressure drop across a U-bend

As before, of the terms used in the section 5.3.9, only the gravitational term will differ, and in the frictional pressure drop, an equivalent length of 0.7m is used as prescribed by ASHRAE (1985).

$$\Delta P_{\text{grav}} = \text{DBPT}(P_w/100, T_w)g.S_T \quad \dots(5.3.71)$$

The rest of the terms remain the same.

5.3.11 Gas side pressure drop theory

Theory for the gas side pressure drop was obtained from Mills (1995), for flow through staggered tube banks. The first step is to calculate the mean film temperature for each row, which is based on the tube wall temperature and the average of the inlet and outlet bulk gas temperatures. The wall temperature of each control volume is approximated after which an average is taken over each row...

$$T_{\text{wall}} = T_{\text{gas}} - (T_{\text{gas}} - T_w)/100 \quad \dots(5.3.72)$$

$$T_{\text{wall,av}} = (\Sigma T_{\text{wall}})_{\text{row}} / (CV_{\text{tube}} \cdot N_t) \quad \dots(5.3.73)$$

Then an average gas temperature for each row is approximated...

$$T_{\text{av}} = 0.5(T_{\text{wall,av}} + 0.5(T_{\text{gas,in}} + T_{\text{gas,out}})) \quad \dots(5.3.74)$$

Once a mean film temperature is determined, the gas properties can be evaluated.

The average gas density is...

$$\rho = 354.26 T_{\text{av}}^{-1.003} \quad \dots(5.3.75)$$

and the average gas kinematic viscosity...

$$\nu = (0.0010752 T_{\text{av}}^{1.68058448}) \cdot 10^{-6} \quad \dots(5.3.76)$$

The equation for the empty duct velocity is ...

$$V_o = \dot{m}_{\text{gas}} / (\rho_{\text{gas}} \cdot H \cdot L_t) \quad \dots(5.3.77)$$

while the maximum velocity is determined by...

$$V_{\text{max}} = V_o \cdot \max \left\{ \frac{S_T}{S_T - D}, \frac{S_T/2}{[S_L^2 + (S_T/2)^2]^{0.5} - D} \right\} \quad \dots(5.3.78)$$

From this, the maximum Reynolds number can be determined as...

$$Re_{\text{max}} = V_{\text{max}} \cdot Od_t / \nu \quad \dots(5.3.79)$$

The dimensionless transverse and longitudinal pitch is determined by...

$$P_T = S_T / Od_t \quad \dots(5.3.80)$$

$$P_L = S_L / Od_t \quad \dots(5.3.81)$$

By using the ratio of the transverse and longitudinal pitch...

$$Z = P_T / P_L \quad \dots(5.3.82)$$

along with figure 4.44b, p318 Mills (1995), χ and f can be determined.

The end result is the following equation which predicts the pressure drop across a single row...

$$\Delta P_{\text{gas}} = \chi \cdot \rho \cdot V_{\text{max}}^2 \cdot f / 2 \quad \dots(5.3.83)$$

5.3.12 Fin efficiency

The fin efficiency theory is used as described by Kröger (1998) for radial fins. The efficiency is determined by two constants...

$$b = (2h_{\text{gas}} / (k_f \cdot t_f))^{0.5} \quad \dots(5.3.84)$$

$$\phi = ((\text{Od}_t + 2H_f) / \text{Od}_t - 1) \cdot (1 + 0.35 \text{Ln}((\text{Od}_t + 2H_f) / \text{Od}_t)) \quad \dots(5.3.85)$$

which gives the fin efficiency as...

$$F_{\text{eff}} = (\tanh(b \cdot \text{Od}_t \cdot \phi / 2)) / (b \cdot \text{Od}_t \cdot \phi / 2) \quad \dots(5.3.86)$$

5.3.13 Overall heat transfer coefficient for a control volume

In order to simplify the equation for the overall heat transfer coefficient, it has been split into three parts:

$$\text{term1} = \frac{1}{h_w A_w} \quad \dots(5.3.87)$$

$$\text{term2} = \frac{\ln(\text{Od}_t / \text{Id}_t)}{2\pi k_t p_f} \quad \dots(5.3.88)$$

$$\text{term3} = \frac{1}{h_{\text{gas}} \left(2F_{\text{eff}} \left(\frac{\pi(\text{Od}_t + 2H_f)^2}{4} - \frac{\pi \text{Od}_t^2}{4} \right) + \pi \text{Od}_t (p_f - t_f) \right)} \quad \dots(5.3.89)$$

The overall heat transfer coefficient for the control volume is then the inverted sum of all three parts...

$$UA_{\text{cv}} = (\text{term1} + \text{term2} + \text{term3})^{-1} \quad \dots(5.3.90)$$

5.3.14 Heat exchanger effectiveness

The heat exchanger effectiveness is determined by using the NTU-method (Number of Transfer Units) as described by Kröger (1998).

First the average water temperature and pressure, as well as the average gas temperature across the heat exchanger is calculated as...

$$T_{w,av} = (T_{w,inlet} + T_{w,outlet})/2 \quad \dots(5.3.91)$$

$$P_{w,av} = (P_{w,inlet} + P_{w,outlet})/2 \quad \dots(5.3.92)$$

$$T_{gas,av} = (T_{gas,inlet} + T_{gas,outlet})/2 \quad \dots(5.3.93)$$

The specific heat for both the water and gas is determined with $T_{gas,av}$ in Kelvin ...

$$Cp_w = CPBPT(P_{w,av}/100, T_{w,av}) \quad \dots(5.3.94)$$

$$Cp_{gas} = 9.7465 \times 10^{-15} T_{gas,av}^6 - 3.3779 \times 10^{-11} T_{gas,av}^5 + 4.6182 \times 10^{-8} T_{gas,av}^4 - 3.2123 \times 10^{-5} T_{gas,av}^3 + 0.012464 T_{gas,av}^2 - 2.5903 T_{gas,av} + 1230.2 \quad \dots(5.3.95)$$

The maximum and minimum capacity as well as the capacity ratio can be determined as follows...

$$C_{max} = \max\{\dot{m}_w Cp_w, \dot{m} Cp_{gas}\} \quad \dots(5.3.96)$$

$$C_{min} = \min\{\dot{m}_w Cp_w, \dot{m} Cp_{gas}\} \quad \dots(5.3.97)$$

$$C = C_{min} / C_{max} \quad \dots(5.3.98)$$

By taking the total overall heat transfer coefficient as the sum of the heat transfer coefficients of each control volume over the heat exchanger, the number of transfer units can be determined as...

$$n = UA_{tot} / C_{min} \quad \dots(5.3.99)$$

after which the heat exchanger effectiveness is determined by...

$$eff = \frac{1 - e^{(-C(1-e^{-n}))}}{C} \quad \dots(5.3.100)$$

for C_{max} mixed and C_{min} unmixed.

5.3.15 Gas heat transfer coefficient

The calculation of the gas heat transfer coefficient is as follow:

Minimum flow area...

$$A_{cv,crit} = (S_T - Od_t)(p_f - t_f) \quad \dots(5.3.101)$$

Frontal area...

$$A_{cv,fr} = S_T \cdot p_f \quad \dots(5.3.102)$$

Area ratio...

$$\sigma_{gas} = A_{cv,crit}/A_{cv,fr} \quad \dots(5.3.103)$$

Hydraulic diameter of the control volume...

$$D_{hyd,cv} = 4A_{cv,crit} \cdot S_L / A_{gas} \quad \dots(5.3.104)$$

Mass velocity through the minimum free flow area of the core...

$$G_{ai} = \dot{m}_{gas} / (A_{fr} \cdot \sigma_{gas}) \quad \dots(5.3.105)$$

Dynamic viscosity...

$$\mu_{gas} = (0.3399(T_{gas,in} + 273.15)^{0.6988})10^{-6} \quad \dots(5.3.106)$$

Specific heat with $T_{gas,in}$ in Kelvin ...

$$Cp_{gas} = 9.7465 \times 10^{-15} T_{gas,in}^6 - 3.3779 \times 10^{-11} T_{gas,in}^5 + 4.6182 \times 10^{-8} T_{gas,in}^4 - 3.2123 \times 10^{-5} T_{gas,in}^3 + 0.012464 T_{gas,in}^2 - 2.5903 T_{gas,in} + 1230.2 \quad \dots(5.3.107)$$

Reynolds number...

$$Re_{gas} = G_{ai} \cdot D_{hyd,cv} / \mu_{gas} \quad \dots(5.3.108)$$

Conductivity with $T_{gas,in}$ in Kelvin ...

$$k_{gas} = 1.5335 \times 10^{-11} T_{gas,in}^3 - 3.4122 \times 10^{-8} T_{gas,in}^2 + 8.0835 \times 10^{-5} T_{gas,in} + 0.0052078 \quad \dots(5.3.109)$$

Prandtl number...

$$Pr_{gas} = \mu_{gas} \cdot Cp_{gas} / k_{gas} \quad \dots(5.3.110)$$

Stanton number...

$$Stan = (0.1353 Re_{gas}^{-0.3733}) / Pr_{gas}^{0.667} \quad \dots(5.3.111)$$

Heat transfer coefficient...

$$h_{gas} = Stan \cdot G_{ai} \cdot Cp_{gas} \quad \dots(5.3.112)$$

5.3.16 Water liquid heat transfer coefficient

The calculation of the water liquid heat transfer coefficient is as follow:

Dynamic viscosity of water with T_w in Kelvin...

$$\mu_w = (6.85237 \times 10^{-13} T_w^6 - 1.84821 \times 10^{-9} T_w^5 + 2.06206 \times 10^{-6} T_w^4 - 0.00121859 T_w^3 + 0.40256 T_w^2 - 70.5636 T_w + 5138.27) 10^{-4} \quad \dots(5.3.113)$$

Reynolds number...

$$Re_w = 4 \dot{m}_w / (\pi I_d \mu_w) \quad \dots(5.3.114)$$

Specific heat (*IAPWS-IF97*)...

$$C_{p_w} = CPLBT(T_w) \quad \dots(5.3.115)$$

Conductivity with T_w in Kelvin...

$$k_w = 2.65607 \times 10^{-15} T_w^6 - 6.18308 \times 10^{-12} T_w^5 + 5.81552 \times 10^{-9} T_w^4 - 2.80589 \times 10^{-6} T_w^3 + 7.16693 \times 10^{-4} T_w^2 - 0.0870087 T_w + 3.95284 \quad \dots(5.3.116)$$

Prandtl number...

$$Pr_w = \mu_w \cdot C_{p_w} / k_w \quad \dots(5.3.117)$$

Nusselt number...

$$Nu_w = 0.0243 Re_w^{0.8} \cdot Pr_w^{0.4} \quad \dots(5.3.118)$$

Water liquid heat transfer coefficient...

$$h_w = Nu_w \cdot k_w / I_d \quad \dots(5.3.119)$$

5.3.17 Water vapour heat transfer coefficient

As mentioned previously, the vapour heat transfer coefficient is determined in almost the same manner as the liquid heat transfer coefficient, with the exception that the vapour properties differ from the liquid properties. (Note again that the subscripts are still “w” which refer to water and not to the liquid phase as such.)

Dynamic viscosity of water vapour with T_w in Kelvin...

$$\mu_w = 6E-8 T_w^{0.9266} \quad \dots(5.3.120)$$

Reynolds number...

$$Re_w = 4 \dot{m}_w / (\pi Id_t \mu_w) \quad \dots(5.3.121)$$

Specific heat (*LAPWS-IF97*)...

$$Cp_w = CPVBT(T_w) \quad \dots(5.3.122)$$

Conductivity with T_w in Kelvin ...

$$k_w = 0.00001 T_w^{1.256} \quad \dots(5.3.123)$$

Prandtl number with T_w in Kelvin ...

$$Pr_w = 6E-8 T_w^2 - 0.0002 T_w + 1.0314 \quad \dots(5.3.124)$$

Nusselt number...

$$Nu_w = 0.0243 Re_w^{0.8} Pr_w^{0.4} \quad \dots(5.3.125)$$

Water vapour heat transfer coefficient...

$$h_w = Nu_w k_w / Id_t \quad \dots(5.3.126)$$

5.3.18 Final energy balance calculations

This last theory section discusses the total amount of energy transferred in the whole heat transfer process. In addition, the energy values calculated by the control volume simulation are verified by heat transfer theory calculations.

The total amount of energy transferred from the gas to the water is...

$$\text{EnergyTransf} = (\Sigma Q_{\text{transf}})_{H.E.} \quad \dots(5.3.127)$$

while the maximum available energy that can be transferred is given by...

$$\text{AvailEnergy} = \text{EnergyTransf} / \text{eff} \quad \dots(5.3.128)$$

where “eff” refers to the heat exchanger effectiveness.

In the data file created by the simulation program, there are alternative energy values for both water and gas. These values have been generated using bulk heat transfer theory where for instance the water heat transfer is divided into three sections; preheating, latent heat (boiling) and superheating. If the water does not reach the superheated state, the quality of the water is taken into account to calculate the correct energy content.

The equations are as follow:

For water...

$$PH = \dot{m}_w(CPLBT(T_{w,@Tsat}) \cdot T_{sat} - CPLBT(T_{w,inlet}) \cdot T_{w,inlet}) \quad \dots(5.3.129)$$

$$BH = \dot{m}_w((x \cdot HVB(T_{w,@Tsat}) + (1 - x) \cdot HLBT(T_{w,@Tsat})) - HLBT(T_{w,@Tsat})) \quad \dots(5.3.130)$$

$$SH = \dot{m}_w(CPVBT(T_{w,outlet}) \cdot T_{w,outlet} - CPVBT(T_{w,@Tsat}) \cdot T_{w,@Tsat}) \quad \dots(5.3.131)$$

$$Water_{energy} = PH + BH + SH \quad \dots(5.3.132)$$

For gas (where the Cp values are determined as previously stated)...

$$Gas_{energy} = \dot{m}_{gas}(CP_{gas,inlet} \cdot T_{inlet} - CP_{gas,outlet} \cdot T_{outlet}) \quad \dots(5.3.133)$$

5.3.19 Conclusion

The equations explained in section 5.3, have all been used in the simulation. Section 5.5 refers to the relevant calculations done by the program and discusses the results in detail.

Along with this thesis, a CD was created which contains the code of the simulation program as well as all generated data used in this thesis. The data files can be opened in Microsoft Excel. A comma must be used as the delimiter to ensure that the file opens correctly.

In the theory discussed above, various other resources were used that were not specifically named. These sources are Çengel and Boles (1994), Holman (1992), Premoli et al. (1970) and White (1999).

5.4 MICROSOFT® EXCEL 2002 SPREADSHEET

5.4.1 Introduction

As previously mentioned, an Excel spreadsheet was used as familiarisation tool with the heat exchanger theory. It consists of a single iteration of the whole system with average temperature values used across each phase of the heat exchanger used to determine the fluid and gas properties. The simulation is a fairly robust and inaccurate model, but served its purpose none the less. Appendix G contains some screen prints of the simulation spreadsheet.

5.4.2 Main sheet

The main sheet serves as an introduction to the simulations. It gives a description of all the necessary inputs needed as well as the outputs calculated. The whole spreadsheet simulation works on a colour coded principle to enable the user to easily identify the data categories: YELLOW \Rightarrow variables or user inputs; BLUE \Rightarrow table data which the user has to choose from the property tables; BROWN \Rightarrow calculated data automatically done by the spreadsheet; GREEN \Rightarrow the final answers supplied by the simulation. Also on the main sheet is a summary of all the heat exchanger geometries.

5.4.3 Energy balance

This sheet contains an overview of the whole process and is presented in the form of an energy balance. It contains a figure where the user can graphically see the temperature distribution through the heat exchanger.

The main disadvantage of the simulation is the fact that it is not an iterative process. The outlet temperature of the gas must be randomly chosen after which the simulation determines the appropriate energy balance and resulting temperatures. By using this figure, the user can then see whether the chosen outlet temperature is viable or not, because of certain restrictions specified on the sheet. This is a very crude way of determining the resulting energy transfers, but by using the spreadsheet the user gains an insight as to how a heat exchanger works and how the input values influence each other.

5.4.4 Different phase stages

Preheating stage:

The preheating stage uses water as working medium and the heat transfer calculations are done until the quality of the water becomes greater than 0. This stage mainly serves as a means to establish the theory involved in preheating water. When the heat exchanger specifications are typed onto the sheet, they are automatically uploads to the remainder of the phase sheets. The preheating sheet calculates the heat transfer on the exhaust side as well as the water side, after which the effectiveness of the heat exchanger is determined. Finally the total heat transfer done by the preheating stage is calculated. The supposed amount of energy transfer needed, is read from the energy balance sheet and checked against the value calculated on the preheating sheet. The aim of calculating each stage separately is to determine the number of finned tubes and rows needed for each stage of the heat exchanger, i.e. the amount energy transferred is varied by altering the number of tubes or rows.

Boiler stage:

The boiler stage works in much the same way as the preheating stage, except that the water flow in the boiler is mixed liquid and vapour. In an effort to simplify the calculations, the liquid and vapour is examined separately. The calculations remain the same for both with only the fluid and vapour properties changing. The result is an upper and lower limit for the number of tubes and rows necessary to attain the specified energy transfer set by the energy balance sheet.

Superheating phase:

The last stage is the superheating stage. Here the working fluid is vapour. All that has to be changed from the theory of the preheating stage is the fluid properties. The rest of the sheet contains the same calculations as the other two stages and results in the total energy transferred to the steam (checked against the energy balance sheet), as well as the amount of tubes and rows needed by the superheated stage to enable the necessary energy transfer.

5.4.5 Rankine cycle

The second last sheet refers to a Rankine cycle analysis of the specified system. The reason for incorporating this sheet into the simulation is to determine how much energy can be recovered from the system using a Rankine cycle and what range of efficiencies can be accomplished by doing so.

5.4.6 Exhaust and water pressure drops

The last sheet contains a pressure drop analysis on the exhaust side and the water side of the heat exchanger. On the water side the sheet takes into account the frictional pressure loss as well as the losses incurred by the U-bends. The U-bends are accounted for by using the equivalent length of 0.7m set by ASHRAE (1985) for each U-bend. The main disadvantage that the pressure calculations have is the fact that they only take the frictional pressure drop in the tubes into account when determining the total pressure loss. The accelerational and gravitational pressure loss is not included in these calculations. Pressure drop theory through fin tube bundles, as explained by Mills (1995), is used to determine the exhaust side pressure drop.

5.4.7 Conclusions

Although the spreadsheet simulation is only a small stepping-stone in the whole project, its value has been to steepen the gradient of the learning curve. Nearly all of the basic heat exchanger theory features in the spreadsheet (except for the obvious two-phase correlations) and helped to refresh the basic thermodynamic knowledge obtained in undergraduate studies. However, the simulation is very inaccurate and its results can understandably not be compared to that of the iterative control volume simulation program which was written in Microsoft® Visual Basic and is explained in the next section.

5.5 MICROSOFT® VISUAL BASIC 6.0 SIMULATION PROGRAM (HESP)

5.5.1 Introduction

The simulation program is called the “Heat Exchanger Simulation Program (HESP)”. The aim of the program is to use fintube heat transfer theory in order to estimate the resulting pressures and temperatures when water and exhaust gasses are used inside a mixed cross flow, shell-and-fintube heat exchanger.

The analysis was divided into three parts: the preheated stage, the boiler stage and the superheated stage. For both the preheated- and superheated stage, single-phase theory was used, while two-phase theory was used for the boiler stage. This included the Friedel frictional two-phase pressure gradient correlation – Whalley (1987), Chen’s boiling heat transfer to saturated fluids in convective flow correlation – Chen (1963) and the CISE void fraction correlation – Whalley (1987) (*see appendix F*).

The program is valid for all pressures and temperatures, as long as the outlet pressure inside the heat exchanger, on the water side, is at or above atmospheric pressure, i.e. the inlet pressure must be sufficient to overcome the pressure losses inside the heat exchanger fintubes.

The program uses the following known values: the water inlet temperature, pressure and mass flow rate as well as the exhaust inlet temperature, pressure and mass flow rate. Because the fluid and air flow is cross flow, the water outlet will be on the same side as the exhaust gas inlet and visa versa. This makes the iteration process essential in the determination of the correct outlet values of both the water and exhaust gas.

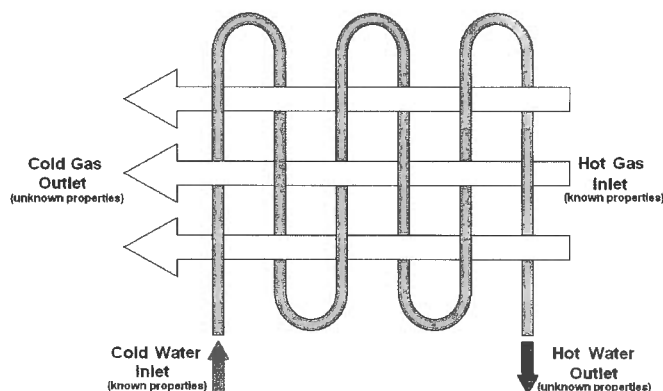


Figure 5.5: Flow directions inside the heat exchanger

By approximating an outlet temperature for the exhaust gas (1max), the temperatures for both the water outlet and exhaust gas inlet can be determined. The error between the correct and estimated exhaust gas inlet temperatures is then considered. Depending on whether the estimated temperature is too high or too low, the approximated value is decreased or increased by a certain set value (1min).

Once the correct exhaust gas inlet temperature has been bracketed by two approximated outlet values (which results in one inlet temperature higher (1max) and one lower (1min) than the correct exhaust inlet temperature), the Davis-Swann method is used to determine the correct exhaust gas outlet temperature. This entails that the average of the bracket is taken as the new approximated value (2max), and depending on whether this value results in a higher or lower estimation of the correct exhaust inlet temperature; it will become the new maximum or minimum value of the bracket.

This process is repeated until the approximated inlet temperature (4answ) corresponds with the specified inlet temperature of the exhaust gas.

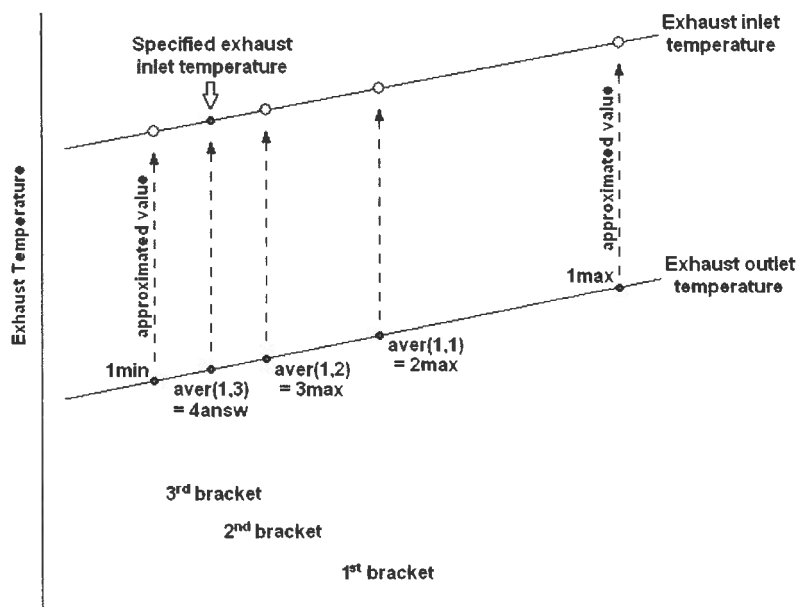


Figure 5.6: Davis-Swann method (Papalambros and Wilde, 2000)

The information source on the Davis-Swann iteration method was Papalambros and Wilde (2000). A full explanation as to how the simulation program is operated can be found in appendix H. The main programming aid used to write the simulation program was Schneider (1999).

5.5.2 Simulation

To illustrate how the program works, an example will be done after which the results will be discussed.

Inlet conditions	Gas	Water	Units
Temperature	400	25	[°C]
Pressure	101.4	1000	[kPa]
Mass flow rate	0.0233	0.0015	[kg/s]

Table 5.1: Gas/fluid input values

When the data in table 5.1 is fed into the program along with the default geometry values (which are set to the heat exchanger in question) and the calculation process is initiated, the following iterations result in a converging exhaust inlet temperature and error.

In figure 5.7 the first approximated value was taken at 220°C. This value could have been taken higher or lower, which would have influenced the amount of iterations. The level of accuracy needed will also influence the amount of iterations. The smaller the error, the higher the number of iterations, and visa versa.

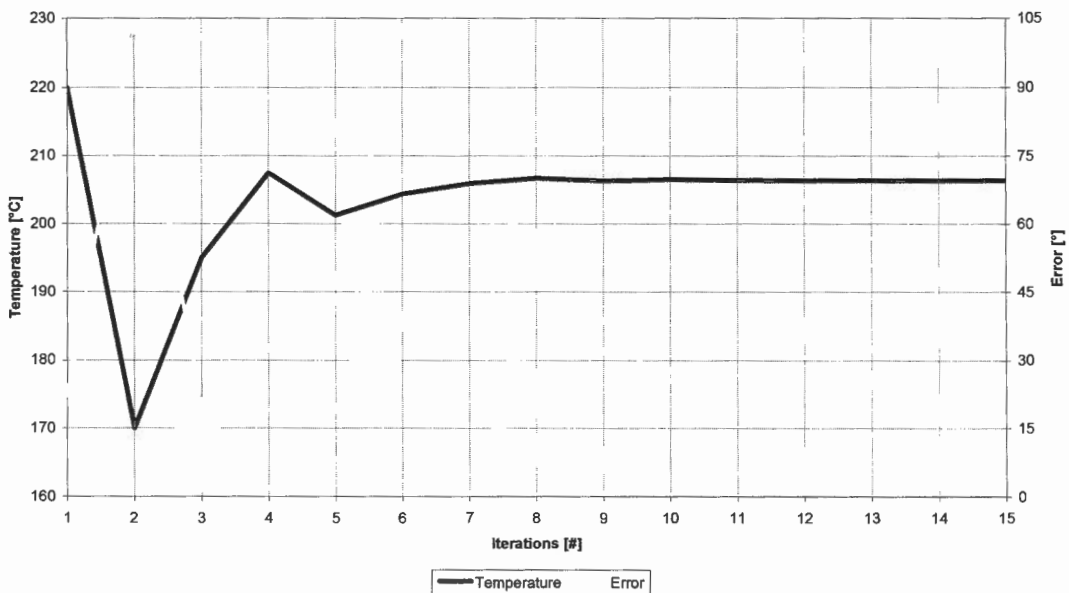


Figure 5.7: Temperature and error convergence

The table below shows a summary of the relevant simulation data.

<u>Input Data:</u>		<u>Implicit Geometries:</u>	
Exhaust Temperature In	399.996 [°C]	Tube Thickness	0.003 [m]
Exhaust Pressure In	101.4 [kPa]	Heat Exchanger Height	0.35874 [m]
Exhaust Mass Flow Rate	0.023333 [kg/s]	Heat Exchanger Frontal Area	0.107622 [m ²]
Water Temperature In	25 [°C]	Area Exposed to Exhaust	0.00098643 [m ²]
Water Pressure In	1000 [kPa]	Area Exposed to Water	0.00012566 [m ²]
Water Mass Flow Rate	0.0015 [kg/s]	<u>Output Data:</u>	
Tube Thermal Conductivity	18 [W/m.K]	Available Energy	5.308 [kW]
Tube Length	0.3 [m]	Energy Recovery	4.649 [kW]
Tube Outer Diameter	0.022 [m]	H.E. Effectiveness	87.59 [%]
Tube Inner Diameter	0.016 [m]	Average Fin Efficiency	96.27 [%]
Longitudinal Pitch	0.0371 [m]	Exhaust Energy Transf (HTT)	4.681 [kW]
Transverse Pitch	0.04288 [m]	Water Energy Transf (HTT)	5.812 [kW]
Fin Thermal Conductivity	18 [W/m.K]	Exhaust Outlet Temperature	206.383 [°C]
Fin Thickness	0.0005 [m]	Exhaust Outlet Pressure	101.4 [kPa]
Fin Pitch	0.0025 [m]	Exhaust Pressure Drop	0.000122 [kPa]
Fin Height	0.005 [m]	Water Outlet Temperature	291.763 [°C]
# Tubes per Row	8 [#]	Water Outlet Pressure	982.839 [kPa]
# Rows in Heat Exchanger	5 [#]	Water Pressure Drop	17.161 [kPa]

Table 5.2: Simulation program input and output summary

As presented by the results of the simulation program in table 5.2, the maximum transferable energy from the exhaust to the water is 5.308kW, while the amount of energy recovered by the water is only 4.649kW. The difference in these two values (659W) is due to the effectiveness of the heat exchanger and does not include any losses that would occur in the system.

None the less, the theoretical effectiveness of the heat exchanger is still relatively high at 87.59%, while the average fin efficiency across the heat exchanger is even higher at 96.27%. The high fin efficiency can be attributed to the fact that the fin height of 5mm was optimised.

The next output values of the water and exhaust energy transfer (*indicated by HTT, see table 5.2*) has been calculated using bulk heat transfer theory as described in section 5.3.18. These values are different from the values based on the control volume simulation, but are used to give an idea of the magnitude of transferred energy expected in the simulation. Lastly, the outlet temperatures, pressures and pressure drops of the water and exhaust are presented.

The following pages contain figures plotted from the data generated by the simulation program.

Figure 5.8 contains the water temperature curve as well as three curves for the exhaust temperature. Of the two stepped curves, the top one is the inlet temperature to every control volume, while the bottom curve is the outlet temperature. The dotted black curve is a fit through these two stepped curves and provides a good indication as to what the temperature distribution inside the heat exchanger will be.

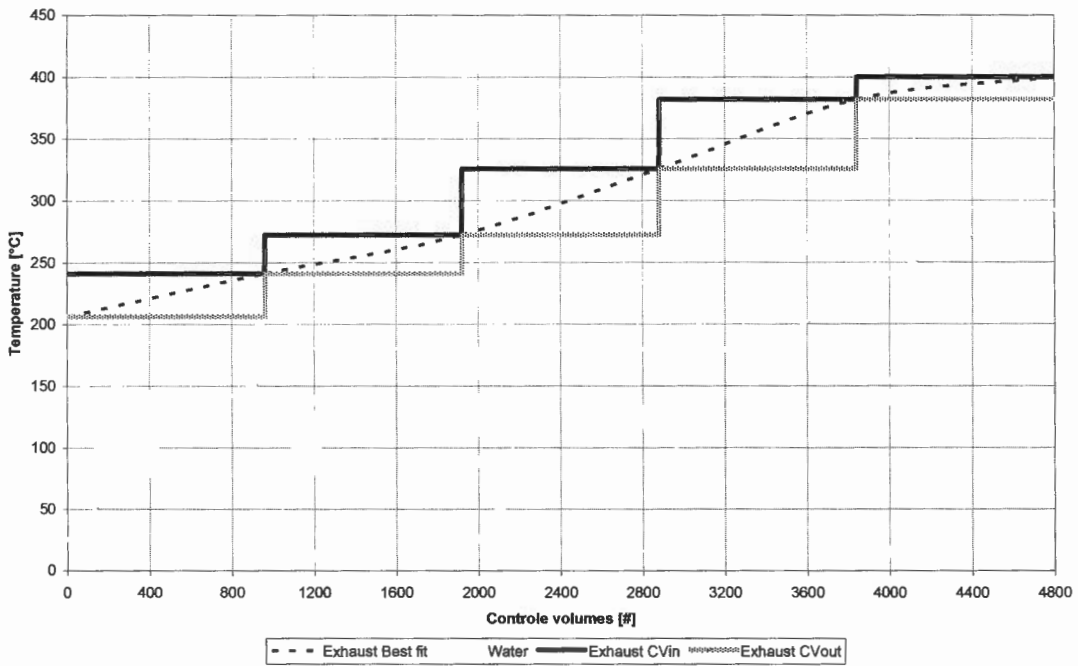


Figure 5.8: Exhaust and water temperature distribution across the heat exchanger

The temperature pinch point can clearly be seen at the 1197th control volume. The energy transfer can be maximized by minimizing the difference between the exhaust and water temperature at this point. The beginning of the 2nd row is marked by a steeper gradient in the water temperature at the 961st control volume. This pronounced change is due to the fact that the exhaust temperature changes from one row to the next. Thus the water entering the 2nd row comes into contact with the hotter exhaust gas which will increase the overall heat transfer coefficient.

It can also be seen that less energy is transferred to the water as the quality of the water rises. This is expected, as the density of the water vapour mixture decreases with the increase in quality. It results in a lower heat transfer coefficient and is confirmed by

figure 5.9 where the heat transfer drops dramatically when the water nears the 100% quality mark. This occurrence is also in part due to dryout that occurs inside the tubing when all the water evaporates.

Figure 5.8 also indicates a slight drop in the water temperature as the quality increases. This is due to the pressure drop inside the tubes, and subsequent saturation temperature drop of the water.

As mentioned earlier, the heat transfer in the heat exchanger acts exactly as suggested by two-phase heat transfer theory (*see section 4.2.2*). In figure 5.9 it is evident that the heat transfer coefficient increases for most part of the vaporization process when nucleate boiling is dominant. When the heat transfer coefficient curve reaches its apex, the nucleate boiling is suppressed while a mist flow inside the tube is formed. It is also after the 3200th control volume that the partial dryout of the tube initiates. Both the water quality and heat transfer coefficient curves have substantial gradient changes. In the case of the heat transfer coefficient there are discontinuities where the coefficient increases by between 125 and 250W/m².K. These changes occur at control volumes 1196 when single phase theory changes to two-phase theory, and at 1920 and 2880 where the exhaust temperature steps down after every row, as illustrated in figure 5.8. The two-phase theory, Chen (1963) correlation, is exhaust temperature dependant.

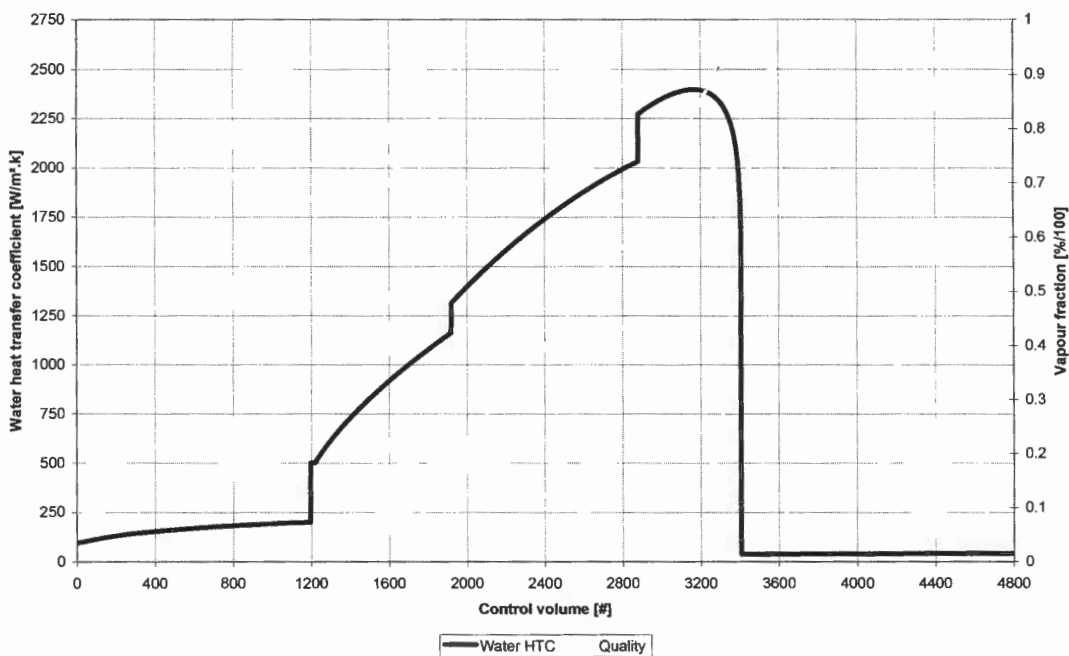


Figure 5.9: Water heat transfer coefficient and quality using equation 5.5.2

Attempts have been made to eradicate these discontinuities which led to an equation that is dependant only on the water temperature. The resulting data, shown in figure 5.10, gave an average energy transfer error increase equal to 2%, compared to the data in figure 5.9.

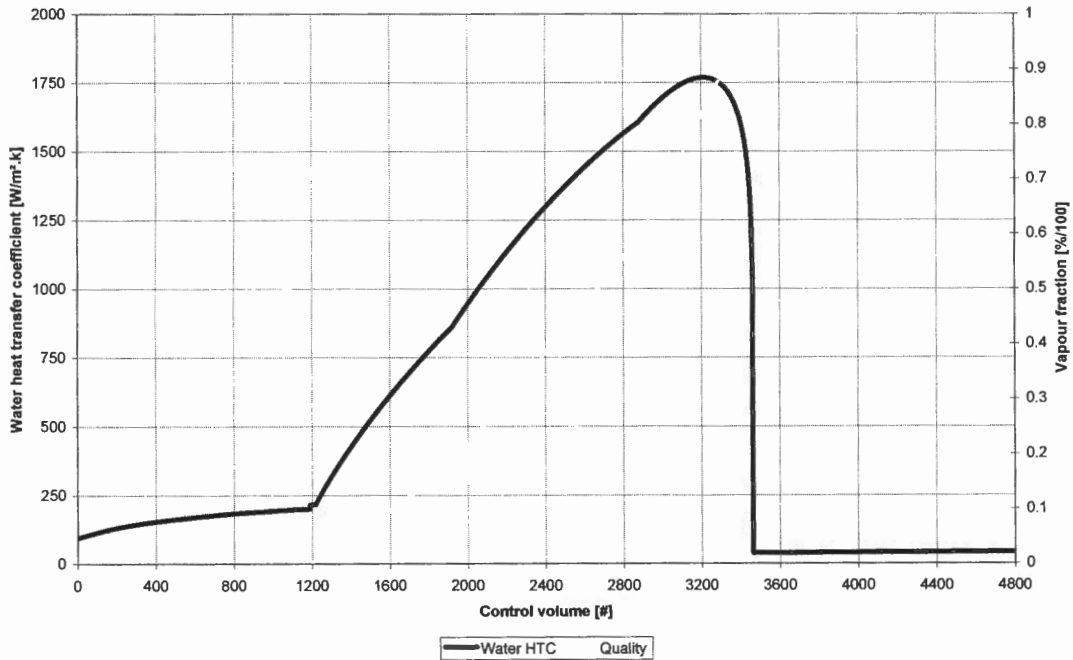


Figure 5.10: Water heat transfer coefficient and quality using equation 5.5.3

As illustrated above, the point where the water reaches 100% quality is slightly retarded compared to figure 5.9, due to the fact that the energy transfer rate to the water is less. The equation for T_{wall} , where ΔT_{sat} (equation F18) is dependant on T_{wall} , is...

$$\Delta T_{sat} = T_{wall} - T_{sat} \quad \dots(5.5.1)$$

Where the equation for T_{wall} used in figure 5.9 is...

$$T_{wall} = \frac{[T_{gas} - T_w]}{500} + T_w \quad \dots(5.5.2)$$

and the equation for T_{wall} used in figure 5.10 is...

$$T_{wall} = 1.0000577T_w \quad \dots(5.5.3)$$

Because of the error increase, and to show the true reflection of the stepped exhaust temperature function on the properties of the working fluid, equation 5.5.3 was not used in the simulation program, although it reflects a more continuous heat transfer coefficient.

Figure 5.11 show the velocities of both the exhaust gas and the water. Here the exhaust velocity decreases in steps resulting from the fact that the velocity is a function of exhaust temperature. The two-phase water velocity is a function of water mass flow rate, inner

tube diameter and the homogeneous density of the mixture, while the density is a function of the water temperature and quality.

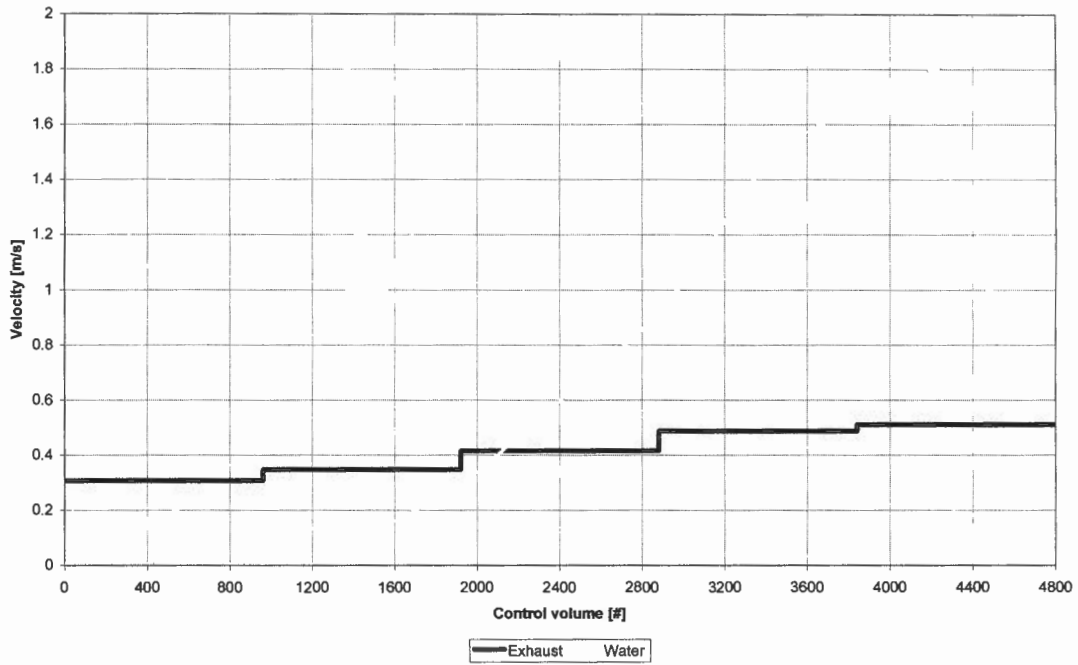


Figure 5.11: Exhaust and water velocities across the heat exchanger

Figure 5.12 show the pressure drop over the heat exchanger on both the exhaust and water side. A stepped curve is evident in both cases.

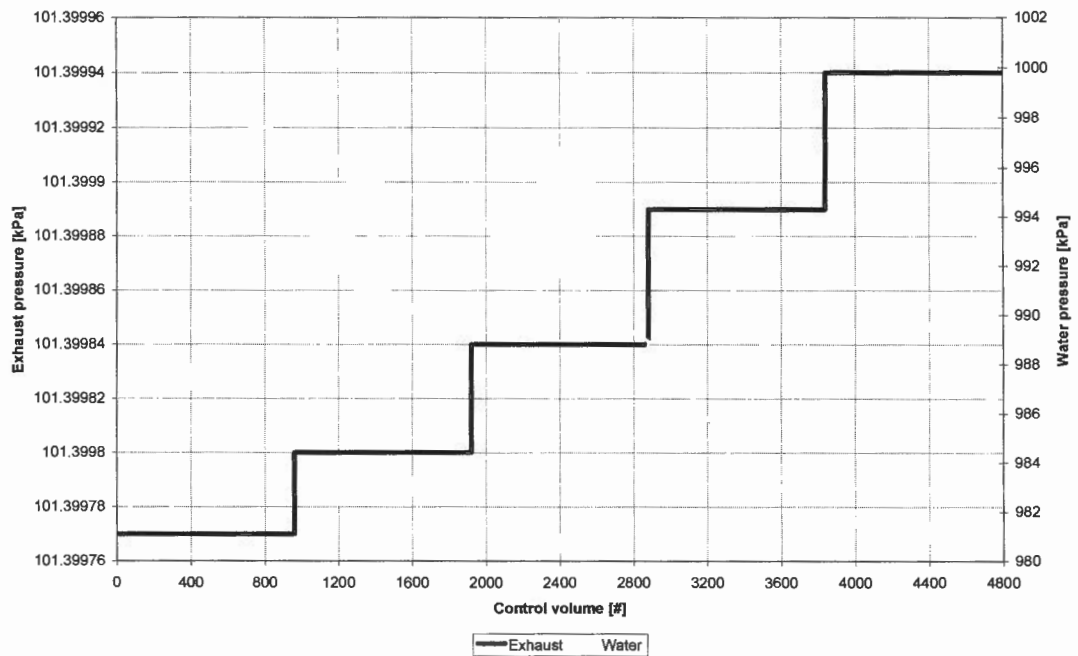


Figure 5.12: Pressure drop across the heat exchanger

The exhaust pressure takes a step down every time the flow passes through a fintube row, while the water pressure drop consists of four components: friction in the tubes;

gravitational pressure drop from one tube to the next; accelerational pressure drop of the fluid flow; and U-bends (which accounts for the vertical drops in pressure).

In theory the U-bends can be converted to equivalent tube lengths. The equivalent length prescribed by ASHRAE (1985) is 0.7m, i.e. the heat exchanger is seen as one straight tube. Another assumption made is that the U-bends are well insulated so that no heat loss occurs. In practise the insulation has been done using insulating wool.

The specific heat of the exhaust gas also follows a decreasing stepped curve as expected. The water specific heat reacts differently. In the preheated and superheated sections it increases, while it decreases in the two-phase region. The reason for this is that the water and vapour temperature increases in the preheated and superheated sections, which would lead to an increase in specific heat. On the other hand, the water in the two-phase region is vaporising and the temperature should stay relatively constant. However, it starts to drop due to pressure losses inside the tubes, which force the saturation temperature down. Thus, the specific heat of the mixture also drops.

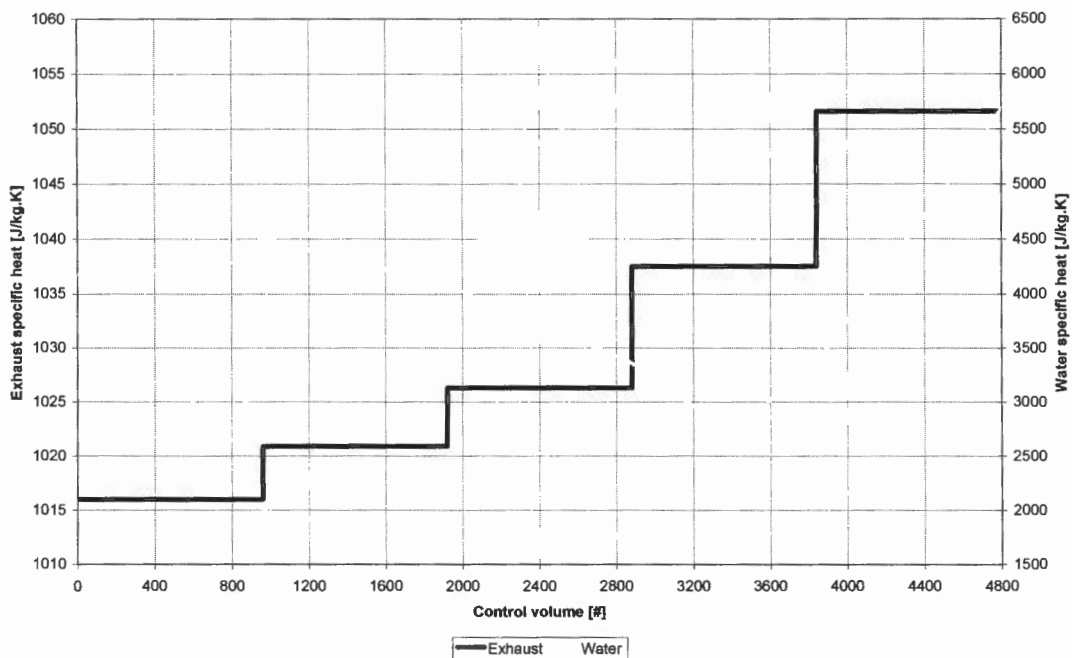


Figure 5.13: Exhaust and water specific heat across the heat exchanger

The data in figure 5.14, corresponds to data provided by Odeh et al. (1998) where the modelling of a parabolic trough with direct steam generation was done. The first horizontal line indicates water or the preheated region, the vertical line indicates the two-

phase region and the last horizontal line indicates the steam or superheated region. The reason why the simulation data of the heat exchanger correspond with that of Odeh, who is simulating a parabolic trough, is because a heat exchanger is nothing more than a parabolic trough with the collector replaced by fins and the absorption-tube neatly folded into a zigzagged configuration.

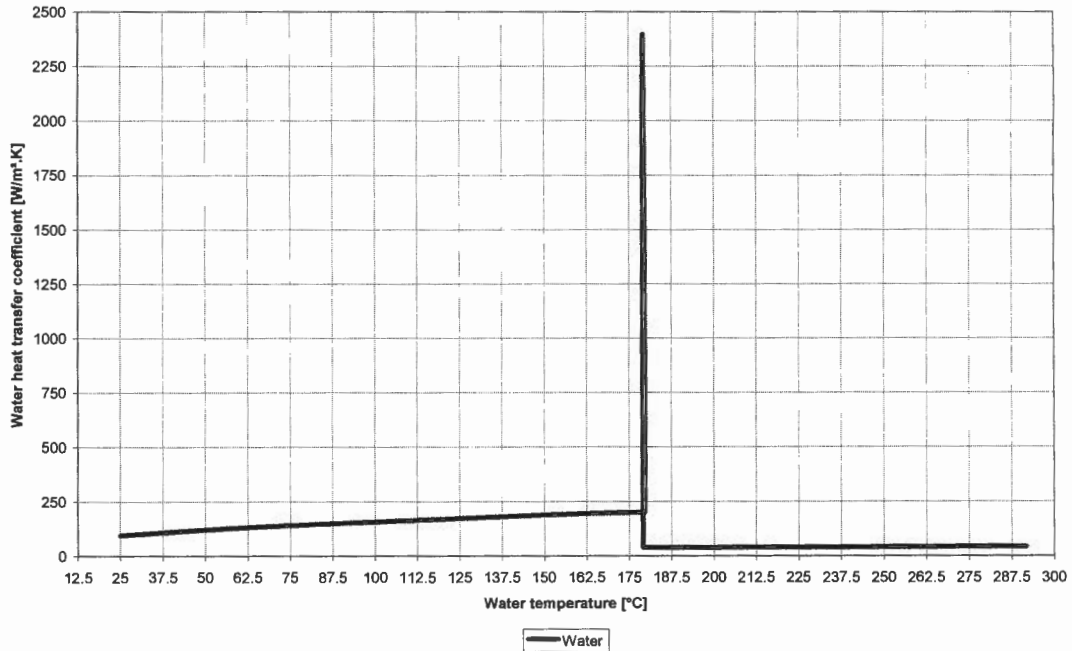


Figure 5.14: Water heat transfer coefficient vs. temperature

5.5.3 Conclusions

The data generated by the heat exchanger simulation program seems promising in that the results obtained is as would be expected from the various thermodynamical theories considered such as described in chapter 4, section 5.3 and appendix F. The definite step in exhaust temperature is the only part of the simulation that could be improved on, as there would not be such a dramatic change in temperature across the fintube rows, but a gradual sloped temperature decrease. In that respect, the fitted curve over the stepped exhaust temperature in figure 5.8 is probably the best representation of the actual temperature fall. In section 7.4 the simulated results versus the experimental results will be discussed.

6. STRESS ANALYSIS

6.1 INTRODUCTION

In section 4.2.7 it was decided to use stainless steel in the construction of the fintubes. To ensure the safe use of this material in the heat exchanger application, the stress distribution in the U-bends and fintubes (caused by the internal pressure of the heat exchanger) were analysed.

As the fintubes and U-bends were to be welded together, the analysis was constrained in such a way as to simulate these conditions. The welding method used, was TIG-welding, and was expertly done by a qualified technician. As the U-bends were interference fitted inside the fintubes before welding took place, there was assured to be no leakage past the welds. In practise proper welds are considered to be stronger than the original material. Thus, it was assumed that the welded joints would withstand the pressure build-up inside the heat exchanger if the finite element analysis showed that the material would be strong enough to hold.

Stainless steel 316 seamless tubes were used for the U-bends and stainless steel 316L hollow bar was used for the fintubes. A total of 39 U-bends were used while 40 fin-tubes were turned out of 4 lengths of hollow bar. The design drawings for both the U-bends and the fintubes can be seen in appendix K, drawing numbers MSc.T-PW7 and MSc.T-PW1.

Data acquired on the stainless steel used from ASME (2001) are as follows:

	Nominal Composition	Max Allowable Stress @ 37°C [MPa]	Max Allowable Stress @ 454°C [MPa]	Min Tensile Strength @ STD [MPa]	Min Yield Strength @ STD [MPa]
Stainless Steel 316L Fintubes	16Cr-12Ni-2Mo	115.13	87.55	482.58	172.35
Stainless Steel 316 U-bends	16Cr-12Ni-2Mo	137.88	108.24	517.05	206.82

Table 6.1: Stainless steel data from ASME (2001)

6.2 FINITE ELEMENT ANALYSIS

The stress analysis for this project has been done on both a U-bend and fintube computer model using MSC/NASTRAN for Windows Version 2.0 (finite element analysis

package). The fintube was modelled as a 2D-wall section consisting of three fins and 3840 axisymmetric elements, while the U-bend was modelled as a 3D-tube consisting of 1720 2D-plate elements.

The analysis program breaks the model geometry up into small elements and calculates the internal stresses, after which it produces a graphical representation of the stress distribution inside the analysed part. In the case of the U-bend analysis, the principal stresses and the Von Mises stress for both the top and bottom (inside and outside) of the plate elements were analysed. During the fintube analysis, the azimuth (or hoop) stress, the radial stress, the axial stress and the Von Mises stress were examined. In this section only the Von Mises stresses will be shown. Appendix M contains the rest of the analysis results with the result discussions incorporated on pages M7-8.

The Von Mises yield criterion states that when the equivalent stress (based on the difference in the principal stresses present in a material) exceeds the yield stress, the material is deemed to have yielded. The equation used by Von Mises is ...

$$\sigma_e = \frac{1}{\sqrt{2}} \left[(\sigma_1 - \sigma_2)^2 + (\sigma_2 - \sigma_3)^2 + (\sigma_3 - \sigma_1)^2 \right]^{1/2} \quad \dots(6.2.1)$$

where σ_e is the equivalent stress and σ_1 , σ_2 and σ_3 are the principal stresses present in the material. Table 6.1 presents the allowable stresses inside stainless steel for the maximum and minimum applicable temperatures of this project. It must be noted that these values already contain a safety factor according to the ASME (2001) code standard.

6.2.1 U-bend

The bottom (inside) Von Mises stress present in the U-bend, as seen in figure 6.1, indicates that the stress varies between 12.78 and 5.34MPa. This is well inside the allowable stress of 108.24MPa as prescribed by ASME (2001) in table 6.1.

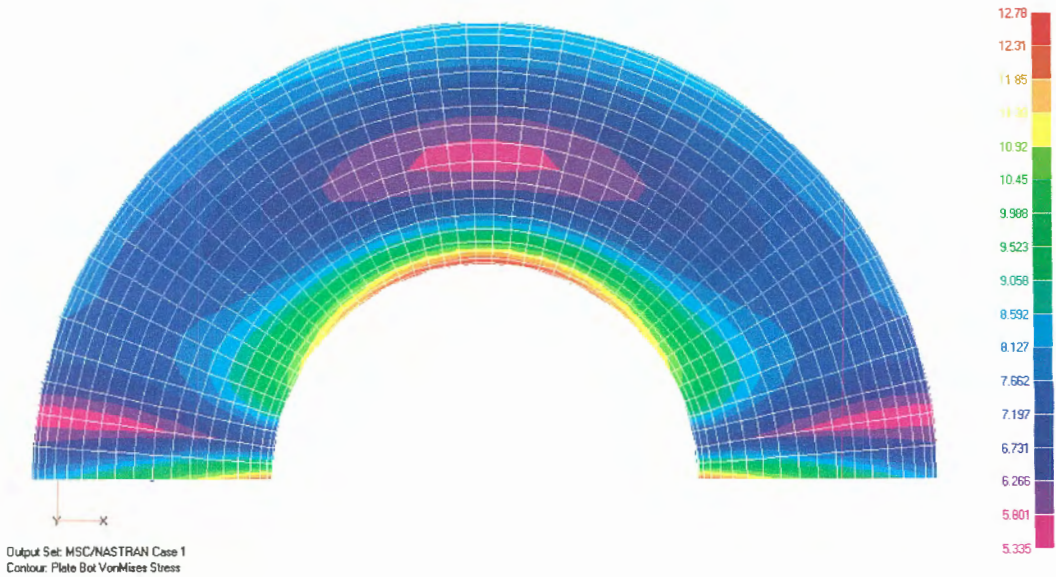


Figure 6.1: U-bend NASTRAN analysis: Bottom Von Mises stress [MPa]

The top (outside) Von Mises stress present in the U-bend, as seen in figure 6.2, indicates that the stress varies between 10.46 and 1.743MPa. The outside of the U-bend will experience a much lower stress distribution than the inside of the tube and it is therefore also lower than the allowable stress of 108.24MPa as prescribed by ASME (2001) in table 6.1.

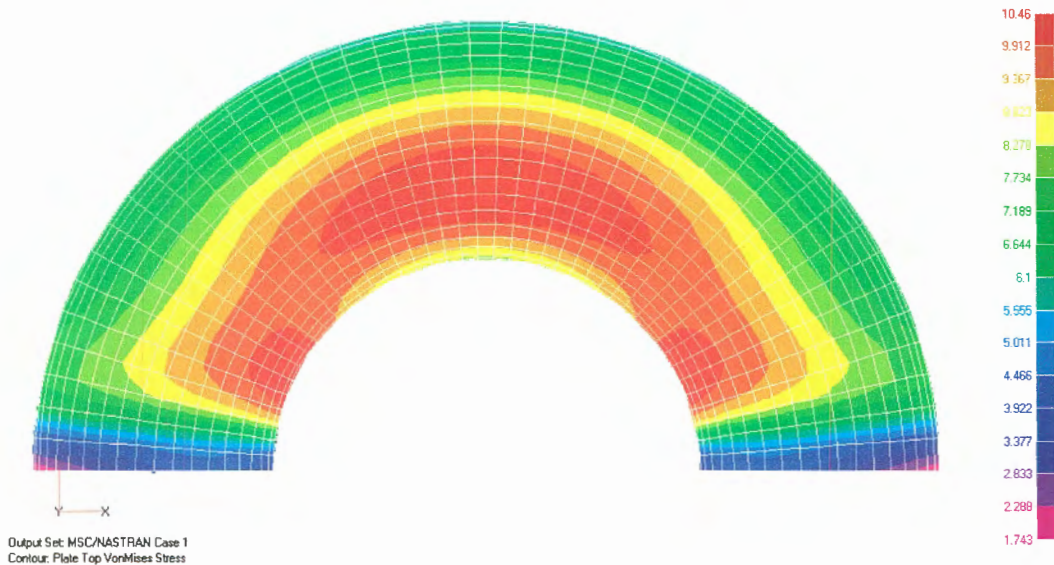


Figure 6.2: U-bend NASTRAN analysis: Top Von Mises stress [MPa]

6.2.2 Fintube

The fintube Von Mises stress distribution, seen in figure 6.3, also show stress variations far below the allowable stress of 87.55MPa as indicated in table 6.1. The fintube will experience stresses ranging from 2.19 to 6.63MPa. It should be noted that only the stress distribution around the centre fin, shown in appendix M, have been taken as the correct stresses, because of end-effects that may have had an influence on the calculation of the outside fin stress distributions.

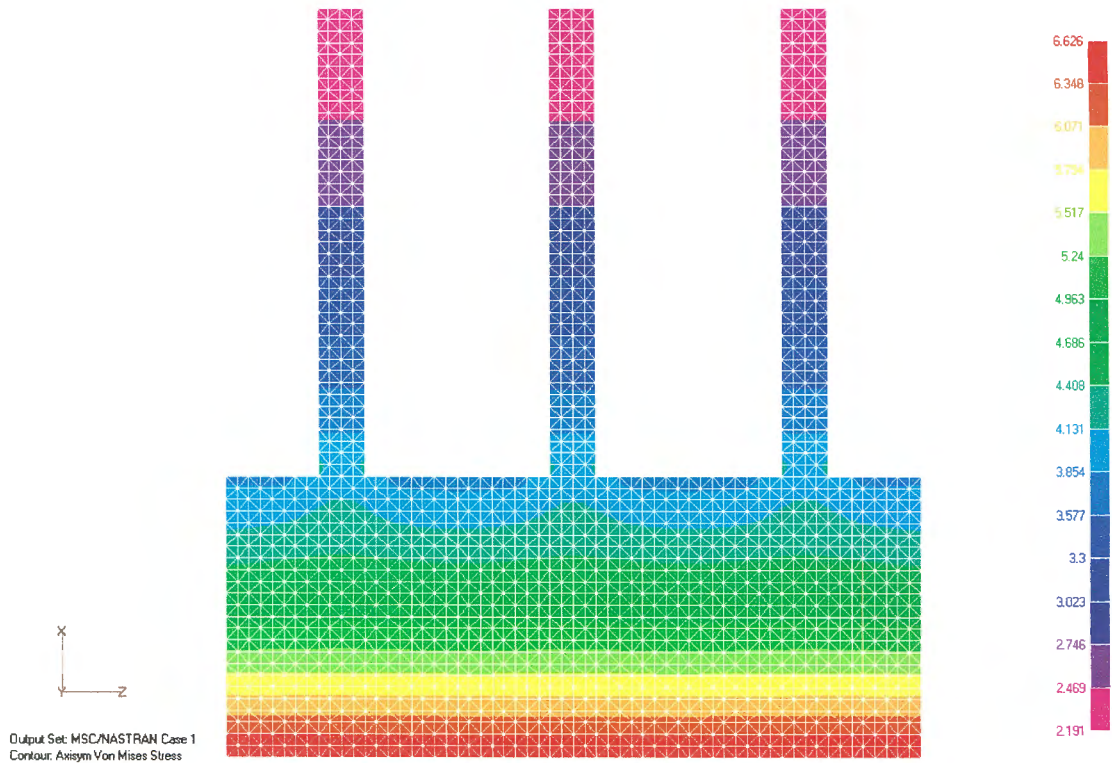


Figure 6.3: Fintube NASTRAN analysis: Von Mises stress [MPa]

6.3 CONCLUSION

From the NASTRAN results it is evident that the U-bends and fintubes are expected to hold at the various pressures that it will be subjected to. As a precaution the fully assembled heat exchanger was pressure tested with cold water up to a pressure of 3000kPa (30bar). The working pressure would not exceed 2000kPa (20bar) under experimental testing conditions. Therefore, along with the appropriate precautional methods (pressure relief valves, etc. as will be discussed in section 7.3), the heat exchanger was deemed safe for this project.

7. PRACTICAL TESTING OF THE HEAT EXCHANGER

With the theoretical simulation of the heat exchanger completed, the final design and construction of the system will be discussed in this chapter.

7.1 SYSTEM DESIGN

Mechanical Desktop R5 was used to create the technical drawings. The main parts consist of the following (*see appendix K*):

Heat exchanger	<u>Drawing nr.</u>
• Fintube	MSc.T-PW1
• Tube U-bend	MSc.T-PW2
• Side plate	MSc.T-PW3
• Side corner	MSc.T-PW4
• Shell flange	MSc.T-PW5
• Cover	MSc.T-PW6
• End cap (1)	MSc.T-PW7
• End cap (2)	MSc.T-PW8
• Heat exchanger assembly (1)	MSc.T-PW9
• Heat exchanger assembly (2)	MSc.T-PW10
Ducting	
• Duct development	MSc.T-PW11
• Ducting flange	MSc.T-PW12
• Ducting pipe flange	MSc.T-PW13
• Ducting assembly	MSc.T-PW14
Inlet pipe	
• Exhaust inlet pipe	MSc.T-PW15

During the design of the fintube, various considerations had to be taken into account.

- 1) Fin thickness and height
- 2) Fin spacing
- 3) Tube wall thickness
- 4) Length of each tube

The fintube was manufactured using a parting-tool cutter and an NC-machine (numerically controlled machine). A fin thickness of 0.5mm was chosen as the minimum machine-able thickness and the height was optimised at 5mm, using an Excel spreadsheet. The fin spacing was determined by the smallest available parting-tool seat, which was 2mm. The tube wall thickness was adversely determined by the hollowbar availability (3mm) and the length of tube was taken at 306mm to ensure the successful integration with existing laboratory equipment (*see MSc.T-PW1*).

The tube U-bend was relatively difficult to obtain and was manufactured by an outside contractor. Taking into account the available tubing, centre-to-centre distance, material deformation and the possible interference of the fintubes, the following specifications were decided upon (*see MSc.T-PW2*):

Tube geometry	17.15mm OD, 13.85mm ID
Centre-to-centre distance	42.88mm

The rest of the heat exchanger was designed around these two parts, taking the restrictions of the laboratory into account. The primary design consideration was that the whole system would have had to fit in the existing ducting between the continuous combustion unit and the exhaust outlet pipe already installed as designed and implemented by Lotun (2001).

7.2 CONSTRUCTION AND TROUBLESHOOTING

The next phase in the project was the construction phase. All of the designed parts (excluding the U-bends, side plates and side corners) were manufactured by SMD (*Sentrale Meganiese Dienste*), Department of Mechanical Engineering, University of Stellenbosch. The manufacturing of the fintubes were the most difficult and time consuming. As mentioned before, the fintubes were machined out of stainless steel hollow bar with the help of an NC-machine. Due to concentricity errors in the hollow bar manufacturing, “chatter” and the resulting deformation (even shearing) of the fins and tube wall was a problem. An example is shown in figure 7.1:

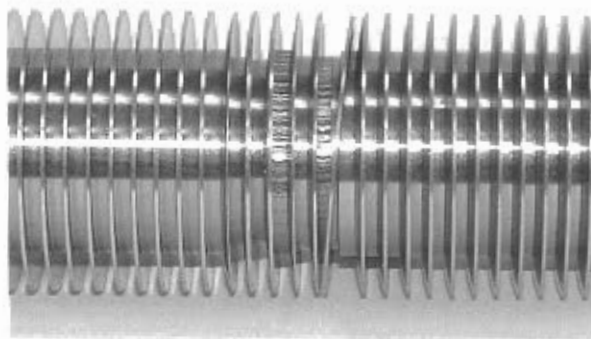


Figure 7.1: Deformation and shearing of the fintube

The problem was solved successfully by progressively feeding the hollowbar into the NC-machine. The resulting fintube can be seen in figure 7.2:

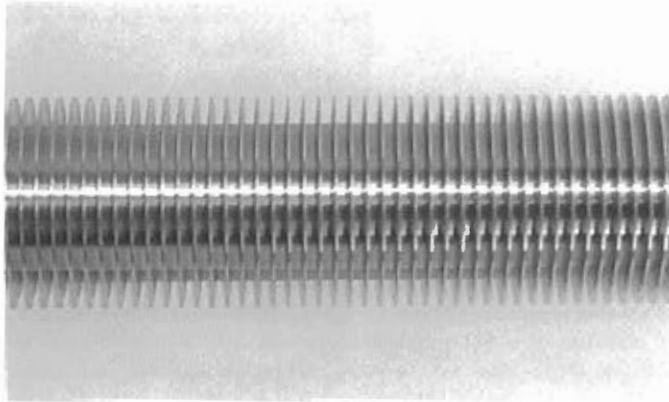


Figure 7.2: Completed fintube

The method by which the fintubes were manufactured is normally used in industry. Only aluminium fins are usually extruded or rolled onto the tube, forming the various fin configurations shown in figure 4.18. In the case of stainless steel this is only possible for a very small fin height. The biggest drawback of using NC-machining is the fact that a lot of material is wasted during the machining process.

The fintubes were interference fitted inside the U-bends and were TIG-welded together, after which each tube was tack-welded to the side-plate. Figure 7.3 shows the preparation done for the assembly process by Mr Graham Hamerse, an SMD technician. Figure 7.4 shows the final product.

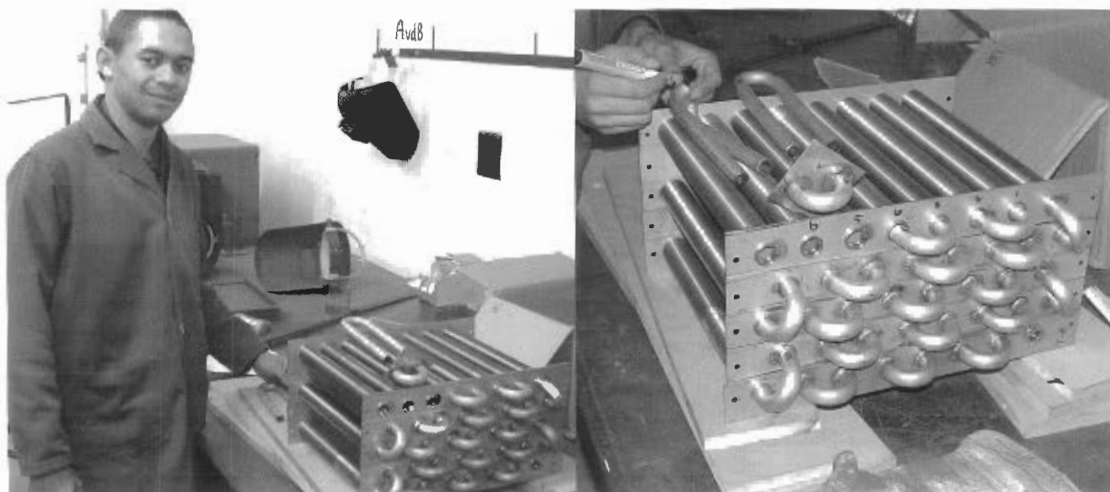


Figure 7.3: Preparation for the assembly process

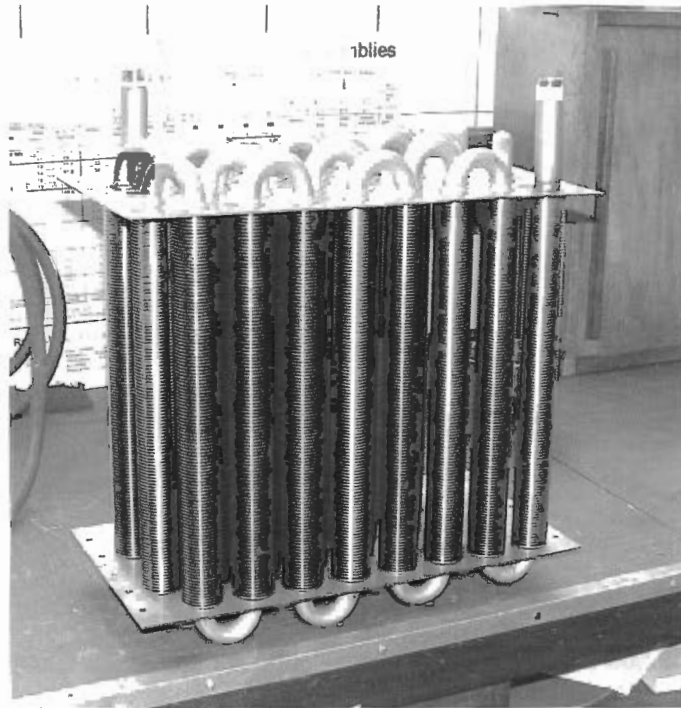


Figure 7.4: Final product of the sub assembly

The heat exchanger was assembled one row at a time. Each row was tack-welded to the next by welding the side-plates together. The end caps (covering the U-bends) and covers (sealing the heat exchanger perimeter) were made next, as shown in figure 7.5. Both have been fastened with nuts and bolts to allow the easy dismantling of the heat exchanger for cleaning purposes when necessary.

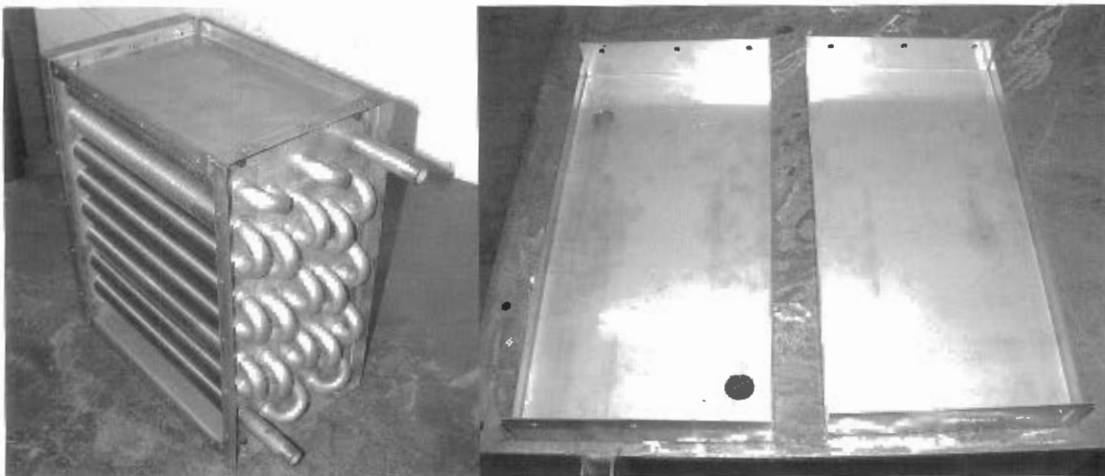


Figure 7.5: Heat exchanger cover (left), end caps covering the U-bends (right)

After the completion of the heat exchanger, the inlet manifolds (which connects the heat exchanger with the pipes through which the exhaust gas flowed) were manufactured. The final products are shown in figure 7.6.



Figure 7.6: Diffuser/nozzle ducting (left), connecting pipe (right)

At this stage, the main parts of the recovery system have been completed and installed in the laboratory. The only major modification done to the system after the initial installation was a service hatch in the diffuser ducting. This would enable the easy inspection and cleaning of the fin tubes. To ensure that the hatch would seal completely during testing, it was fitted with a bolting mechanism and a silicon O-ring. Figure 7.7 shows the service hatch and the exhaust inlet temperature thermocouple.

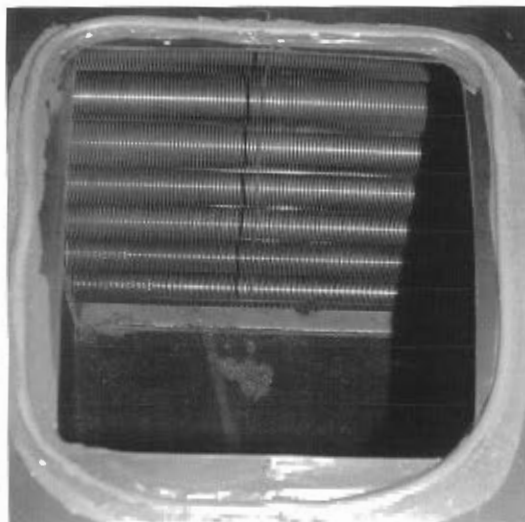


Figure 7.7: Service hatch on the diffuser ducting

7.3 FINAL SYSTEM CONFIGURATION AND TESTING

The following section discusses the testing of the system, which included the measuring of various temperatures, pressures and flow rates. The necessary fail safes were also incorporated to ensure safe running conditions and that the system would be able to handle any pressure spikes that could result from air in the water supply of the pump.

The pump was fitted with a speed control device, which would make it easier to control the pressure. A valve was installed at the inlet and outlet of the heat exchanger to vary the flow and pressure inside the fintubes. A pressure relieve valve was included between these two valves to ensure that the pressure inside the heat exchanger did not exceed 2000kPa (20bar). The actual testing of the system showed that it was more effective to vary the pressure inside the heat exchanger with the valve at the outlet while keeping the valve at the inlet open. The speed control was also used for pressure control, but was less effective. The water mass flow was controlled at the flow meter connected to the water source.

Pressure gauges were installed at the inlet and outlet of the heat exchanger and at the inlet and outlet of the exhaust ducting. The temperatures were measured using K-type, high temperature thermocouples. One was placed at the inlets and outlets of the heat exchanger and at various points on the exhaust ducting. In addition, the top, middle and bottom temperatures of each row were measured by TIG-welding nine high temperature thermocouples to certain U-bends (*see figures 7.9 and 7.10*).

One of the problems that occurred was the steam at the outlet of the heat exchanger. Steam at such a high temperature is very dangerous: therefore it had to be disposed of in a safe manner. There were two choices: a condenser could be installed to condense the steam to water and then connect the water outlet to the drain system, or the steam could be blown into an un-pressurised container where the water would assemble at the bottom of the container and the steam would blow out at the top.

The latter solution was chosen because of its simplicity and effectiveness. The steam released into the atmosphere would not be a problem as the volume encompassed by the laboratory is quite large. This would also solve the problem at the two-phase stage when

water and steam would be blown out of the heat exchanger. In addition a steam separator was connected to the system between the heat exchanger outlet and the steam trap. This would divert the flow through a 90° angle (because of layout restrictions in the laboratory) and help to separate the water from the steam flow.

The final system configuration is shown in figure 7.8 below.

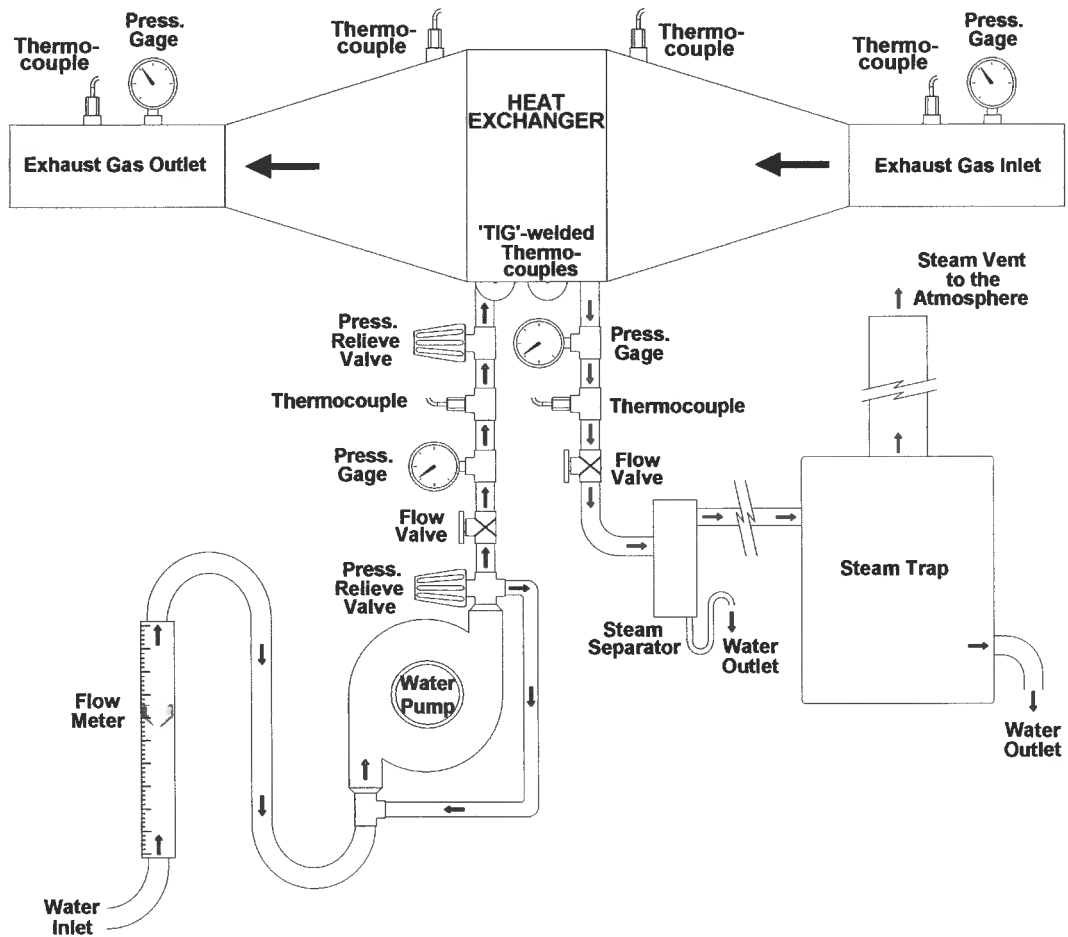


Figure 7.8: Final system configuration

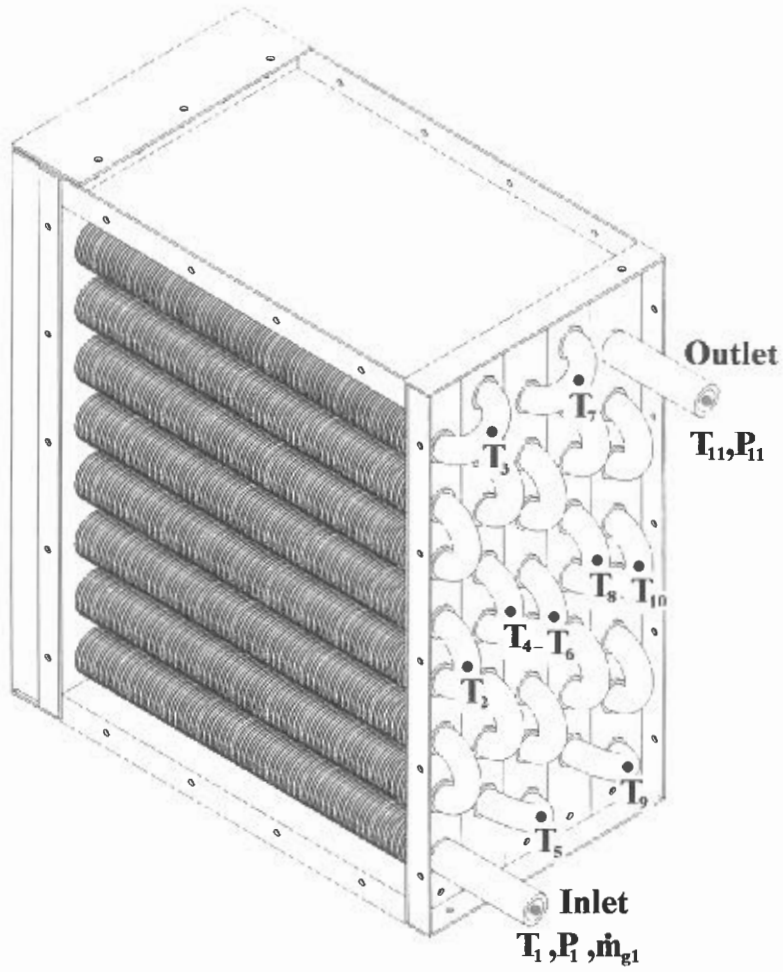


Figure 7.9: Measurements taken on the heat exchanger

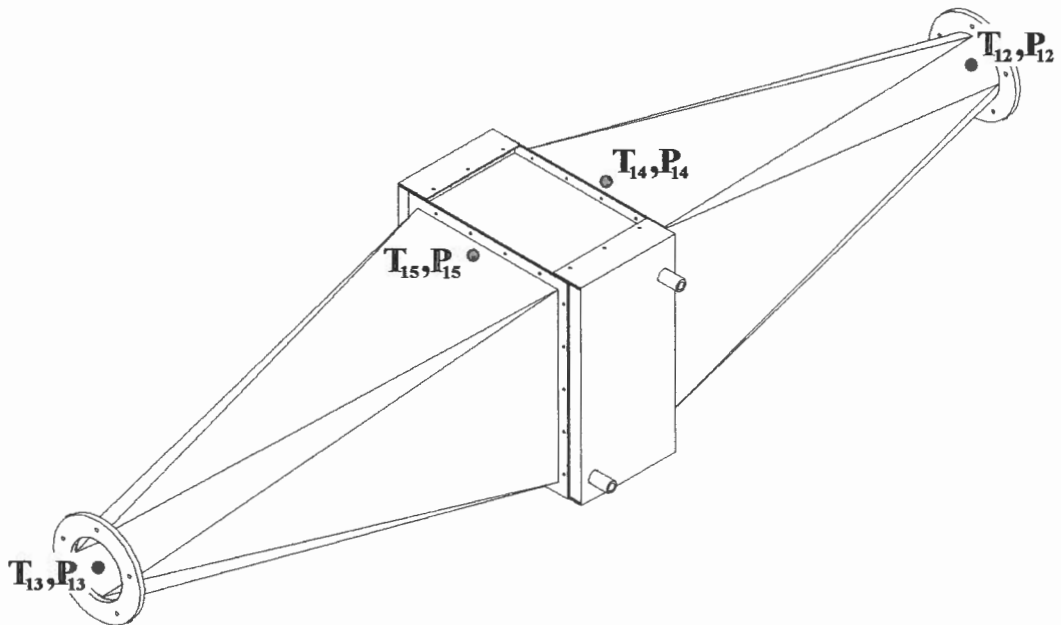


Figure 7.10: Measurements taken on the inlet manifold

7.4 EXPERIMENTAL VERSUS SIMULATED RESULTS

7.4.1 Testing strategy

The testing of the system had to be done in such a way as to cover the greatest possible range of mass flows and pressures to ensure the accurate characterisation of the heat exchanger. As simulated data was already available, it could be used as a starting point to set the testing criteria.

There were a few limitations in the practical testing that had to be taken into account:

- 1) The water flow meter could only supply a minimum of 0.00332kg/s (0.2l/min), which limited the temperature range of the resulting steam. Another limitation of the specific flow meter was that the flow measurement was only accurate at low mass flow rates, which further limited the testing range.
- 2) The exhaust gas temperature was limited to a maximum of 540°C as the failsafe mechanism of the continuous combustion unit activates and shuts the system down when the cooling water reaches 50°C.
- 3) A steam quality of less than 100% was very difficult to measure accurately due to plug flow inside the heat exchanger.
- 4) Increased losses were expected between the heat exchanger and the continuous combustion unit due to the un-insulated piping and ducting, but because of time and cost limitations the piping could not be insulated.
- 5) The last and most frustrating limitation was the fact that a single test run could only last for an hour at a time. The reason was that the nozzle of the gas bottle froze over due to the evaporation and accompanying temperature drop of the propane liquid inside the bottle. Another bottle was later purchased so that the two could be changed around when one froze over, but this still limited testing to two hours a day.

7.4.2 Testing procedure

For the startup and duration of the testing, certain protocol had to be followed to ensure the safety of everyone in the laboratory. The procedure followed was as follows:

(Note: The activation of the exhaust fan at *CAE* is optional but influences the results.)

SYSTEM STARTUP

- 1) Ensure that the inlet (BLACK) and outlet (BLUE) valves on the heat exchanger are open and that the water collectors are underneath the steam separator and steam trap outlets.
- 2) Ensure that the ends of the RED silicon tube and GREEN pressure relief pipe leads to the drainage system.
- 3) Close the CCU exhaust piping with the BLACK lid and open the butterfly valve at the T-junction (by setting the nut in the VERTICAL position).
- 4) Connect the CCU and speed control to the electrical output.
- 5) Connect the water pump to the speed control.
- 6) Startup the PC, run IMPVIEW and start logging the temperature data.
- 7) Open the water supply to the heat exchanger and set the desired water flow rate.
- 8) Follow the startup procedure for the CCU as prescribed by appendix E.
- 9) Set the air fuel ratio of the CCU to the desired values.
- 10) Keep track of the water mass flow rate to the heat exchanger and as soon as the mass flow rate drops, activate the speed control and run the water pump.

Note: This is very important, as air is sucked into the system by the pump when there is no backpressure from the heat exchanger, which results in surging or pressure spikes in the system fluid that could damage the heat exchanger.

- 11) Set the desired pressure inside the heat exchanger by closing and opening the BLUE outlet valve.
- 12) Commence with testing by varying the water flow rate and pressure inside the heat exchanger.

Note: The BLACK inlet valve of the heat exchanger is left completely open during the testing procedure.

SYSTEM SHUTDOWN

- 1) When testing is completed or the CCU gas supply is depleted, follow the CCU shutdown procedure as prescribed by appendix E, leaving the fan on while shutting the heat exchanger down.
- 2) Open the BLUE heat exchanger outlet valve a little bit at a time with intervals between each turn. Care should be taken not to induce any thermal or pressure shocks in the system (This step could take up to 3 or 4 minutes).
- 3) Once the heat exchanger is depressurised, the water pump and speed control can be switched off and disconnected from the electrical input.
- 4) The water mass flow rate to the heat exchanger can be increased to shorten the heat exchanger cool down period.
- 5) Once the temperatures inside the heat exchanger drops to acceptable levels, the water supply can be turned off, along with the fan of the CCU.
- 6) Ensure that the power to the CCU is disconnect, and the water supply to the CCU is closed.
- 7) Remove the BLACK lid from the CCU exhaust piping and close the butterfly valve at the T-junction (by setting the nut in the HORIZONTAL position).
- 8) Stop the data logging in IMPVIEW and do the necessary data conversions.
- 9) Shut down the PC.

7.4.3 Result discussion

The results obtained from the heat exchanger testing procedure are automatically stored in an Excel file by IMPVIEW (data processing software package). There were 15 temperature inputs from the heat exchanger and ducting, with specified time steps between each data point taken. By specifying the water and exhaust temperatures, mass flow rates and pressures, it is possible to simulate certain conditions inside the heat exchanger using the Visual Basic simulation program, with the condition that the experimental data points are taken when thermal stability has been reached inside the heat exchanger. This stabilisation process takes a while to complete and limits the amount of usable data points that can be taken in one test run. Another problem encountered in the testing process occurred when the quality of the steam exiting the heat exchanger was lower than 100%. Because of the presence of plug flow under these conditions, it was difficult to obtain an accurate measurement as to what the actual steam quality was. The

measurements taken with regard to the heat transferred to the water, was higher than that extracted from the exhaust gas. This will be further discussed in conjunction with figure 7.13. The water plugs also influenced the pressure difference between the inlet and outlet of the heat exchanger.

Table 7.1 contains data assembled from tests run on the heat exchanger. These tests were run at various exhaust and water mass flow rates as well as different water pressures. The exhaust temperatures shown above were measured at the inlet and outlet of the heat exchanger (*points 14 and 15 on figure 7.10*), while the water temperatures were measured at the inlet and outlet of the heat exchanger (*points 1 and 11 on figure 7.9*).

Test nr.	Exhaust Mass flow [kg/s]	Exhaust Inlet Temp [°C]	Exhaust Outlet Temp [°C]	H.E. Eff [%]	Sim Outlet Temp [°C]	Temp diff. Error [%]
1	0.019931	366.7	126.8	71.27	137.8	-4.56
2	0.019931	371.6	144.9	71.16	151.7	-3.00
3	0.019792	353.5	146.4	70.93	146.2	0.11
4	0.019792	338.0	135.7	70.94	137.6	-0.97
5	0.019792	344.9	133.9	71.01	134.9	-0.46
6	0.023333	340.5	141.5	74.75	148.2	-3.34
7	0.023333	338.7	148.4	74.68	153.8	-2.82
8	0.020764	359.7	128.0	66.14	134.3	-2.72
9	0.020764	374.0	130.5	66.25	134.4	-1.60
10	0.020764	381.6	138.5	66.24	139.9	-0.57
11	0.020764	377.9	144.4	72.24	148.9	-1.93

Test nr.	Water Mass flow [kg/s]	Water Inlet Temp [°C]	Water Outlet Temp [°C]	Water Quality [%]	H.E. Press [kPa]	Sim Outlet Temp [°C]	Temp diff. Error [%]
1	0.003320	22.8	161.0	28.76	600	157.2	-2.72
2	0.003320	25.0	194.1	29.57	1350	192.7	-0.81
3	0.003320	25.2	189.4	30.36	1200	187.3	-1.30
4	0.003320	25.4	171.6	29.26	800	169.4	-1.48
5	0.003320	25.5	160.7	31.88	600	157.4	-2.44
6	0.003320	25.5	170.9	40.58	800	169.3	-1.12
7	0.003320	25.5	186.8	32.40	1150	185.3	-0.91
8	0.004150	23.1	170.9	28.47	800	169.4	-0.99
9	0.004150	23.4	164.1	29.33	650	160.6	-2.53
10	0.004150	23.7	176.4	25.86	900	174.4	-1.29
11	0.003320	23.9	175.188	30.95	900	174.335	-0.56

Table 7.1: Heat exchanger experimental testing and simulation results

The heat exchanger effectiveness in the data shown above is fairly low. This is because of the high water mass flow rates that were flowing through the heat exchanger and accounts for the low water quality present inside the heat exchanger. The data also shows the simulation error for both the exhaust and water temperature differences. The average error made in the simulated exhaust temperature difference across the entire test point range is

-1.99% below the measured differences, i.e. the transferred energy values are on average simulated lower than what is actually measured. The average error made in the simulated water temperature difference is -1.47% below actual measured differences. These errors are illustrated in figure 7.11. Table 7.2 shows the energy content of the exhaust gas and water as well as the simulated energy transfer.

Test nr.	Exhaust Energy [W]	Water Energy [W]	Sim Energy [W]	Exhaust based		Water based	
				Losses [W]	Error [%]	Losses [W]	Error [%]
1	5106.169	3960.185	4653	453.169	8.87	1145.984	22.44
2	4851.736	4446.414	4479	372.736	7.68	405.322	8.35
3	4379.069	4420.625	4186	193.069	4.41	-41.556	-0.95
4	4249.539	4109.277	4038	211.539	4.98	140.262	3.30
5	4440.286	4138.979	4234	206.286	4.65	301.307	6.79
6	4936.045	4877.039	4573	363.045	7.35	59.005	1.20
7	4726.299	4524.932	4401	325.299	6.88	201.367	4.26
8	5129.209	5109.112	4771	358.209	6.98	20.097	0.39
9	5417.938	5039.898	5078	339.938	6.27	378.040	6.98
10	5428.376	4961.052	5126	302.376	5.57	467.324	8.61
11	5214.320	4309.104	4857	357.320	6.85	905.216	17.36

Table 7.2: Heat exchanger experimental and simulated energy balance

As mentioned earlier, some of the energy contents present in the outlet water are highly irregular as can be seen from test numbers 1, 3 and 11. There could be two possible explanations for this phenomenon:

- 1) The inaccuracy in the quality measurement due to plug flow.
- 2) Losses incurred inside the heat exchanger.

The second theory can certainly apply to test number 1 and 11, although it does not seem likely due to the fact that none of the other tests showed such a dramatic energy loss. The results from test number 3 were most likely due to the inaccurate measurement of the water quality, but were included in order to illustrate the error.

The simulated energy transfer was compared to both the exhaust gas and water heat transferred. The difference between the water and simulated energy transfer would normally be the smallest, which some of the tests indicate, but the average taken from the data clearly indicates that the exhaust gas measurements are much more reliable. On average, the simulated energy transfer differs from the exhaust energy transfer by 6.41%, while the difference between the simulated and measured water transfer is 7.16%. The difference between the simulated and actual exhaust transfer can be ascribed to energy losses inside the heat exchanger.

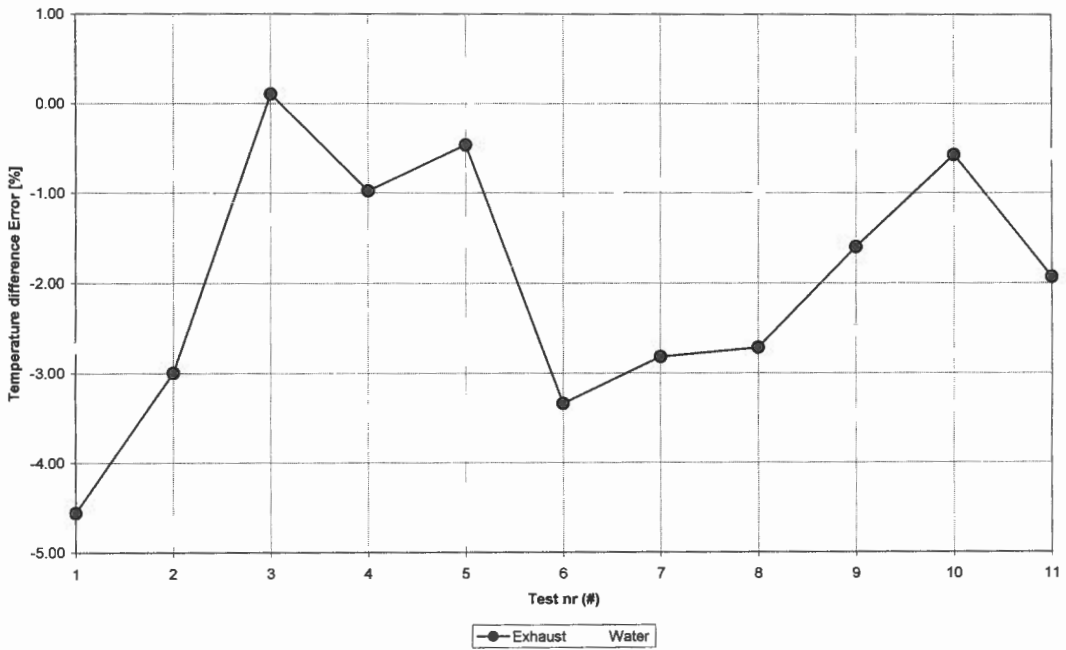


Figure 7.11: The error between the simulated and measured exhaust and water temperatures

From figure 7.12 it is clear that the simulated energy transfer from the exhaust to the water is less than the actual measured value. The simulated exhaust temperature is higher than the measured temperature, because less energy has been lost by the exhaust gas, while the simulated water temperature is lower than the measured temperature because the water received less energy.

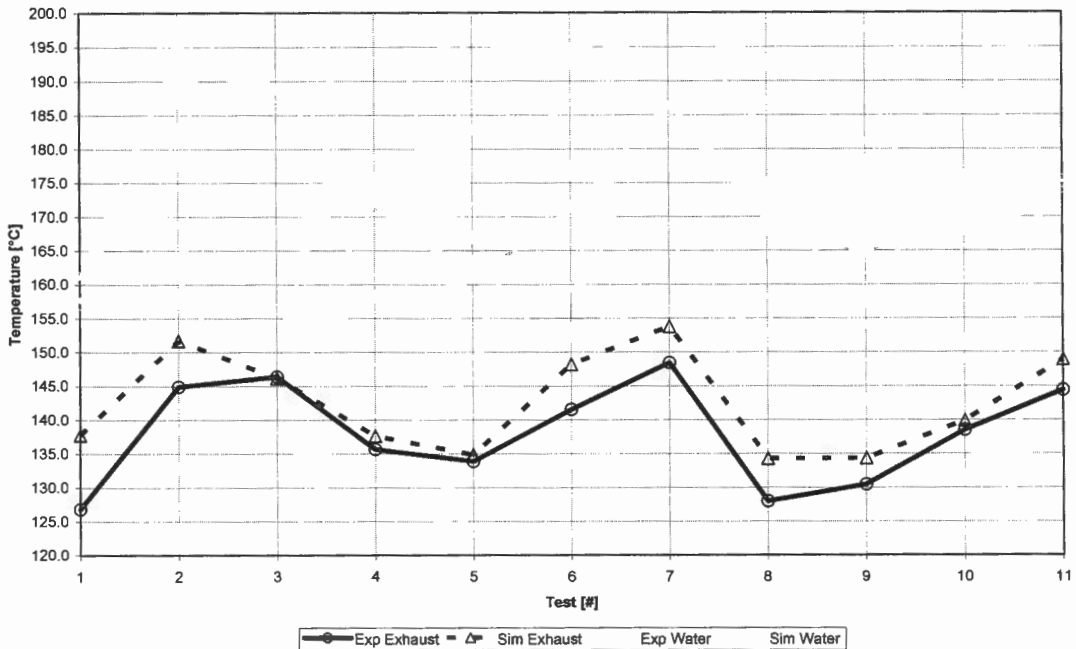


Figure 7.12: Experimental and simulated exhaust and water temperatures

Figure 7.13 shows the energy balance for both the experimental and simulated cases. The experimental case is much more scattered than the simulated case, presumably in part due to the fact that the steam quality that was measured, varied due to the pulsating/plug flow present inside the heat exchanger. The simulated values on the other hand, form a relatively straight line beneath the equilibrium line, where the distance between the simulated and equilibrium line can be ascribed to losses.

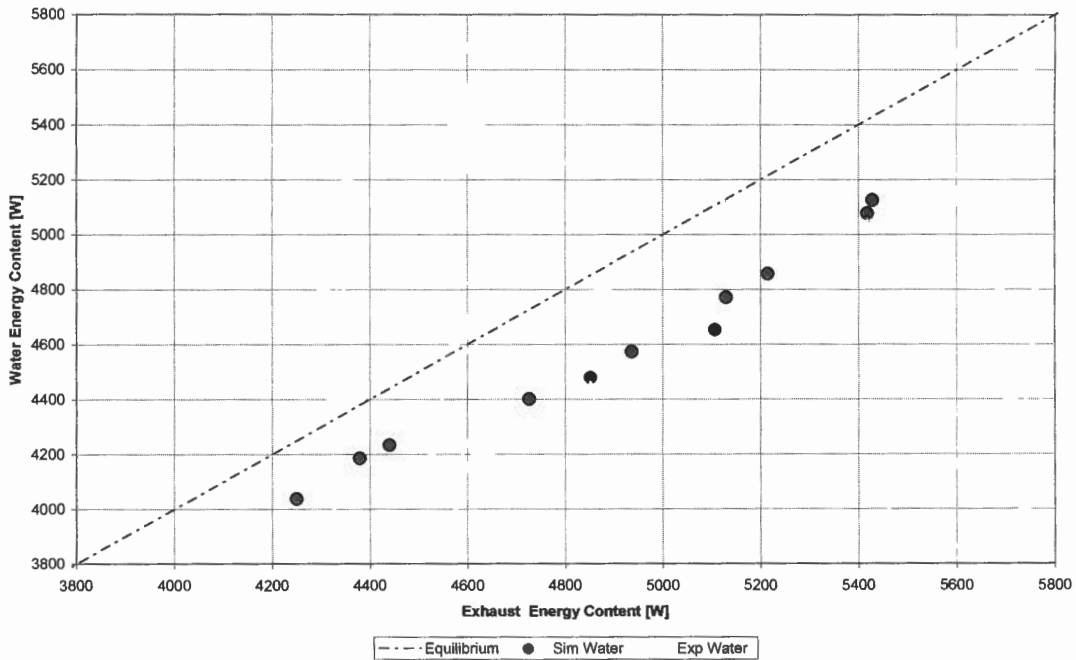


Figure 7.13: Heat exchanger experimental and simulated energy balance

Test number 3 can clearly be seen where it is above the equilibrium line. Test number 1 and 11 on the other hand lies on the other extreme. These three values do not reflect the same behaviour as the rest of the test points and can be seen as the outer limits of the expected results.

In figure 7.14, test point 9 has been chosen to illustrate the temperature distribution as measured by the thermocouples TIG-welded on the U-bends. Between thermocouples 1 and 4, the figure shows a steeper actual temperature gradient than was predicted by the simulation. These thermocouples are in the first two rows of the heat exchanger as shown in figure 7.15. From then on, the temperature rise gradient flattens and actually becomes negative from thermocouple 8 to 9. This strange phenomenon can be explained by the distribution of hot exhaust gas through the heat exchanger.

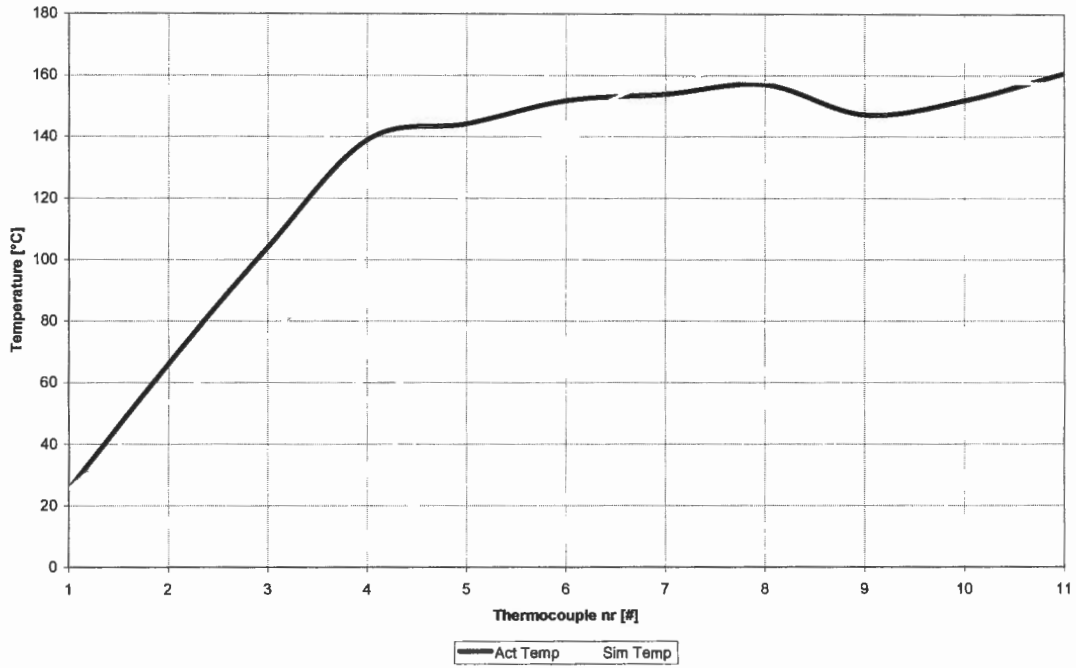


Figure 7.14: Test point 9: Actual versus simulated temperatures inside the heat exchanger

Figure 7.15 also shows the expected exhaust flow. As the exhaust gas enters the ducting, it rises to the top of the ducting, creating turbulent vortices at the bottom of the ducting.

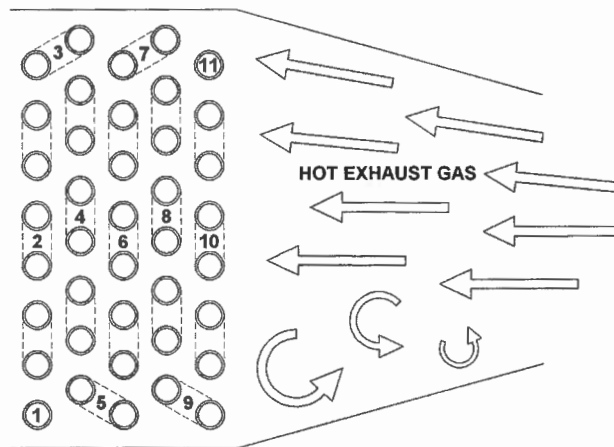


Figure 7.15: Exhaust gas distribution inside the ducting

This anomalous behaviour will result in a better heat transfer through the bottom and sides of the ducting, cooling the exhaust down. The end result is that the lower parts of rows 3, 4 and 5 will see a different (lower) temperature than the top fintubes and will lead to the actual cooling of the liquid-vapour mixture inside the fintubes.

The hypothesis above was checked using convection theory from Mills (1995). First the Grashof number was determined taking $T_{\text{gas}}=344.9^{\circ}\text{C}$, $g=9.81\text{m/s}^2$, $L=0.832\text{m}$, $\text{Pr}=0.69$, $\nu=53.1 \times 10^{-6}\text{m}^2/\text{s}$, $V=1.83\text{m/s}$ and $D_{\text{hyd}}=0.6375\text{m}$:

$$Gr = \frac{\beta \Delta T g L^3}{\nu^2} \quad \dots(7.4.1)$$

where...

$$\Delta T = T_{\text{gas}} - T_s \quad \dots(7.4.2)$$

$$\beta = 1/T_{\text{av}} = 2/(T_{\text{gas}} + T_s) \quad \dots(7.4.3)$$

and T_{av} is in Kelvin.

The Reynolds number is determined by...

$$Re = \frac{V \cdot D_{\text{hyd}}}{\nu} \quad \dots(7.4.4)$$

and the Rayleigh number by...

$$Ra = Gr \cdot Re \quad \dots(7.4.5)$$

The following results were calculated by using a range of values for T_s along with figure 4.42, p. 312 from Mills (1995).

T_s [°C]	Gr Grashof	Re Reynolds	Ra Rayleigh	Ducting Flow condition
25	1399847002	2197	965894431	Mixed/Turb
100	990583202	2197	683502409	Mixed/Turb
200	532432715	2197	367378573	Mixed/Turb
300	151221599	2197	104342903	Mixed/Turb
320	82534725	2197	56948960	Mixed/Turb
340	16079866	2197	11095108	Mixed/Turb

Table 7.3: Flow conditions inside the ducting

The results show that mixed convection conditions occur inside the ducting. According to Mills (1995) this will result in a secondary motion where the exhaust gas will flow upwards along the wall and downwards in the central region forming a vortex which will increase the heat transfer and result in a lower exhaust temperature. A way of eliminating this would be to ensure the equal distribution of the hot exhaust gas through the ducting with the help of guide vanes.

Another interesting phenomenon shown by figure 7.14 is the fact that the inlet gradient between thermocouples 1 and 4 is much steeper than predicted by the simulation program. The explanation for this occurrence probably has a connection to the exhaust extraction fan. In experimental testing a change in the heat transfer coefficients was noted when the fan was switched on, while no notable change in the air mass flow rate at the continuous combustion unit was measured. This means that either the air flow meter is inaccurate, or there is a low pressure zone between the heat exchanger and the exhaust fan which accelerates the air and results in a higher heat transfer coefficient - the latter being the most plausible explanation as the simulated pressure drop (approximately 1Pa) is much lower than the actual pressure drop (approximately 8-10Pa) across the heat exchanger.

Figure 7.16 shows similar temperature behaviour at other test points as has been described with respect to figure 7.14. From this figure, it is also evident that test points 5 and 9 as well as test points 8 and 10 follow the same temperature path for the last half of the heat exchanger, despite the fact that they have different starting gradients.

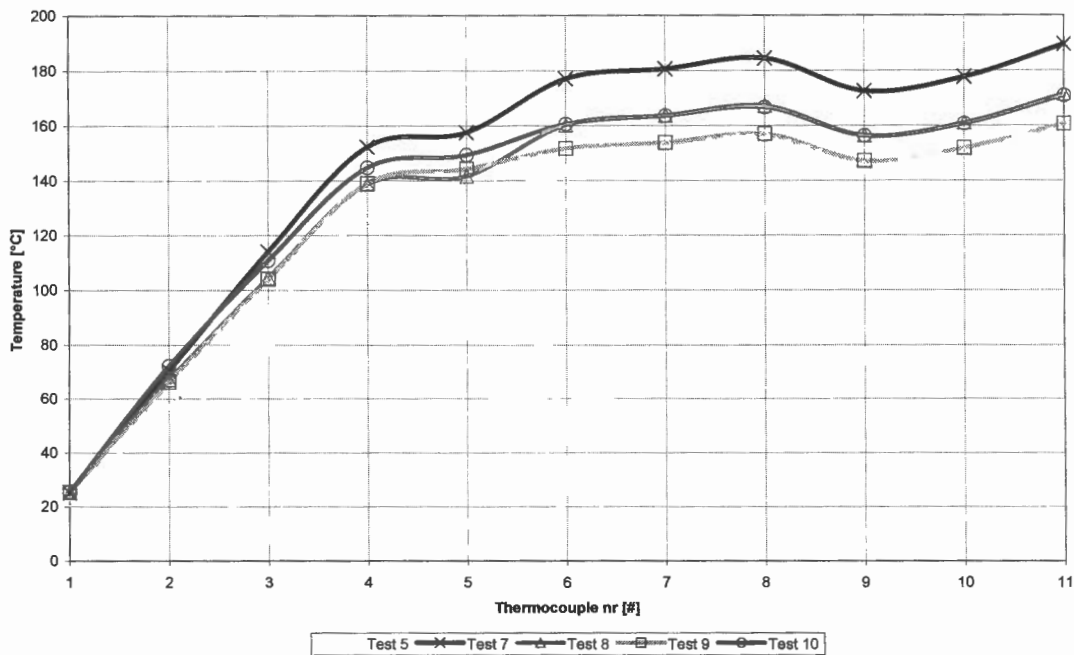


Figure 7.16: Test point comparisons

The explanation for this occurrence is the fact that points 5 and 9 are both at 600kPa (6bar), while points 8 and 10 are at 800kPa (8bar). The similar pressures mean that they will evaporate at the same saturation temperatures. The fact that all of them have different exhaust gas temperatures and/or flow rates, explains the different temperature gradients at the beginning of each curve.

7.4.4 Further simulated testing

Various simulated tests were done to better understand the working of the heat exchanger. Arbitrary input values were chosen to illustrate the crossover where the quality increases from $x < 1$ to $x > 1$.

The data was generated by keeping the inlet temperatures and mass flow rates constant, only varying the inlet pressures. The input values to the simulation program are presented in table 7.4.

Inlet conditions	Gas	Water	Units
Temperature	600	30	[°C]
Pressure	101.4	2000	[kPa]
Mass flow rate	0.0236	0.003735	[kg/s]

Table 7.4: Input values to the simulation program

The obtained results are presented in the figures that follow.

Figure 7.17 shows the water temperature properties as the inlet pressure of the heat exchanger is increased. Between inlet pressures of 400 and 1200kPa, the outlet temperatures drop, but as soon as the pressure rises above 1300kPa, the temperature starts to increase again. It is also evident that T_{sat} rises as the pressure increase.

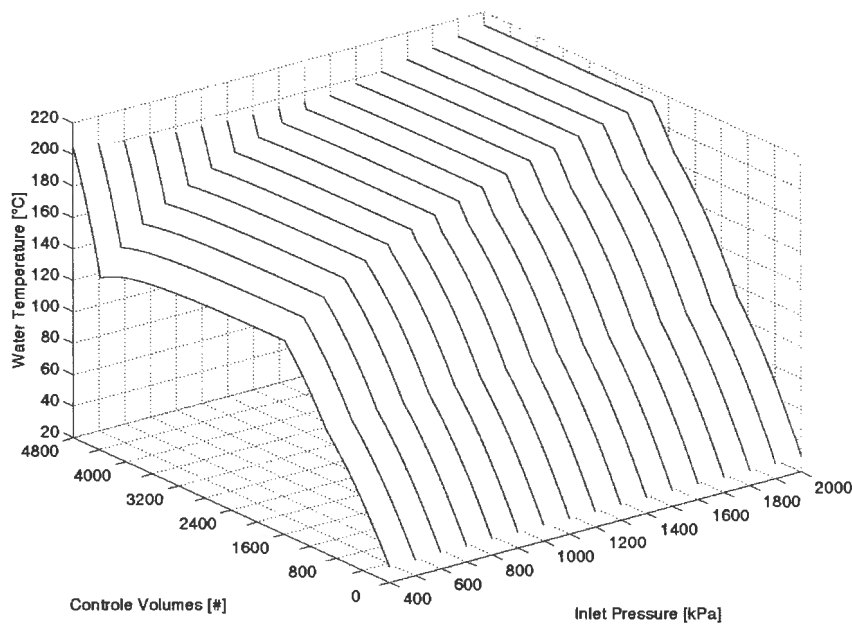


Figure 7.17: Water temperature distribution

Figure 7.18 shows the pressure loss inside the fintubes when the inlet pressure rises.

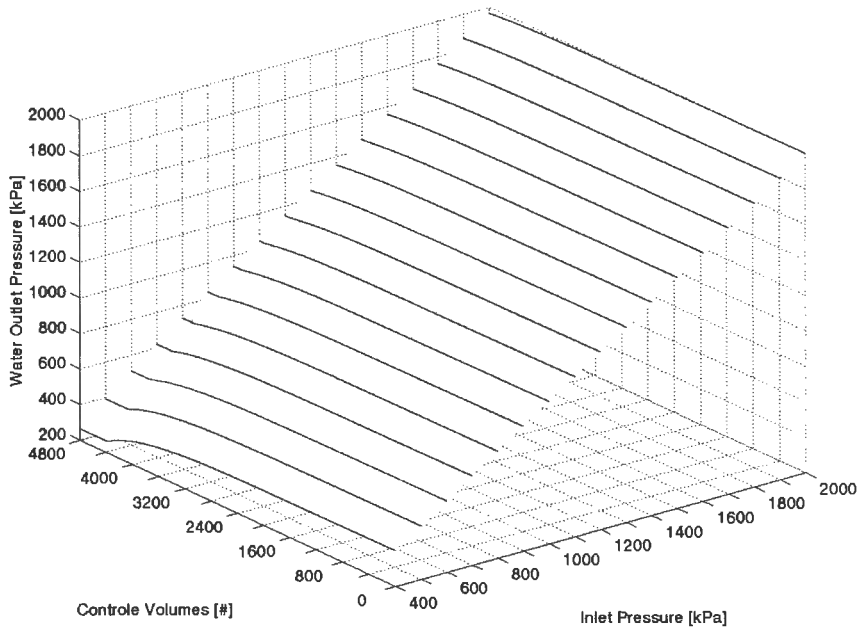


Figure 7.18: Water outlet pressures

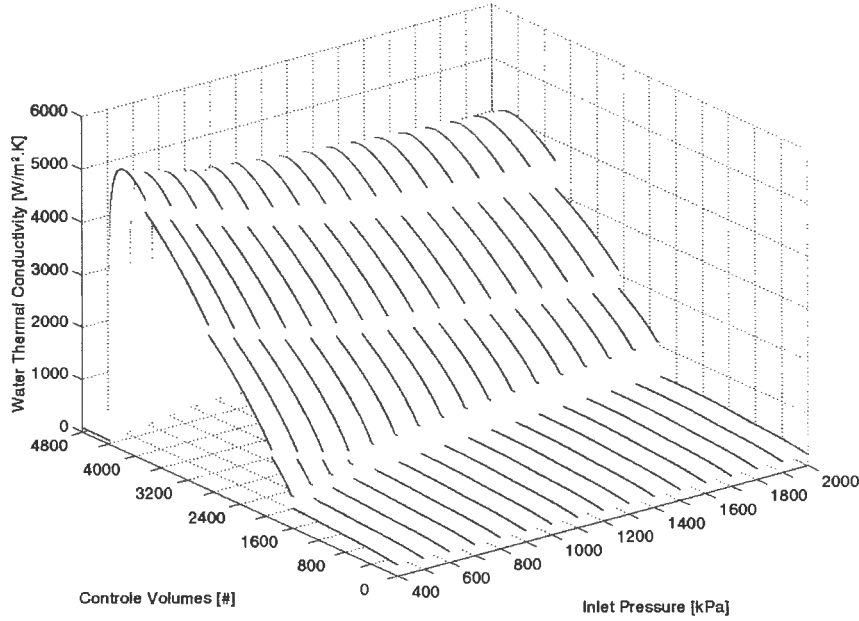


Figure 7.19: Water thermal heat transfer coefficient

The heat transfer coefficient peaks at a lower value for every pressure increase. This would indicate that the amount of energy transferred must decrease as the pressure increases.

Figures 7.20 and 7.21 confirms the previous statement as it is evident that when the pressure rises, so the quality of the water drops (meaning that the water is receiving less energy) which implies that the water enthalpy will also drop.

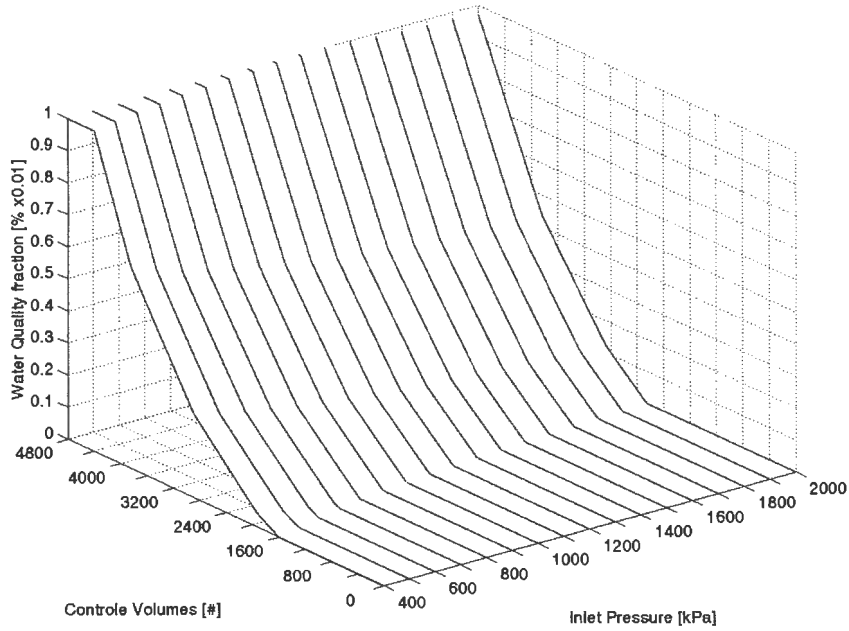


Figure 7.20: Water quality

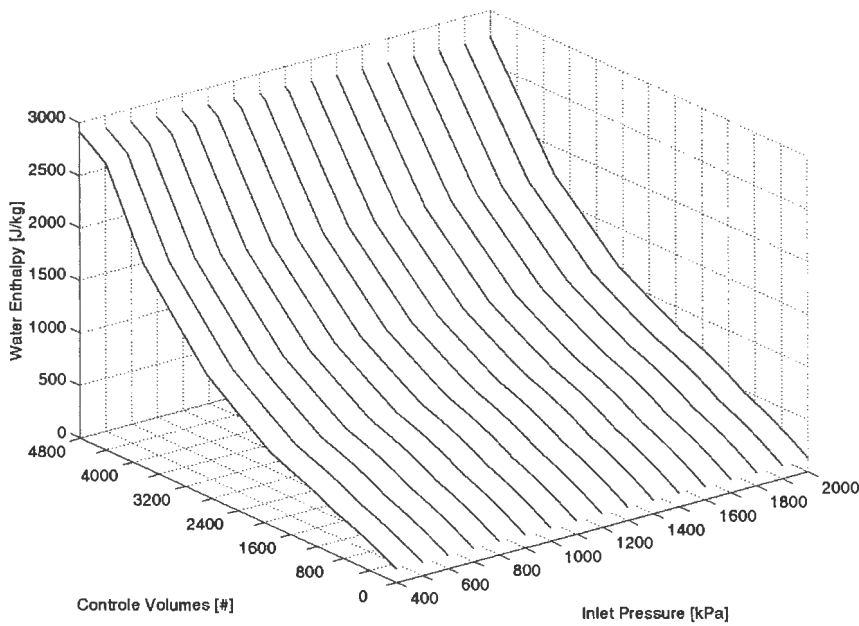


Figure 7.21: Water enthalpy

But why then the interesting temperature behaviour? The reason for the fall and rise of the water temperature as seen in figure 7.17, would be because of the specific heat of the water. As the temperature of liquid water rises ($x=0$), so does the specific heat. When the saturation temperature is reached, the water temperature starts to drop due to pressure losses in the tube ($0 < x < 1$). This will imply that the specific heat would also drop. But as the evaporation process is completed ($x > 1$), the steam temperature as well as the specific heat will rise again. Another factor is that for every pressure rise, there is a higher saturated temperature. From the data shown above it is clear that the outlet properties of the water move back along the quality line, starting at superheated and ending at a liquid-vapour mixture. Combined with the higher saturation temperature, this would explain the temperature slump.

7.4.5 Conclusion

From the discussion in section 7.4.3, it is clear that there are a few discrepancies in both the experimental and simulation data, with the biggest discrepancy being the fact that the steam quality in experimental testing is very difficult to measure accurately.

With regard to the simulation program, the biggest problem is the fact that, despite taking all the flow regimes and fluid phases into account, the program under predicts the energy transfer in the system by about 2%.

None the less, the error that is made when compared to the exhaust heat transfer is relatively small (6.41% including losses that occur inside the heat exchanger), while the average simulated exhaust temperature difference error is -1.99% below the actual measured temperature differences and the average simulated water temperature difference error is -1.47% below the actual measured temperature differences.

The difference in exhaust gas and water energy transfer can also be explained by the elevated heat transfer coefficient between thermocouples 1 and 4 as explained in section 7.4.3.

By comparing the simulated values to the experimental values, it is clear that the simulation program is fairly accurate in its predictions and is therefore successful in its attempt to simulate the specified heat exchanger.

Concerning section 7.4.4, it has been proven that by increasing the pressure inside the heat exchanger for a certain water and exhaust mass flow rate, the actual energy transfer will be reduced. This implies that if a turbocharger were to be connected to the system and the pressure inside the heat exchanger was increased in order to maximise the pressure drop over the turbocharger, less energy would actually be recovered from the exhaust gas.

The results of this chapter, along with appendix D, gives an indication as to the system efficiency that can be expected if a turbine were to be connected to the heat exchanger outlet. As can be seen, the efficiency of the system rises when the turbine inlet pressure rises. Thus, despite the fact that less energy is recovered in the heat exchanger, the system efficiency will still rise, as more energy will be harvested in the turbine section.

8. PROJECT CONCLUSION

The proposed thesis has a relevant subject, not only because of the depletion of fossil fuels, but is also justified in the light of recent fuel price fluctuations around the world. The results obtained in this thesis also show that the proposed recovery system will result in a significant improvement in energy usage.

From the research, current available high speed generators have efficiencies of up to 95%, which means that the critical element would be the achievable efficiency of the turbine. The heat exchanger design done in this project has simplified matters considerably, as a turbine's main working mechanisms are mass flow and pressure drop related.

The designing, construction and testing of a high pressure heat exchanger was done successfully and has now paved the way for further research in this area of energy recovery. The next phase of the project should entail the integration and testing of the turbine section with the heat exchanger, after which the generator aspect can be addressed.

As has been seen in the heat exchanger testing, efficiencies of up to 74% were reached with a relatively high water mass flow rate which was dictated by the available flow meter. By using the simulation program, efficiencies of up to 85% can theoretically be achieved by using a lower water mass flow rate.

From the literature review as well as the research done in under- and postgraduate studies, it is clear that the possibilities regarding electrical power generation from the recovery of waste heat are promising. The main obstacle is the acquisition of a suitable high speed generator. For this project though, these matters were not the primary concern.

In closing, this project along with those of Joubert (1996), Koorts (1998) and Lotun (2001), is the first stage in the successful development of an electrical generation system and will provide valuable information for possible follow-up studies.

9. RECOMMENDATIONS

Recommendations for this project concern the improvement of the environment and hardware control in the laboratory in order to increase the measuring accuracy of experimental testing, as well as the installation of certain hardware in the laboratory for safety reasons.

The first recommendation would be the insulation of the ducting- and pipe- work in the laboratory. This will decrease the safety risk to anyone in the laboratory as well as minimize heat loss. As previously stated, the losses that are currently occurring are in the range of 12%, which is substantial.

Another potential hazard, which has been temporarily dealt with in this project is the handling of waste steam. At this stage the superheated steam is blown into a steam trap and vented into the laboratory atmosphere. A more permanent solution such as a integrated steam outlet inside the laboratory would be more satisfactory.

The use of 9kg propane gas bottles as fuel for the continuous combustion unit has proven to be a significant source of frustration as the bottle nozzles tended to freeze shut just as the test run in progress was beginning to deliver good results. Two bottles were later used alternately, but the system still needed to be warmed up again after the bottles were exchanged. As the continuous combustion unit is used in practical tutorials for university students and CAE has a permanent source of propane gas, it is recommended that a pipeline is installed that connects to the continuous combustion unit with CAE's gas tank.

The exhaust gasses are vented, using the same exhaust fan that is connected to CAE's engine test cells, directly beneath the laboratory. The fan sucks the exhaust at a constant rate, except when one of the test cells is activated. The suction on the continuous combustion unit then decreases and influences the air mass flow rate over the heat exchanger, resulting in a lower heat transfer coefficient and the changing of the test conditions and results.

REFERENCES

AlliedSignal Ltd. (2002), “Automotive Turbochargers”, Skelmersdale, Lancs, England

Al Rabghi O.M., Bierutty M., Akyurt M., Najjar Y. and Alp T. (1993), “Recovery and utilization of waste heat”, A review paper, Heat Recovery Systems and CHP, Vol. 13, pp. 463-670

“ASHRAE Handbook 1985 Fundamentals, SI Edition”, American Society of Heating, Refrigerating and Air-Conditioning Engineers, Inc., Atlanta, p.34.17

ASME (2001), Section II, Part D - Properties, “Maximum Allowable Stress Values for Ferrous Materials”, Table A1

Benham P.P., Crawford R.J. and Armstrong C.G. (1997), “Mechanics of Engineering Materials”, 2nd Edition, Addison Wesley Longman Limited, England

Benson R.S. and Whitehouse N.D. (1979), “Internal Combustion Engines”, Pergamon International Library, Great Britain, Vol. 2, Chapter 10

Bolland O., Førde M. and Hånde B. (1995), “Air bottoming cycle use of gas turbine waste heat for power generation”, *ASME*, New York, 95-CTP-50, pp. 1-12

Bowman Power (2002)

Site: <http://www.bowmanpower.com>

Carey V.P. (1991), “Liquid-Vapor Phase-Change Phenomena”, Series in Chemical and Mechanical Engineering, Chapter 12

Çengel Y.A. and Boles M.A. (1994), “Thermodynamics – An Engineering Approach”, 2nd Edition, McGraw-Hill, Inc., New York, Computer Programs

Chen J.C. (1963), “A correlation for boiling heat transfer to saturated fluids in convective flow”, ASME paper 63-HT-34. Presented at the 6th National Heat Transfer Conference, Boston

Combustion Laboratory Unit (1997), “Experimental operating and maintenance manual”, P.A. Hilton Limited, England

Corrado C.N. Jr. (1985), “Economic power generation at sea”, Vol. 223, no. 3, pp. 34

Crawford P., Aston R.W., Smith M.L., Marloth R.T., Es-said O.S. and Iyer S. (1997), “Corrosion of a stainless steel chemical hood”, *Engineering Failure Analysis*, Vol. 5, no. 1, pp. 53-56

Ferguson C.R. (1986), “Internal Combustion Engines: Applied Thermosciences”, John Wiley & Sons Inc., Canada, Chapters 1 & 7

Forster H.K. and Zuber N. (1955), “Dynamics of vapour bubbles and boiling heat transfer”, *AIChEJ.*, Vol. 1, pp. 531-535

Friedel L. (1979), “Improved friction drop correlations for horizontal and vertical two-phase flow”, *European Two-phase Flow Group Meeting*, Ispra, Italy

Holman J.P. (1992), “Heat Transfer”, 7th Edition in SI units, McGraw-Hill Int. (UK) Limited, Singapore

Hopmann U. (2002), “Diesel engine waste heat recovery utilizing electric turbocompound technology”, Caterpillar Inc., 2002 DEER Conference, San Diego, California

Joubert R. de V. (1996), “Waste heat recovery system for marine propulsion plants”, Mechanical Project 478, University of Stellenbosch, November

Koehler J., Tgethoff W.J., Westpalen D. and Sonnekalb M. (1997), “Absorption refrigeration systems for mobile applications utilising exhaust gasses”, *Heat and Mass Transfer*, Vol. 32, pp. 333-340

Koorts T. (1998), “Waste energy recovery system”, Mechanical Project 478, University of Stellenbosch, August

Kröger D.G. (1998), “Air-cooled Heat Exchangers and Cooling Towers”, Department Mechanical Engineering, University of Stellenbosch, Chapters 2 & 3 and pp. 5.4.13

Lotun D. (1999), “Design and evaluation through simulation and experimental apparatus of a small scale waste heat driven electrical power generation plant”, Postgraduate Thesis Proposal, University of Stellenbosch, December

Lotun D. (2001), “Design and evaluation through simulation and experimental apparatus of a small scale waste heat recovery system”, MEng Thesis, University of Stellenbosch, September

Malan S.F. and Paterson A.E. (1993), “Introduction to Aluminium”, Aluminium Federation of South Africa, 3rd Edition

Micro Hydropower Basics (2000)

Site: <http://www.microhydropower.net/turbines.html>

Mills A.F. (1995), “Heat and Mass Transfer”, University of California, Los Angeles, Chapter 4 and Appendix A

Najjar Y.S.H. (2000), “Efficient use of energy by utilizing gas turbine combined systems”, *Applied Thermal Engineering*, Vol. 21, Elsevier Science Ltd., pp. 407-438

Odeh, S.D., Morrison G.L. and Behnia M. (1998), “Modelling of parabolic trough direct steam generation solar collectors”, Solar Thermal Energy Laboratory, University of New South Wales, *Solar Energy*, Vol. 62, Nr. 6, pp. 395-406

Oomori H. and Shigeru O. (1993), “Waste heat recovery of passenger car using a combination of rankine bottoming cycle and evaporative engine cooling system”, Toyota Motor Corp. *SAE Journal*, March, pp. 159-164

Papalambros P.Y. and Wilde D.J. (2000), “Principles of Optimal Design, Modelling and Computation”, 2nd Edition, Cambridge University Press, Chapter 7

Passos J.C. and Reinaldo R.F. (2000), "Analysis of pool boiling within smooth and grooved tubes", *Experimental Thermal and Fluid Science*, Vol. 22, pp. 35-44

Premoli A., Francesco D. and Prina A. (1970), "An empirical correlation for evaluating two-phase mixture density under adiabatic conditions", *European Two-phase Flow Group Meeting*, Milan

Sayers A.T. (1990), "Hydraulic and Compressible Flow Turbomachines", University of Cape Town, Chapters 4 & 7

Schneider D.I. (1999), "An Introduction to Programming Using Visual Basic 6.0", 4th Edition, Prentice Hall, New Jersey

Schwack A. and Harms T.M. (2000), "Continuous combustion chamber – thermodynamics B", Laboratory exercise, Mechanical Engineering Department, University of Stellenbosch

Serway R.A. (1996), "Physics for Scientists and Engineers", 4th Edition, Saunders Golden Sunburst Series

Shigley J.E. and Mischke J.R. (1989), "Mechanical Engineering Design", 5th Edition, McGraw Hill, Chapters 2 & 9

South African Stainless Steel Development Association (Sassda) (2003), "Stainless Steel Buyers Guide, 2003 / 2004", Published 2003 Sassda

TurbochargersNZ (2001)

Site: <http://www.turbochargersnz.com>

TurboGenset (2003)

Site: <http://www.turbogenset.com>

Volkswagen (2003)

Site: <http://www.cs.rochester.edu/u/jag/vw/engine/turbo/turbo.html>

Wagner W., Cooper J.R., Dittmann A., Kijima J., Kretschmar H.-J., Kruse A., Mareš R., Oguchi K., Sato H., Stöcker I., Šifner O., Takaishi Y., Tanishita I., Trübenbach J. and Willkommen Th. (1997), "The IAPWS industrial formulation 1997 for the thermodynamical properties of water and steam", *Journal of Engineering for Gas Turbines and Power*, Vol. 122, pp. 150-182

Wang C., Chen I. Y., Yang Y. and Chang Y. (2003), "Two-phase flow pattern in small diameter tubes with the presence of horizontal return bend", *International Journal of Heat and Mass Transfer*, Vol. 46, pp. 2975-2981

Wang C., Chen I. Y., Yang Y. and Hu R. (2002), "Influence of horizontal return bend on the two-phase flow pattern in small diameter tubes", *Experimental Thermal and Fluid Science*, pp. 2975-2981

Whalley P.B. (1987), "Boiling, Condensation, and Gas-Liquid Flow", Department of Engineering Science, University of Oxford, Oxford, Chapters 1-6, 16, 17, 20

White F.M. (1999), "Fluid Mechanics", 4th Edition, McGraw-Hill, Singapore, Chapters 9 & 11

Wipplinger K.P.M. (2000), Internal combustion engine practical, Thermodynamics B, Presented by the Centre for Automotive Engineering, University of Stellenbosch, December

Wipplinger K.P.M. (2001), "Waste heat recovery using generated steam and a turbocharger", Mechanical Project 478, University of Stellenbosch, November

Yu W., France D.M., Wambsganss M.W. and Hull J.R. (2002), "Two-phase pressure drop, boiling heat transfer, and critical heat flux to water in a small-diameter horizontal tube", *International Journal of Multiphase Flow*, Vol. 28, pp. 927-941

APPENDIX A
MANUFACTURER'S
TURBOCHARGER DESIGN DRAWING
(ALLIEDSIGNAL, 2002)

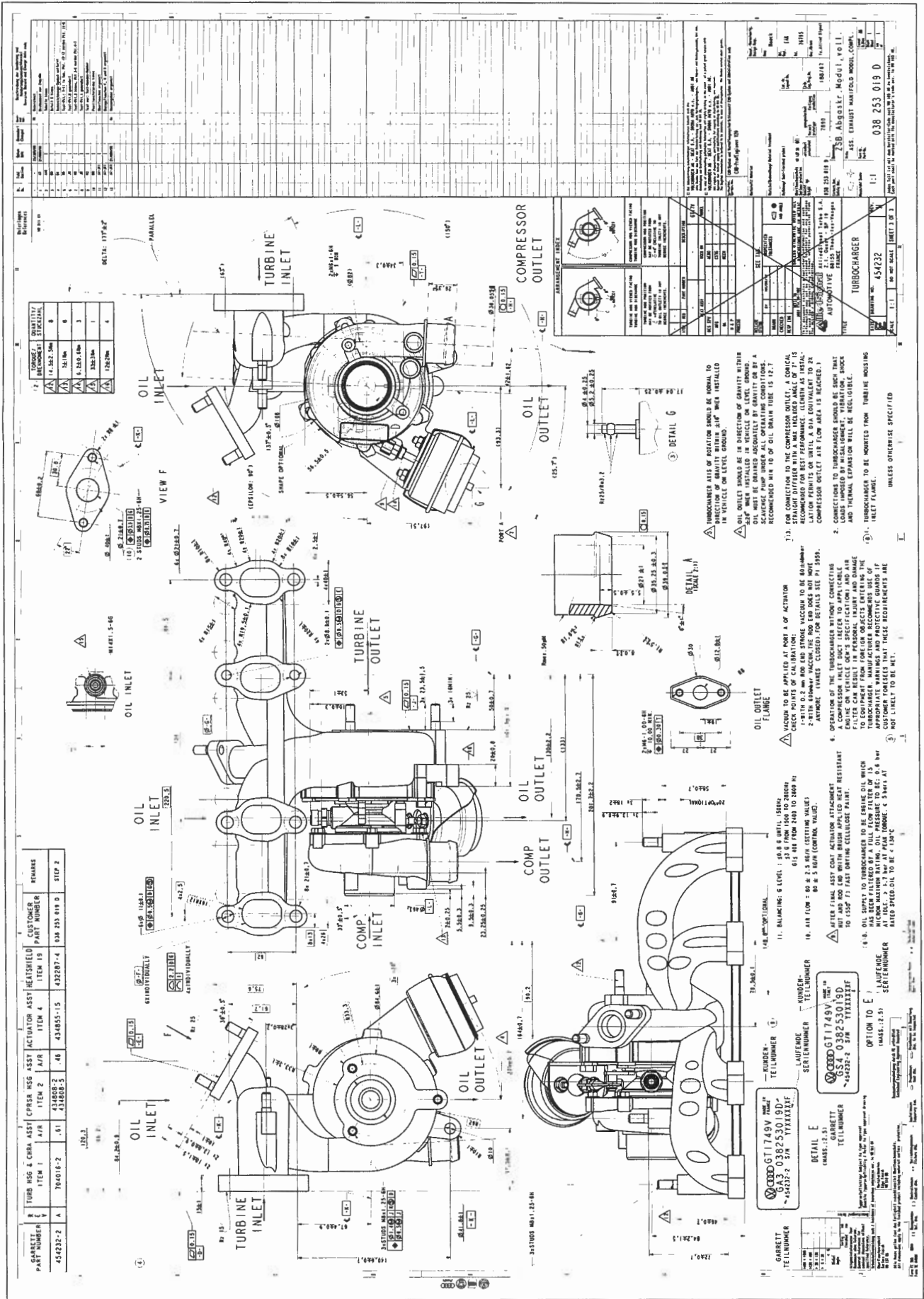


Figure A1: Turbocharger design drawing

APPENDIX B
MANUFACTURER'S
TURBOCHARGER MAPS
(ALLIEDSIGNAL, 2002)

GT17V Step2 NS111(Ø43) TRIM 70 0.65 A/R 1/10 Opening			
	PRT	WT	ETATM
[rpm]	P1t/P2s	[lbs/min]	[%]
Speed 1	1.46	3.65	0.46
50469	1.52	3.81	0.47
	1.54	3.89	0.48
	1.56	3.94	0.49
	1.58	3.99	0.49
	1.59	4.01	0.49
	1.59	4.02	0.49
Speed 2	1.66	4.04	0.45
61812	1.75	4.22	0.48
	1.81	4.30	0.48
	1.83	4.35	0.49
	1.86	4.39	0.49
	1.88	4.42	0.49
	1.89	4.44	0.49
Speed 3	1.91	4.37	0.48
73209	2.05	4.55	0.50
	2.12	4.63	0.51
	2.17	4.68	0.51
	2.22	4.72	0.51
	2.24	4.74	0.52
	2.26	4.75	0.52

Table B1: Turbocharger map: 1/10 open

GT17V Step2 NS111(Ø43) TRIM 70 0.65 A/R 1/5 Opening			
	PRT	WT	ETATM
[rpm]	P1t/P2s	[lbs/min]	[%]
Speed 1	1.36	4.22	0.50
50174	1.40	4.40	0.53
	1.43	4.50	0.54
	1.45	4.57	0.54
	1.46	4.64	0.54
	1.47	4.65	0.54
	1.48	4.66	0.54
Speed 2	1.52	4.71	0.51
61395	1.58	4.89	0.54
	1.63	5.01	0.55
	1.65	5.08	0.55
	1.67	5.11	0.55
	1.69	5.15	0.55
	1.70	5.18	0.55
Speed 3	1.73	5.16	0.52
72637	1.83	5.36	0.55
	1.89	5.46	0.56
	1.93	5.52	0.57
	1.96	5.57	0.57
	1.98	5.59	0.57
	1.99	5.61	0.58
Speed 4	2.00	5.56	0.54
83704	2.14	5.73	0.57
	2.23	5.82	0.57
	2.28	5.86	0.58
	2.32	5.91	0.59
	2.34	5.93	0.59
	2.36	5.94	0.59
Speed 5	2.33	5.83	0.56
94741	2.51	5.99	0.58
	2.63	6.07	0.59
	2.70	6.10	0.59
	2.75	6.13	0.60
	2.78	6.15	0.60
	2.80	6.15	0.60

Table B2: Turbocharger map: 1/5 open

GT17V Step2 NS111(Ø43) TRIM 70 0.65 A/R 2/5 Opening			
	PRT	WT	ETATM
[rpm]	P1t/P2s	[lbs/min]	[%]
Speed 1	1.26	5.33	0.56
50441	1.29	5.56	0.59
	1.31	5.71	0.60
	1.32	5.77	0.61
	1.33	5.81	0.62
	1.33	5.87	0.62
	1.34	5.89	0.62
Speed 2	1.38	6.00	0.56
61606	1.43	6.27	0.60
	1.45	6.42	0.61
	1.47	6.49	0.62
	1.49	6.55	0.62
	1.50	6.63	0.62
	1.51	6.65	0.62
Speed 3	1.54	6.65	0.57
72807	1.61	6.93	0.61
	1.65	7.07	0.62
	1.68	7.15	0.63
	1.70	7.22	0.63
	1.72	7.25	0.63
	1.73	7.27	0.63
Speed 4	1.73	7.15	0.60
84048	1.83	7.43	0.62
	1.90	7.58	0.63
	1.93	7.66	0.64
	1.96	7.72	0.65
	1.98	7.75	0.65
	2.00	7.73	0.65
Speed 5	1.98	7.59	0.62
95022	2.11	7.82	0.64
	2.20	7.95	0.65
	2.25	8.00	0.65
	2.29	8.04	0.66
	2.31	8.06	0.66
	2.32	8.08	0.66
Speed 6	2.31	7.94	0.64
106066	2.46	8.09	0.65
	2.56	8.17	0.66
	2.62	8.22	0.66
	2.67	8.23	0.67
	2.68	8.25	0.67
	2.66	8.23	0.67

Table B3: Turbocharger map: 2/5 open

GT17V Step2 NS111(Ø43) TRIM 70 0.65 A/R 3/5 Opening			
	PRT	WT	ETATM
[rpm]	P1t/P2s	[lbs/min]	[%]
Speed 1	1.22	6.45	0.57
50666	1.24	6.75	0.62
	1.25	6.93	0.62
	1.26	7.03	0.63
	1.27	7.14	0.63
	1.27	7.18	0.64
	1.27	7.20	0.64
Speed 2	1.31	7.36	0.57
61821	1.35	7.75	0.61
	1.37	7.92	0.62
	1.38	8.04	0.63
	1.39	8.13	0.63
	1.40	8.19	0.63
	1.41	8.24	0.64
Speed 3	1.44	8.19	0.59
73121	1.50	8.58	0.62
	1.53	8.78	0.63
	1.55	8.90	0.64
	1.57	8.99	0.64
	1.59	9.06	0.65
	1.59	9.06	0.65
Speed 4	1.60	8.86	0.60
84373	1.68	9.24	0.63
	1.74	9.44	0.64
	1.77	9.55	0.64
	1.80	9.62	0.65
	1.81	9.66	0.65
	1.82	9.67	0.65
Speed 5	1.82	9.46	0.61
95590	1.93	9.76	0.63
	2.01	9.94	0.64
	2.05	10.01	0.64
	2.08	10.06	0.65
	2.10	10.07	0.65
	2.10	10.07	0.66
Speed 6	2.12	9.93	0.62
107117	2.25	10.12	0.63
	2.34	10.22	0.64
	2.40	10.28	0.64
	2.43	10.30	0.65
	2.44	10.30	0.65
	2.41	10.27	0.65

Table B4: Turbocharger map: 3/5 open

GT17V Step2 NS111(Ø43) TRIM 70 0.65 A/R 4/5 Opening			
	PRT	WT	ETATM
[rpm]	P1t/P2s	[lbs/min]	[%]
Speed 1	1.20	7.53	0.54
50535	1.22	7.87	0.58
	1.23	8.07	0.59
	1.24	8.20	0.60
	1.25	8.31	0.60
	1.25	8.37	0.60
	1.25	8.41	0.60
Speed 2	1.29	8.51	0.52
61787	1.33	9.00	0.56
	1.35	9.23	0.58
	1.36	9.39	0.58
	1.37	9.49	0.59
	1.38	9.56	0.59
	1.38	9.62	0.59
Speed 3	1.42	9.58	0.53
72978	1.47	10.02	0.56
	1.51	10.27	0.57
	1.53	10.39	0.58
	1.55	10.36	0.59
	1.55	10.59	0.59
	1.56	10.61	0.59
Speed 4	1.58	10.33	0.53
84300	1.66	10.78	0.56
	1.71	11.00	0.57
	1.74	11.13	0.58
	1.76	11.21	0.58
	1.78	11.26	0.59
	1.78	11.29	0.59
Speed 5	1.81	10.95	0.53
95601	1.92	11.28	0.55
	2.00	11.46	0.56
	2.03	11.54	0.57
	2.06	11.58	0.57
	2.08	11.62	0.58
	2.09	11.62	0.58
Speed 6	2.15	11.30	0.53
106826	2.28	11.47	0.54
	2.37	11.57	0.55
	2.43	11.59	0.55
	2.46	11.60	0.56
	2.46	11.62	0.56
	2.46	11.61	0.56

Table B5: Turbocharger map: 4/5 open

GT17V Step2 NS111(Ø43) TRIM 70 0.65 A/R Fully Open			
	PRT	WT	ETATM
[rpm]	P1t/P2s	[lbs/min]	[%]
Speed 1	1.21	8.45	0.47
50317	1.23	8.81	0.50
	1.24	9.03	0.52
	1.24	9.15	0.52
	1.25	9.26	0.53
	1.25	9.34	0.53
	1.26	9.36	0.53
Speed 2	1.30	9.59	0.45
61318	1.34	10.04	0.49
	1.36	10.27	0.50
	1.37	10.39	0.51
	1.38	10.52	0.52
	1.39	10.59	0.52
	1.39	10.65	0.52
Speed 3	1.44	10.56	0.45
72507	1.49	11.06	0.48
	1.52	11.29	0.50
	1.54	11.44	0.51
	1.56	11.54	0.51
	1.57	11.62	0.51
	1.57	11.66	0.52
Speed 4	1.62	11.37	0.45
83795	1.70	11.81	0.48
	1.75	12.02	0.49
	1.78	12.13	0.50
	1.80	12.20	0.51
	1.82	12.27	0.51
	1.83	12.28	0.51
Speed 5	1.87	11.88	0.45
95000	1.99	12.17	0.47
	2.06	12.34	0.48
	2.10	12.38	0.49
	2.15	12.48	0.48
	2.16	12.45	0.49
	2.16	12.46	0.49
Speed 6	2.28	12.04	0.44
106205	2.42	12.16	0.46
	2.52	12.20	0.46
	2.59	12.19	0.46
	2.63	12.19	0.46
	2.65	12.20	0.46
	2.61	12.21	0.46

Table B6: Turbocharger map: fully open

APPENDIX C
AIR BASED FEASIBILITY
&
CHOKING CALCULATIONS

C1 - SYSTEM FEASIBILITY CALCULATIONS

This appendix shows the theoretical calculations carried out to determine the feasibility of an air based recovery system using the Brighton gas turbine cycle. Figure C1 is a representation of such a recovery system and shows the parameters needed for the calculations to follow, which utilises a software package accompanying Çengel and Boles (1994). Please note that the calculations have been done in the following order: the input data is determined; the program processing takes place; and the resulting efficiencies are shown.

C1.1 - CALCULATIONS

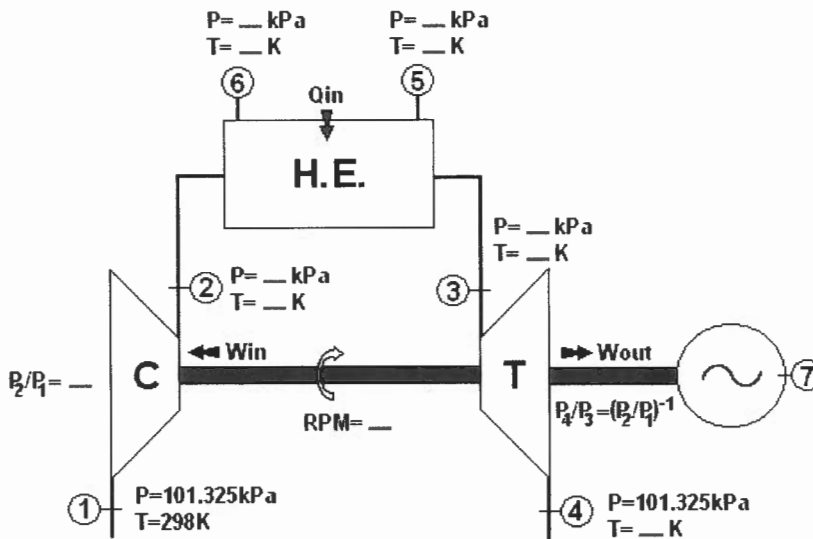


Figure C1: Recovery system diagram

Below can be seen the data generated for the ideal Brayton recovery system. The data shows a very low maximum obtainable efficiency of 12.19%.

Compressor efficiency		80 [%]
Turbine efficiency		80 [%]
Generator efficiency		95 [%]
Comp inlet pressure	{1}	101.325 [kPa]
Comp inlet temperature	{1}	24 [°C]
Turbine inlet temperature	{3}	600 [°C]
Pressure ratio	{1-2}	4 [-]
Program Processing		
Wout		51.76 [kJ/kg]
Overall cycle efficiency		12.19 [%]

Table C1: Ideal Brayton cycle

C1.2 - UTILISING THE TURBOCHARGER-MAPS

The following data was generated using the turbocharger-maps (*as in appendix B*) in conjunction with the simulation software as supplied by Çengel and Boles (1994).

Proposed H.E. properties without air-cooler & P.R. = 1.15 & Eff. @ 65%

Compressor efficiency		65 [%]	
Turbine efficiency		65 [%]	
Generator efficiency		95 [%]	
H.E. mass flow	{5}	0.055 [kg/s]	
H.E. inlet	{5}	360 [°C]	641.93 [kJ/kg]
H.E. inlet pressure	{5}	101.345 [kPa]	
H.E. outlet temperature	{6}	24 [°C]	297.33 [kJ/kg]
H.E. outlet pressure	{6}	101.325 [kPa]	
Comp Mass flow	{1}	0.02495 [kg/s]	
Comp inlet temperature	{1}	24 [°C]	
Comp inlet pressure	{1}	101.325 [kPa]	
Heat supplied	{5-6}	18.953 [kJ/s]	
Pressure ratio	{1-2}	1.15 [-]	
Pressure	{2,3}	116.52375 [kPa]	
Heat transferred	{5-6}	759.639279 [kJ/kg]	
Program Processing			
Wout		7.5800 [kJ/kg]	
		189.1210 [W]	
Generator	{7}	179.6650 [W]	
Overall cycle efficiency		0.9978 [%]	

Table C2: Case study 1

Proposed H.E. properties without air-cooler & P.R. = 1.2 & Eff. @ 60%

Compressor efficiency		60 [%]	
Turbine efficiency		60 [%]	
Generator efficiency		95 [%]	
H.E. mass flow	{5}	0.055 [kg/s]	
H.E. inlet	{5}	360 [°C]	641.93 [kJ/kg]
H.E. inlet pressure	{5}	101.345 [kPa]	
H.E. outlet temperature	{6}	24 [°C]	297.33 [kJ/kg]
H.E. outlet pressure	{6}	101.325 [kPa]	
Comp Mass flow	{1}	0.01512 [kg/s]	
Comp inlet temperature	{1}	24 [°C]	
Comp inlet pressure	{1}	101.325 [kPa]	
Heat supplied	{5-6}	18.95 [kJ/s]	
Pressure ratio	{1-2}	1.2 [-]	
Pressure	{2,3}	121.59 [kPa]	
Heat transferred	{5-6}	1253.51 [kJ/kg]	
Program Processing			
Wout		18.01 [kJ/kg]	
		272.31 [W]	
Generator	{7}	258.70 [W]	
Overall cycle efficiency		1.44 [%]	

Table C3: Case study 2

Insulated piping without air-cooler & P.R. = 1.2 & Eff. @ 65%

Compressor efficiency		65 [%]	
Turbine efficiency		65 [%]	
Generator efficiency		95 [%]	
H.E. mass flow	{5}	0.055 [kg/s]	
H.E. inlet	{5}	450 [°C]	738.33 [kJ/kg]
H.E. inlet pressure	{5}	101.345 [kPa]	
H.E. outlet temperature	{6}	24 [°C]	297.33 [kJ/kg]
H.E. outlet pressure	{6}	101.325 [kPa]	
Comp Mass flow	{1}	0.02722 [kg/s]	
Comp inlet temperature	{1}	24 [°C]	
Comp inlet pressure	{1}	101.325 [kPa]	
Program Processing			
Wout		13.52 [kJ/kg]	
		368.01 [W]	
Generator	{7}	349.61 [W]	
Overall cycle efficiency		1.52 [%]	

Table C4: Case study 3

Insulated piping without air-cooler & P.R. = 1.3 & Eff. @ 65%

Compressor efficiency		65 [%]	
Turbine efficiency		65 [%]	
Generator efficiency		95 [%]	
H.E. mass flow	{5}	0.055 [kg/s]	
H.E. inlet	{5}	450 [°C]	738.33 [kJ/kg]
H.E. inlet pressure	{5}	101.345 [kPa]	
H.E. outlet temperature	{6}	24 [°C]	297.33 [kJ/kg]
H.E. outlet pressure	{6}	101.325 [kPa]	
Comp Mass flow	{1}	0.02570 [kg/s]	
Comp inlet temperature	{1}	24 [°C]	
Comp inlet pressure	{1}	101.325 [kPa]	
Heat supplied	{5-6}	24.26 [kJ/s]	
Pressure ratio	{1-2}	1.3 [-]	
Pressure	{2,3}	131.72 [kPa]	
Heat transferred	{5-6}	943.77 [kJ/kg]	
Program Processing			
Wout		21.11 [kJ/kg]	
		542.53 [W]	
Generator	{7}	515.40 [W]	
Overall cycle efficiency		2.24 [%]	

Table C5: Case study 4

Insulated piping without air-cooler & P.R. = 1.8 & Eff. @ 75%

Compressor efficiency		75 [%]	
Turbine efficiency		75 [%]	
Generator efficiency		95 [%]	
H.E. mass flow	{5}	0.055 [kg/s]	
H.E. inlet	{5}	500 [°C]	792.64 [kJ/kg]
H.E. inlet pressure	{5}	101.345 [kPa]	
H.E. outlet temperature	{6}	24 [°C]	297.33 [kJ/kg]
H.E. outlet pressure	{6}	101.325 [kPa]	
Comp Mass flow	{1}	0.07258 [kg/s]	
Comp inlet temperature	{1}	24 [°C]	
Comp inlet pressure	{1}	101.325 [kPa]	
Heat supplied	{5-6}	27.24 [kJ/s]	
Pressure ratio	{1-2}	1.8 [-]	
Pressure	{2,3}	182.39 [kPa]	
Heat transferred	{5-6}	375.34 [kJ/kg]	
Program Processing			
Wout		12.66 [kJ/kg]	
		918.86 [W]	
Generator	{7}	872.92 [W]	
Overall cycle efficiency		3.37 [%]	

Table C6: Case study 5

Insulated piping without air-cooler & P.R. = 2 & Eff. @ 75%

Compressor efficiency		75 [%]	
Turbine efficiency		75 [%]	
Generator efficiency		95 [%]	
H.E. mass flow	{5}	0.055 [kg/s]	
H.E. inlet	{5}	600 [°C]	903.03 [kJ/kg]
H.E. inlet pressure	{5}	101.345 [kPa]	
H.E. outlet temperature	{6}	24 [°C]	297.33 [kJ/kg]
H.E. outlet pressure	{6}	101.325 [kPa]	
Comp Mass flow	{1}	0.08014 [kg/s]	
Comp inlet temperature	{1}	24 [°C]	
Comp inlet pressure	{1}	101.325 [kPa]	
Heat supplied	{5-6}	33.31 [kJ/s]	
Pressure ratio	{1-2}	2 [-]	
Pressure	{2,3}	202.65 [kPa]	
Heat transferred	{5-6}	415.69 [kJ/kg]	
Program Processing			
Wout		19.17 [kJ/kg]	
		1536.28 [W]	
Generator	{7}	1459.47 [W]	
Overall cycle efficiency		4.61 [%]	

Table C7: Case study 6

C1.3 - CONCLUSION

From the calculations based on the turbocharger-maps, it can be seen that the overall efficiency steadily increases as the pressure ratio and heat exchanger temperature is increased. The increase however is not sufficient to obtain system efficiencies above 4.6%. According to these results it will not be worthwhile to construct an air based recovery system.

C2 - CHOKING

Despite of the previous conclusion, there has also been looked at the possibility of choking inside the heat exchanger proposed by Lotun (2001). Ignoring bending losses inside the heat exchanger, the following calculations can be made with regard to the maximum mass flow allowed by the heat exchanger before choking of the air flow occurs.

C2.1 - CALCULATIONS

From White (1999), p. 586 eq. 9.46(b) ...

$$\dot{m}_{\max} = 0.6847 A^* \rho_o (RT_o)^{1/2} \quad \dots \text{(C1)}$$

where

\dot{m}_{\max} : maximum possible mass flow rate

A^* : pipe diameter

ρ_o : air density

R : air constant

T_o : air temperature

From data recorded by Lotun (2001), the following values were chosen:

$$A^* = 5.9583\text{E-}5 \text{ m}^2$$

$$\rho_o = 0.7464 \text{ kg/m}^3$$

$$R = 287 \text{ J/(kg.K)}$$

$$T_o = 473 \text{ K}$$

This results a maximum flow rate of

$$\dot{m}_{\max} = 0.011219 \text{ kg/s}$$

This value is much lower than the values calculated in table C1. The minimum value calculated for an efficiency of 24.89% was 0.0393kg/s. This means that the heat exchanger will most possibly cause the air, entering from the compressor side, to choke and thus limit the air flow entering the turbine.

By using equation C1, it can be determined that in order to obtain an air mass flow rate of 0.04kg/s, the tube inner diameter should be at least 16.45mm.

C2.2 - CONCLUSION

The recommendation concluded from these calculations, is thus that the heat exchanger proposed by Lotun (2001) will have to be replaced by a heat exchanger with an inner tube diameter larger than 16.45mm if an air based recovery system is to be used.

APPENDIX D
WATER BASED FEASIBILITY
CALCULATIONS

D1 - SYSTEM FEASIBILITY CALCULATIONS UTILISING THE SIMPLE RANKINE CYCLE

The following table shows the theoretical calculation results done to determine the feasibility of a water based simple Rankine recovery system utilising the software supplied with Çengel and Boles (1994).

Simple Rankine Cycle with Varying Turbine Pressures												
Compressor efficiency	[%]	80										
Turbine efficiency	[%]	80										
Generator efficiency	[%]	95										
Turbine inlet temperature	[°C]	600	600	600	600	600	600	600	600	600	600	600
Turbine inlet pressure	[kPa]	200	300	400	500	600	700	800	900	1000	1100	
Turbine outlet temperature	[°C]	505.64	453.99	420.47	395.68	374.86	358.85	344.34	333.04	321.83	313.38	
Turbine outlet pressure	[kPa]	101	101	101	101	101	101	101	101	101	101	101
Turbine work output	[kJ/kg]	203.703	311.695	381.239	432.331	473.97	505.874	534.705	556.996	579.115	595.532	
Pump work input	[kJ/kg]	0.129	0.26	0.39	0.521	0.651	0.782	0.912	1.042	1.173	1.303	
W _{net}	[kJ/kg]	203.57	311.44	380.85	431.81	473.32	505.09	533.79	555.95	577.94	594.23	
Overall Efficiency	[%]	6.2	9.48	11.6	13.15	14.42	15.4	16.27	16.96	17.63	18.13	

Table D1: Water based feasibility results

D1.1 - CONCLUSION

The recommendation concluded from these results, is that the simple Rankine cycle is a much more efficient way of recovering energy than the air based Brighton cycle discussed in appendix C. The same data was also applied to a two stage reheat Rankine cycle and showed an improvement of 1-2%. The efficiency increase will however have to be compared to the additional expense of adding another turbine and constructing the reheat system in later studies, to justify the two stage cycle.

APPENDIX E

CONTINUOUS COMBUSTION UNIT

E1 - CONTINUOUS COMBUSTION UNIT

E1.1 - INTRODUCTION

The Hilton Combustion Demonstration Unit was built approximately in 1970 by P.A. Hilton Ltd, England, UK. It offers a wide range of application, from simple demonstrations for boiler operators to research and development projects. One of the main uses of this unit is to offer a series of experiments for undergraduate and postgraduate students regarding combustion with heat transfer and temperature measurement. Another main use of the unit is to provide this heat exchanger project with sufficient energy in the form of hot exhaust gases.

E1.2 - ASSEMBLY

The main assembly parts of this unit can be summarized as follow:

Burner:	Schildrop No.3 Combustion Burner
Air Supply:	3 stage centrifugal blower
Observation Chamber:	double shell stainless steel tube 460mm internal diameter 910mm length 5 observation windows
Controls:	Automatic safety control system Manual controls for air and fuel Liquid and gaseous fuel metering valve Main chamber cooling water flow control valve
Electrical Supply:	240/1/50
Instrumentation:	Air flow: Orifice plate Fuel flow: Glass tube Rotameter 0-13kg/h Manometer Gas. 0-19kg/h Water flow: Glass tube Rotameter 0-1600kg/h Water temp.: Inlet and Outlet Air temp.: Inlet Exhaust gas: Thermocouple 0-1000 °C

E1.3 - OPERATING NOTES

The unit runs either on liquid or on gaseous fuel. The fuel is mixed with air to a specific air/fuel ratio. The flow rate can be varied over a wide range of air/fuel ratios, e.g. between 10:1 and 50:1 for air/propane. As soon as the air/fuel mixture is blown into the combustion chamber it has to be ignited immediately by activating the ignition electrode. After this procedure a flame can be seen through the observation windows along the chamber. The chamber is water cooled to avoid damage to the unit itself and to the environment as well as for obtaining information about the released energy absorbed by the water. The integrated control displays allow the collection of all information needed to calculate for instance heat balance, energy balance, flame radiation and heat transfer.

Several safety features, like flame failure solenoid valves, ultra violet flame detector, water outlet temperature sensor, etc., ensure safe working conditions.

The operating procedure was previously recorded by Schwack and Harms (2000).

E2 - CONTINUOUS COMBUSTION UNIT OPERATION *(SCHWACK AND HARMS, 2000)*

E2.1 - RUNNING ON GASEOUS FUEL

1. Ensure that all fuel valves are closed.
2. Zero the air flow using the calibration adjustment on the side of the unit.
3. Drain any condensate in the combustion chamber by unscrewing the drain knob below the combustion chamber.
4. Open the water in the following order:
 - a) Open main (**RED**) water valve at the waste heat exchanger completely.
 - b) Open main (**BLACK**) water supply.
 - c) Open secondary (**RED**) water supply valve completely.
5. Switch on the mains (**grid**) at lead.
6. Switch the mains (**RED**) switch on the combustion unit.
7. Push the fan start button.
8. Open the air inlet to maximum (**position 8**).

9. Open the gas bottle completely.
10. Set the air mass flow rate to 50kg/h.
11. Start the combustion as follow:
 - a) Make sure the reset switch is in the off (**UP**) position.
 - b) Press the instrument reset switch button (**PURPLE**).
 - c) Set the reset switch to the on position (**DOWN**).
 - d) Wait for the solenoid to open (a "**TAK**" sound will be heard).
 - e) **PRESS AND HOLD** the black ignition switch.
 - f) While still holding the ignition open, turn the fuel knob and set the fuel flow to 4-5kg/h.
 - g) After a flame has been established hold the ignition switch for a further 5 seconds.
12. If ignition is not successful:
 - a) Close the gas flow knob on the combustion unit.
 - b) Turn off the fuel supply at the main supply (**gas bottle**).
 - c) Open the air flow valve to its maximum (**position 8**).
 - d) Wait 2 minutes to purge any unburned fuel from the combustion chamber.
 - e) Repeat procedure 9 to 11.
13. Shut down Procedure:
 - a) Turn of the fuel supply at the source (**gas bottle**).
 - b) Switch off the reset switch.
 - c) Progressively move the air flow control to maximum (**position 8**).
 - d) Wait for 2 minutes for any gasses and unburned fuel to purge.
 - e) Press the stop (**RED**) button to switch off fan.
 - f) Switch the mains switch off.
 - g) Disconnect the mains.
 - h) Close the water valve in the following order: **BLACK** and **RED** valves at the main supply, then the **BLUE** on the panel.

E2.2 - SWITCHING OVER TO LIQUID FUEL

Important: Run the combustion unit on the gaseous fuel for at least 10 minutes to allow the normal operating conditions to be reached.

1. Slowly open the liquid fuel valve (**bottom right on panel**) and simultaneously slowly close the gas fuel using the control valve on the unit (the colour of the flame will change from blue to bright yellow and the exhaust note might also change).

Note: The switching over will be achieved by progressively and simultaneously performing the above. The whole procedure should take about **30 seconds**.

2. If the gas fuel is no longer required, turn off at the main supply (**gas bottle**).

3. Shut down procedure:

- a) Turn off the liquid fuel control valve on the panel.
- b) Switch off the reset switch.
- c) Progressively move the air flow control to its maximum (**position 8**)
- d) Wait 2 minutes for all gasses and any unburned fuel to purge
- e) Press stop (**RED**) button to switch off the fan
- f) Switch off electricity at unit (**RED**) and mains
- g) Disconnect mains
- h) Close the water valve in the following order: **BLACK** and **RED** valves at the main supply, then the **BLUE** on the panel.

The information sources for this appendix were Combustion Laboratory Unit (1997) and Schwack and Harms (2000).

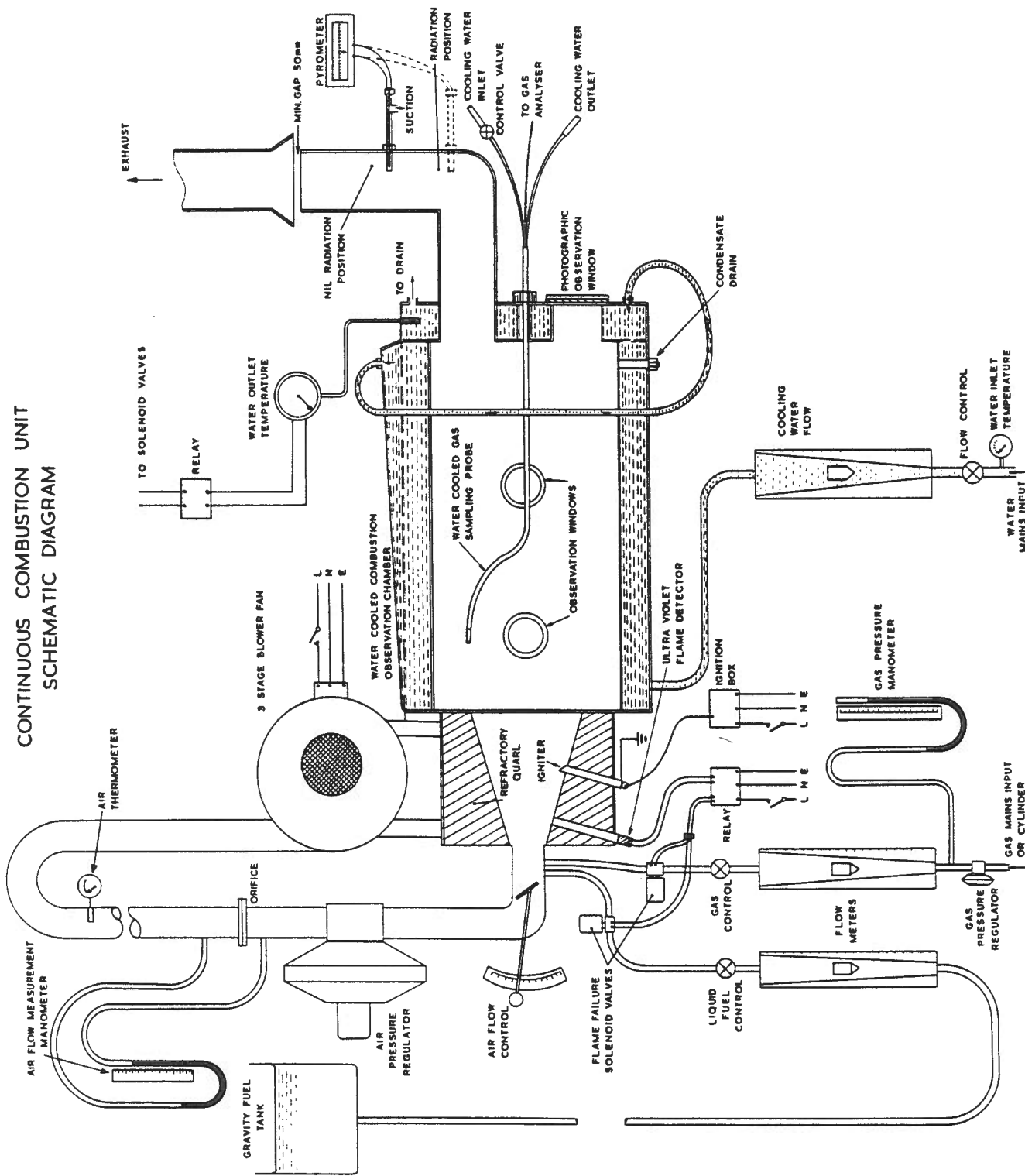


Figure E1: Continuous combustion unit

APPENDIX F

CORRELATIONS

F1 - FRIEDEL CORRELATION FOR FRICTIONAL TWO-PHASE PRESSURE GRADIENT (as from Whalley (1987))

The Friedel (1979) correlation is probably the most generally available correlation for the frictional two-phase pressure gradient. It is written in terms of a two-phase multiplier...

$$\phi_{lo}^2 = \frac{\left(-\frac{dp}{dz}\right)_F}{\left(-\frac{dp}{dz}\right)_{lo}} \quad \dots(\text{F1})$$

where $(-dp/dz)_F$ is the frictional pressure gradient (N/m^3) in the two-phase flow, and $(-dp/dz)_{lo}$ is the frictional pressure gradient (N/m^3) in single-phase liquid flow with the same mass flow rate as the total two-phase flow rate. Then...

$$\phi_{lo}^2 = E + \frac{3.24FH}{Fr^{0.045}We^{0.035}} \quad \dots(\text{F2})$$

$$E = (1-x)^2 + x^2 \frac{\rho_l C_{fgo}}{\rho_g C_{flo}} \quad \dots(\text{F3})$$

$$F = x^{0.78} (1-x)^{0.224} \quad \dots(\text{F4})$$

$$H = \left(\frac{\rho_l}{\rho_g}\right)^{0.91} \left(\frac{\mu_g}{\mu_l}\right)^{0.19} \left(1 - \frac{\mu_g}{\mu_l}\right)^{0.7} \quad \dots(\text{F5})$$

$$Fr = \frac{G^2}{gd\rho_h^2} \quad \dots(\text{F6})$$

$$We = \frac{G^2 d}{\sigma\rho_h} \quad \dots(\text{F7})$$

$$\rho_h = \left(\frac{x}{\rho_g} + \frac{1-x}{\rho_l}\right)^{-1} \quad \dots(\text{F8})$$

where x is the quality; ρ_g is the gas density [kg/m^3]; ρ_l is the liquid density [kg/m^3]; C_{fgo} and C_{flo} are the friction factors for the total mass flux flowing with the gas and liquid properties respectively; μ_g is the gas viscosity [N.s/m^2]; μ_l is the liquid viscosity [N.s/m^2]; σ is the surface tension [N/m]; and g is the acceleration due to gravity ($=9.81\text{m/s}^2$).

Note that the definition of the Weber number (We) is not the same as that used in the CISE correlation for the determination of the void fraction (Eq. F16).

F2 - CISE CORRELATION FOR VOID FRACTION*(as from Whalley (1987))*

The correlation of Premoli et al. (1970), usually known as the CISE correlation is a correlation in terms of the slip ratio S . The void fraction, α , is then given by...

$$\alpha = \frac{1}{1 + \left(S \frac{1-x}{x} \frac{\rho_g}{\rho_l} \right)} \quad \dots(\text{F9})$$

The slip ratio is then given by...

$$S = 1 + E_1 \left(\frac{y}{1 + yE_2} - yE_2 \right)^{0.5} \quad \dots(\text{F10})$$

where...

$$y = \frac{\beta}{1 - \beta} \quad \dots(\text{F11})$$

$$\beta = \frac{\rho_l x}{\rho_l x + \rho_g (1 - x)} \quad \dots(\text{F12})$$

$$E_1 = 1.578 \text{Re}^{-0.19} \left(\frac{\rho_l}{\rho_g} \right)^{0.22} \quad \dots(\text{F13})$$

$$E_2 = 0.0273 \text{We} \text{Re}^{-0.51} \left(\frac{\rho_l}{\rho_g} \right)^{-0.08} \quad \dots(\text{F14})$$

$$\text{Re} = \frac{Gd}{\mu_l} \quad \dots(\text{F15})$$

$$\text{We} = \frac{G^2 d}{\sigma \rho_l} \quad \dots(\text{F16})$$

where x is the quality; ρ_g is the gas density [kg/m^3]; ρ_l is the liquid density [kg/m^3]; d is the tube diameter [m]; μ_l is the liquid viscosity [$\text{N}\cdot\text{s/m}^2$]; G is the total (liquid+gas) mass flux [$\text{kg/m}^2\text{s}$]; and σ is the surface tension [N/m].

Note that the definition of the Weber number (We) is not the same as that used in the Friedel correlation for frictional two-phase pressure gradient (Eq. F7).

F3 - CHEN CORRELATION FOR BOILING HEAT TRANSFER TO SATURATED FLUIDS IN CONVECTIVE FLOW (as from Chen (1963))

The Chen correlation uses the superpositioning of nucleation and forced convection mechanisms. The convective transfer is expressed as a function of the two-phase Reynolds number after Lockhart-Martinelli, and the nucleation transfer is obtained from the nucleate boiling correlation of Forster and Zuber (1955). The Chen correlation can be expressed as...

$$h = h_{mic} + h_{mac} \quad \dots(F17)$$

with the total heat transfer coefficient equal to the sum of a microscopic (nucleate boiling) contribution, h_{mic} , and a macroscopic (bulk convective) contribution, h_{mac} , where...

$$h_{mic} = 0.00122 \frac{k_l^{0.79} C_{pl}^{0.45} \rho_l^{0.49}}{\sigma^{0.5} \mu_l^{0.29} h_{lg}^{0.24} \rho_g^{0.24}} \Delta T_{sat}^{0.24} \Delta P_{sat}^{0.75} S \quad \dots(F18)$$

$$h_{mac} = 0.023 \left[\frac{G(1-x)D}{\mu_l} \right]^{0.8} \left[\frac{\mu C_p}{k} \right]_l^{0.4} \frac{k_l}{D} F \quad \dots(F19)$$

where...

$$S = \frac{1}{1 + 2.53 \times 10^{-6} F^{1.25} \frac{G(1-x)D}{\mu_l}} \quad \dots(F20)$$

$$F = \begin{cases} 1.0 & \dots \frac{1}{X_{tt}} \leq 0.1 \\ 2.35 \left(\frac{1}{X_{tt}} + 0.213 \right)^{0.736} & \dots \frac{1}{X_{tt}} > 0.1 \end{cases} \quad \dots(F21)$$

$$X_{tt} = \left(\frac{1-x}{x} \right)^{0.9} \left(\frac{\rho_g}{\rho_l} \right)^{0.5} \left(\frac{\mu_l}{\mu_g} \right)^{0.1} \quad \dots(F22)$$

where G is the mass flux [$\text{kg/m}^2\text{s}$]; D is the tube diameter [m]; h_{lg} is the latent heat of vaporization [J/kg]; C_p is the specific heat [J/kg.K]; x is the local quality; μ_l is the liquid viscosity [N.s/m^2]; μ_g is the gas viscosity [N.s/m^2]; K is the thermal conductivity [W/m.K]; σ is the surface tension [N/m]; ΔT_{sat} is the wall superheat [K]; ΔP_{sat} is the difference between the saturation pressures calculated from the wall temperature and the fluid temperature [Pa]; S is the suppression factor; F the enhancement factor; X_{tt} is the turbulent-turbulent Lockhart-Martinelli parameter.

APPENDIX G
MICROSOFT® EXCEL 2002 SPREADSHEET

<p>Discription: This spreadsheet attempts to determine the heat exchanger geometry for a given energy balance.</p>		<p>Calculation Results</p>					
<p>Energy Balance (Energy Balance)</p> <p>Inputs: Mass flow rates Pressures Efficiencies Graphdata Inlet and Outlet exhaust temperatures Energy balance for Pre-heater, Boiler and Super-heater stages</p> <p>Outputs: Energy balance for Pre-heater, Boiler and Super-heater stages</p>		<p>Heat Exchanger Design</p> <p>Tubing: Stainless Steel 304 k 18 [W/m.K] Fin: Stainless Steel 304 k 18 [W/m.K] Heat Exchanger Width W 0.300 [m] Heat Exchanger Height H 0.359 [m] Staggered tube configuration Longitudinal tube pitch Sl 0.0371 [m] Transverse tube pitch St 0.0429 [m] Outer tube diameter Odt 0.022 [m] Tube thickness tt 0.003 [m] Fin pitch Pf 0.0025 [m] Fin thickness tf 0.0005 [m] # Tubes in a row Nt 4 [-] # of rows Nr 12 [-] Heat Exchanger Length L,he 0.474 [m] Total Tube Length L,t 14.4 [m] Water side pressure drop Inlet Pressure Pin 2000 [kPa] Pressure Drop dP 6 [kPa] Outlet Pressure Pout 1994 [kPa] Exhaust side pressure drop Pressure Drop dP 0.05 [kPa] 0.06 [kPa]</p>					
<p>Heat Exchanger Geometry (Pre-heater, Boiler W, Boiler S, Super-heater)</p> <p>Inputs: Average exhaust Temperature in specified stage Average water Temperature in specified stage Conductivity of material used for tubes and fins Know properties of heat exchanger geometry</p> <p>Outputs: Average heat transfer coefficient for specified stage Heat exchanger effectivity for specified stage Number of tube-rows needed to achieve specified energy balance for each stage</p>		<p>The Rankine Cycle Used in Energy balance spreadsheet</p> <p>Pressure Drops Shows the pressure drop across and inside the heat exchanger</p>					
<p>Legend</p> <table border="1"> <tr><td>Variables</td></tr> <tr><td>Table data</td></tr> <tr><td>Calculated data</td></tr> <tr><td>Final Answers</td></tr> </table>		Variables	Table data	Calculated data	Final Answers		
Variables							
Table data							
Calculated data							
Final Answers							

Figure G.1: Main excel sheet

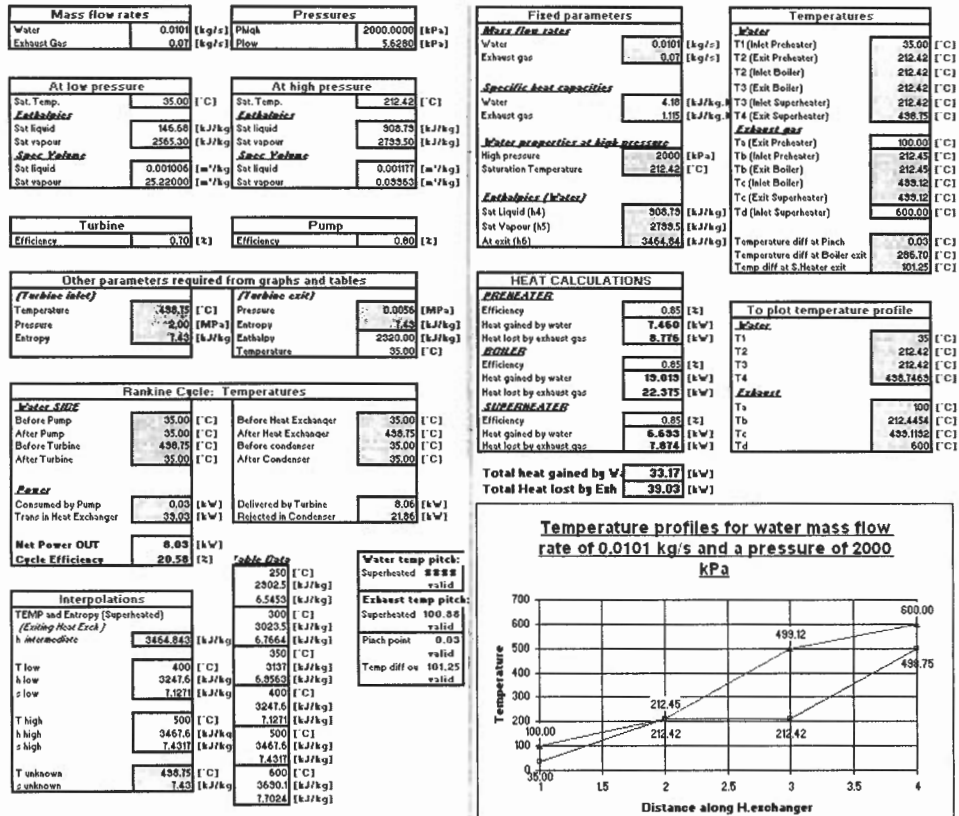


Figure G.2: Energy balance excel sheet

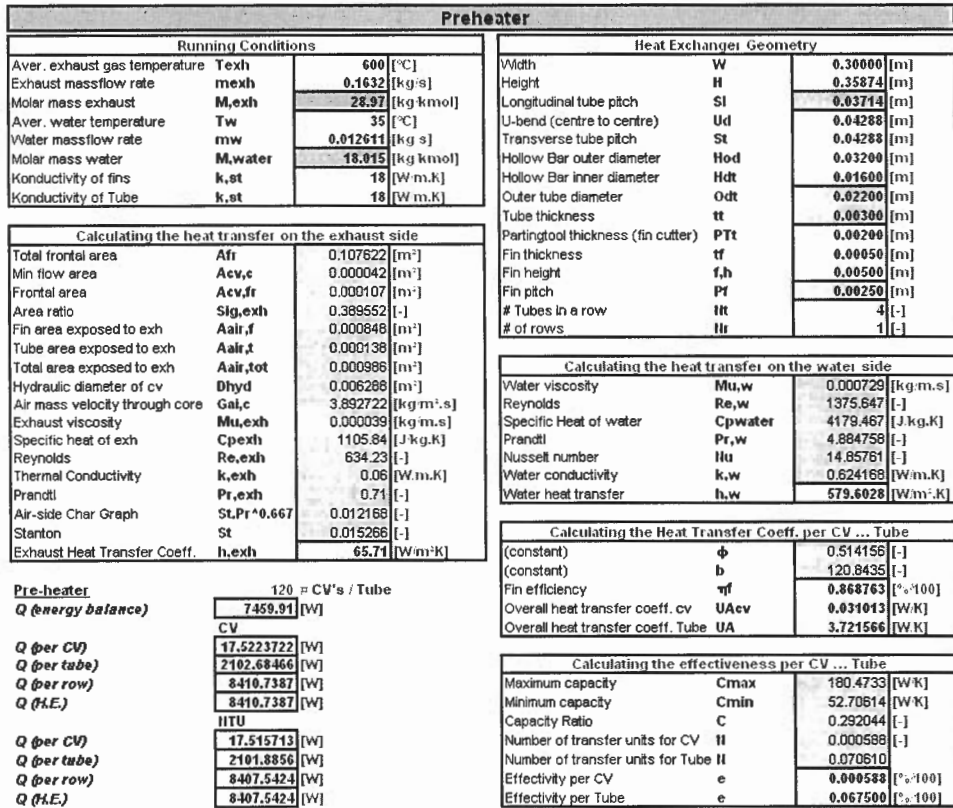


Figure G.3: Preheating excel sheet

Boiler (Water only)			
Running Conditions		Heat Exchanger Geometry	
Aver. exhaust gas temperature	T_{exh}	Width	W
Exhaust massflow rate	m_{exh}	Height	H
Molar mass exhaust	M_{exh}	Longitudinal tube pitch	Sl
Aver. water temperature	T_w	U-bend (centre to centre)	Ud
Water massflow rate	m_w	Transverse tube pitch	St
Molar mass water	M_{water}	Hollow Bar outer diameter	Hod
Conductivity of fins	k_{al}	Hollow Bar inner diameter	Hdt
Conductivity of Tube	k_{st}	Outer tube diameter	Odt
		Tube thickness	tt
		Partingtool thickness (fin cutter)	PTt
		Fin thickness	tf
		Fin height	fh
		Fin pitch	Pf
		# Tubes in a row	lt
		# of rows	lr
Calculating the heat transfer on the exhaust side			
Total frontal area	A_{fr}	Water viscosity	μ_{w}
Min flow area	$A_{cv,c}$	Reynolds	Re_w
Frontal area	$A_{cv,fr}$	Specific Heat of water	C_{pwater}
Area ratio	Sig_{exh}	Prandtl	Pr_w
Fin area exposed to exh	$A_{air,f}$	Nusselt number	lnu
Tube area exposed to exh	$A_{air,t}$	Water konstant	k_w
Total area exposed to exh	$A_{air,tot}$	Water heat transfer	h_w
Hydraulic diameter of cv	D_{hyd}		
Air mass velocity through core	Gal_c	Calculating the Heat Transfer Coeff. of the Heat Exchanger	
Exhaust viscosity	$\mu_{u,exh}$	(constant)	ϕ
Specific heat of exh	C_{pexh}	(constant)	b
Reynolds	Re_{exh}	Fin efficiency	η_f
Thermal Conductivity	k_{exh}	Overall heat transfer coeff. cv	UA_{cv}
Prantel	Pr_{exh}	Overall heat transfer coeff. Tube	UA
Air-side Char Graph	$St.Pr^{*0.667}$		
Starton	St	Calculating the effectiveness of the Heat Exchanger	
Exhaust Heat Transfer Coeff.	h_{exh}	Maximum capacity	C_{max}
		Minimum capacity	C_{min}
		Capacity Ratio	C
		Number of transfer units for CV	II
		Number of transfer units for Tub	II
		Effectivity per CV	e
		Effectivity per Tube	e
Boiler $120 = CV's / Tube$			
Q (energy balance)	19018.65		
Q (per CV)	5.2888492		
Q (per tube)	634.66190		
Q (per row)	2538.6476		
Q (f.l.e.)	20309.1809		
HTU			
Q (per CV)	5.2866248		
Q (per tube)	634.39497		
Q (per row)	2537.5799		
Q (f.l.e.)	20300.639		

Figure G.4: Boiler (water only) excel sheet

Boiler (Steam only)			
Running Conditions		Heat Exchanger Geometry	
Aver. exhaust gas temperature	T_{exh}	Width	W
Exhaust massflow rate	m_{exh}	Height	H
Molar mass exhaust	M_{exh}	Longitudinal tube pitch	Sl
Aver. water temperature	T_w	U-bend (centre to centre)	Ud
Water massflow rate	m_w	Transverse tube pitch	St
Molar mass water	M_{water}	Hollow Bar outer diameter	Hod
Conductivity of fins	k_{al}	Hollow Bar inner diameter	Hdt
Conductivity of Tube	k_{st}	Outer tube diameter	Odt
		Tube thickness	tt
		Partingtool thickness (fin cutter)	PTt
		Fin thickness	tf
		Fin height	fh
		Fin pitch	Pf
		# Tubes in a row	lt
		# of rows	lr
Calculating the heat transfer on the exhaust side			
Total frontal area	A_{fr}	Water viscosity	$\mu_{u,s}$
Min flow area	$A_{cv,c}$	Reynolds	Re_s
Frontal area	$A_{cv,fr}$	Specific Heat of steam	$C_{p,s}$
Area ratio	Sig_{air}	Prandtl	Pr_s
Fin area exposed to exh	$A_{air,f}$	Nusselt number	lnu
Tube area exposed to exh	$A_{air,t}$	Water konstant	k_s
Total area exposed to exh	$A_{air,tot}$	Water heat transfer	h_s
Hydraulic diameter of cv	D_{hyd}		
Air mass velocity through core	Gal_c	Calculating the Heat Transfer Coeff. of the Heat Exchanger	
Exhaust viscosity	$\mu_{u,exh}$	(constant)	ϕ
Specific heat of exh	C_{pexh}	(constant)	b
Reynolds	Re_{exh}	Fin efficiency	η_f
Thermal Conductivity	k_{exh}	Overall heat transfer coeff. cv	UA_{cv}
Prantel	Pr_{exh}	Overall heat transfer coeff. Tube	UA
Air-side Char Graph	$St.Pr^{*0.667}$		
Starton	St	Calculating the effectiveness of the Heat Exchanger	
Exhaust Heat Transfer Coeff.	h_{exh}	Maximum capacity	C_{max}
		Minimum capacity	C_{min}
		Capacity Ratio	C
		Number of transfer units for CV	II
		Number of transfer units for Tub	II
		Effectivity per CV	e
		Effectivity per Tube	e
Boiler $120 = CV's / Tube$			
Q (energy balance)	19018.65		
Q (per CV)	3.3714739		
Q (per tube)	404.57687		
Q (per row)	1618.3075		
Q (f.l.e.)	19419.6896		
HTU			
Q (per CV)	3.3696809		
Q (per tube)	404.36171		
Q (per row)	1617.4469		
Q (f.l.e.)	19409.362		

Figure G.5: Boiler (steam only) excel sheet

Superheater			
Running Conditions		Heat Exchanger Geometry	
Aver. exhaust gas temperature	Texh	552	[°C]
Exhaust massflow rate	mexh	0.1632	[kg/s]
Molar mass exhaust	M,exh	28.97	[kg kmol]
Aver. water temperature	Ts	345	[°C]
Water massflow rate	mww	0.012611	[kg/s]
Molar mass water	M,water	18.015	[kg kmol]
Conductivity of fins	k,al	18	[W.m.K]
Conductivity of Tube	k,st	18	[W.m.K]
Calculating the heat transfer on the exhaust side		Calculating the heat transfer on the steam side	
Total frontal area	Afr	0.107822	[m²]
Min flow area	Aev,c	0.000042	[m²]
Frontal area	Aev,fr	0.000107	[m²]
Area ratio	Sigair	0.389552	[-]
Fin area exposed to exh	Aair,f	0.000848	[m²]
Tube area exposed to exh	Aair,t	0.000138	[m²]
Total area exposed to exh	Aair,tot	0.000986	[m²]
Hydraulic diameter of cv	Dhyd	0.006288	[m]
Air mass velocity through core	Gair,c	3.89	[kg m⁻².s]
Exhaust viscosity	Mu,exh	0.000037	[kg m.s]
Specific heat of exh	Cp,exh	1096.13	[J kg.K]
Reynolds	Re,exh	659.80	[-]
Thermal Conductivity	k,exh	0.08	[W.m.K]
Prantel	Pr,exh	0.71	[-]
Air-side Char Graph	St.Pr*0.667	0.011990	[-]
Stanton	St	0.015068	[-]
Exhaust Heat Transfer Coeff.	h,exh	64.29	[W.m².K]
Superheater		120 = CV's / Tube	
Q (energy balance)		6692.69	[W]
Q (per CV)		5.2553112	[W]
Q (per tube)		630.63735	[W]
Q (per row)		2522.5494	[W]
Q (I.E.)		7567.6482	[W]
HITU			
Q (per CV)		5.2523364	[W]
Q (per tube)		630.28037	[W]
Q (per row)		2521.1215	[W]
Q (I.E.)		7563.3644	[W]
Calculating the Heat Transfer Coeff. of the Heat Exchanger		Calculating the effectiveness of the Heat Exchanger	
(constant)	φ	0.514156	[-]
(constant)	b	119.524349	[-]
Fin efficiency	ηf	0.871174	[%=100]
Overall heat transfer coeff. cv	UAcv	0.025388	[W.K]
Overall heat transfer coeff. Tube	UA	36.558687	[W.K]
Maximum capacity	Cmax	178.8890	[W.K]
Minimum capacity	Cmin	25.62690	[W.K]
Capacity Ratio	C	0.143258	[-]
Number of transfer units for CV	NTU	0.000991	[-]
Number of transfer units for Tub	NTU	1.426575	[-]
Effectivity per CV	e	0.000990	[%=100]
Effectivity per Tube	e	0.719973	[%=100]

Figure G.6: Superheating excel sheet

The Rankine Cycle	
Mass flow rates	
Water	0.01006 [kg/s]
Pressures	
Phigh	2008.00 [kPa]
Plow	6.83 [kPa]
Spec Vol at Plow	
Sat Liquid	0.00104 [m³/kg]
Sat vapour	25.22 [m³/kg]
Spec Vol at Phigh	
Sat Liquid	0.00118 [m³/kg]
Sat vapour	0.09963 [m³/kg]
Work done by Pump	
Ideal	2.34738 [kJ/kg]
Actual (per kg)	2.93422 [kJ/kg]
Work done by Turbine	
Ideal	1144.84 [kJ/kg]
Actual (per kg)	801.39 [kJ/kg]
Total work	0.02952 [kW]
Total work	8.06118 [kW]
Heat Abs in Waste Heat Exch	
Total rate of absorp	39.03 [kW]
Heat Rejected in Condenser	
Total rate of reject	21.8614 [kW]
Nett Work Out	8.03167 [kW]
Energy Entering Boiler	39.03 [kW]
Cycle Efficiency	20.5808 [%]

Figure G.7: Rankine cycle excel sheet

APPENDIX H
MICROSOFT® VISUAL BASIC 6.0
SIMULATION PROGRAM

H1 - VISUAL BASIC SIMULATION PROGRAM

H1.1 - INTRODUCTION

A computer simulation program was written in order to optimize the system design process. The simulation program is written in Microsoft® Visual Basic 6.0, Copyright ©1987-1998 Microsoft Corp. It is called the “Heat Exchanger Simulation Program (HESP)” and uses fin-tube theory to estimate the resulting pressures and temperatures when water and exhaust gasses are used inside a cross flow, shell-and-fintube heat exchanger.

The analysis was broken up into three parts: the preheated stage, the boiler stage and the superheated stage. For both the preheated- and superheated stage, single-phase theory was used, while two-phase theory was used for the boiler stage. This included the Friedel correlation for frictional two-phase pressure gradient – Whalley (1987), Chen’s correlation for boiling heat transfer to saturated fluids in convective flow – Chen (1963) and the CISE correlation for void fraction – Whalley (1987) (*see appendix F*).

The following appendix will provide a simple explanation as to how the program works as well as a detailed flow chart showing the program functions and sub functions.

H1.2 - PROGRAM STARTUP

When the program file “HESP.exe” is executed, the following window will appear on your screen.

Heat Exchanger Simulation Program - Finned Tubes

Running Conditions		Heat Exchanger Geometry			
Gas Inlet Temp	600 [°C]	Tube Conductivity	18 [W/m.K]	Fin Conductivity	18 [W/m.K]
Gas Inlet Press	101.4 [kPa]	Tube Length	0.3 [m]	Fin Thickness	0.0005 [m]
Gas Mass Flow	0.1632 [kg/s]	Outer Tube Diameter	0.022 [m]	Fin Pitch	0.0025 [m]
Water Inlet Temp	25 [°C]	Inner Tube Diameter	0.016 [m]	Fin Height	0.005 [m]
Water Inlet Press	2000 [kPa]	Longitudinal Tube Pitch	0.0371 [m]	Nr of Tubes/Row	8 [#]
Water Mass Flow	0.012611 [kg/s]	Transverse Tube Pitch	0.04288 [m]	Nr of Rows	5 [#]

Implicit Geometries		Simulation Results			
Tube Thickness	0.003 [m]	Nr of Control Volumes/Tube	[#]	Starting Temperature	220 [°C]
H.E. Height	0.35874 [m]	Total nr of Control Volumes	[#]	Accuracy to nearest °C	0.005 [°C]
Frontal Area	0.107622 [m²]			Iterations	
Area Exp to Gas	0.0009864 [m²]	Gas Inlet Temp	[°C]	Error	[°C]
Area Exp to Water	0.0001256 [m²]	Gas Outlet Temp	[°C]		

Analysis Progress		Gas Side		Water Side	
Nr of Tubes done	[#]	Gas Outlet Temp	[°C]	Water Outlet Temp	[°C]
Tube Distance Remaining	[m]	Gas Outlet Press	[kPa]	Water Outlet Press	[kPa]
		Gas Side Press Drop	[kPa]	Water Side Press Drop	[kPa]

Max Energy Transfer	[kW]	H.E. Effectiveness	[%]
Actual Heat Transfer	[kW]	Average Fin Efficiency	[%]

File Name: Results

Buttons: Implicit Geometries, Default Values, Run Simulation, Exit Program

Figure H1: Main interface

The interface is divided into different sections to simplify the use of the program. The first section is captioned “Running Conditions” and contains all the fields necessary to enter the starting conditions of the water and exhaust gas.

Running Conditions

Gas Inlet Temp	600 [°C]
Gas Inlet Press	102 [kPa]
Gas Mass Flow	0.1632 [kg/s]
Water Inlet Temp	25 [°C]
Water Inlet Press	2000 [kPa]
Water Mass Flow	0.012611 [kg/s]

Figure H2: Running conditions

It should be noted that the SI-units appear in blue and must be applied to ensure accurate results.

The next section is captioned “Heat Exchanger Geometry”. The section contains all the fields necessary for the input of the various heat exchanger geometries. You will notice that the tube- and fin conductivities will not necessarily stay the same during an actual test, but to simplify the calculations, average values will have to be used as inputs.

Heat Exchanger Geometry					
Tube Conductivity	<input type="text" value="18"/>	[W/m.K]	Fin Conductivity	<input type="text" value="18"/>	[W/m.K]
Tube Length	<input type="text" value="0.3"/>	[m]	Fin Thickness	<input type="text" value="0.0005"/>	[m]
Outer Tube Diameter	<input type="text" value="0.022"/>	[m]	Fin Pitch	<input type="text" value="0.0025"/>	[m]
Inner Tube Diameter	<input type="text" value="0.016"/>	[m]	Fin Height	<input type="text" value="0.005"/>	[m]
Longitudinal Tube Pitch	<input type="text" value="0.0371"/>	[m]	Nr of Tubes/Row	<input type="text" value="8"/>	[#]
Transverse Tube Pitch	<input type="text" value="0.04268"/>	[m]	Nr of Rows	<input type="text" value="5"/>	[#]

Figure H3: Heat exchanger geometries

The next section is the “Implicit Geometries” section. This section provides the geometries that are implied by the inputs of the previous section and can be updated by left-clicking with the mouse on the “Implicit Geometries” button located at the bottom-left corner of the window.

Implicit Geometries	
Tube Thickness	<input type="text" value="0.003"/> [m]
H.E. Height	<input type="text" value="0.35874"/> [m]
Frontal Area	<input type="text" value="0.107622"/> [m ²]
Area Exp to Gas	<input type="text" value="0.0009864"/> [m ²]
Area Exp to Water	<input type="text" value="0.0001256"/> [m ²]

Figure H4: Implicit geometries

It should be noted that the input boxes in this section are light-brown, while the input boxes in the previous sections are yellow. The brown boxes indicate that the values are program calculated, while the yellow boxes are user defined inputs.

By left-clicking with the mouse on the “Default Values” button, you can load the optimum input values applicable to this project. These values are stored in the

“Default.txt” file and can be edited at any time by opening the text file in Windows Explorer.

After the implicit geometries have been calculated, part of the “Simulation Results” section will become active showing the amount of control volumes per tube as well as the total amount of control volumes contained inside the heat exchanger. Indicated as inputs in this section, is an estimation of the temperature at which the exhaust gasses will leave the heat exchanger and the accuracy to which the program will determine the starting temperature. The duration of the simulation will depend on the gas temperature chosen and the specified accuracy.

Simulation Results			
Nr of Control Volumes/Tube	120 (#)	Starting Temperature	220 (°C)
Total nr of Control Volumes	4800 (#)	Accuracy to nearest °C	0.005 (°C)
		Iterations	
Gas Inlet Temp	Error	Gas Outlet Temp	
(°C)	(°C)	(°C)	
Gas Side		Water Side	
Gas Outlet Temp	(°C)	Water Outlet Temp	(°C)
Gas Outlet Press	(kPa)	Water Outlet Press	(kPa)
Gas Side Press Drop	(kPa)	Water Side Press Drop	(kPa)
Max Energy Transfer	(kW)	H.E. Effectiveness	(%)
Actual Heat Transfer	(kW)	Average Fin Efficiency	(%)

Figure H5: Simulation results

The last input that can be specified is the file in which the results will be stored after the completion of the simulation run. This file name can be entered into the text box at the bottom-left corner of the window. The default filename is “Sim_Results.txt”.

File Name: Results

Figure H6: Save file text box

When all the inputs have been entered, the “Run Simulation” button can be left-clicked with the mouse. This will start the simulation process and may take a few minutes, depending on the capabilities of your PC.

The program will now keep you up to date with the simulation results by displaying them in the “Simulation Results” section. You will notice that the error becomes smaller as the simulation progresses. There is also a progress bar which indicates the number of control volumes processed and the stage in which the calculations are currently evolved. In addition another section, “Analysis Progress”, is also activated and shows the length of tube as the number of control volumes increase. Once the simulation has reached a satisfactory answer (specified by the gas inlet temperature and the accuracy needed), the following window will appear. This indicates that the program is busy writing the data to the specified file.

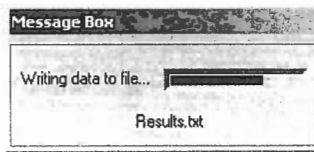


Figure H7: Writing data to text file

The main interface will now appear as follow:

Heat Exchanger Simulation Program - Finned Tubes

Running Conditions Gas Inlet Temp: 600 [°C] Gas Inlet Press: 101.4 [kPa] Gas Mass Flow: 0.1632 [kg/s] Water Inlet Temp: 25 [°C] Water Inlet Press: 2000 [kPa] Water Mass Flow: 0.012611 [kg/s]		Heat Exchanger Geometry Tube Conductivity: 18 [W/m.K] Tube Length: 0.3 [m] Outer Tube Diameter: 0.022 [m] Inner Tube Diameter: 0.016 [m] Longitudinal Tube Pitch: 0.0371 [m] Transverse Tube Pitch: 0.04288 [m] Fin Conductivity: 18 [W/m.K] Fin Thickness: 0.0005 [m] Fin Pitch: 0.0025 [m] Fin Height: 0.005 [m] Nr of Tubes/Row: 8 [#] Nr of Rows: 5 [#]																	
Implicit Geometries Tube Thickness: 0.003 [m] H.E. Height: 0.35874 [m] Frontal Area: 0.107622 [m²] Area Exp to Gas: 0.0009864 [m²] Area Exp to Water: 0.0001256 [m²]		Simulation Results Nr of Control Volumes/Tube: 120 [#] Total nr of Control Volumes: 4800 [#] Starting Temperature: 220 [°C] Accuracy to nearest °C: 0.005 [°C] Iterations: 14 Gas Inlet Temp: 599.99544 [°C] Error: 0.00456 [°C] Gas Outlet Temp: 361.34033 [°C] Superheater: 4800																	
Analysis Progress Nr of Tubes done: 40 [#] Tube Distance Remaining: 0 [m]		<table border="1"> <tr> <th colspan="2">Gas Side</th> <th colspan="2">Water Side</th> </tr> <tr> <td>Gas Outlet Temp</td> <td>361.34 [°C]</td> <td>Water Outlet Temp</td> <td>328.539 [°C]</td> </tr> <tr> <td>Gas Outlet Press</td> <td>101.386 [kPa]</td> <td>Water Outlet Press</td> <td>1730.626 [kPa]</td> </tr> <tr> <td>Gas Side Press Drop</td> <td>0.014192 [kPa]</td> <td>Water Side Press Drop</td> <td>269.374 [kPa]</td> </tr> </table>		Gas Side		Water Side		Gas Outlet Temp	361.34 [°C]	Water Outlet Temp	328.539 [°C]	Gas Outlet Press	101.386 [kPa]	Water Outlet Press	1730.626 [kPa]	Gas Side Press Drop	0.014192 [kPa]	Water Side Press Drop	269.374 [kPa]
Gas Side		Water Side																	
Gas Outlet Temp	361.34 [°C]	Water Outlet Temp	328.539 [°C]																
Gas Outlet Press	101.386 [kPa]	Water Outlet Press	1730.626 [kPa]																
Gas Side Press Drop	0.014192 [kPa]	Water Side Press Drop	269.374 [kPa]																
Implicit Geometries: Default Values Run Simulation: Exit Program		Max Energy Transfer: 50.727 [kW] H.E. Effectiveness: 82.25 [%] Actual Heat Transfer: 41.722 [kW] Average Fin Efficiency: 87.58 [%]																	

File Name: Results

Figure H8: Finished simulated run

At the bottom of the “Simulation Results” section, the gas side and water side results are now displayed as well as various heat exchanger performance characteristics. These are only the final answers. To view the results as the simulation progressed, open “Sim_Results.txt” in Microsoft Excel or any other data processing program. (The file name may vary depending on the name specified in the file name text box.)

In addition, the following window will also appear:

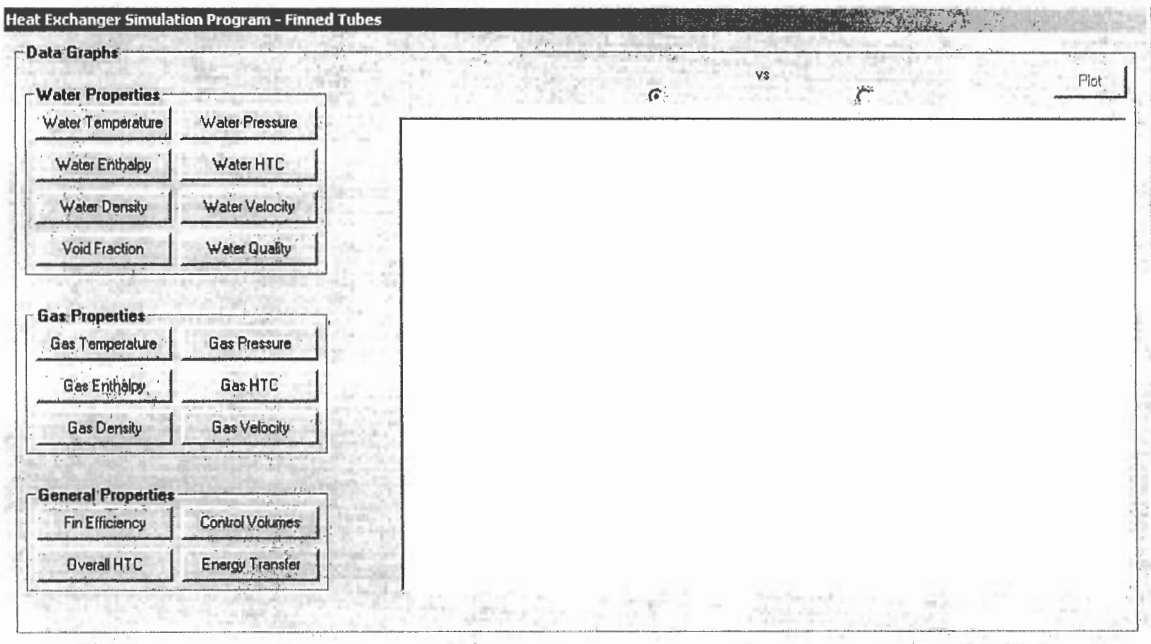


Figure H9: Plot interface

This window will enable you to plot the generated data on screen and will give you a rough impression of the simulation results. First you will have to choose the data arrays that you want to plot. You can achieve this by doing the following:

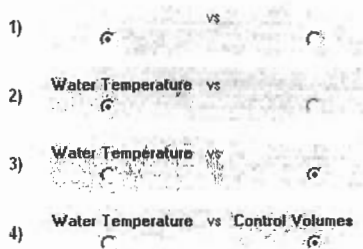


Figure H10: Choosing the axis

- 1) You will notice that the option button on the left is activated. This represents the Y-axis of the figure.

- 2) Now choose from the three sections on the left, “Water Properties”, “Gas Properties” or “General Properties” and left-click on the data array that you want displayed on the Y-axis. For instance “Water Temperature”.
- 3) Then select the right option button, representing the X-axis, by left-clicking on it.
- 4) Now choose from the three sections on the left, “Water Properties”, “Gas Properties” or “General Properties” and left-click on the data array that you want displayed on the X-axis. For instance “Control Volumes”.

After the procedures above have been done, simply left-click on the “Plot” button and the data will be plotted on the figure as follow:

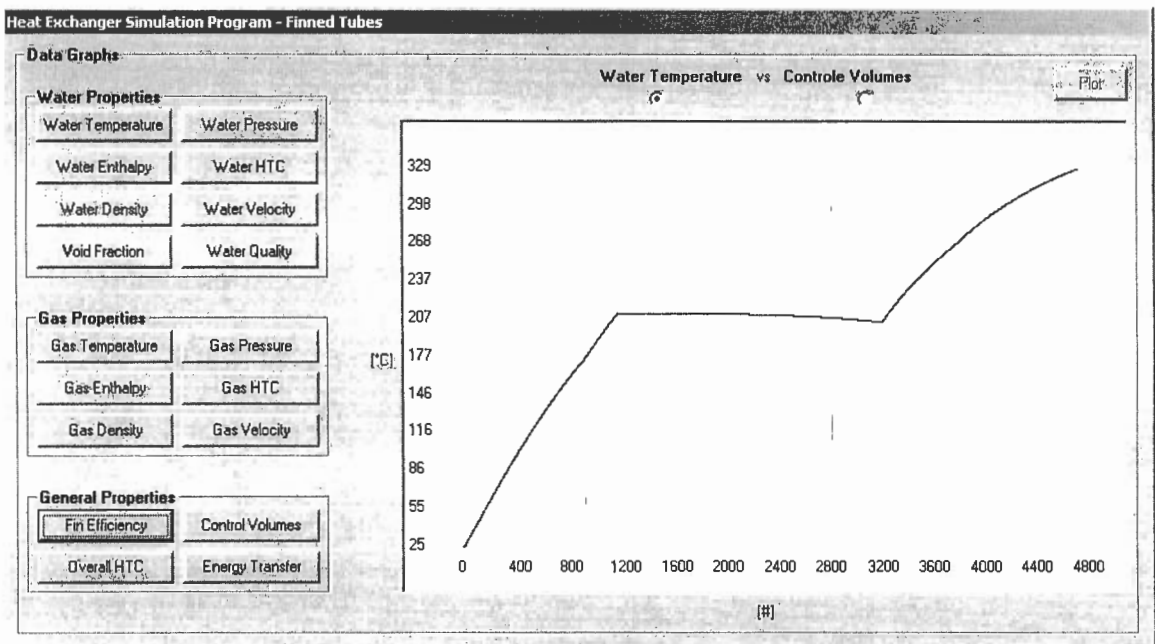


Figure H11: Water plot

It should be noted that the vertical light-blue line passing through the plot represents the end of the preheated stage, while the vertical light-red line represents the end of the boiling stage. The vertical grey lines represent each row in the heat exchanger.

If the “Gas Temperature” is plotted against “Control Volumes”, the figure appears quite different:

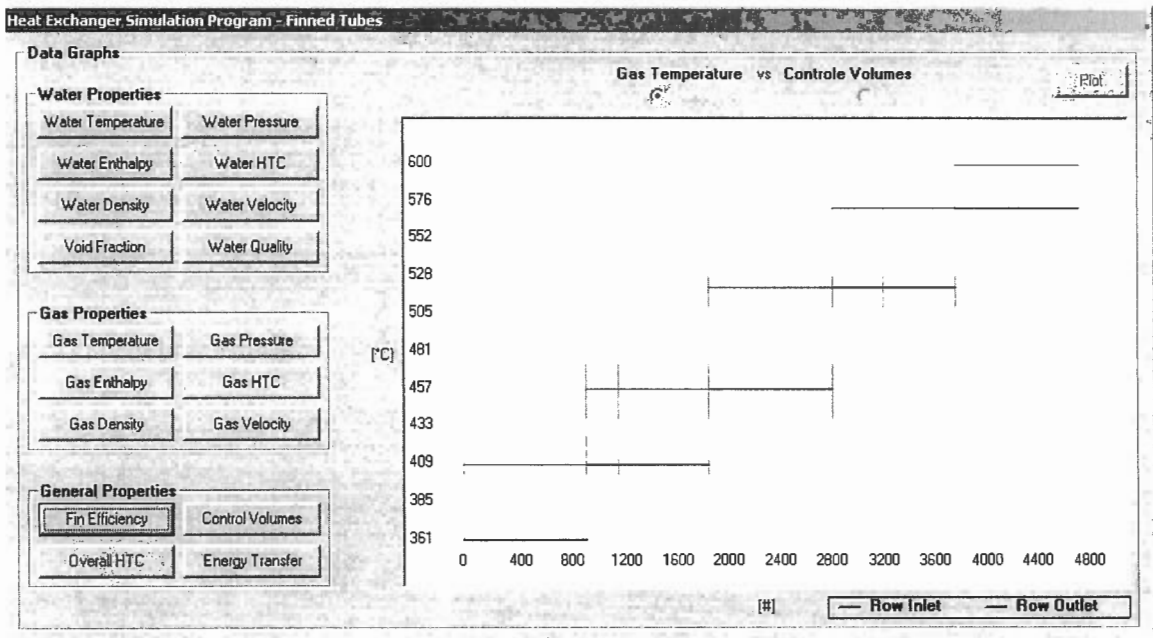


Figure H12: Gas plot

The reason that there are only horizontal lines on the plot is that only the bulk temperature is logged before and after each row. As indicated in the legend (bottom-right corner) the red lines show the inlet temperature to each row and the black lines show the outlet temperature.

It should be noted that on the plot area, the gas inlet is actually on the right and the outlet on the left, while the water inlet is on the left and the outlet on the right. This is due to the cross-flow taking place inside the heat exchanger.

To return to the main interface window, you simply left-click on the part protruding from behind the plot window and you can now change the input values and run the simulation again until you are satisfied with the results.

APPENDIX I
MICROSOFT® VISUAL BASIC 6.0 PROGRAM
FUNCTION AND VARIABLE LISTING
&
FLOW CHART

I1 - GLOBAL PROGRAM FUNCTIONS AND VARIABLES

I1.1 - GLOBAL FUNCTIONS

```

Public Declare Function DBPT Lib "if97-rub.dll" (PBAR As Double,TCEL As Double)As Double
Public Declare Function HBPT Lib "if97-rub.dll" (PBAR As Double,TCEL As Double)As Double
Public Declare Function CPBPT Lib "if97-rub.dll" (PBAR As Double,TCEL As Double)As Double
Public Declare Function TBP Lib "if97-rub.dll" (PBAR As Double)As Double
Public Declare Function PBT Lib "if97-rub.dll" (TCEL As Double)As Double
Public Declare Function TBPH Lib "if97-rub.dll" (PBAR As Double,H As Double)As Double
Public Declare Function HLBT Lib "if97-rub.dll" (TCEL As Double)As Double
Public Declare Function HVBT Lib "if97-rub.dll" (TCEL As Double)As Double
Public Declare Function DLBT Lib "if97-rub.dll" (TCEL As Double)As Double
Public Declare Function DVBT Lib "if97-rub.dll" (TCEL As Double)As Double
Public Declare Function CPLBT Lib "if97-rub.dll" (TCEL As Double)As Double
Public Declare Function CPVBT Lib "if97-rub.dll" (TCEL As Double)As Double
Public Declare Function VLBT Lib "if97-rub.dll" (TCEL As Double)As Double
Public Declare Function tanH Lib "MathLib.dll" (ByVal X As Double)As Double

```

I1.2 - SIMULATION INPUTS

```

Public pi As Double ' 3.141592654
Public FTair As Double ' final air temp
Public TairIn(1 To 30000) As Double ' exhaust temp [°C]
Public TairOut(1 To 30000) As Double ' exhaust temp [°C]
Public Pair As Double ' exhaust press [kPa]
Public FPair(1 To 30000) As Double ' exhaust press [kPa]
Public mair As Double ' exhaust mass flow rate [kg/s]
Public Tw(1 To 30000) As Double ' water temp [°C]
Public Pw(1 To 30000) As Double ' water press [kPa]
Public mw As Double ' water mass flow rate [kg/s]
Public kt As Double ' tube conductivity [W/m.K]
Public Lt As Double ' tube length [m]
Public Odt As Double ' tube outer diameter [m]
Public Idt As Double ' tube inner diameter [m]
Public SL As Double ' tube longitudinal pitch [m]
Public ST As Double ' tube transverse pitch [m]
Public kf As Double ' fin conductivity [W/m.K]
Public tf As Double ' fin thickness [m]
Public Pf As Double ' fin pitch [m]
Public Hf As Double ' fin height [m]
Public Nt As Double ' nr of tubes per row [#]
Public Nr As Double ' nr of rows in HE [#]

```

I1.3 - IMPLICIT GEOMETRIES

```

Public tt As Double ' tube wall thickness [m]
Public H As Double ' approx. HE height [m]
Public Afr As Double ' total frontal area [m²]
Public Aair As Double ' CV area exposed to air [m²]
Public Aw As Double ' CV area exposed to water [m²]

```

I1.4 - SIMULATION VARIABLES

```

Public CV As Double ' current CV during simulation
Public CVtube As Double ' total amount of CV's per tube
Public CVtot As Double ' total amount of CV's in HE
Public Itter As Double ' current iteration during simulation
Public UAcv(1 To 30000) As Double ' CV overall heat transfer coeff. [W/K]
Public UA_tot As Double ' HE overall heat transfer coeff. [W/K]
Public X(1 To 30000) As Double ' water/steam quality [%]
Public G(1 To 30000) As Double ' mass flux [kg/m².s]
Public alfa(1 To 30000) As Double ' void fraction [%]
Public h_enth(1 To 30000) As Double ' fluid/steam enthalpy [J/kg]
Public TubeNr(1 To 30000) As Double ' keeps track of finished nr of tubes
Public TubeDist(1 To 30000) As Double ' keeps track of remaining tube length
Public Sigma As Double ' water surface tension [N/m]
Public Twall(1 To 30000) As Double ' approx. wall temperature inside tube [°C]

```

11.5 - ENERGY VARIABLES

```
Public Qtransf(1 To 30000) As Double ' amount of heat transferred per CV
Public Tlout(1 To 30000) As Double ' liquid temp out of CV [°C]
Public Tgout(1 To 30000) As Double ' gas temp out of CV [°C]
```

11.6 - CHEN'S CORRELATION

```
Public hmac As Double ' heat transfer component (Chen) [W/m².K]
Public hmic As Double ' heat transfer component (Chen) [W/m².K]
```

11.7 - FIN AND HE VARIABLES

```
Public Feff(1 To 30000) As Double ' fin efficiency [%]
Public EnergyTransf As Double ' temporary variable
Public FinEff As Double ' temporary variable
Public AirEnergy As Double ' temporary variable
Public eff As Double ' HE affectivity [%]
Public PDrop As Double ' pressure drop on airside [kPa]
```

11.8 - EXHAUST VARIABLES

```
Public h_air(1 To 30000) As Double ' exhaust heat transfer coeff. [W/m².K]
Public dPair(1 To 30000) As Double ' exhaust pressure drop [kPa]
Public Vmax(1 To 30000) As Double ' max flow velocity between pipes [m/s]
Public Cp_air(1 To 30000) As Double ' exhaust specific heat [J/kg.K]
Public Acv_crit As Double ' min flow area [m²]
Public Acv_fr As Double ' frontal area [m²]
Public Sig_air As Double ' exhaust ratio
Public Dhyd_cv As Double ' hydraulic diameter of cv [m²]
Public Gai As Double ' core exhaust mass velocity [kg/m².s]
Public Mu_air As Double ' exhaust viscosity [kg/m.s]
Public Re_air As Double ' exhaust Reynolds nr
Public kair As Double ' exhaust conductivity [W/m.K]
Public Pr_air As Double ' exhaust Prandtl nr
Public konst As Double ' constant
Public Stan As Double ' Stanton nr
```

11.9 - WATER VARIABLES

```
Public Tsat(1 To 30000) As Double ' water saturation temp, based on press
Public h_w(1 To 30000) As Double ' water heat transfer coeff. [W/m².K]
Public D_w(1 To 30000) As Double ' water density [kg/m³]
Public Vel_w(1 To 30000) As Double ' water velocity [m/s]
Public Cp_w(1 To 30000) As Double ' water specific heat [J/kg.K]
Public Mu_w(1 To 30000) As Double ' water viscosity [kg/m.s]
Public Re_w As Double ' water Reynolds nr
Public kw As Double ' water conductivity [W/m.K]
Public Pr_w As Double ' water Prandtl nr
Public Nu_w As Double ' water Nusselt nr
```

11.10 - STEAM VARIABLES

```
Public Cp_s(1 To 30000) As Double ' steam specific heat [J/kg.K]
Public Mu_s(1 To 30000) As Double ' steam viscosity [kg/m.s]
Public Re_s As Double ' steam Reynolds nr
Public ks As Double ' steam conductivity [W/m.K]
Public Pr_s As Double ' steam Prandtl nr
Public Nu_s As Double ' steam Nusselt nr
```

11.11 - GENERAL CALCULATION VARIABLES

```
Public i As Double ' temporary variable
Public j As Double ' temporary variable
Public k As Double ' temporary variable
Public GasDX As Boolean ' temporary variable
Public GasDY As Boolean ' temporary variable
Public MasterRun As Boolean ' master running condition
Public Run As Boolean ' sub running condition
Public SaveSim As String ' simulation save file
Public Fault As Double ' maximum allowable error in program results
```

I2 - FORM1

I2.1 - PREHEATER

I2.1.1 - Private Sub Bend_Losses_1PhaseW()

Dim U As Double	' determining Friction Pressure Gradient
Dim Re As Double	' Reynolds
Dim Cf As Double	' friction coefficient
Dim Tau As Double	' shear stress
Dim dPgrav As Double	' gravitational pressure drop
Dim dPfric As Double	' frictional pressure drop
Dim dPaccel As Double	' acceleration pressure drop
Dim dP As Double	' total pressure drop
Dim EqLength As Double	' 0.7m per bend

I2.1.2 - Private Sub Preheater()

Dim Qair_tot As Double	' energy transferred to water per row
------------------------	---------------------------------------

I2.1.3 - Private Sub Press_Drop_1PhaseW()

Dim Digt0 As Double	' previous density ⁻¹
Dim Digt1 As Double	' current density ⁻¹
Dim U As Double	' determining Friction Pressure Gradient
Dim Re As Double	' Reynolds
Dim Cf As Double	' friction coefficient
Dim Tau As Double	' shear stress
Dim dPgrav As Double	' gravitational pressure drop
Dim dPfric As Double	' frictional pressure drop
Dim dPaccel As Double	' acceleration pressure drop
Dim dP As Double	' total pressure drop
Dim t0 As Double	' water average temperature
Dim t1 As Double	' water average temperature
Dim theta As Double	' tube angle to horizontal

I2.2 - BOILER

I2.2.1 - Private Sub Boiler()

Dim Ttemp As Double	' temporary variable
Dim Xtemp As Double	' temporary variable

I2.2.2 - Private Sub Bend_Losses_2Phase()

Dim U As Double	' determining Friction Pressure Gradient
Dim Re As Double	' Reynolds
Dim Cf As Double	' friction coefficient
Dim Tau As Double	' shear stress
Dim dPgrav As Double	' gravitational pressure drop
Dim dPfric As Double	' frictional pressure drop
Dim dPaccel As Double	' acceleration pressure drop
Dim dP As Double	' total pressure drop
Dim t As Double	' water average temperature
Dim EqLength As Double	' 0.7m per bend
Dim Mu_l As Double	' liquid viscosity

I2.2.3 - Private Sub Chen()

Dim Xtt As Double	' Martinelli parameter
Dim S As Double	' suppression correction factor
Dim hfz As Double	' nucleate boiling heat transfer coefficient
Dim hfg As Double	' enthalpy
Dim f As Double	' enhancement factor
Dim Ref As Double	' liquid Reynolds nr
Dim hl As Double	' saturated water heat transfer coefficient
Dim Retp As Double	' enhanced Reynolds nr
Dim dPsat As Double	' pressure difference
Dim dTsats As Double	' temperature difference
Dim Mu_l As Double	' liquid viscosity
Dim Mu_v As Double	' vapour viscosity
Dim Rhohomo As Double	' homogeneous density

I2.2.4 - Private Function Phase_Mult(Rho As Double)

Dim We As Double	' Friedel correlation constant
Dim Fr As Double	' Friedel correlation constant


```
Dim H As Double ' Friedel correlation constant
Dim f As Double ' Friedel correlation constant
Dim E As Double ' Friedel correlation constant
Dim Rego As Double ' Reynolds, gas-only
Dim Refo As Double ' Reynolds, fluid-only
Dim Cfgo As Double ' Friction, gas-only
Dim Cffo As Double ' Friction, fluid-only
Dim Mu_l As Double ' liquid viscosity
Dim Mu_v As Double ' vapour viscosity
```

12.2.5 - Private Sub Press_Drop_2Phase()

```
Dim Rhohomo As Double ' homogeneous density
Dim Rhosep As Double ' separated density
Dim Refo As Double ' Reynolds, fluid-only
Dim Cffo As Double ' friction factor, fluid-only
Dim dFlo As Double ' pressure drop, fluid-only
Dim dPgrav As Double ' gravitational pressure drop
Dim dPfric As Double ' frictional pressure drop
Dim dPaccel As Double ' acceleration pressure drop
Dim dP As Double ' total pressure drop
Dim Digt0 As Double ' previous density-1
Dim Digt1 As Double ' current density-1
Dim theta As Double ' tube angle to horizontal
Dim Mu_l As Double ' liquid viscosity
```

12.3 - SUPERHEATER

12.3.1 - Private Sub Bend_Losses_1PhaseS()

```
Dim U As Double ' determining Friction Pressure Gradient
Dim Re As Double ' Reynolds
Dim Cf As Double ' friction coefficient
Dim Tau As Double ' shear stress
Dim dPgrav As Double ' gravitational pressure drop
Dim dPfric As Double ' frictional pressure drop
Dim dPaccel As Double ' acceleration pressure drop
Dim dP As Double ' total pressure drop
Dim t As Double ' water average temperature [°C]
Dim EqLength As Double ' 0.7m per bend
```

12.3.1 - Private Sub Press_Drop_1PhaseS()

```
Dim Digt0 As Double ' previous density(-1)
Dim Digt1 As Double ' current density(-1)
Dim U As Double ' determining Friction Pressure Gradient
Dim Re As Double ' Reynolds
Dim Cf As Double ' friction coefficient
Dim Tau As Double ' shear stress
Dim dPgrav As Double ' gravitational pressure drop
Dim dPfric As Double ' frictional pressure drop
Dim dPaccel As Double ' acceleration pressure drop
Dim dP As Double ' total pressure drop
Dim t0 As Double ' water average temperature [°C]
Dim t1 As Double ' water average temperature [°C]
Dim theta As Double ' tube angle to horizontal
```

12.3.1 - Private Sub Superheater()

12.4 - MASTER FUNCTIONS

12.4.1 - Private Sub Form_Load()

12.4.2 - Private Sub Run_Simulation_Click()

```
Dim Error As Double ' calculated and simulated temperature error
Dim Bracket As Boolean ' tests whether the temp has been bracketed
Dim FileName2 As String ' 2nd filename for writing errors
Dim Bracket1, Bracket2, Bracket3 As Double ' bracket values used in iteration
Dim inc As Double ' temp inc/dec in iterations
```

I2.5 - GENERAL SUB FUNCTIONS

I2.5.1 - Private Sub Activate1()

I2.5.2 - Private Sub Activate2()

I2.5.3 - Private Sub Air_HeatTransfer()

I2.5.4 - Private Sub AirPressureDrop()

```
Dim TwallAv As Double ' average wall temperature
Dim Tav As Double ' average temperature
Dim Rho As Double ' air density
Dim v As Double ' air viscosity
Dim Vo As Double ' empty duct velocity
Dim konst As Double ' calculation constant
Dim Remax As Double ' maximum Reynolds number
Dim Pt As Double ' dimensionless transverse pitch
Dim Pl As Double ' dimensionless longitudinal pitch
Dim Ex As Double ' temporary factor variable
Dim Z, i, j, k As Double ' temporary variables
Dim f As Double ' friction factor
```

I2.5.5 - Private Sub Clear_Text()

I2.5.6 - Private Sub Disable1()

I2.5.7 - Private Sub Disable2()

I2.5.8 - Private Sub Fin_Eff_UA()

```
Dim b As Double ' fin efficiency constant
Dim term1, term2, term3 As Double ' fin efficiency constant
Dim phi As Double ' fin efficiency constant
```

I2.5.9 - Private Sub HE_Effctvns()

```
Dim Cmax As Double ' maximum capacity
Dim Cmin As Double ' minimum capacity
Dim C As Double ' capacity ratio
Dim n As Double ' number of transfer units
Dim Tw_aver As Double ' average water temperature
Dim Tair_aver As Double ' average air temperature
Dim UA_tot As Double ' overall heat transfer coefficient
Dim Cp_l As Double ' liquid specific heat
Dim Cp_g As Double ' gas specific heat
```

I2.5.10 - Private Sub Implicit_Geometries()

I2.5.11 - Private Sub Imp_Geom_Click()

I2.5.12 - Private Sub Load_Config(Name As String)

```
Dim FileName As String ' local file name to which will be written
```

I2.5.13 - Private Sub Load_Default_Click()

I2.5.14 - Private Sub Read_Inputs()

I2.5.15 - Private Sub Results()

I2.5.16 - Private Sub Save_Click()

I2.5.17 - Private Sub Save_Config()

```
Dim FileName As String ' local file name to which will be written
```

I2.5.18 - Private Function Void()

```
Dim beta As Double ' CISE void fraction correlation constant
Dim Y As Double ' CISE void fraction correlation constant
Dim Re As Double ' CISE void fraction Reynolds number
Dim We As Double ' CISE void fraction Weber number
Dim E1 As Double ' CISE void fraction correlation constant
Dim E2 As Double ' CISE void fraction correlation constant
```

I2.5.19 - Private Sub WaterLiq_HeatTransfer()

I2.5.20 - Private Sub WaterVap_HeatTransfer()

I2.5.21 - Private Sub Write_Data()

```
Dim FileName As String ' local file name to which will be written
```

I3 - FORM2**I3.1 - GLOBAL FORM VARIABLES**

Dim Ydata(1 To 30000) As Double	' 1 st Y-axis data set
Dim Ydata2(1 To 30000) As Double	' 2 nd Y-axis data set
Dim Xdata(1 To 30000) As Double	' 1 st X-axis data set
Dim Xdata2(1 To 30000) As Double	' 2 nd X-axis data set
Dim TwoP, SingleP As Double	' validation variables
Dim DigX, DigY As Long	' X and Y decimal accuracy
Dim i, j As Double	' temporary variables
Dim Plus1X, Plus1Y As Boolean	' control volume axis variables
Dim RedL, BlackL As String	' temporary variables
Dim NrX, NrY As Double	' number of plots on chart

I3.2 - PLOT OPTIONS

I3.2.1 - Private Sub Command1_Click()	' Water Temperature
I3.2.2 - Private Sub Command2_Click()	' Gas Temperature
I3.2.3 - Private Sub Command3_Click()	' Water Heat Transfer Coefficient
I3.2.4 - Private Sub Command4_Click()	' Gas Heat Transfer Coefficient
I3.2.5 - Private Sub Command5_Click()	' Overall Heat Transfer Coefficient
I3.2.6 - Private Sub Command6_Click()	' Energy Transferred
I3.2.7 - Private Sub Command7_Click()	' Water Pressure
I3.2.8 - Private Sub Command8_Click()	' Water Quality
I3.2.9 - Private Sub Command9_Click()	' Water Enthalpy
I3.2.10 - Private Sub Command10_Click()	' Fin Efficiency
I3.2.11 - Private Sub Command11_Click()	' Void Fraction
I3.2.12 - Private Sub Command12_Click()	' Gas Velocity
I3.2.13 - Private Sub Command16_Click()	' Water Density
I3.2.14 - Private Sub Command17_Click()	' Control Volumes
I3.2.15 - Private Sub Command18_Click()	' Gas Pressure
I3.2.16 - Private Sub Command19_Click()	' Gas Enthalpy
I3.2.17 - Private Sub Command20_Click()	' Gas Density
I3.2.18 - Private Sub Command21_Click()	' Water Velocity

I3.3 - PLOT FUNCTIONS**I3.3.1 - Private Sub Form_Load()****I3.3.2 - Private Sub Hide_Block()****I3.3.3 - Private Sub Plot_Data_Click()**

Dim dX As Single	' X axis intervals
Dim dY As Single	' Y axis intervals
Dim Xlengte As Double	' X axis length
Dim Ylengte As Double	' Y axis length
Dim Ymax, Ymin, Xmax, Xmin As Double	' maximum and minimum limits

I3.3.4 - Private Sub Plot_Chart(Data As Double)

Dim temp As Double	' temporary variable
Dim TwoPhase As Boolean	' two-phase variable
Dim temp2(1 To 30000) As Double	' dummy variable for double plots

I3.3.5 - Private Sub Show_Block()

APPENDIX J

ENERGY AVAILABILITY

J1 - ENERGY AVAILABILITY SAMPLE CALCULATIONS

J1.1 - INTRODUCTION

This appendix contains information and calculations on the amount of energy available to the recovery system. The data shown were taken from practical testing results and is an accurate representation of the performance obtainable from the continuous combustion unit.

J1.2 - SAMPLE CALCULATIONS

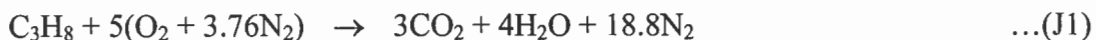
Table J.1 contains the enthalpy values from Çengel and Boles (1994) for each component of the combustion gas at their measured temperatures. An air/propane ratio of 16:1 was used and the reactants were at 28°C and the products at 562°C.

Substance	h_f°	h_{298}°	<u>Reactants</u>	<u>Products</u>
	[kJ/kmol]	[kJ/kmol]	h_r	h_p
			[kJ/kmol]	[kJ/kmol]
C ₃ H ₈ (gas)	-103850	-
O ₂	0	8682	8765.4	-
N ₂	0	8669	8752.1	24816
CO ₂	-393520	9364	-	33990.5
H ₂ O (gas)	-241820	9904	-	29258

Table J.1: Combustion enthalpy values

Given that the air inlet temperature was 28°C, the water inlet temperature was 21°C, the water mass flow rate was 1500kg/hr and the propane mass flow rate was kept constant at 4kg/hr.

The combustion equation is shown in equation J1...



The energy distribution of the various components of combustion can be determined using the following equation ...

$$Q_{\text{comp}} = N_{\text{comp}}(h_f^\circ + h - h_{298}^\circ) \quad \dots(\text{J2})$$

where h_f° = enthalpy of formation of substance
 h = enthalpy at the actual temperature of substance
 h_{298}° = reference enthalpy of substance at 298K

The total energy of the components per unit mole of fuel, where $h_{r,\text{propane}} = h_{298^\circ}$, is ...

$$\begin{aligned} Q_{\text{reactants}} &= (1 \text{ kmole } \text{C}_3\text{H}_8) [(-103850 + h_{r,\text{propane}} - h_{298^\circ}) \text{ kJ/kmole}] \\ &+ (5 \text{ kmole } \text{O}_2) [(0 + 8765.4 - 8682) \text{ kJ/kmole}] \\ &+ (18.8 \text{ kmole } \text{N}_2) [(0 + 8752.1 - 8669) \text{ kJ/kmole}] \quad \dots(\text{J3}) \\ &= \underline{-101871 \text{ kJ/kmole}} \end{aligned}$$

$$\begin{aligned} Q_{\text{products}} &= (3 \text{ kmole } \text{CO}_2) [(-103850 + h_r - h_{298^\circ}) \text{ kJ/kmole}] \\ &+ (4 \text{ kmole } \text{H}_2\text{O}) [(0 + 8765.4 - 8682) \text{ kJ/kmole}] \\ &+ (18.8 \text{ kmole } \text{N}_2) [(0 + 8752.1 - 8669) \text{ kJ/kmole}] \quad \dots(\text{J4}) \\ &= \underline{-1692981 \text{ kJ/kmole}} \end{aligned}$$

$$\begin{aligned} Q_{\text{out}} &= Q_{\text{reactants}} - Q_{\text{products}} \quad \dots(\text{J5}) \\ &= -101871 - (-1692981) \\ &= \underline{1591110 \text{ kJ/kmole}} \end{aligned}$$

Taking the molar mass of C_3H_8 as 44.097kg/kmole and converting the answer to kW by multiplying with $4\text{kg/hr}_{\text{propane}}$ and dividing by 3600sec...

$$Q_{\text{out}} = \underline{40.091\text{kW}}$$

The amount of energy absorbed by the water jacket can be determined as follows:

$$C_{p,\text{water}} = 4.18\text{kJ}/(\text{kg}^\circ\text{C}) ; \dot{m} = 1500\text{kg/hr} ; T_{\text{water,in}} = 21^\circ\text{C} ; T_{\text{water,out}} = 40^\circ\text{C}$$

$$\begin{aligned} Q_{\text{water}} &= C_{p,\text{water}} \cdot \Delta T \cdot \dot{m} \quad \dots(\text{J6}) \\ &= 4.18(40-20)(1500/3600) \\ &= \underline{33.900 \text{ kW}} \end{aligned}$$

The amount of energy lost due to natural convection from the endplate of the chamber to the environment can be determined as follows as from Holeman (1992):

$$\begin{aligned} T_{\text{film}} &= (850+293)/2 \quad \dots(\text{J7}) \\ &= 571\text{K} \end{aligned}$$

Using the diameter of 0.6m we obtain...

$$\text{GrPr} = 6.96 \times 10^8 \quad \dots(\text{J8})$$

From table 7.1 we get $C = 0.53$ and $m = 0.25$ which gives...

$$\begin{aligned} \text{Nu} &= 0.53(\text{GrPr})^{0.25} \quad \dots(\text{J9}) \\ &= 86 \end{aligned}$$

and

$$\begin{aligned} h &= 0.044(\text{Nu}/d) && \dots(\text{J10}) \\ &= \underline{6.3\text{W}/\text{m}^2\text{K}} \end{aligned}$$

The end plate surface is...

$$\begin{aligned} A &= \pi r^2 && \dots(\text{J11}) \\ &= \underline{0.283\text{m}^2} \end{aligned}$$

The heat transfer due to convection at the back of the combustion chamber with $T_{\text{wall}} = 562^\circ\text{C}$ and $T_{\text{inf}} = 28^\circ\text{C}$ is then...

$$\begin{aligned} Q_{\text{end plate}} &= h \cdot A \cdot \Delta T && \dots(\text{J12}) \\ &= \underline{0.957\text{ kW}} \end{aligned}$$

Thus the available energy is...

$$Q_{\text{out}} = Q_{\text{water jacket}} + Q_{\text{end plate}} + Q_{\text{exhaust}} \quad \dots(\text{J13})$$

thus $Q_{\text{exhaust}} = Q_{\text{out}} - Q_{\text{water jacket}} + Q_{\text{end plate}}$

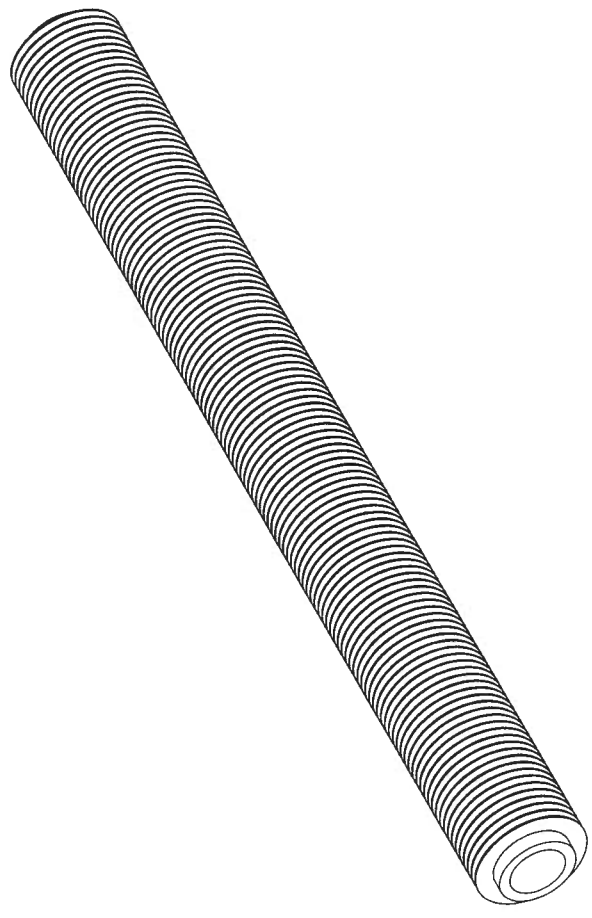
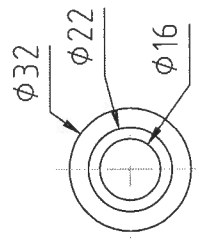
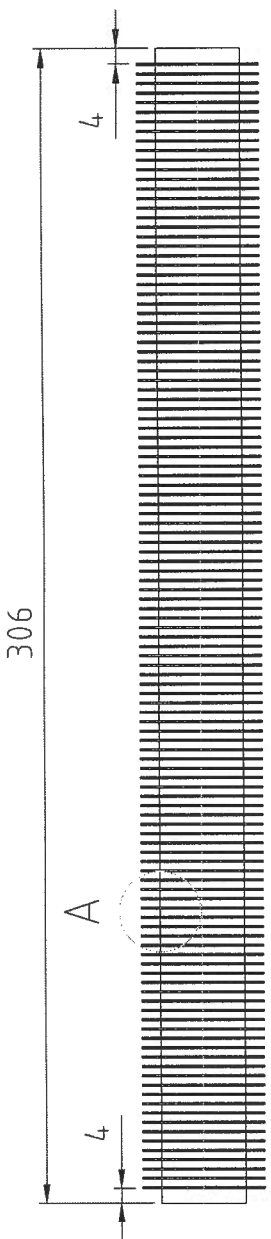
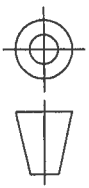
$$= \underline{5.234\text{kW}}$$

J1.3 - CONCLUSION

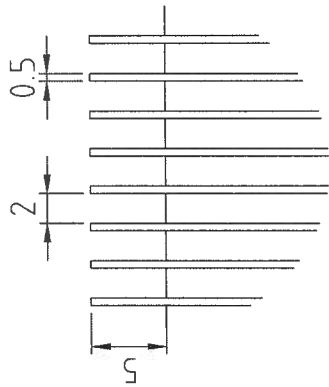
The value above is only an approximation of the maximum amount of recoverable energy and ignores the losses incurred along the pipeline leading to the heat exchanger due to convection and radiation. Thus from measuring the temperature of the exhaust gas just before it enters the heat exchanger and if the mass flow rate of air from the continuous combustion unit is known, the actual amount of energy can be determined. From experimental data (*see appendix L*), it has been found that the amount of energy that reaches the heat exchanger has an average value between 4.6kW. That means that on average a heat loss of 0.634kW occurs between the continuous combustion unit and the heat exchanger, depending on the gas mass flow rate and temperature.

APPENDIX K

HEAT EXCHANGER DESIGN DRAWINGS



DETAIL A

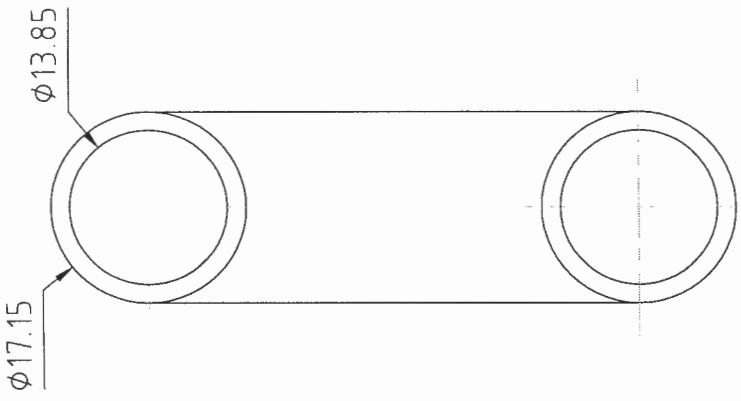
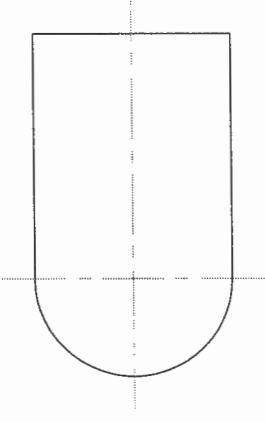
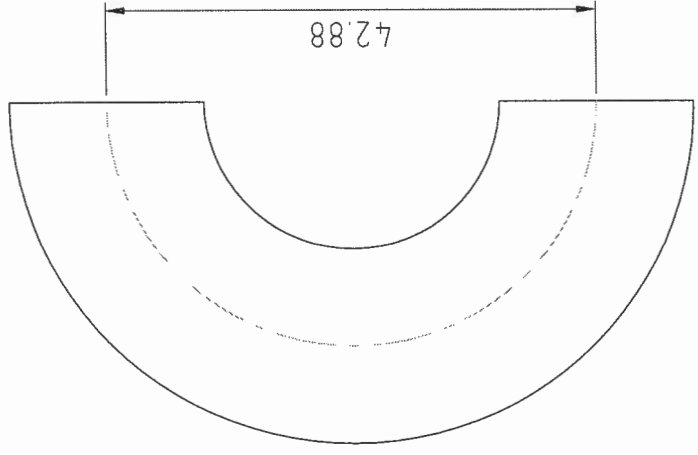
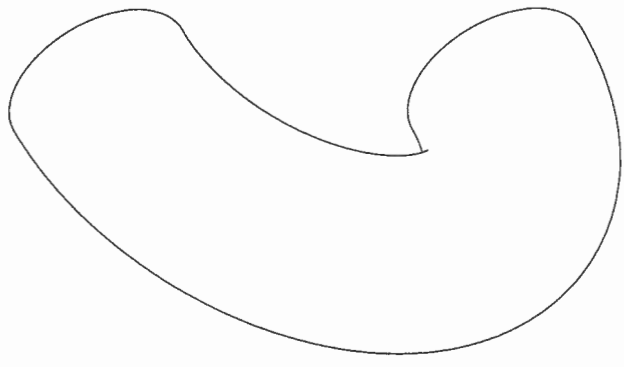
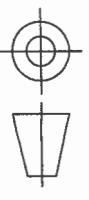


LENGTH	TOLERANCE
<1	0.02
1-100	0.1
>100	0.5

1	FINTUBE	1	STAINLESS STEEL	OD32mm ID16mm x 306mm
ITEM	DETAILS	NUMBER	MATERIAL	SPECS
SCALE	N.T.S.	TITLE: FINTUBE		
UNITS	MM	PAGE No. 1 OF 15 PAGES No. MSc.T - PW1		
DATE	04/06/2003	CHECKED		

UNIVERSITY OF STELLENBOSCH

STUDENT No. 12911259 DESIGNER P WIPPLINGER

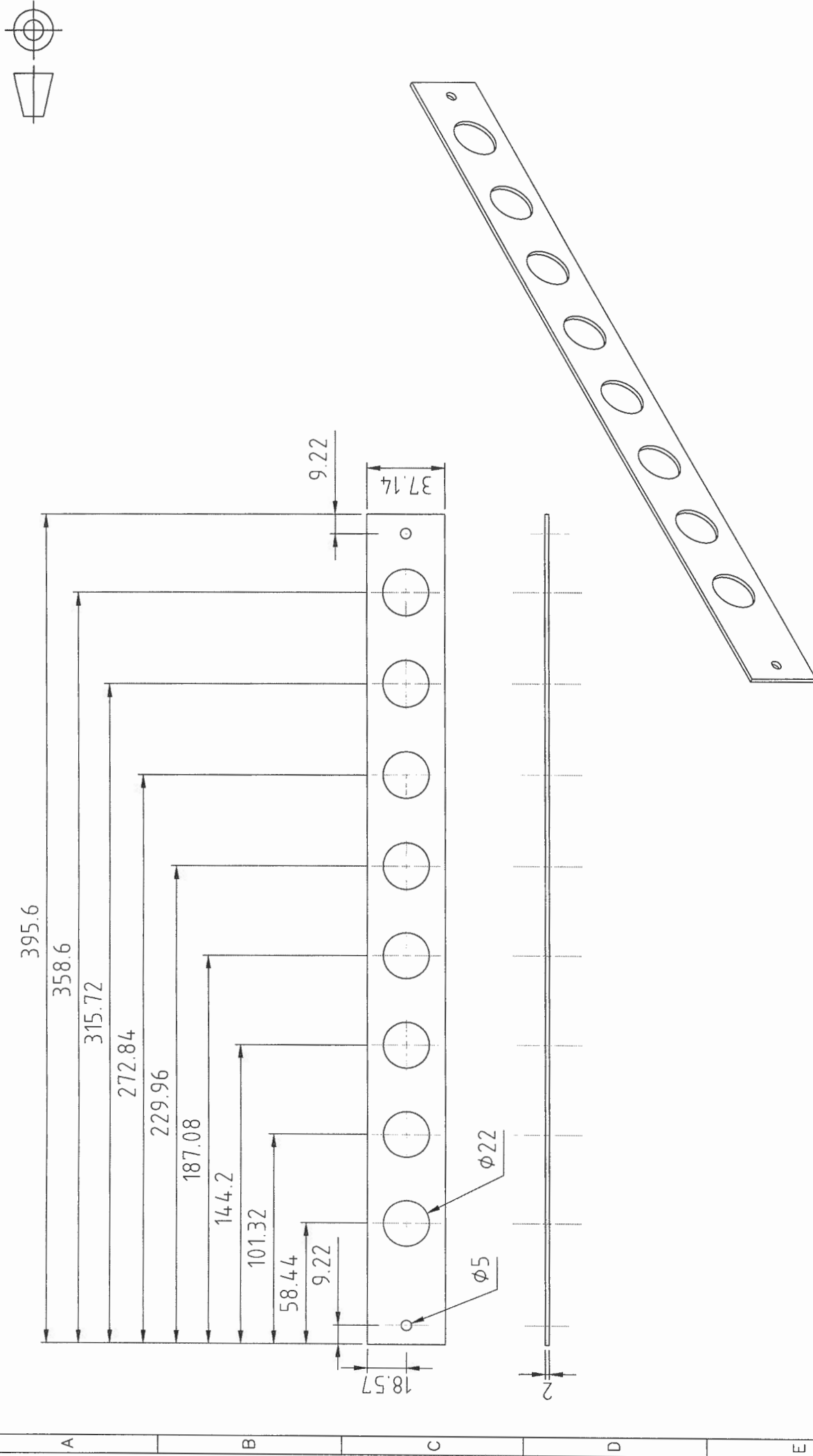


LENGTH	TOLERANCE
<1	0.02
1-100	0.1
>100	0.5

1	U-BEND	4.0	STAINLESS STEEL	OD17.15mm x ID13.85mm
ITEM	DETAILS	NUMBER	MATERIAL	SPECS
SCALE	N.T.S.	TITLE: TUBE U-BEND		
UNITS	MM	PAGE No. 2 OF 15 PAGES		
DATE	10/06/2003	No. M.Sc.T - PW2		

UNIVERSITY OF STELLENBOSCH

STUDENT No. 12911259 DESIGNER P WIPPLINGER CHECKED

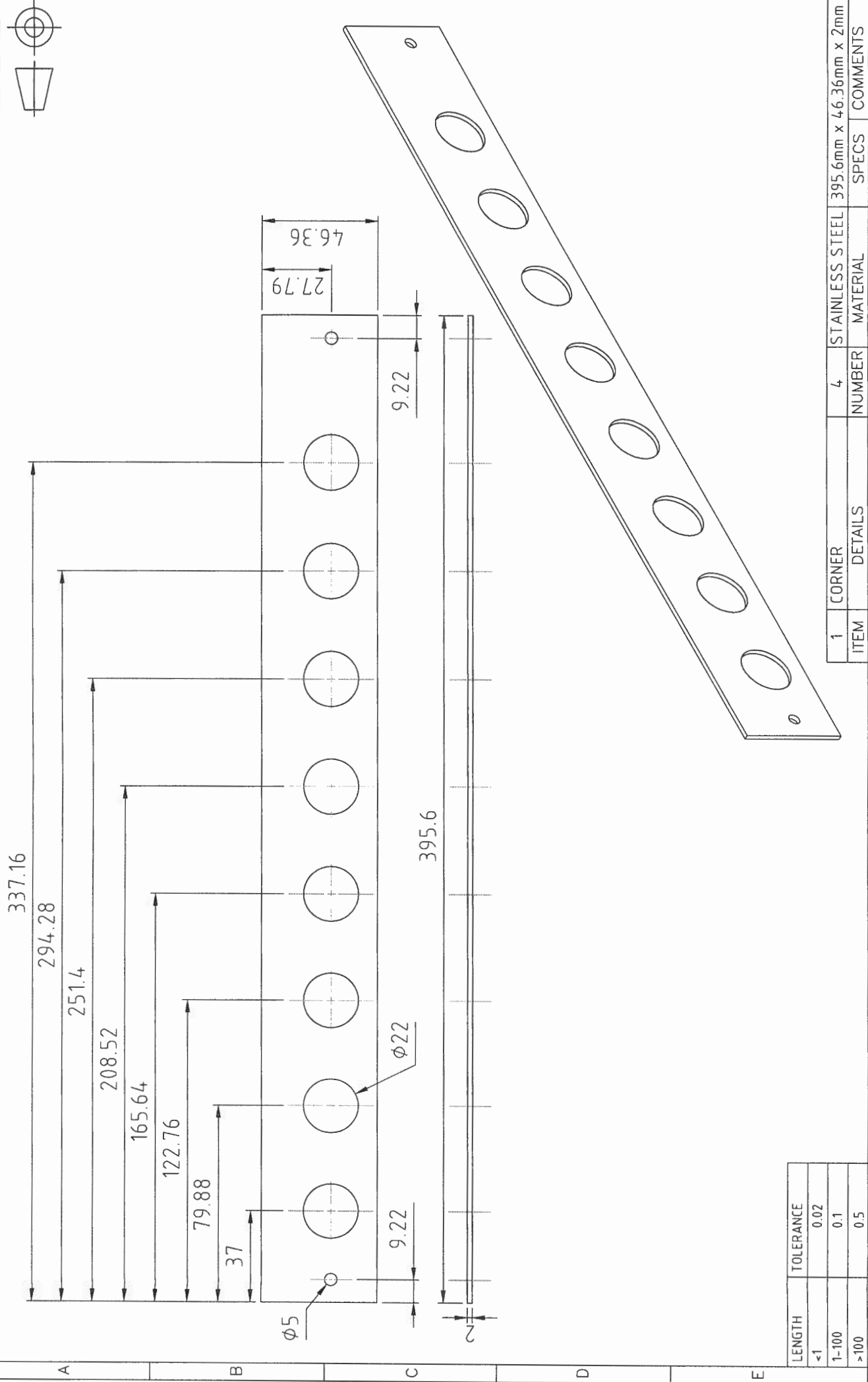
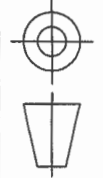


LENGTH	TOLERANCE
<1	0.02
1-100	0.5
>100	1

1	SIDE PLATE	6	STAINLESS STEEL	395.6mm x 19.75mm
ITEM	DETAILS	NUMBER	MATERIAL	SPECS
SCALE	N.T.S.	TITLE: SIDE PLATE		
UNITS	MM	PAGE No. 3 OF 15 PAGES No. Msc.T - PW3		
DATE	04/06/2003	PAGE No. 3 OF 15 PAGES No. Msc.T - PW3		

UNIVERSITY OF STELLENBOSCH

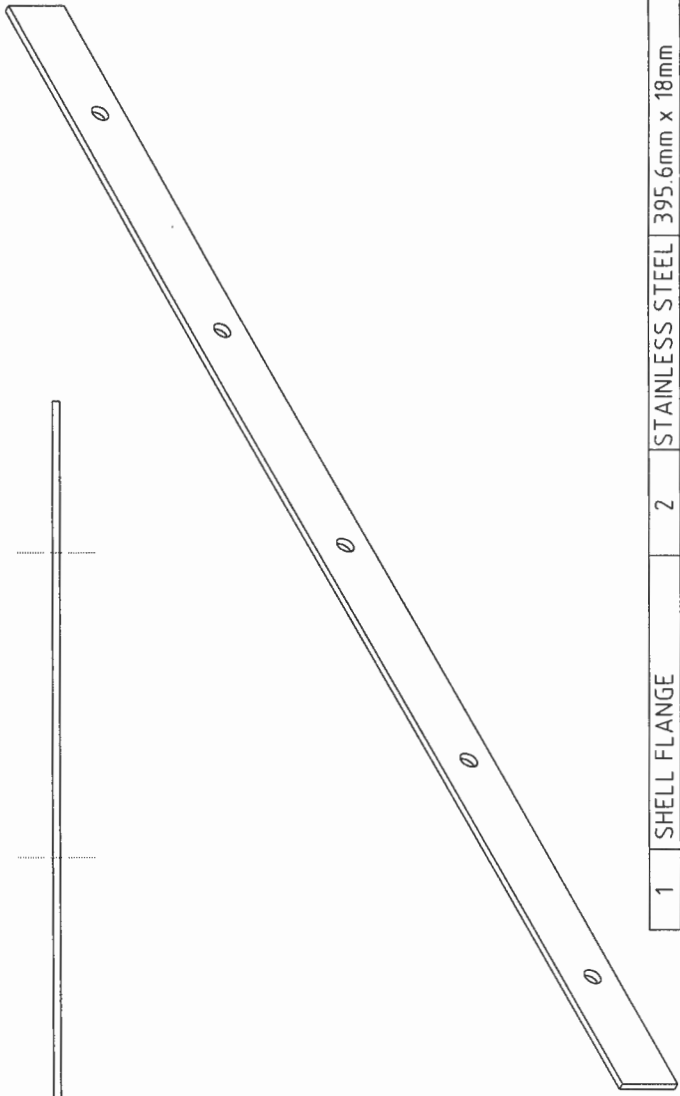
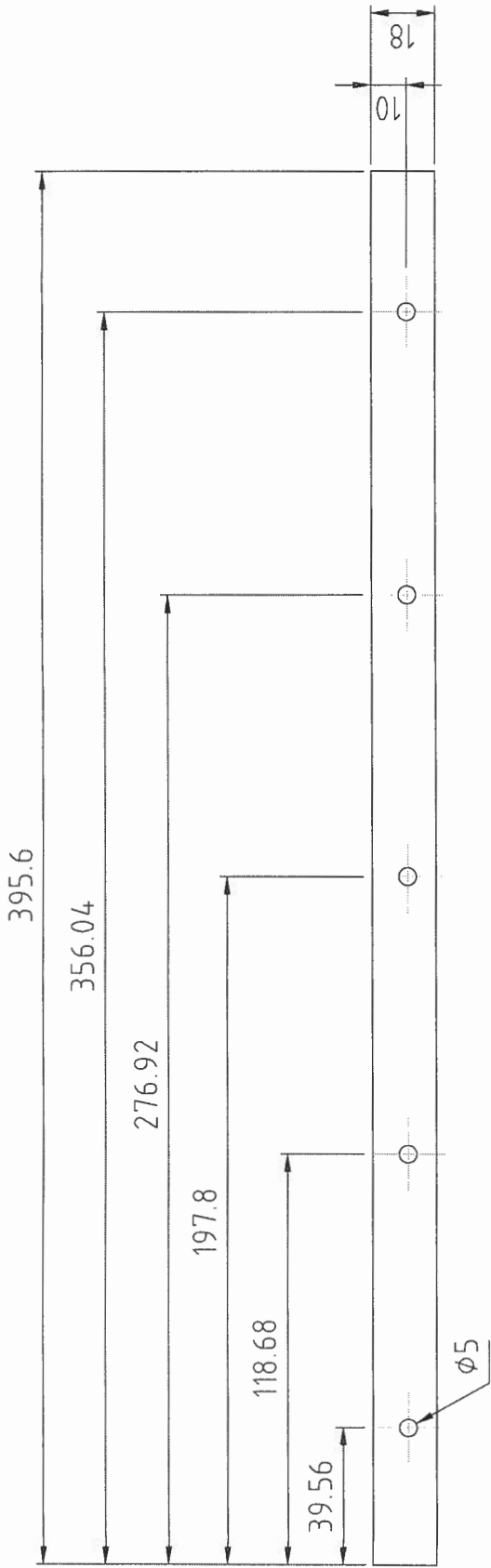
STUDENT No. 12911259 DESIGNER P WIPPLINGER CHECKED



LENGTH	TOLERANCE
<1	0.02
1-100	0.1
>100	0.5

ITEM	CORNER	DETAILS	NUMBER	MATERIAL	SPECS	COMMENTS
1	CORNER	DETAILS	4	STAINLESS STEEL	395.6mm x 46.36mm x 2mm	
SCALE	N.T.S.	TITLE: SIDE CORNER				
UNITS	MM	PAGE No. 4 OF 15 PAGES No. MSc.T - PW4				
DATE	10/06/2003	DESIGNER P WIPPLINGER CHECKED				

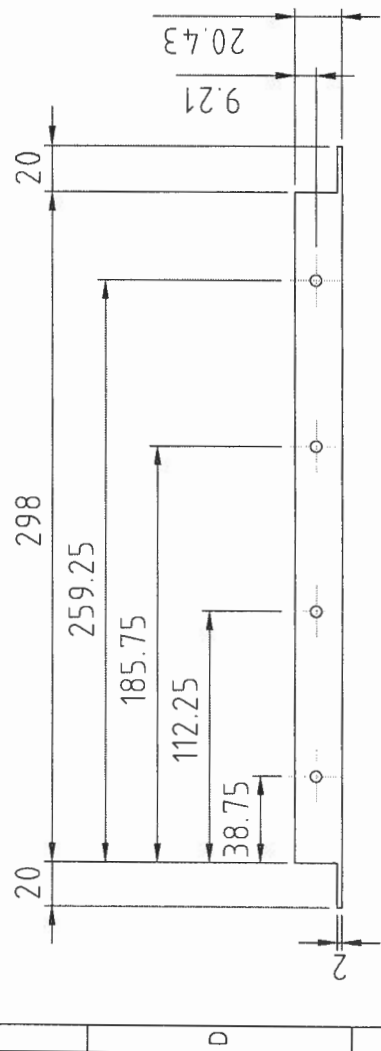
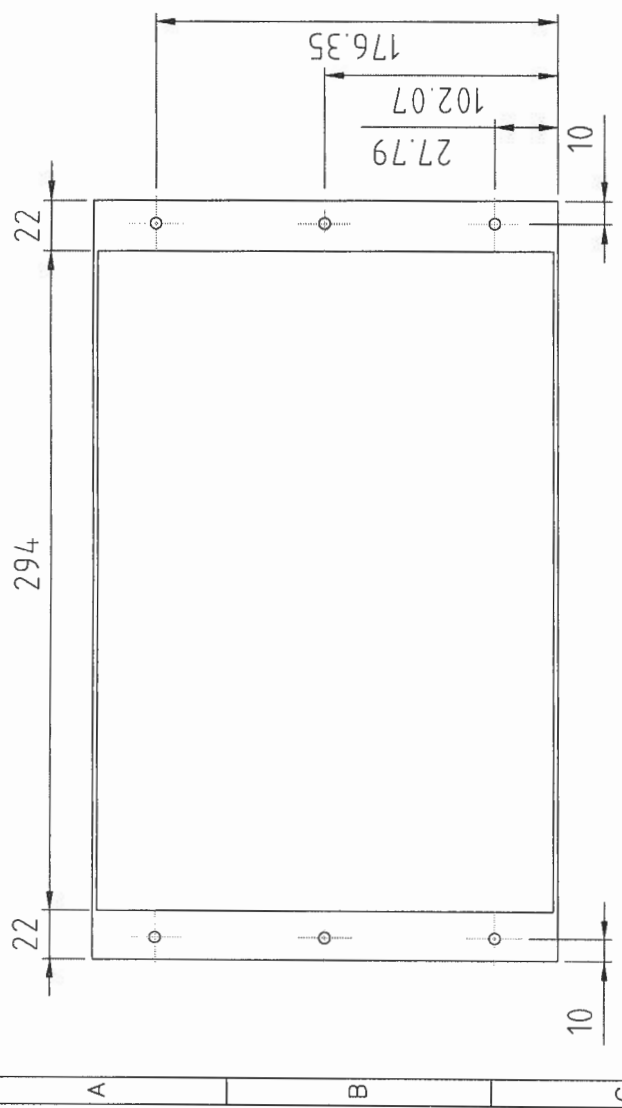
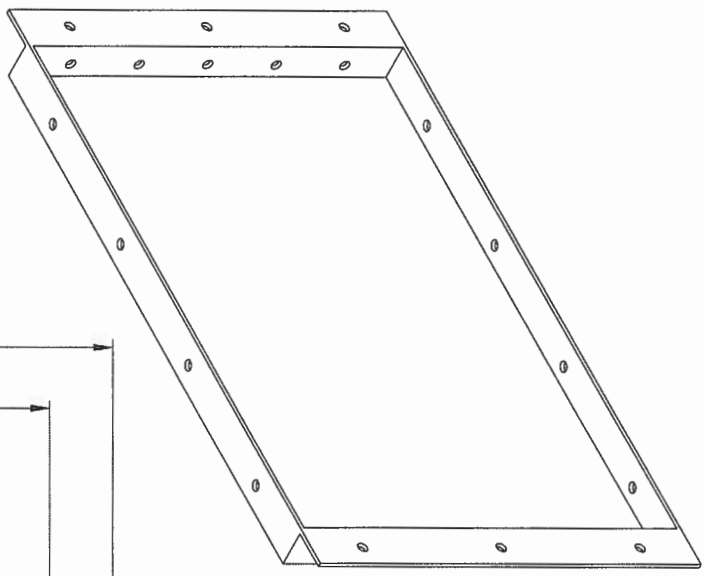
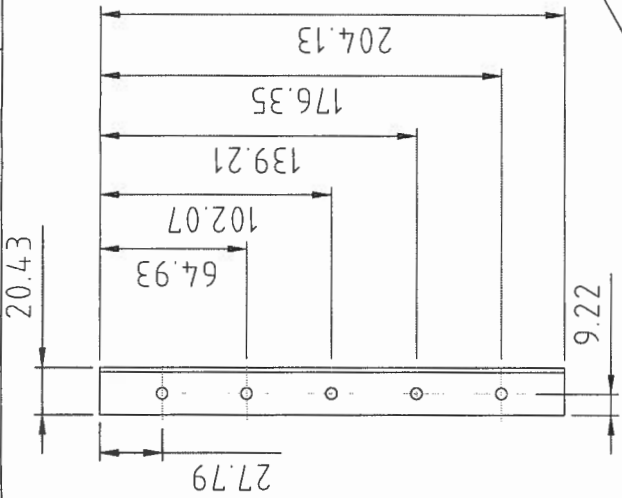
UNIVERSITY OF STELLENBOSCH



LENGTH	TOLERANCE
<1	0.02
1-100	0.5
>100	1

1	SHELL FLANGE	2	STAINLESS STEEL	395.6mm x 18mm
ITEM	DETAILS	NUMBER	MATERIAL	SPECS
SCALE	N.T.S.	TITLE: SHELL FLANGE		
UNITS	MM	PAGE No. 5 OF 15 PAGES No. MSc.T - PW5		
DATE	10/06/2003			

UNIVERSITY OF STELLENBOSCH



LENGTH	TOLERANCE
<1	0.02
1-100	0.1
>100	0.5

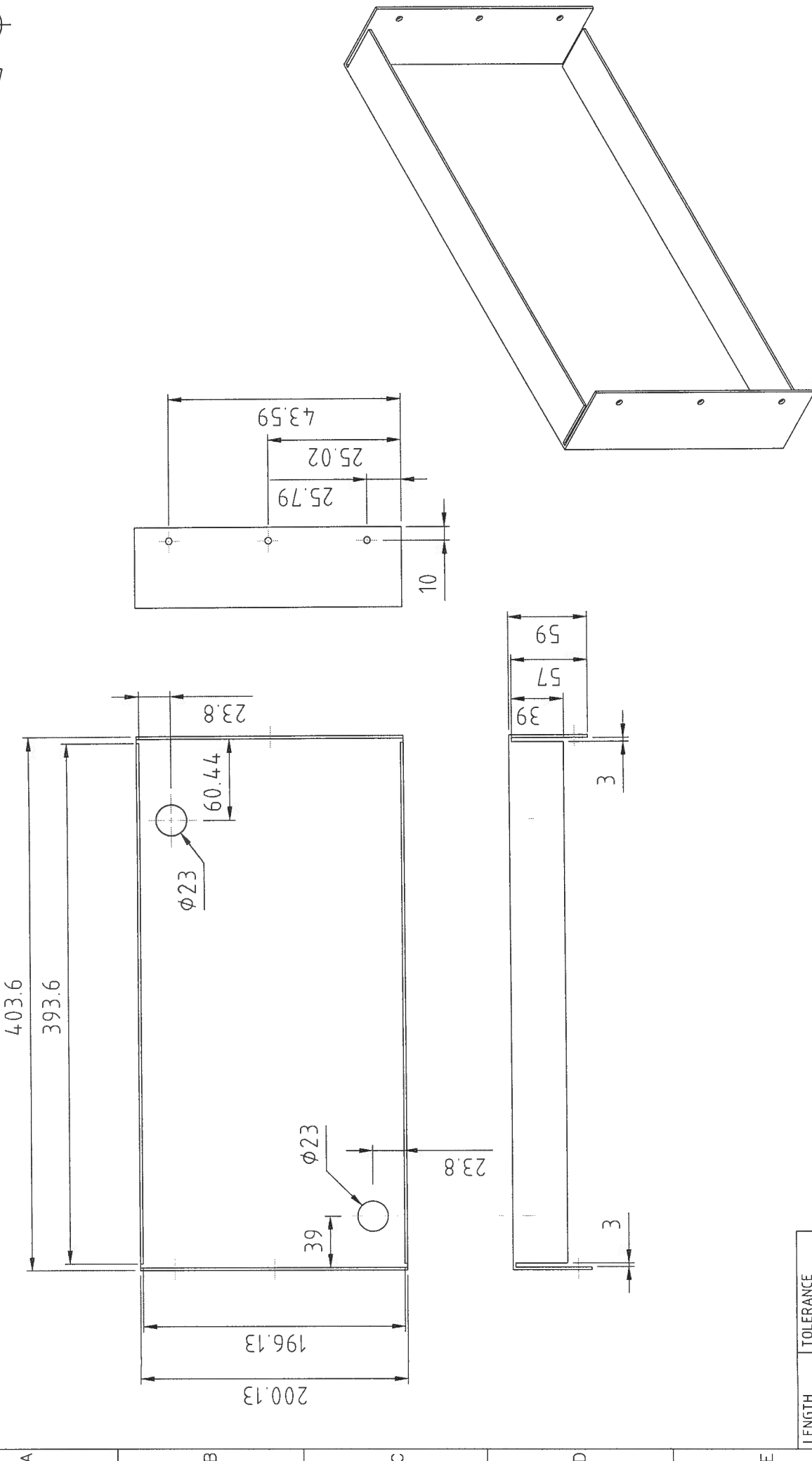
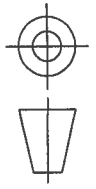
1	COVER			2	STAINLESS STEEL	373mm x 241mm x 2mm
ITEM	DETAILS	NUMBER	MATERIAL	SPECS	COMMENTS	

SCALE N.T.S.		TITLE: COVER
UNITS	MM	

DATE 10/06/2003	PAGE No. 6 OF 15 PAGES	No. Msc.T - PW6
-----------------	------------------------	-----------------

UNIVERSITY OF STELLENBOSCH

STUDENT No. 12911259 DESIGNER P WIPPLINGER CHECKED



LENGTH	TOLERANCE
<1	0.02
1-100	0.1
>100	0.5

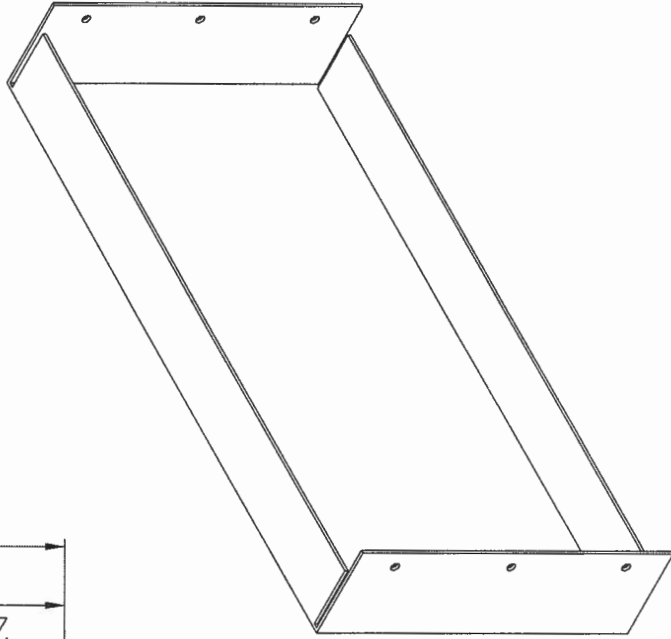
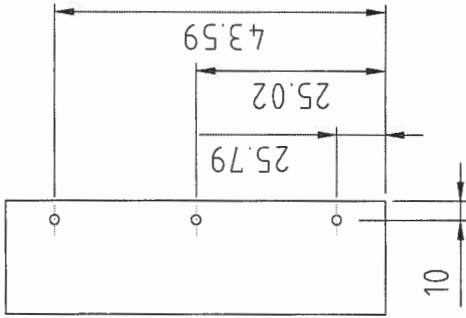
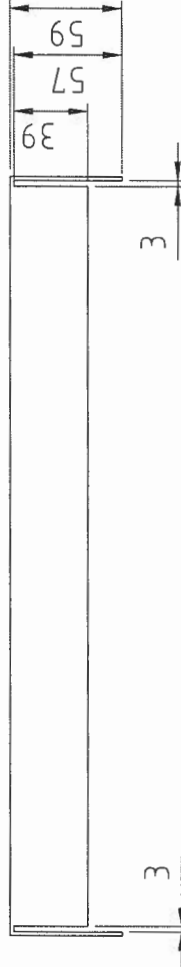
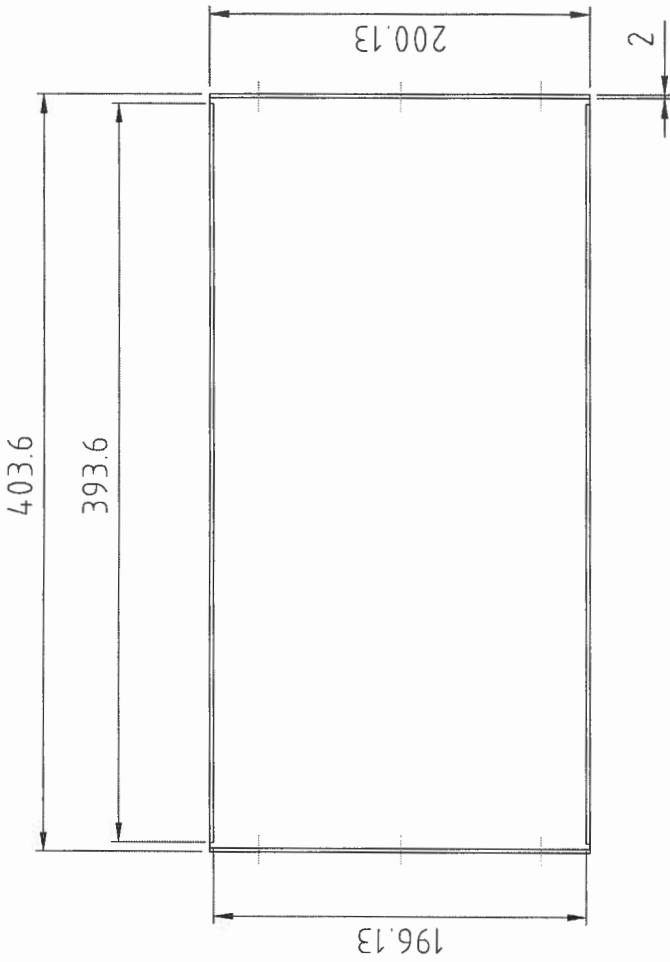
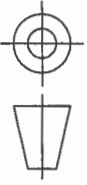
1	END CAP (1)	1	STAINLESS STEEL	493.6mm x 250.13mm x 2mm
ITEM	DETAILS	NUMBER	MATERIAL	SPECS
SCALE	N.T.S.	TITLE: END CAP (1)		
UNITS	MM	PAGE No. 7 OF 15 PAGES		
DATE	30/07/2003	No. Msc.T - PW7		

UNIVERSITY OF STELLENBOSCH

STUDENT No. 12911259

DESIGNER P WIPPLINGER

CHECKED



LENGTH	TOLERANCE
<1	0.02
1-100	0.1
>100	0.5

ITEM	END CAP (2)	DETAILS	NUMBER	MATERIAL	SPECS	COMMENTS
1			1	STAINLESS STEEL	493.6mm x 250.13mm x 2mm	

UNIVERSITY OF STELLENBOSCH

TITLE: END CAP (2)

STUDENT No. 12911259

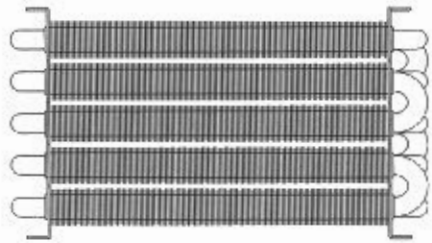
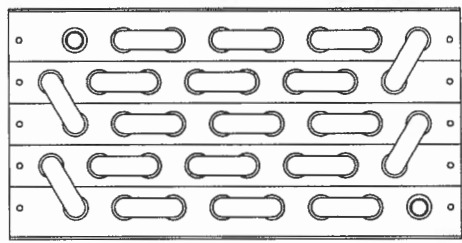
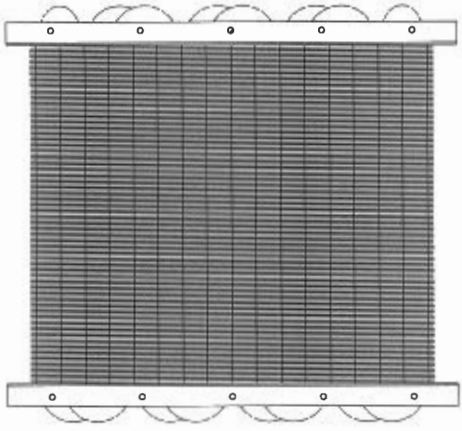
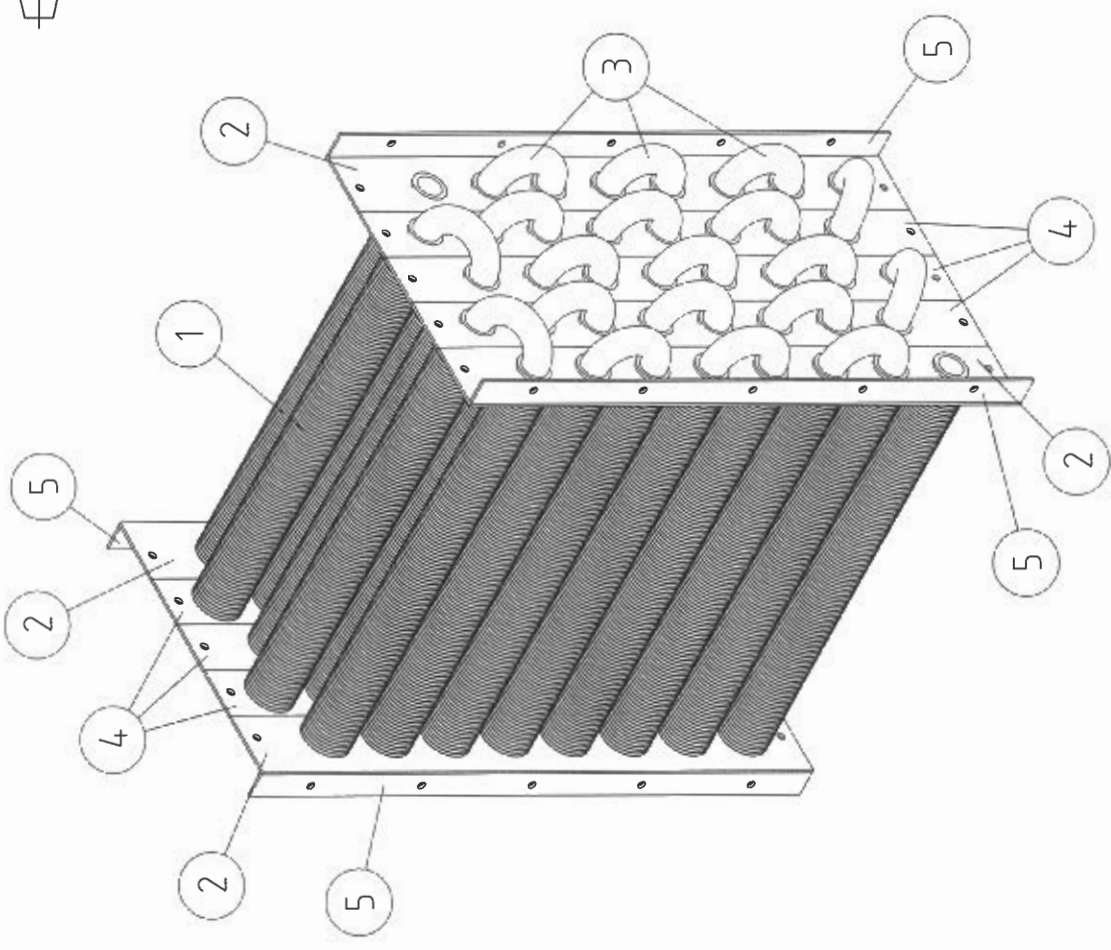
DESIGNER P WIPPLINGER

CHECKED

DATE 30/07/2003

PAGE No. 8 OF 15 PAGES

No. MSc.T - PW8



ITEM	DETAILS	NUMBER	MATERIAL	SPECS	COMMENTS
5	SHELL FLANGE	4	STAINLESS STEEL	Msc.T - PW5	
4	SIDE PLATE	6	STAINLESS STEEL	Msc.T - PW3	
3	TUBE U-BEND	39	STAINLESS STEEL	Msc.T - PW2	
2	SIDE CORNER	4	STAINLESS STEEL	Msc.T - PW4	
1	FIN TUBE	40	STAINLESS STEEL	Msc.T - PW1	

UNIVERSITY OF STELLENBOSCH

TITLE: HEAT EXCHANGER ASSEMBLY (1)

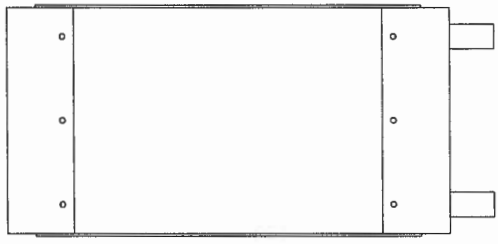
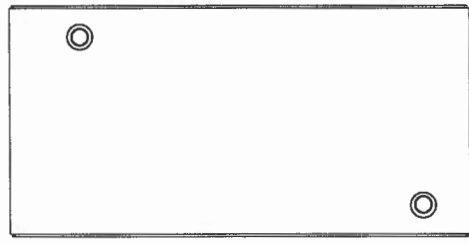
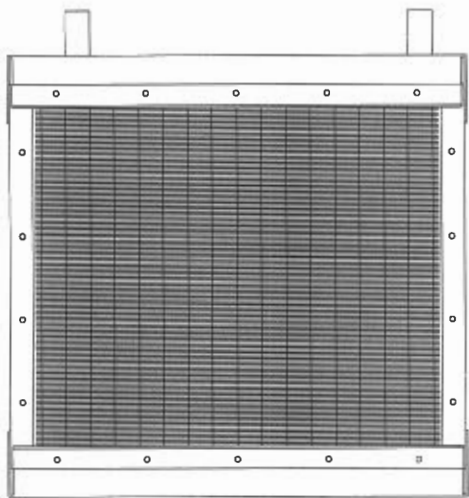
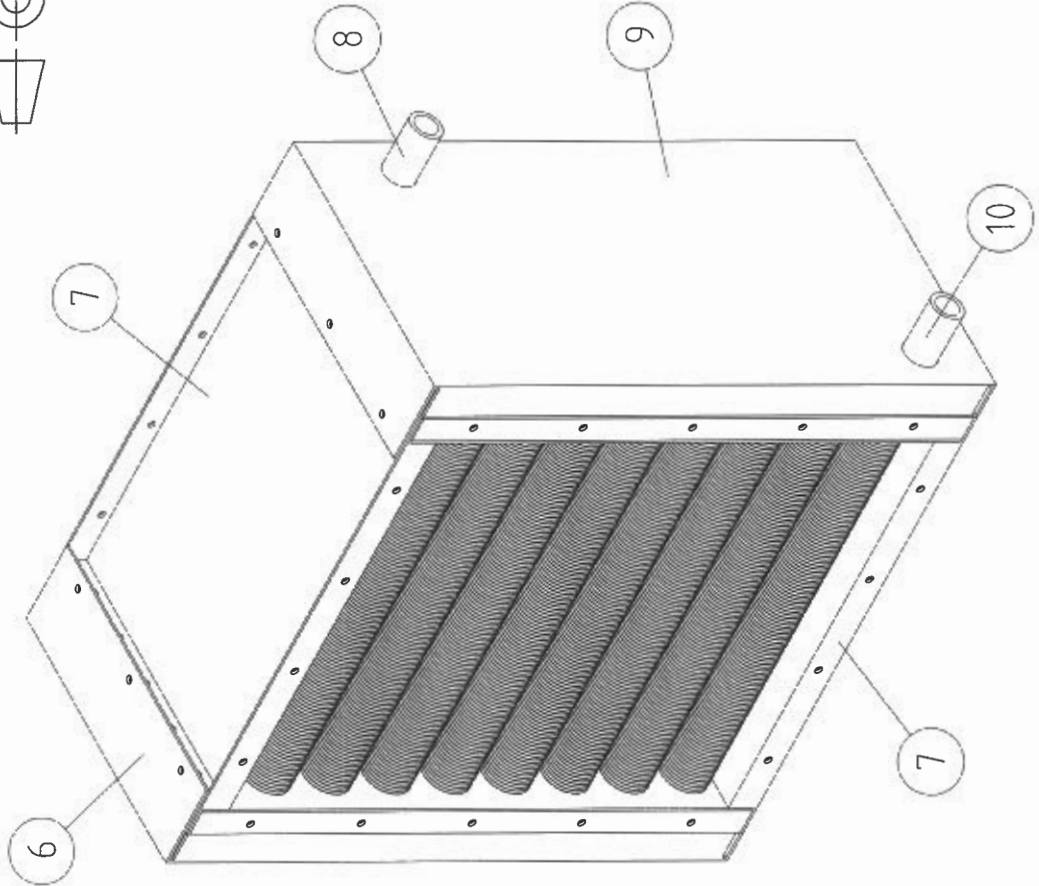
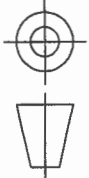
DATE 11/06/2003 PAGE No. 9 OF 15 PAGES No. Msc.T - PW9

DESIGNER P WIPPLINGER

CHECKED

STUDENT No. 12911259

A B C D E



10	INLET	1	STAINLESS STEEL		
9	END CAP (1)	1	STAINLESS STEEL	Msc.T - PW7	
8	OUTLET	1	STAINLESS STEEL		
7	COVER	2	STAINLESS STEEL	Msc.T - PW6	
6	END CAP (2)	1	STAINLESS STEEL	Msc.T - PW8	
ITEM	DETAILS	NUMBER	MATERIAL	SPECS	COMMENTS

SCALE N.T.S.
 UNITS MM
 DATE 11/06/2003
 TITLE: HEAT EXCHANGER ASSEMBLY (2)
 PAGE No. 10 OF 15 PAGES No. Msc.T - PW10

UNIVERSITY OF STELLENBOSCH

CHECKED

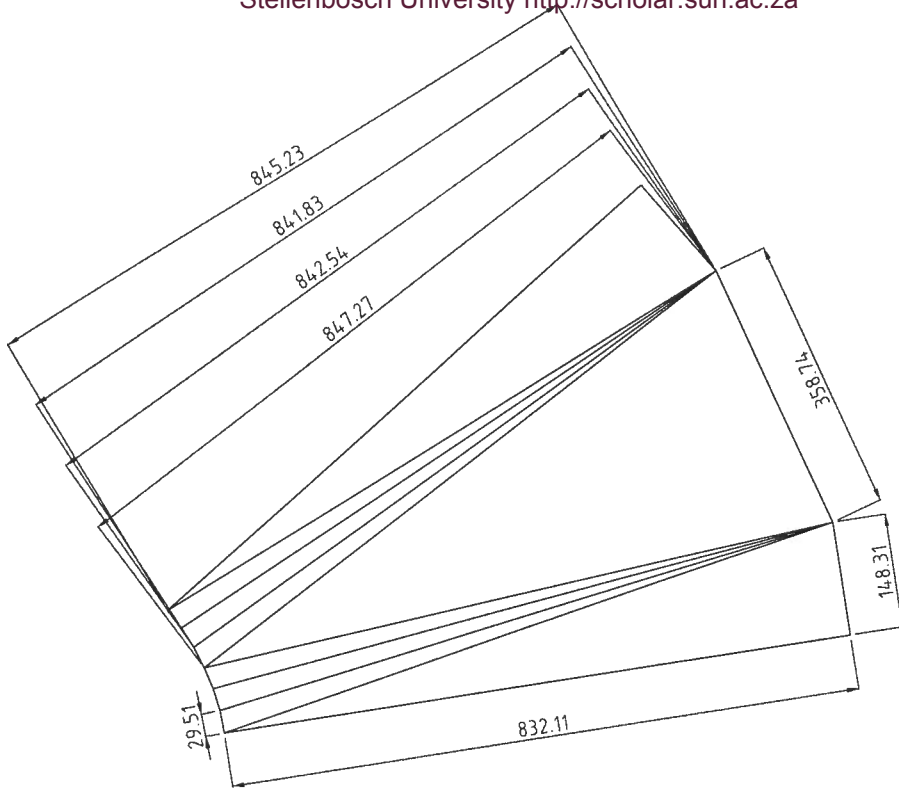
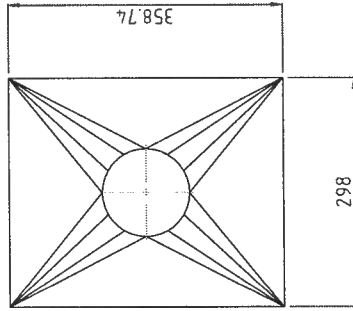
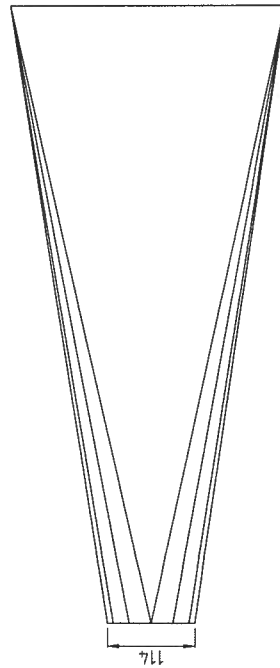
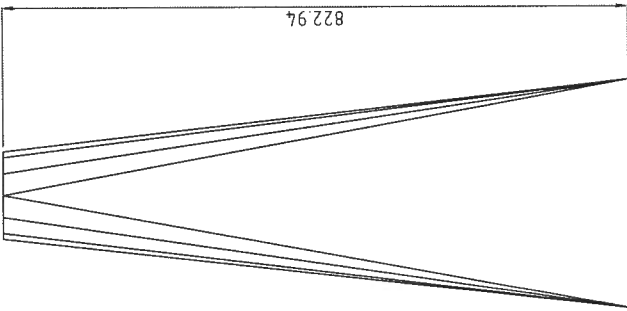
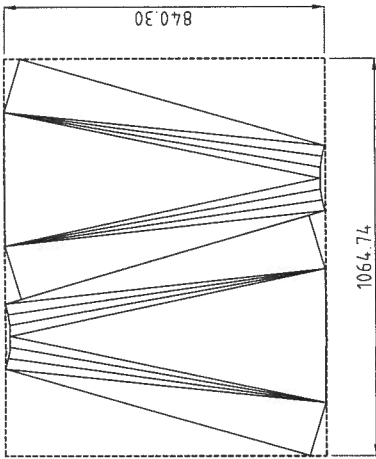
DESIGNER P WIPPLINGER

STUDENT No. 12911259

A B C D E



DUCT CUTTING FROM PLATE

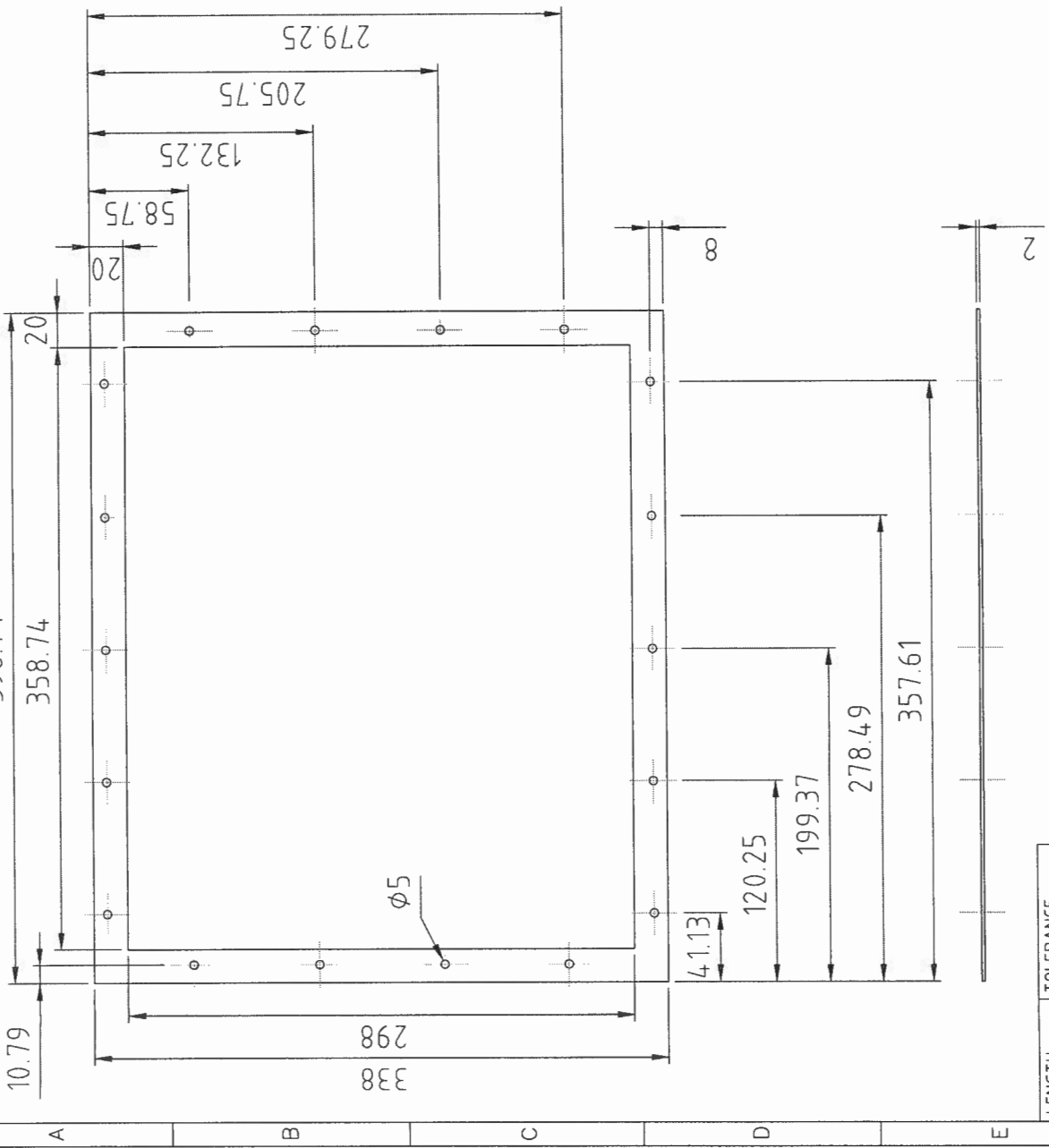
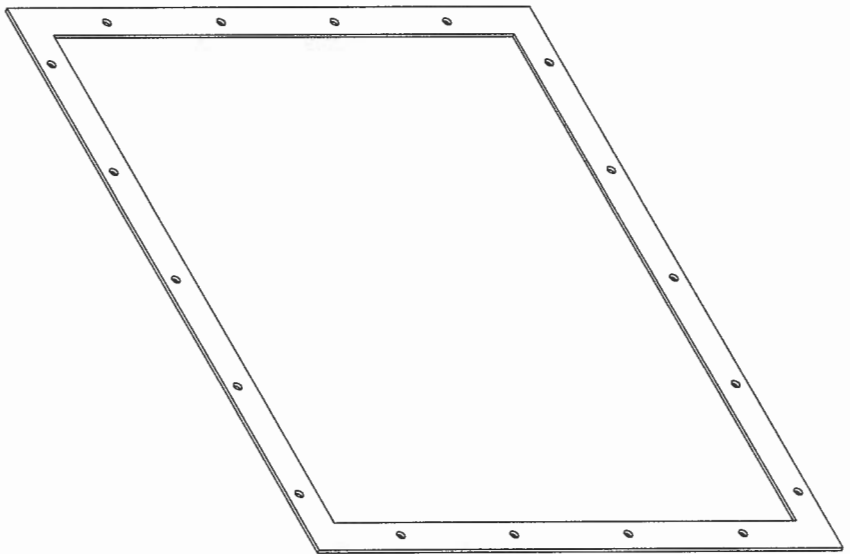
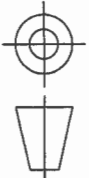


LENGTH	TOLERANCE
<1	0.02
1-100	0.5
>100	1

ITEM	DUCT UNFOLDING	NUMBER	SHEET METAL	1064.74mm x 840.30mm
1	DUCT UNFOLDING	2	SHEET METAL	1064.74mm x 840.30mm
SCALE	DETAILS	MATERIAL	SPECS	COMMENTS
N.T.S.	N.T.S.			
UNITS	MM			

UNIVERSITY OF STELLENBOSCH

TITLE: DUCT UNFOLDING

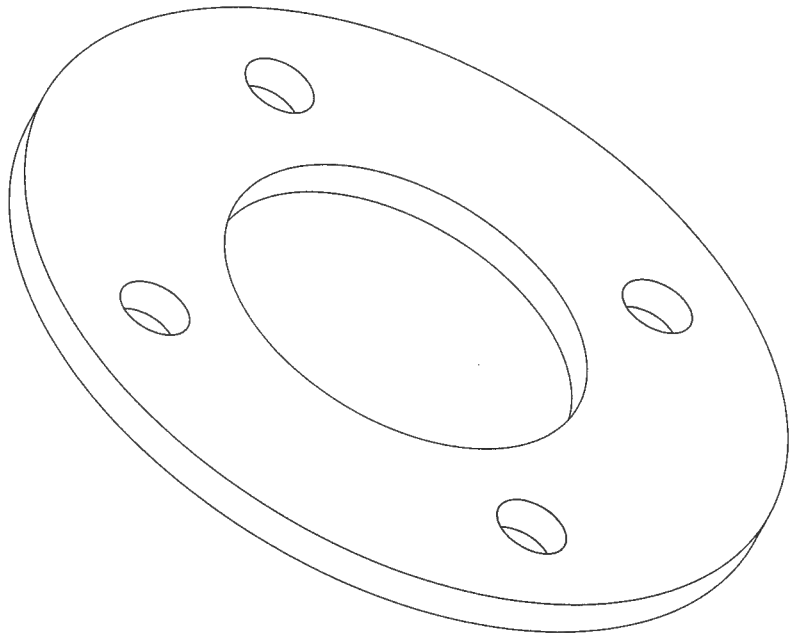
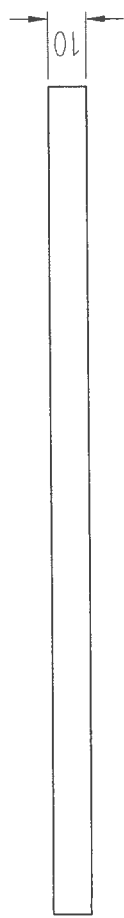
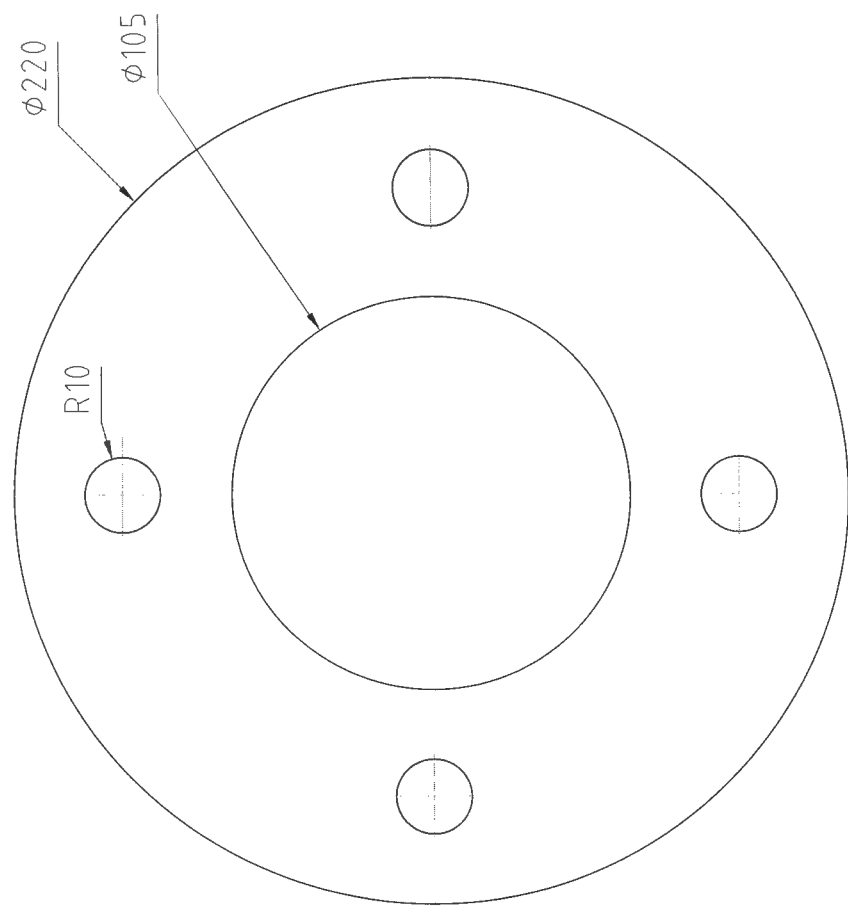
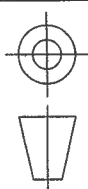


LENGTH	TOLERANCE
<1	0.02
1-100	0.1
>100	0.5

1	DUCTING FLANGE	2	STAINLESS STEEL	395.6mm x 46.36mm x 2mm
ITEM	DETAILS	NUMBER	MATERIAL	SPECS
SCALE	N.T.S.	TITLE: DUCTING FLANGE		
UNITS	MM	PAGE No. 12 OF 15 PAGES INO. MSc.T - PW12		
DATE 10/06/2003				

UNIVERSITY OF STELLENBOSCH

STUDENT No. 12911259 DESIGNER P WIPPLINGER CHECKED

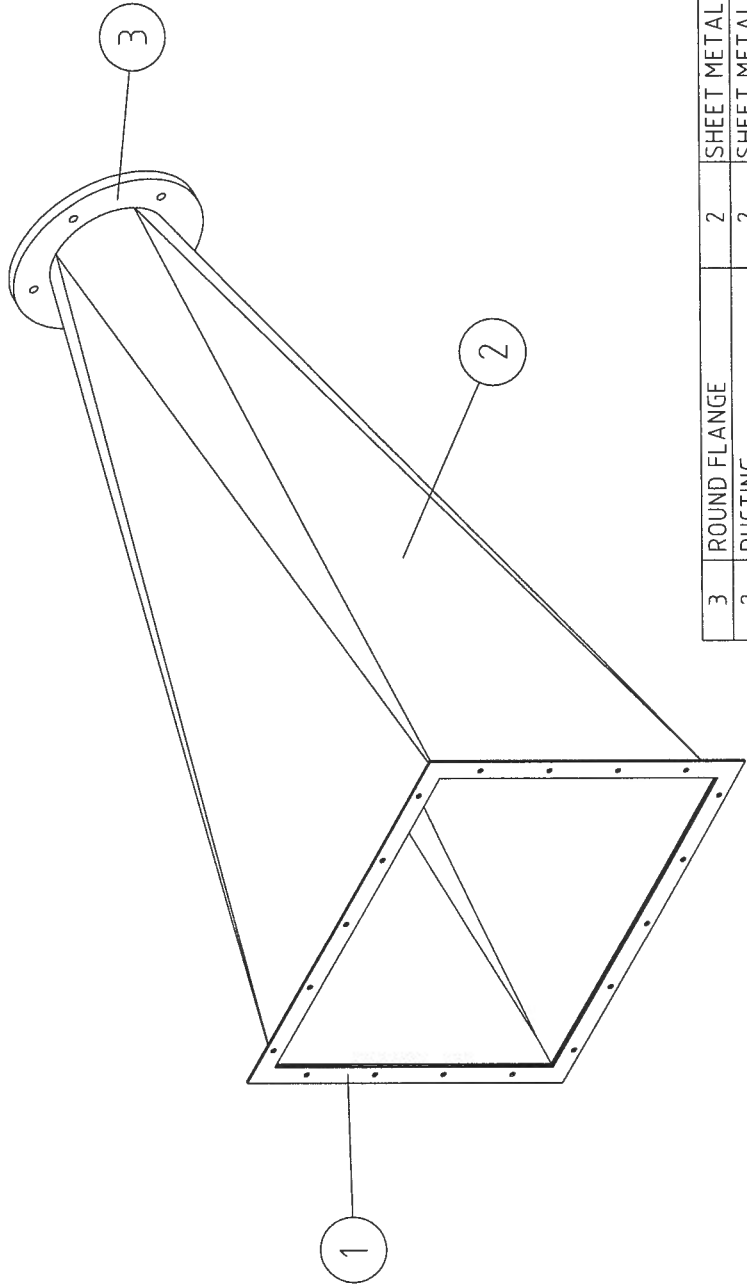
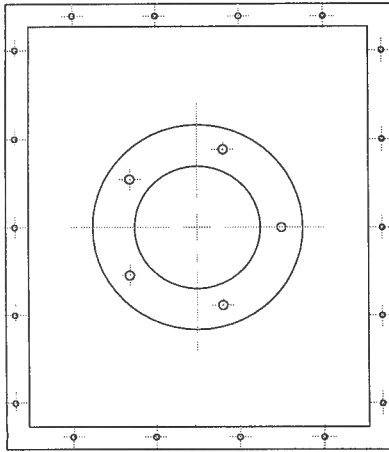
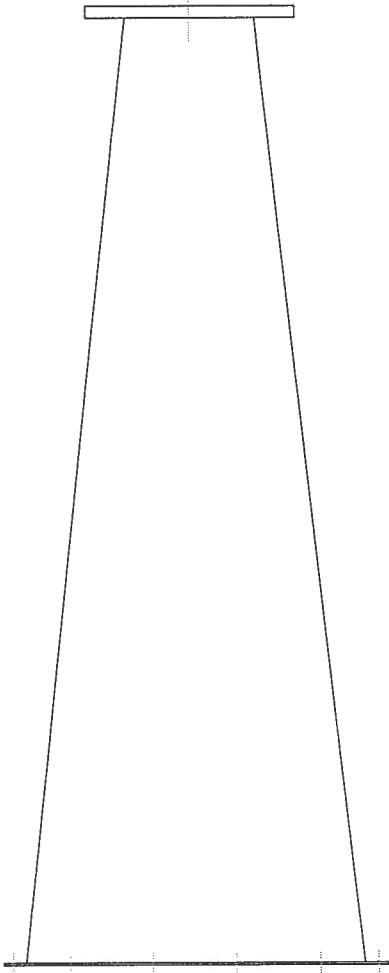
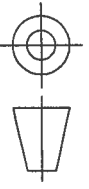


A B C D E

1	DUCTING PIPE FLANGE	2	METAL SHEET	2200Dx10mm
ITEM	DETAILS	NUMBER	MATERIAL	SPECS
SCALE	N.T.S.	TITLE: DUCTING PIPE FLANGE		
UNITS	MM	PAGE No. 13 OF 15 PAGES No. Msc.T - Pw13		
DATE	14/08/2003			

UNIVERSITY OF STELLENBOSCH

STUDENT No. 12911259 DESIGNER P WIPPLINGER CHECKED



LENGTH	TOLERANCE
<1	0.02
1-100	0.1
>100	0.5

ITEM	DETAILS	NUMBER	MATERIAL	SPECS	COMMENTS
3	ROUND FLANGE	2	SHEET METAL		
2	DUCTING	2	SHEET METAL	Msc.T - Pw11	
1	RECTANGULAR FLANGE	2	SHEET METAL	Msc.T - Pw12	

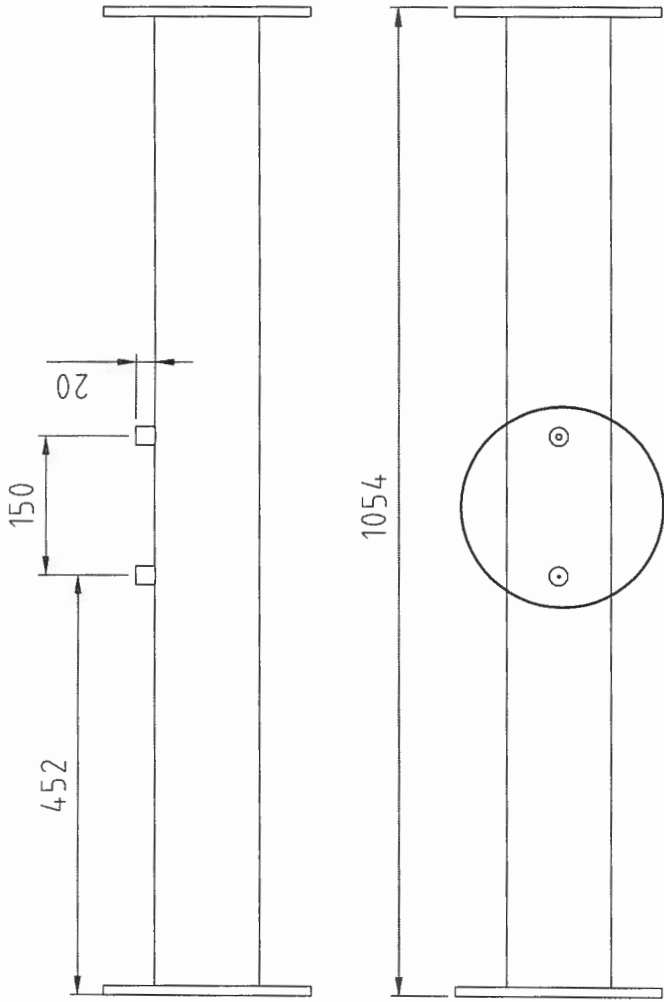
UNIVERSITY OF STELLENBOSCH

STUDENT No. 12911259 DESIGNER P WIPPLINGER CHECKED

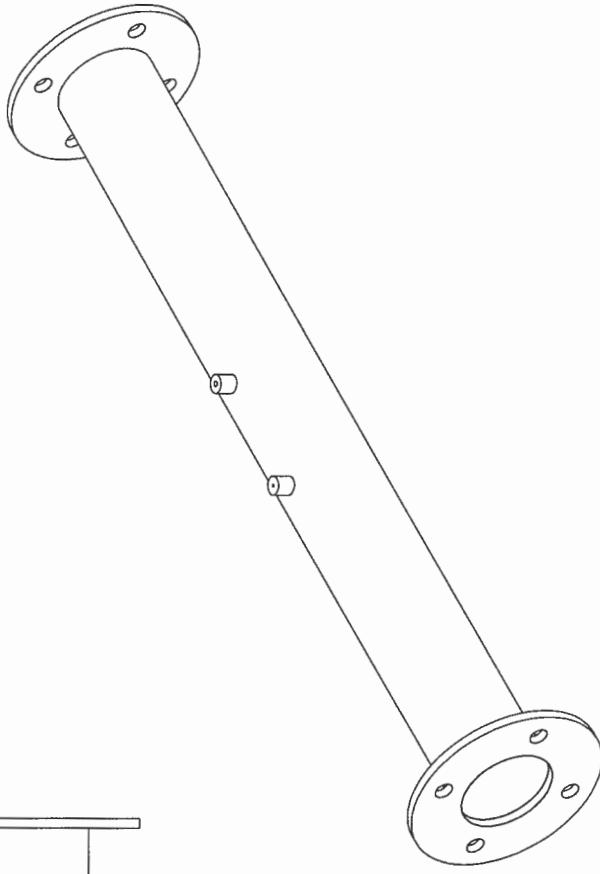
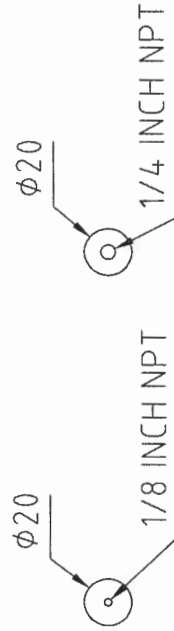
SCALE N.T.S. TITLE: DUCTING ASSEMBLY

UNITS MM

DATE 11/06/2003 PAGE No. 14 OF 15 PAGES No. Msc.T - Pw14



DETAIL



4	TEMPERATURE POINT	1	SOLID BAR	200Dx20mm
3	PRESSURE POINT	1	SOLID BAR	200Dx20mm
2	DUCTING FLANGE	2	METAL	MSc.T-PW12
1	PIPE	1	METAL PIPE	1110Dx105IDx1034mm
ITEM	DETAILS	NUMBER	MATERIAL	SPECS
SCALE	N.T.S.	TITLE: EXHAUST INLET PIPE		
UNITS	MM	PAGE No. 15 OF 15 PAGES No. MSc.T - PW15		
DATE	14/08/2003	DESIGNER P WIPPLINGER CHECKED		

LENGTH	TOLERANCE
<1	0.02
1-100	0.1
>100	0.5

UNIVERSITY OF STELLENBOSCH

STUDENT No. 12911259

DESIGNER P WIPPLINGER

CHECKED

DATE 14/08/2003

PAGE No. 15 OF 15 PAGES

No. MSc.T - PW15

APPENDIX L
HEAT EXCHANGER TEST RESULTS

L1 - INTRODUCTION

The following tables document the results for each of the test runs referred to in the thesis. The actual measured data can be found on the CD accompanying the thesis.

<u>Continuous combustion unit</u>				<u>Heat exchanger</u>			
Time	Gas flow [kg/hr]	Fuel flow [kg/hr]	Total flow [kg/hr]	Water flow [l/min]	Water side		Gas side
					Inlet Press [kPa]	Outlet Press [kPa]	Press diff [Pa]
14:34:33	65	4.75	69.75	0.2	-	-	2
14:35:40	65	4.75	69.75	0.2	-	-	2
14:37:00	65	4.75	69.75	0.2	-	-	4
14:39:00	65	4.75	69.75	0.2	600	550	4
14:40:00	65	4.75	69.75	0.2	600	550	4
: :	Gasbottle is empty						
14:49:00	65	4.75	69.75	0.2	1300	1400	5
14:50:47	65	4.75	69.75	0.2	1400	1450	5
14:52:40	65	4.75	69.75	0.2	1450	1500	5
14:53:06	65	4.75	69.75	0.2	1300	1400	5
14:55:09	65	4.75	69.75	0.2	1100	1100	5
14:56:47	65	4.75	69.75	0.2	1000	1000	5
14:57:16	65	4.75	69.75	0.2	1000	1000	5
: :	Stable						
14:59:00	57.5	4.25	61.75	0.2	900	900	5
15:03:00	57.5	4.25	61.75	0.2	900	900	5
: :	Stable						
15:04:10	65	4.25	69.25	0.2	900	900	5
15:05:00	65	4.25	69.25	0.2	900	900	5
15:08:15	65	4.25	69.25	0.2	950	950	5
: :	Stable						
15:10:10	75	4.25	79.25	0.2	1000	1000	5
15:11:10	75	4.25	79.25	0.2	1000	1000	5
15:15:09	75	4.25	79.25	0.2	1000	1000	5
	Stable						
16:15:50	Shutdown procedure						

Table L1: Test data on 27-10-2003

<u>Continuous combustion unit</u>				<u>Heat exchanger</u>			
Time	Gas flow [kg/hr]	Fuel flow [kg/hr]	Total flow [kg/hr]	Water flow [l/min]	Water side		Gas side
					Inlet Press [kPa]	Outlet Press [kPa]	Press diff [Pa]
10:14:34	67	4.75	71.75	0.2	-	-	0
10:16:44	67	4.75	71.75	0.2	400	300	2
10:18:34	67	4.75	71.75	0.2	500	400	4
	Exhaust fan is shut down						
14:59:04	67	4.75	71.75	0.2	-	-	
15:00:59	67	4.75	71.75	0.2	200	100	6
15:02:40	67	4.75	71.75	0.2	400	300	8
15:05:04	67	4.75	71.75	0.2	500	400	8
15:08:11	67	4.75	71.75	0.2	550	470	8
15:11:03	67	4.75	71.75	0.2	600	550	8
15:12:33	67	4.75	71.75	0.2	600	550	8
	Stable						
15:14:23	67	4.75	71.75	0.2	1100	1120	
15:16:43	67	4.75	71.75	0.2	1100	1120	8
15:17:40	67	4.75	71.75	0.2	1200	1220	8
15:18:42	67	4.75	71.75	0.2	1250	1320	8
15:23:18	67	4.75	71.75	0.2	1350	1400	8
15:24:04	67	4.75	71.75	0.2	1350	1500	8
	Stable						
15:25:10	67	4.25	71.25	0.2	1300	1400	8
15:26:30	67	4.25	71.25	0.2	1275	1350	8
15:29:05	67	4.25	71.25	0.2	1250	1300	8
15:30:00	67	4.25	71.25	0.2	1200	1300	8
15:31:22	67	4.25	71.25	0.2	1200	1300	8
	Stable						
15:33:10	Gasbottle is empty						
15:37:00	67	4.25	71.25	0.2	200	100	8
15:38:32	67	4.25	71.25	0.2	600	500	8
15:40:50	67	4.25	71.25	0.2	750	750	8
15:41:30	67	4.25	71.25	0.2	800	800	8
15:42:38	67	4.25	71.25	0.2	800	800	8
15:43:30	67	4.25	71.25	0.2	800	800	8
	Stable						

Table L2: Test data on 30-10-2003

<u>Continuous combustion unit</u>				<u>Heat exchanger</u>			
Time	Gas flow [kg/hr]	Fuel flow [kg/hr]	Total flow [kg/hr]	Water flow [l/min]	Water side		Gas side
					Inlet Press [kPa]	Outlet Press [kPa]	Press diff [Pa]
15:44:02	67	4.25	71.25	0.2	800	800	8
15:45:26	67	4.25	71.25	0.2	700	700	8
15:48:20	67	4.25	71.25	0.2	680	650	8
15:49:10	67	4.25	71.25	0.2	680	650	8
15:51:07	67	4.25	71.25	0.2	600	550	8
15:52:14	67	4.25	71.25	0.2	600	550	8
	Stable						
15:54:00	80	4	84	0.2	600	550	8
15:56:20	80	4	84	0.2	600	550	8
15:57:10	80	4	84	0.2	650	600	8
15:58:00	80	4	84	0.2	700	650	8
15:58:50	80	4	84	0.2	750	750	8
16:00:00	80	4	84	0.2	800	800	8
16:01:50	80	4	84	0.2	800	800	8
	Stable						
16:01:56	80	4	84	0.2	900	900	11
16:03:10	80	4	84	0.2	950	1000	10
16:04:03	80	4	84	0.2	10	1100	10
16:04:57	80	4	84	0.2	1100	1150	10
16:07:15	80	4	84	0.2	1150	1250	10
	Stable						
16:09:30	Shutdown procedure						

Table L3: Test data on 30-10-2003 (continued)

<u>Continuous combustion unit</u>				<u>Heat exchanger</u>			
Time	Gas flow [kg/hr]	Fuel flow [kg/hr]	Total flow [kg/hr]	Water flow [l/min]	Water side		Gas side
					Inlet Press [kPa]	Outlet Press [kPa]	Press diff [Pa]
08:31:50	75	4.75	79.75	0.25	-	-	4
08:32:50	70	4.75	74.75	0.25	-	-	6
08:34:38	70	4.75	74.75	0.25	-	-	6
08:35:36	70	4.75	74.75	0.25	500	400	8
08:38:16	70	4.75	74.75	0.25	600	600	8
08:41:14	70	4.75	74.75	0.25	600	600	8
08:41:44	70	4.75	74.75	0.25	700	700	8
08:43:30	70	4.75	74.75	0.25	750	750	8
08:45:00	70	4.75	74.75	0.25	800	800	9
08:48:00	70	4.75	74.75	0.25	800	800	9
	Stable						
08:54:25	70	4.75	74.75	0.25	700	700	10
08:56:40	70	4.75	74.75	0.25	650	650	10
08:58:30	70	4.75	74.75	0.25	650	650	10
	Stable						
08:59:19	70	4.75	74.75	0.25	750	750	10
09:00:46	70	4.75	74.75	0.25	800	800	10
09:02:17	70	4.75	74.75	0.25	900	900	10
09:03:12	70	4.75	74.75	0.25	900	900	10
09:04:40	70	4.75	74.75	0.25	900	900	10
	Stable						
09:05:25	70	4.75	74.75	0.2	900	900	10
09:07:50	70	4.75	74.75	0.2	900	900	10
09:09:50	70	4.75	74.75	0.2	900	900	10
	Stable						
09:10:55	Shutdown procedure						

Table L4: Test data on 5-10-2003

APPENDIX M

STRESS ANALYSIS

M1 - FINITE ELEMENT ANALYSIS RESULTS

M1.1 - U-BEND

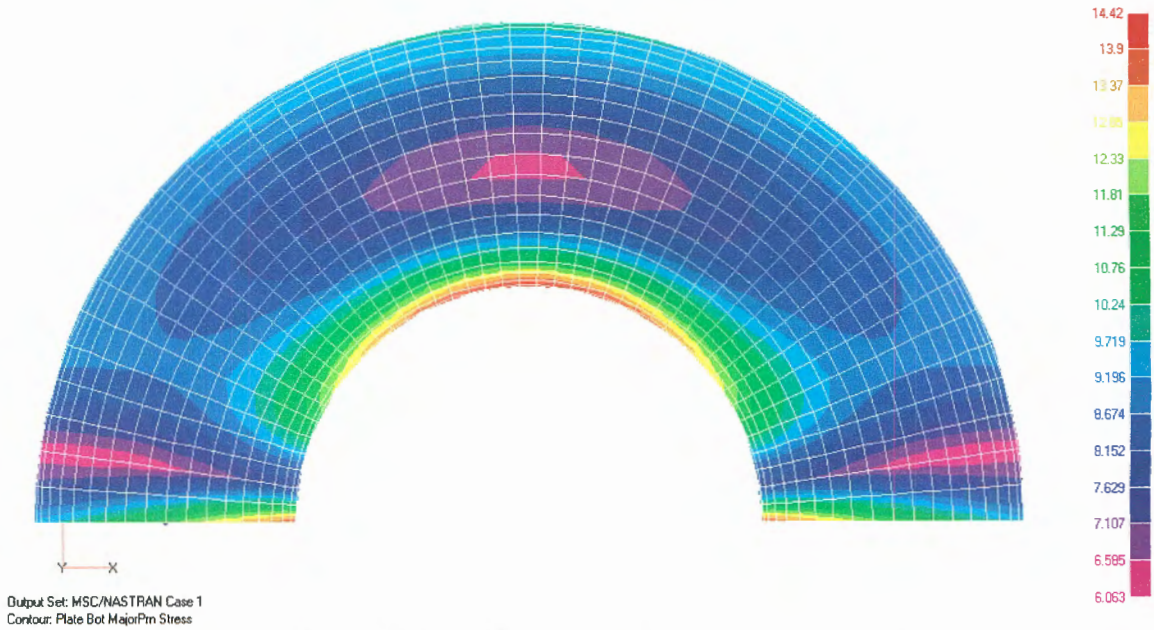


Figure M1: U-bend NASTRAN analysis: Bottom major principal stress [MPa]

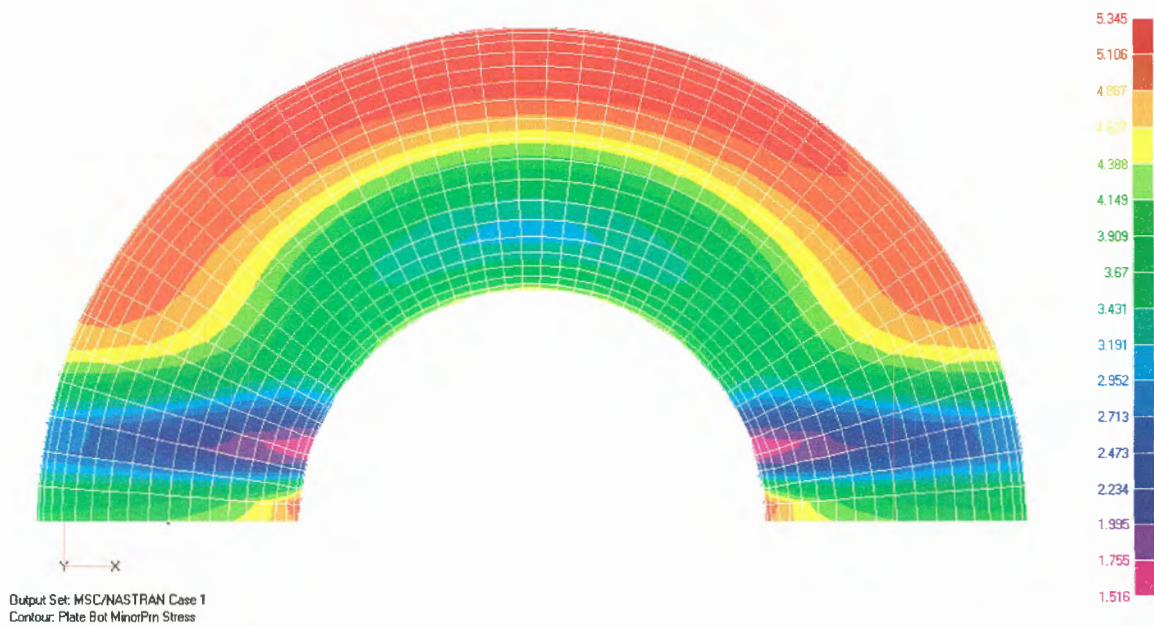


Figure M2: U-bend NASTRAN analysis: Bottom minor principal stress [MPa]

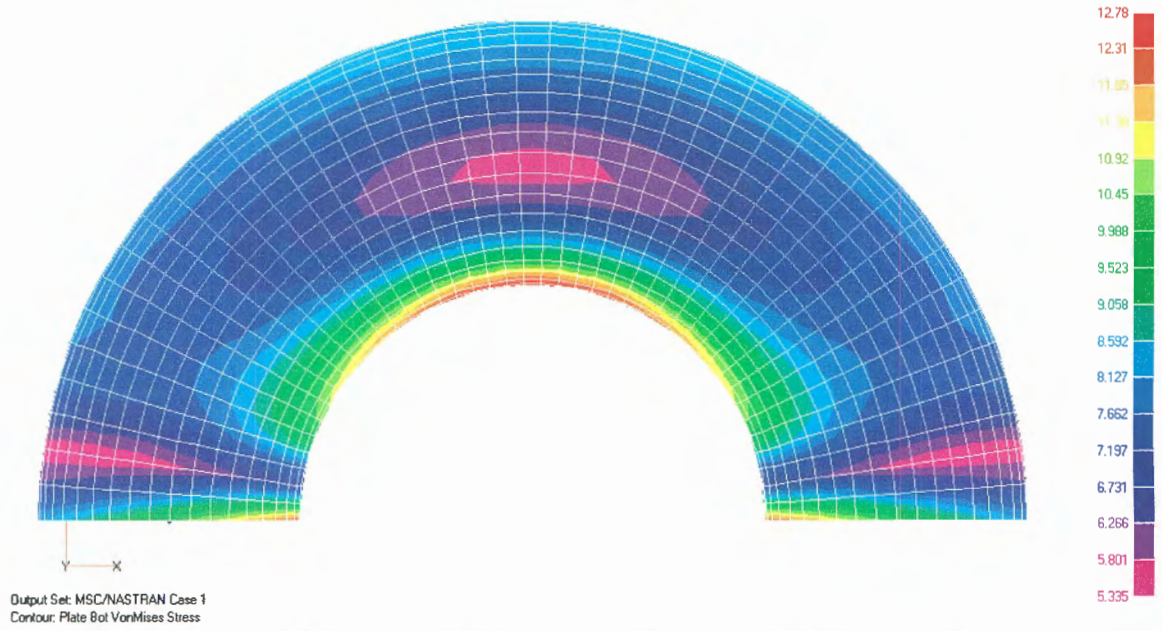


Figure M3: U-bend NASTRAN analysis: Bottom Von Mises stress [MPa]

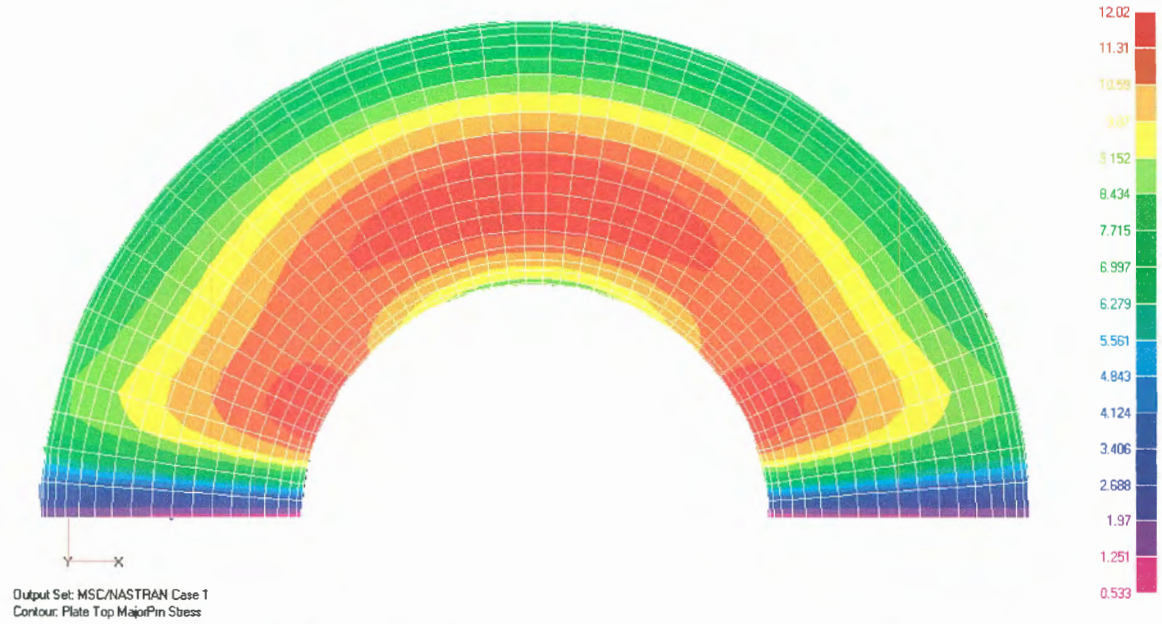


Figure M4: U-bend NASTRAN analysis: Top major principal stress [MPa]

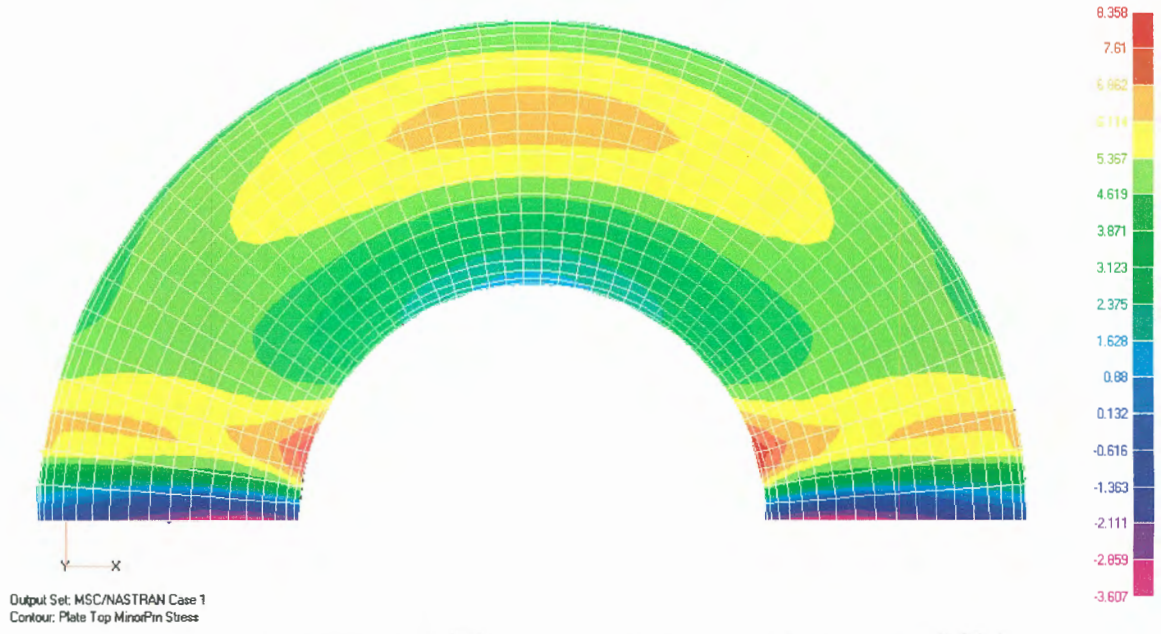


Figure M5: U-bend NASTRAN analysis: Top minor principal stress [MPa]

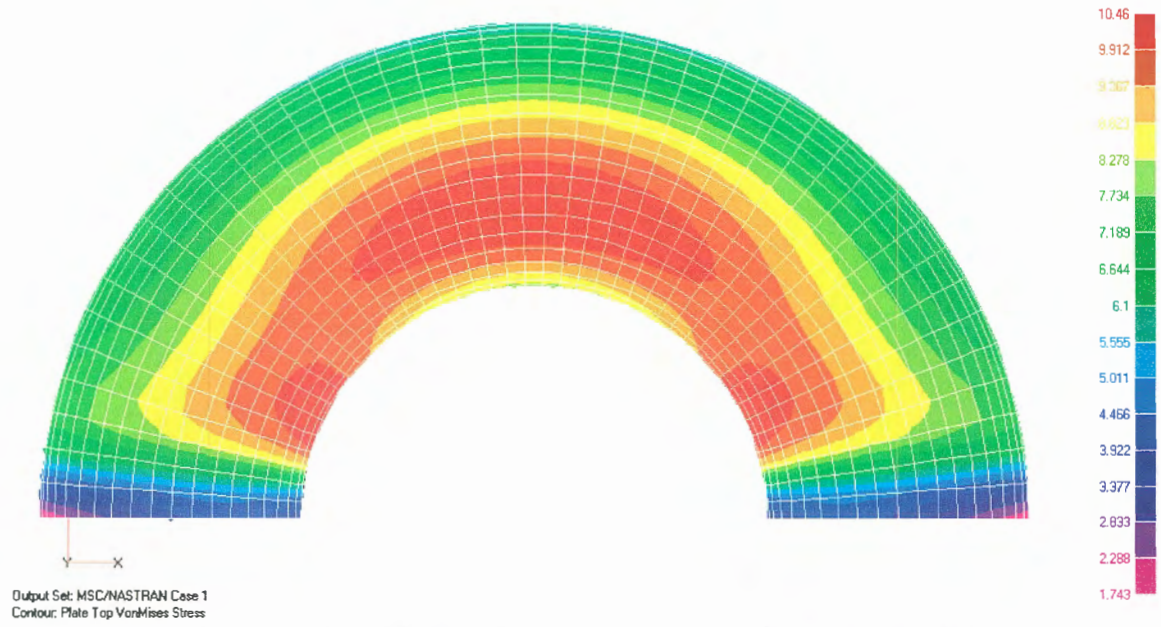


Figure M6: U-bend NASTRAN analysis: Top Von Mises stress [MPa]

M1.2 - FINTUBE

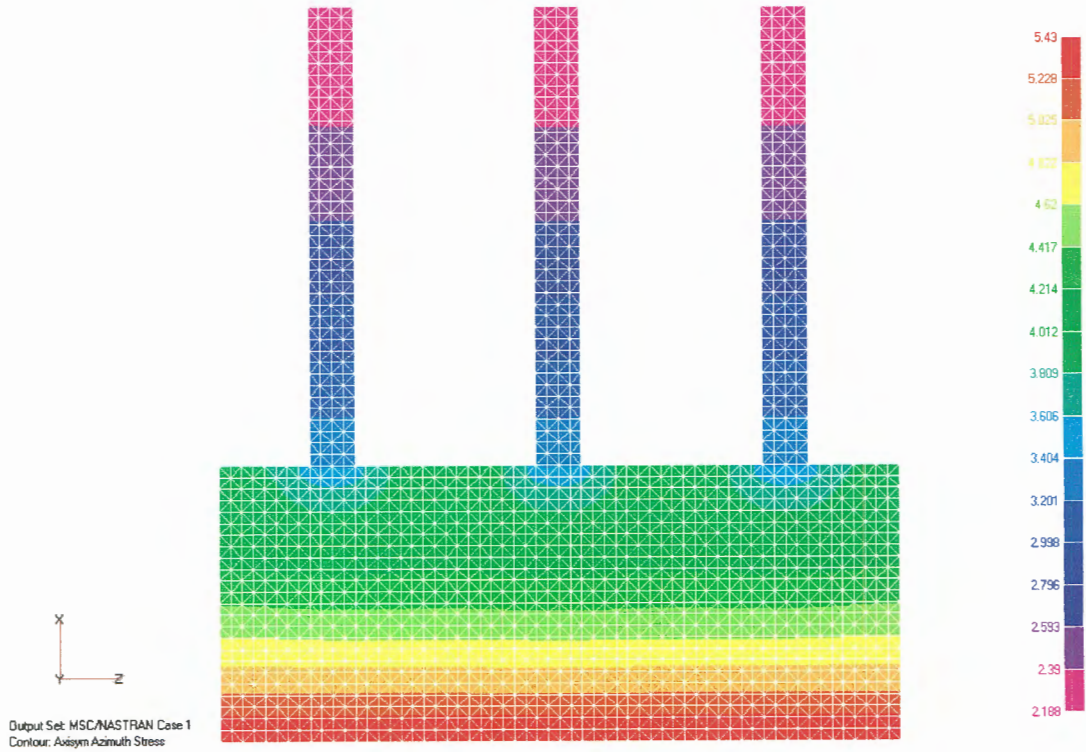


Figure M7: Fintube NASTRAN analysis: Azimuth Stress [MPa]

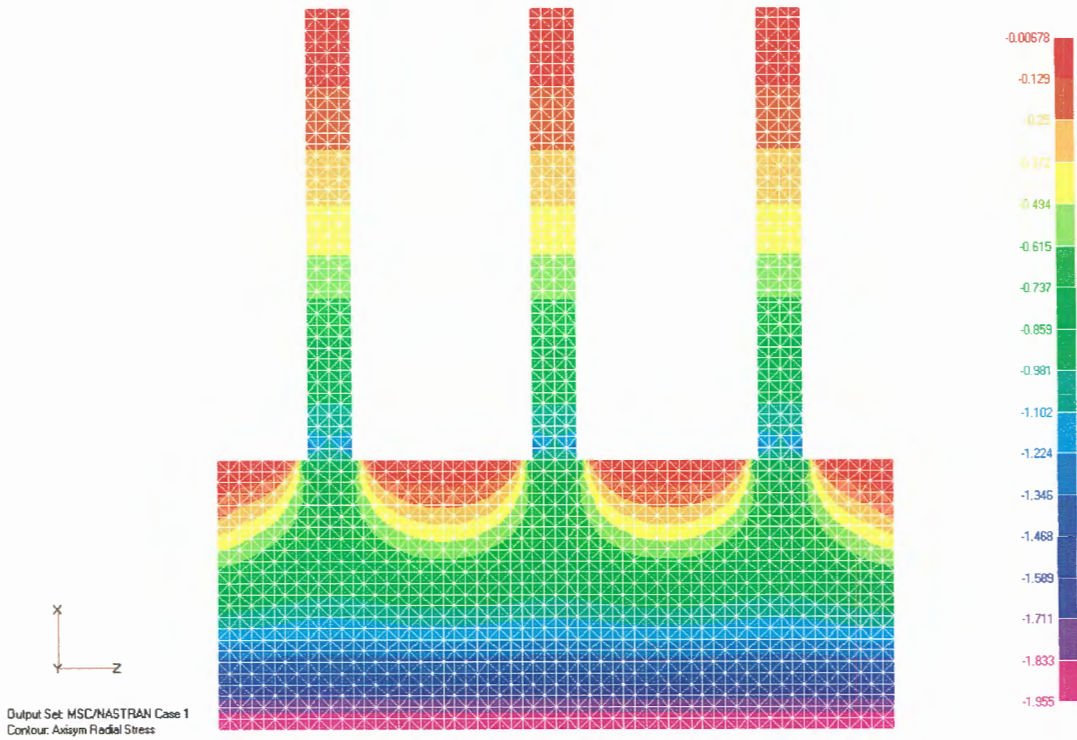


Figure M8: Fintube NASTRAN analysis: Radial Stress [MPa]

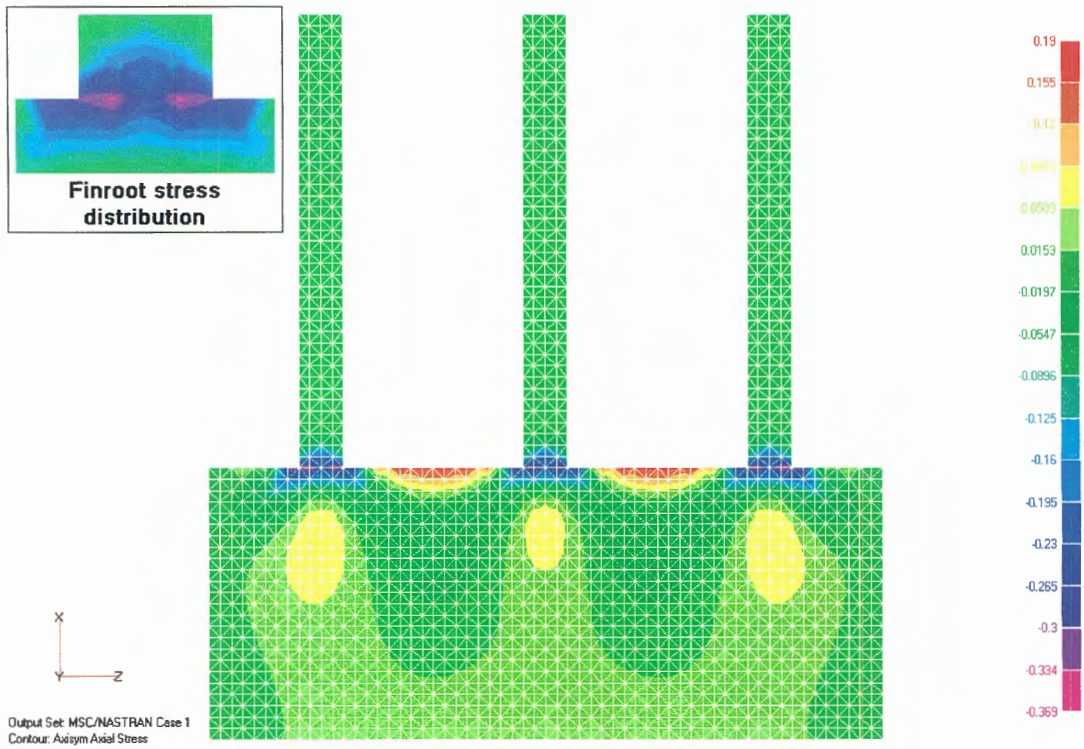


Figure M9: Fintube NASTRAN analysis: Axial Stress [MPa]

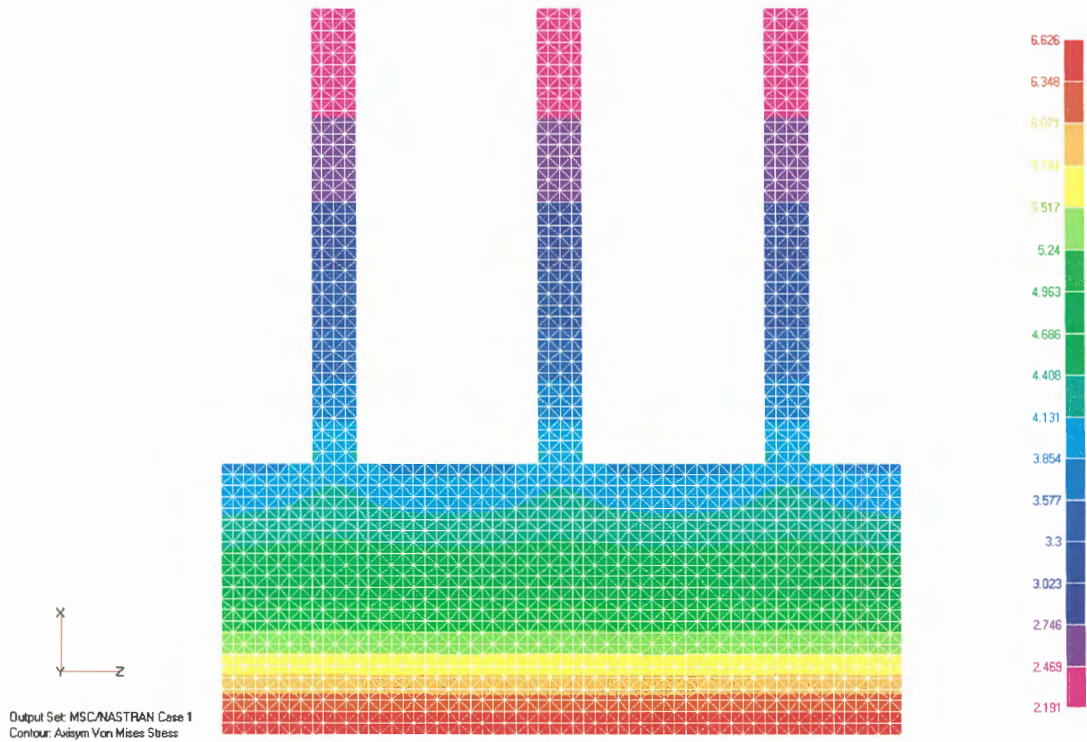


Figure M10: Fintube NASTRAN analysis: Von Mises Stress [MPa]

M1.3 - CONCLUSIONS DRAWN FROM THE U-BEND ANALYSIS*

Load:

The model had an inside pressure of 2MPa (20bar) on each element.

Constraints:

Each node at the ends were fixed with respect to the x, y and z axis in order to simulate conditions where there is no room for pressure induced-expansion, i.e. the end centres are kept at a fixed distance from each other and the concentricity of each end is ensured. The concentricity is important as the ends are welded to the fintubes. This results in the maximum possible stress generated in the U-bend (worse case scenario).

Figure M1 – Bottom major principal stress (Mohr-circle theory)

The maximum major principal stress on the inside of the U-bend occurs at the apex and ends of the inner curve where the red elements show tension in the material. The stress throughout the U-bend varies between 6.063 and 14.42MPa.

Figure M2 – Bottom minor principal stress (Mohr-circle theory)

The maximum minor principal stress on the inside of the U-bend occurs on most of the outer curve and at the ends of the inner curve where the red elements show tension in the material. The stress throughout the U-bend varies between 1.516 and 5.345MPa.

Figure M3 – Bottom Von Mises (Von Mises yield criterion)

The Von Mises stress has much the same distribution as the major principal stresses, but the resulting forces are much lower. The maximum Von Mises yield stress occurs at the apex and ends of the inner curve where the red elements show tension in the material. The stress throughout the U-bend varies between 5.335 and 12.78MPa.

Figure M4 – Top major principal stress (Mohr-circle theory)

The maximum major principal stress on the outside of the U-bend (using Mohr-circle theory) occurs on the symmetric mid sections of the inner curve as well as on the sides where the red elements show tension in the material. The stress throughout the U-bend varies between 0.533 and 12.02MPa.

** The stress values listed above have been averaged across each element and are not the absolute values, but it can be assumed to be accurate due to the low stresses involved versus the high allowable stresses.*

Figure M5 – Top minor principal stress (Mohr-circle theory)

The maximum minor principal stress on the outside of the U-bend occurs near both ends on the inner curve. The analysis show that the stress values vary from compression to tension. They vary between -3.607 (compression) to 8.358MPa (tension).

Figure M6 – Top Von Mises (Von Mises yield criterion)

The resulting Von Mises stress again has much the same distribution as the major principal stresses, but with much lower forces. The maximum Von Mises yield stress occurs on the symmetric mid sections of the inner curve as well as on the sides where the red elements indicate tension. The stress varies between 1.743 and 10.46MPa.

For both the inside and outside of the U-bend, the occurring stresses are well below the allowable stress of 108.24MPa according to ASME (2001) (see table 6.1).

M1.4 - CONCLUSIONS DRAWN FROM THE FINTUBE ANALYSIS*

Load:

Calculated stresses assuming an inside pressure of 2MPa (20bar).

Constraints:

One node on the bottom left was fixed in the z-translation axis, while the rest of the nodes were unconstrained.

Figure M7 – Azimuth stress

The maximum azimuth or hoop stress occurs on the inside of the fintube where the red elements show tension in the material. The stress throughout the fintube varies between 2.188 and 5.43MPa.

Figure M8 – Radial stress

The maximum radial stress also occurs on the inside of the fintube (indicated by the purple elements). The stress is negative, showing that there are compressive stresses present in the material. The stress throughout the fintube varies between -0.00687 and -1.955MPa.

Figure M9 – Axial stress

The maximum axial stress occurs at the root of each fin. This is where one would anticipate material failure because of the sharp corners and the accompanying stress concentrations. The analysis confirms this theory and show that the stress values vary from compression stresses in the finroot to tension stresses between the fins on the outside of the tube. The insert picture shows the detail stress distribution in the finroot. Note that the distribution is effected by the grid with which the model is meshed. The grid size was limited by hardware limitations, but the results are deemed to be fairly accurate. The values vary between -3.69 (compression) to 0.19MPa (tension).

Figure M10 – Von Mises stress (Von Mises yield criterion)

The maximum Von Mises stress occurs in the inside tube wall and is indicated by the red elements. The occurring stresses are well below the allowable stress of 87.55MPa according to ASME (2001) (*see table 6.1*). The stress varies between 2.191 and 6.626MPa.